

**Civilian Radioactive Waste Management System  
Management & Operating Contractor**

**Chapter 11  
Total System Performance Assessment-Viability Assessment (TSPA-VA)  
Analyses Technical Basis Document**

**Summary and Conclusions**

**B00000000-01717-4301-00011 REV 00**

**August 14, 1998**

Prepared for:

U.S. Department of Energy  
Yucca Mountain Site Characterization Office  
P.O. Box 30307  
North Las Vegas, Nevada 89036-0307

Prepared by:

TRW Environmental Safety Systems Inc.  
1261 Town Center Drive  
Las Vegas, Nevada 89134

**INFORMATION COPY**

Under Contract Number  
DE-AC08-91RW00134

#### **DISCLAIMER**

This report was prepared as an account of work sponsored by an agency of the United States Government. Neither the United States nor any agency thereof, nor any of their employees, makes any warranty, expressed or implied, or assumes any legal liability or responsibility for the accuracy, completeness, or usefulness of any information, apparatus, product, or process disclosed, or represents that its use would not infringe privately owned rights. Reference herein to any specific commercial product, process, or service by trade name, trademark, manufacturer, or otherwise, does not necessarily constitute or imply its endorsement, recommendation, or favoring by the United States Government or any agency thereof. The views and opinions of authors expressed herein do not necessarily state or reflect those of the United States Government or any agency thereof.

**Civilian Radioactive Waste Management System  
Management & Operating Contractor**

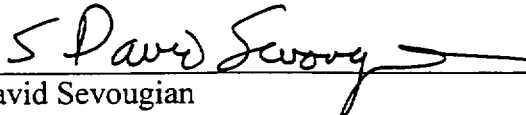
**Chapter 11  
Total System Performance Assessment-Viability Assessment (TSPA-VA)  
Analyses Technical Basis Document**

**Summary and Conclusions**

**B00000000-01717-4301-00011 REV 00**


**August 14, 1998**

Prepared by:

  
\_\_\_\_\_  
David Sevougian  
Performance Assessment Operations

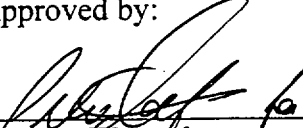
8/14/98  
Date

Checked by:

  
\_\_\_\_\_  
Tim Dale  
Performance Assessment Operations

8/14/98  
Date

Approved by:

  
\_\_\_\_\_  
Robert W. Andrews  
Performance Assessment Operations

11 Aug 98  
Date

INTENTIONALLY LEFT BLANK



## ACKNOWLEDGMENT

### Summary and Conclusions

The following individuals have contributed to the technical content and preparation of this document: Michael L. Wilson, John H. Gauthier, Robert W. Andrews, Vinod Vallikat, Robert J. MacKinnon, B. S. Ramarao, Nelson Erb, Patrick Mattie, David Chace, and Laurence Parisot.

This work was supported by the Yucca Mountain Site Characterization Office as part of the Civilian Radioactive Waste Management Program, which is managed by the U.S. Department of Energy, Yucca Mountain Site Characterization Project.

INTENTIONALLY LEFT BLANK

## CONTENTS

	Page
11. SUMMARY AND CONCLUSIONS .....	11-1
11.1 INFORMATION FLOW IN TSPA-VA .....	11-3
11.1.1 Treatment of Uncertainty in the TSPA-VA .....	11-5
11.1.1.1 Uncertainty Versus Variability .....	11-5
11.1.1.2 Weighting of Alternative Conceptual Models .....	11-7
11.1.1.3 Uncertainty and the Base Case .....	11-8
11.1.1.4 Presentation and Analysis Techniques for Uncertainty .....	11-10
11.2 TSPA-VA MODEL AND CODE ARCHITECTURE .....	11-11
11.2.1 Unsaturated-Zone Flow .....	11-13
11.2.1.1 Climate .....	11-13
11.2.1.2 Mountain-Scale Unsaturated-Zone Flow .....	11-14
11.2.1.3 Seepage into the Drift .....	11-15
11.2.2 Thermal Hydrology .....	11-16
11.2.2.1 Repository-Scale Thermal Hydrology .....	11-16
11.2.2.2 Drift-Scale Thermal Hydrology .....	11-17
11.2.3 Near-Field Geochemical Environment .....	11-18
11.2.4 Waste-Package Degradation .....	11-19
11.2.5 Cladding Degradation .....	11-21
11.2.6 Waste-Form Degradation and Mobilization .....	11-22
11.2.7 Engineered-Barrier-System Transport .....	11-23
11.2.8 Unsaturated-Zone Transport .....	11-25
11.2.9 Saturated-Zone Transport .....	11-26
11.2.10 Biosphere Transport .....	11-27
11.3 UNCERTAINTY/SENSITIVITY ANALYSIS METHODS IN TSPA-VA .....	11-27
11.3.1 Uncertainty Analysis .....	11-28
11.3.2 Sensitivity Analysis Methods .....	11-30
11.3.2.1 Scatter Plots .....	11-30
11.3.2.2 Linear Regression Analysis .....	11-31
11.3.2.3 Stepwise Regression Modeling .....	11-32
11.3.3 Sensitivity Analysis Calculations .....	11-34

11.4 SUMMARY OF TSPA-VA RESULTS .....	11-36
11.4.1 Deterministic Results of the Base Case.....	11-37
11.4.1.1 Ten-Thousand-Year Dose Rates .....	11-39
11.4.1.2 One-Hundred-Thousand-Year Dose Rates .....	11-43
11.4.1.3 One-Million-Year Dose Rates .....	11-48
11.4.1.4 Cumulative Activity Releases from the Repository and the Engineered Barrier System.....	11-51
11.4.1.5 Summary.....	11-52
11.4.2 Probabilistic Results of the Base Case .....	11-53
11.4.2.1 Uncertainty Analysis Results.....	11-53
11.4.2.2 Precision of the Base Case CCDFs.....	11-57
11.4.2.3 Sensitivity Analysis Results.....	11-57
11.4.2.4 Impact of Parameter Uncertainty Ranges on Sensitivity Analyses .....	11-61
11.4.2.5 Summary.....	11-62
11.5 summary of Performance Assessment Work required between the viability assessment and the site recommendation and license application.....	11-63
11.5.1 Model Abstractions .....	11-65
11.5.2 Total System Performance Assessment Analyses.....	11-67
11.5.3 Design Support .....	11-70
11.5.4 Concluding Remarks .....	11-70
11.6 References.....	11-72
APPENDIX A—DESCRIPTION OF TSPA-VA BASE CASE UNCERTAIN PARAMETERS.....	A11-1

## FIGURES

- Figure 11-1. Performance assessment information flow pyramid. .... F11-1
- Figure 11-2. Simplified representation of information flow in TSPA-VA between data, process models, and abstracted models. .... F11-2
- Figure 11-3. Detailed representation of information flow in TSPA-VA. .... F11-3
- Figure 11-4. TSPA-VA code configuration: Information flow among component computer codes. .... F11-4
- Figure 11-5. Configuration of cells in the RIP program for EBS transport in the TSPA-VA base case. CAM means corrosion-allowance material and is the outer waste-package layer made of carbon steel. CRM means corrosion-resistant material and is the inner waste-package layer made of Alloy 22. .... F11-5
- Figure 11-6. Dose rate to an "average" individual withdrawing water from a well penetrating the maximum plume concentration in the SZ, 20 km downgradient from the repository. This figure shows the most important radionuclides in different time periods: Tc-99 and I-129 within the first 10,000 years; Tc-99 and Np-237 within the first 100,000 years; and Np-237 and Pu-242 within the first 1,000,000 years. .... F11-6
- Figure 11-7. Effects of climate change, seepage flux, and waste-package degradation on EBS releases and dose rates in the first 10,000 years after waste emplacement. .... F11-7
- Figure 11-8. Performance of the UZ with respect to Tc-99 during the first 10,000 years after waste emplacement. Shown is the effect of different climate states, the EBS released from various repository regions, and the UZ releases to the various water-table regions. .... F11-8
- Figure 11-9. Performance of the SZ with respect to Tc-99 during the first 10,000 years after waste emplacement. Shown are concentration and releases in six stream tubes (each associated with one of six regions at the water-table level) and the impact of dilution in the SZ. Shown in the upper left corner are the six water-table regions. .... F11-9
- Figure 11-10. Effects of climate change, seepage flux, and waste-package degradation on EBS releases and dose rates in the first 100,000 years after waste emplacement. .... F11-10
- Figure 11-11. Effects of matrix degradation rate and inventory exposure rate on the releases of the three different fuel types: CSNF, DSNF, and HLW. WP means waste package. .... F11-11

- Figure 11-12. Performance of the UZ during the first 100,000 years after waste emplacement with respect to Tc-99, Np-237, and Pu-239. Shown is the importance of sorption in the UZ. EBS means engineered barrier system. LTA means long term average. Pu-242 breakthrough curve is approximate only, see discussion in Section 11.4.1.3..... F11-12
- Figure 11-13. Performance of the SZ during the first 100,000 years after waste emplacement with respect to Tc-99, Np-237, and Pu-239. Shown is the importance of sorption and dilution in the SZ. UZ means unsaturated zone. CDF means cumulative distribution function..... F11-13
- Figure 11-14. Importance of biosphere dose conversion factors (BDCF) in the first 100,000 years after waste emplacement. Also shown is the impact of colloidal transport of irreversibly sorbed Pu-239..... F11-14
- Figure 11-15. Effects of climate change, seepage flux, waste-package degradation, and cladding degradation on waste-package (WP) releases and dose rates in the first 1,000,000 years after waste emplacement. CSNF means commercial spent nuclear fuel. .... F11-15
- Figure 11-16. Waste-package (WP) releases during 1,000,000 years after waste emplacement for the three inventory types: CSNF, DSNF, and HLW. .... F11-16
- Figure 11-17. Effects of SZ dilution and BCDF on 1,000,000-year dose rates. The inset at upper left shows the six water table regions. .... F11-17
- Figure 11-18. Cumulative fractional inventory releases of Tc-99, Np-237, Pu-239, and Pu-242 from the EBS and the 20-km SZ boundary, normalized to the initial inventory. Shown are the effects of sorption and decay of radionuclides. .... F11-18
- Figure 11-19. The base-case distribution of peak-dose rates for three time periods (bottom) and their relation to dose-rate time histories (top). Twenty dose-rate histories do not appear on the top plot because they have no computed dose for the first 100,000 years. .... F11-19
- Figure 11-20. Average contribution to peak-dose rate of different radionuclides for three time periods. Note that for the earlier two time periods, many realizations have no computed dose..... F11-20
- Figure 11-21. Peak-dose-rate vs. time of peak-dose rate for three time periods. Pink dots at the bottom indicate realizations with zero dose (which are off the scale of the log plot). The colored circles refer to the selected realizations highlighted in Figure 11-19, plus one that is not in Figure 11-19 because of having no computed dose for the first 100,000 years. .... F11-21

- Figure 11-22. Number of failed waste packages over time for the selected realizations for 100,000 years. There is no curve for one realization because it has no waste-package failures in the first 100,000 years. The realizations were chosen to have a spread of peak-dose rates and peak-dose times and, therefore, a variety of different behaviors. .... F11-22
- Figure 11-23. Dose-rate time histories for 1,000,000 years for the five selected realizations. Regularly spaced spikes in the curves are caused by the climate changes that occur roughly every 100,000 years..... F11-23
- Figure 11-24. Climate history for one realization. The others look similar. Most of the peak-dose rates occur at one of the two superpluvial climates. .... F11-24
- Figure 11-25. Number of failed waste packages over time for the selected realizations for 1,000,000 years. The waste-package failures starting at about 700,000 years are waste packages with no seeps dripping on them. .... F11-25
- Figure 11-26. Comparison of peak-dose-rate distributions determined from simulations with different numbers of realizations (runs). The distributions are found to be quite similar, indicating reasonable stability with respect to number of realizations. Figure 11-26. Comparison of peak-dose-rate distributions determined from simulations with different numbers of realizations (runs). The distributions are found to be quite similar, indicating reasonable stability with respect to number of realizations. .... F11-26
- Figure 11-27. Most important parameters from stepwise regression analysis for three time periods. These charts show the relative importance of various parameters to the calculated uncertainty in dose rate for the three time periods. Importance of an individual parameter is shown by  $R^2$ -loss, the reduction in goodness of the regression fit when the parameter is left out of the calculation, as described in the text. .... F11-27
- Figure 11-28. Scatter plot of seepage fraction (fraction of waste packages contacted by seeps) for the long-term-average climate against peak dose rate for a 100,000-year period. Pink dots at the bottom indicate realizations with zero dose (which are off the scale of the log plot). The colored circles refer to the selected realizations highlighted in Figure 11-19. .... F11-28
- Figure 11-29. Scatter plot of mean Alloy 22 corrosion rate (in terms of percentile from the uncertainty distribution) against peak-dose rate for a 100,000-year period. Pink dots at the bottom indicate realizations with zero dose (which are off the scale of the log plot). The colored circles refer to the selected realizations highlighted in Figure 11-19. .... F11-29

- Figure 11-30. Scatter plot of seepage fraction (fraction of waste packages contacted by seeps) for the long-term-average climate against peak-dose rate for a 1,000,000-year period. The colored circles refer to the selected realizations shown in Figure 11-23. .... F11-30
- Figure 11-31. Partial rank correlation coefficients as a function of time for six uncertain parameters that are most important to uncertainty in dose rate. This figure illustrates another way to show the change of importance of parameters through time from that shown in Figure 11-27..... F11-31
- Figure 11-32. Dose-rate time histories for 100,000 years for the base case (top) and the modified-parameter case (bottom). .... F11-32
- Figure 11-33. Base case and modified-parameter case distributions of peak-dose rates for the 100,000-year time period. .... F11-33
- Figure 11-34. Most important parameters from stepwise regression analysis for the modified-parameter case. This chart shows the relative importance of various parameters to the calculated uncertainty in dose rate. Importance of an individual parameter is shown by  $R^2$ -loss, the reduction in goodness of the regression fit when the parameter is left out of the calculation. .... F11-34



## TABLES

Table 11T-1. Summary of Input and Output Files, Plot File Names (SigmaPlot), and Data Tracking Numbers (DTNs) Associated with the TSPA-VA figures 11-6 to 11-18 in Section 11.4 and Sections 4.2 and 5 of DOE (1998).....	T11-1
Table 11T-2. Summary of Computer Codes* that Comprise the Total System Model.* ...	T11-12 14 <i>RLA 8/14</i>
Table 11T-3. Summary of Input and Output Files and Data Tracking Numbers Associated with the TSPA-VA (Figures 11-19 through 11-34 in Section 11.4 of this Chapter).*	T11-13 15 <i>RLA 8/14</i>
Table 11T-4. Summary of Computer Codes Used for the Uncertainty and Sensitivity Analysis (Codes were Executed on a Sun Ultra Sparc (UNIX Operating System).*	T11-15 17 <i>RLA 8/14</i>
Table 11T-5. Importance Ranking of Inputs for Engineered-Barrier-System Releases at 1,000,000 Years.....	T11-15 17 <i>RLA 8/14</i>
Table 11T-6. Summary of Calculated, Peak-Dose Rates at 20 km (12.4 Miles).....	T11-15 17 <i>RLA 8/14</i>

INTENTIONALLY LEFT BLANK

ADDENDUM TO CHAPTER 11 – 8/22/98

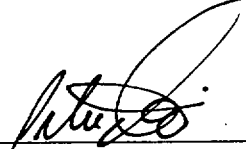
Please note that the following figures were inadvertently omitted from this chapter during the reproduction process. They have been included here for technical consistency and to facilitate the review, although they are not formally part of Revision 00.

Figure 11-3. Detailed representation of information flow in TSPA-VA

Figure 11-5. Configuration of cells in the RIP program for EBS transport in the TSPA-VA base case. CAM means corrosion allowance material and is the outer waste-package layer made of carbon steel. CRM means corrosion resistant material and is the inner waste-package layer made of Alloy 22.

Figure 11-8. Performance of the UZ with respect to Tc-99 during the first 10,000 years after waste emplacement. Shown is the effect of different climate states, the EBS released from various repository regions, and the UZ releases to the various water table regions.

A Performance Report (PR) will be issued to correct this chapter. Revision 01 will also include these figures.

 21-Aug-98  
\_\_\_\_\_  
Peter S. Hastings, Deputy Manager  
Performance Assessment Operations

INTENTIONALLY LEFT BLANK

## ACRONYMS

BDCF	biosphere dose conversion factor
CAM	corrosion-allowance material
CCDF	complementary cumulative distribution function
CRM	corrosion-resistant material
CSNF	commercial spent nuclear fuel
DKM	dual permeability model
DSNF	DOE spent nuclear fuel
DTN	data tracking number
EBS	engineered-barrier system
HLW	high-level waste
LHS	Latin Hypercube sampling
PCC	partial correlation coefficient
SRC	standardized regression coefficients
SZ	saturated zone
TSPA-VA	Total System Performance Assessment-Viability Assessment Technical Basis Document
UZ	unsaturated zone
YMP	Yucca Mountain Project

INTENTIONALLY LEFT BLANK

## 11. SUMMARY AND CONCLUSIONS

This chapter describes the results of combining all of the component Total System Performance Assessment-Viability Assessment Technical Basis Document (TSPA-VA) models, described in the foregoing chapters, into the overall TSPA-VA total system model. The results presented here are the estimated future dose rate to an average individual who obtains his water from a well located 20 km (12.4 mi) downgradient of the potential repository. The well is presumed to be located in the center of the plume of radionuclide releases that may eventually escape from the repository when the waste packages begin to degrade. These predictions of dose rate are presented in Section 11.4 in two forms: (a) plots of dose rate versus time for a single realization of the uncertain component model parameters (the "expected-value" realization, which is the realization that samples the expected values of all input parameters), and (b) complementary cumulative distribution functions (CCDFs) of peak dose rate during a given time span, which show the probability of exceeding a given dose rate at any time during the defined time frame (for example, during the first 10,000 years after repository closure). Plots of performance parameters from various repository subsystems, such as the activity release rate (Curies/year) from the engineered-barrier system (EBS) are also presented in Section 11.4. These subsystem plots demonstrate how the various repository subsystems interact with and influence each other, and also how they influence the dose rate.

This chapter presents an overview of the method for mathematical and numerical modeling of each process and component introduced in Chapters 2 through 9, including their uncertainty, and the approach for combining them into an overall model and computer code. This overview includes discussions about information flow between the models (Section 11.1) and the computer code architecture that facilitates the information flow (Section 11.2).

Besides the methods for modeling the repository system, the other key part of TSPA is how to most transparently analyze and present the key results—in particular, how to show the influence of uncertainty on the performance predictions. The 1997 Energy and Water Appropriations Act requests an analysis of the "probable behavior of the repository." The TSPA-VA base-case models described in Chapters 2 through 9 are intended to encompass this probable behavior. The exact definition of "base case" depends on the choice of parameter ranges for each component model. In this context, the use of the term "range" is important. In particular, the TSPA-VA base-case parameter sets and conceptual models encompass a range of uncertainty for the various parameters rather than just one realization of the parameters. Given the base-case definitions of these various parameter ranges for each of the model components, a base-case total system model is constructed to predict overall repository performance. This model represents an assessment of the likely range of future behavior for the overall repository system, which is essentially a combination of the likely ranges of behavior for the various component models, processes, and corresponding parameters. Section 11.1 provides a definition of the base-case TSPA-VA model in the context of various types of uncertainty regarding physical-chemical parameters, conceptual models, numerical models, and future events.

Lying outside the range of the base-case performance predictions are types of repository behavior considered to be less likely, including:

- Alternative models and/or alternative parameter ranges of the various physical-chemical processes
- Low-likelihood disruptive events, such as volcanism, seismicity, and criticality
- Alternative repository designs.

The last item in the above list is a slightly different form of "uncertainty," since it is directly under the control of the repository designers. However, it remains uncertain because of uncertainty in the various system parameters. As the uncertainty in the system parameters is reduced through experimentation and data collection, the optimal repository design also becomes less uncertain.

Performance predictions for the above three forms of uncertainty are not discussed in this document. Only the TSPA-VA base-case results are shown. The effect of these three uncertainties on dose rate may, however, be found in the DOE publication *Viability Assessment of a Repository at Yucca Mountain* (DOE 1998).

Various sensitivity analysis methods for determining the most influential system parameters are presented in Section 11.3, primarily focusing on linear regression methods. These analyses include methods for displaying the results in a way that transparently demonstrates the key natural and engineered-barrier parameters and features (e.g., plots of correlation coefficients versus time). This helps prioritize future site-characterization efforts and delineate best possible design options.

The final section of this chapter, Section 11.5, identifies the performance-assessment activities necessary for developing the TSPA for the Site Recommendation/License Application. The intent of this section is to summarize the TSPA work between viability assessment and license application.

The main information in this Chapter that is not discussed in DOE (1998) is presented in Section 11.2, which gives a more detailed description of the total system computer-code architecture than given in DOE (1998) and in Section 11.3, which is an amplified discussion of the linear regression model. Other portions of this chapter are for the most part duplicates of the text in Volume 3 of DOE (1998). These have been included in this document for completeness.

Finally, the other key information in this chapter that is not included in DOE (1998) is contained in Tables 11-1, 11-2, and 11-3 (later in the chapter), which identify all the electronic data files necessary to reproduce the dose rate results in the figures of Sections 4 and 5 of Volume 3, Draft B, of DOE (1998), including the total-system-model computer codes, and their associated input and output files. Included are data tracking numbers (DTNs) which identify a location in the Yucca Mountain Project (YMP) Technical Database that contains these electronic files. Table 11-3 also refers to two figures found later in this chapter (11-33 and 11-34) that are not in DOE (1998).



## 11.1 INFORMATION FLOW IN TSPA-VA

A stylized conceptualization of the TSPA-VA model hierarchy and information flow is shown in Figure 11-1. This figure indicates a continuum of information and models, from the most basic, detailed level to the level of the total system model. The data and associated conceptual and process-level models rest at the base of the pyramid. These process-level models may be simplified or abstracted,<sup>1</sup> if necessary, because of computational constraints or lack of information. The abstracted performance-assessment models may have a one-to-one correspondence with the detailed process-level models, or may represent a combined subsystem model<sup>2</sup> covering several aspects of the overall system. The performance-assessment models form the components of the overall TSPA model at the top of the pyramid. Total-system model simulations can then be performed in the computationally intensive probabilistic framework necessitated by a Monte Carlo approach to performance assessments.<sup>3</sup>

For this model-simplification process, there are two key factors in accurately representing the performance of the overall system. First, information passed up the model pyramid must be consistent. For instance, an infiltration flux used to generate liquid flow fields from the detailed process model for the unsaturated zone (UZ) must be used in all subsequent analyses based on those particular flow fields. For example, the same flux must be used when calculating seepage flux in the abstracted seepage subsystem model (see Chapter 2) and when calculating thermal-hydrologic response (temperature and relative humidity) in the near-field environment (see Chapter 3). Second, the parameters that most affect performance in the detailed process models must be appropriately represented in the subsequent subsystem and total system models, including the appropriate uncertainty range of the parameters (see Sections 2.4.3, 3.2.1, 4.5.3, 5.10.3, 6.3, 6.4, 6.5, 7.5.3, 8.4.2, and 9.2.3 in Chapters 2–9).

A key feature of the methodology is the propagation of uncertainty at one level to uncertainty at another level. As Figure 11-1 illustrates, transfer of uncertainty must go in both directions, from bottom up and from top down. When analyzing uncertainty at the bottom levels (data, conceptual models, and process models), the analyses look at the effect of uncertain parameters

---

<sup>1</sup> The word *abstraction* is used to connote the development of a simplified mathematical and/or numerical model that reproduces and bounds the results of an underlying detailed process model.

<sup>2</sup> Examples of various subsystems include the engineered barrier system, the UZ, and the SZ.

<sup>3</sup> Much of the modeling of the repository and its components is complex, uncertain, and variable, involving a variety of coupled processes (thermal-hydrologic-chemical and thermal-hydrologic-mechanical) operating in three spatial dimensions on a variety of different materials (for example, fuel rods, waste packages, invert, and host rock) and changing over time. For these reasons, it is often necessary to make some simplifications to the detailed process-level models. The need for simplification is particularly evident in total system performance assessment, which has a significant component of probabilistic risk analysis. The general approach of using probabilistic risk analysis is appropriate because of the inherent uncertainties in predicting physical behavior many thousands of years into the future in a geologic system with properties that can never be fully characterized deterministically. Because of the large number of uncertain parameters in the component TSPA models, probabilistic risk analysis involves a Monte Carlo method of multiple realizations of system behavior, which requires significant computational resources. For this reason, and also because the lack of certain data makes some detailed models difficult to quantify, model abstractions are often employed.

on surrogate or subsystem performance measures such as the amount of fracture flow in the UZ. The sensitivity of the surrogate measure to component model uncertainty is then used to decide whether to carry this uncertainty through to the total system analyses. However, sometimes important parameters at the subsystem level prove to be unimportant at the overall system level and then this information is passed down the pyramid to indicate the relative unimportance of collecting more physical data about this parameter.

Figure 11-2 is a more detailed, but still quite simplified, look at information flow among the nine-key component models to be described in Section 11.2: UZ flow (and seepage), thermal hydrology, near-field geochemistry, waste-package degradation, waste-form degradation and mobilization, EBS transport, UZ transport, saturated zone (SZ) flow and transport, and biosphere. Figure 11-2 is essentially Figure 11-1 turned sideways and with more detail. It does not show all of the couplings among TSPA-VA component models but gives a good idea of major model connections, abstractions, and information feeds. The term "response surface" appears in most of the abstracted models. This term generally means a multidimensional table of output from one model to be used as input for another model. When interpolating among points in the table, linearity is generally assumed. Usually a response surface has more than one dependent variable (e.g., both time and percolation flux). However, in the usage in Figure 11-2, sometimes time is the only independent variable, and interpolation is not even necessary between the time points (e.g., the data are provided directly "as is" to the next model).

Figure 11-3 is a more detailed description of information flow in the TSPA-VA, showing the principal pieces of information passed between the various component models. These details of information flow are explained in greater depth in the discussion of the TSPA-VA code architecture in Section 11.2. The conceptual and experimental basis for this depiction of information flow is given in detail in Chapters 2 through 9. For example, the division of the repository horizon into six regions based on thermal-hydrologic response and infiltration flux is discussed in Chapter 3, and the division of the SZ water table into six regions—unrelated to the six repository regions—based on stratigraphy and other factors is discussed in Chapter 8.

The decoupling of the physical-chemical processes into component models, shown in Figures 11-2 and 11-3, is facilitated by a natural division of the repository system into a series of sequentially linked spatial domains (e.g., the waste package, emplacement drift, host rock "near" the drift, UZ between the drift and the water table, SZ, and biosphere). This division works best from the standpoint of radionuclide transport, which is the primary consideration of the TSPA models (i.e., to track and predict radionuclide transport from the waste-form domain to the biosphere domain). The TSPA-VA model architecture and information flow becomes, therefore, a sequential calculation in which each spatially based transport model may be run in succession, with output as "mass versus time" from an upstream spatial domain serving as the input of "mass versus time" for the spatial domain immediately downstream. (Upstream and downstream refer to the direction of mass flow.) Although many physical-chemical processes are uncoupled in the present TSPA-VA model, the Project's focus on coupled processes has increased, and modeling efforts are attempting to assess the importance of such effects so that this information may be used to improve future performance assessments (for example see Chapter 4, Section 4.2.2).

### **11.1.1 Treatment of Uncertainty in the TSPA-VA**

This section describes the various types of uncertainty represented in the TSPA-VA models and how these uncertainties affect the predictions of performance. Section 11.1.1.1 lists the four major types of uncertainty, describes the differences between uncertainty and variability, and introduces the modeling tools (e.g., Monte Carlo sampling) for analyzing uncertainty. Section 11.1.1.2 describes how one type of uncertainty, conceptual model uncertainty, is handled in TSPA-VA and how this leads to a definition of the TSPA-VA base case. Section 11.1.1.3 gives more details on how uncertainty is handled in the base case and how the base case might be used to explore the "probable" behavior of the repository. A description then follows about the "expected-value" realization, which is used in Section 11.4.1 to show how the various component models interact with one another. Finally, Section 11.1.1.4 describes the various sensitivity analysis methods employed in TSPA-VA to determine the most important model parameters affecting the total system performance.

#### **11.1.1.1 Uncertainty Versus Variability**

A variable feature, event, or process is one that varies over space or time. Examples include the porosity of a hydrogeologic layer and the temperature and near-field geochemical environment in the repository drifts. If perfect information (complete knowledge) were available, such parameters would best be represented by distributions over space and time.

Uncertainty relates to ignorance or lack of knowledge regarding a feature, event, or process—one whose properties or future outcome cannot be predicted beforehand. Four types of uncertainty are typically considered: (1) value uncertainty, (2) conceptual-model uncertainty, (3) numerical-model uncertainty, and (4) uncertainty regarding future events. The treatment of a feature, event, or process as purely variable or purely uncertain can lead to significantly different modeling results. In general, variability can serve to either dilute or concentrate contamination from a repository in either time or space.

Uncertainty in the treatment of a feature, event, or process results in uncertain forecasts of future repository behavior. Uncertainty and variability are related in that spatial and temporal variability are generally very uncertain. If the variability can be appropriately quantified or measured, then a model can usually be developed to include this variability. If the variability cannot be physically quantified or measured, then it should be treated as uncertainty (lack of knowledge).

However, the ability to model some types of spatial variability can be limited not only by measurement deficiencies but also by computational resources. An example of this is fracture permeability in the volcanic tuffs. Fracture lengths and apertures in the tuff units occur randomly over a wide variety of spatial scales, from the very large such as distinct fault zones (e.g., the Ghost Dance) to the very small (e.g., cracks on the order of millimeters in length and sub-micron in width). It is relatively easy to measure air permeabilities (but not necessarily liquid permeabilities) in these large faults and to include these discrete features in numerical models. It is much harder to include spatial heterogeneity on the millimeter scale in the overall flow-and-transport numerical models because of the difficulties of in situ measurement, the inability to comprehensively characterize small-scale permeability over the entire mountain, and

a lack of computers large enough to model flow and transport on such a fine scale over the entire mountain.

In addition to these considerations, the appropriate quantification of the spatial variability in the models is very much a function of what performance measure is desired at the output side of the model. If a well pumps water over a 100-meter screened interval, the appropriate discretization of the spatial variability may be on the order of 10 meters per numerical grid block; however, if it is desired to measure dripping into the drifts, the appropriate discretization of the grid cells may be on the centimeter scale.

Two basic tools were used in the TSPA to deal with uncertainty and variability: probability theory and alternative conceptual models. The former is used for uncertainty in specific model parameters and the latter for uncertainty in the understanding of a key physical-chemical process controlling system behavior. In particular, uncertain processes often require different conceptual models. For example, different concepts of matrix-fracture coupling in the UZ lead to different flow and transport models. Sometimes, conceptual models are not mutually exclusive (e.g., both matrix and fracture flow might occur) and sometimes they do not exhaustively cover all possibilities (matrix and fracture flow apparently do, although the definition of "matrix" depends on the length scale used in the model). These problems indicate that the use of alternative conceptual models, while often necessary to characterize some types of uncertainty, is not always as rigorous as one might like—an unfortunate result of insufficient knowledge in some areas. Methods used in the TSPA-VA to deal with alternative conceptual models are discussed in Section 11.1.1.2.

For the treatment of uncertainty in specific model parameters and for alternative conceptual models that have been weighted beforehand with specific probabilities, the Monte Carlo sampling method has been used in all TSPAs to date and is the primary method of uncertainty analysis used for this TSPA. The method involves random sampling of the probability distributions for all uncertain input parameters (including any index parameters that might be used to weight alternative conceptual models). Then, numerous realizations of the repository system are calculated based on the sampled realizations of all the inputs. Each total system realization has an associated probability so that there is some perspective on the likelihood of that set of circumstances occurring.<sup>4</sup> The Monte Carlo method yields a range for any chosen performance measure (e.g., peak dose-rate to an individual within a given time period at a given location), along with a probability for each value in the range. In other words, it gives an estimate of repository performance plus "error bars" on the estimate. The performance measures and associated probabilities have traditionally been presented as CCDFs that show the probability of exceeding a given performance-measure value.

---

<sup>4</sup> In the standard Monte Carlo method, each realization is equally likely, so each realization is weighted by 1 divided by the number of realizations. In more elaborate variants, for example using "importance sampling," some realizations can be less probable than others. The TSPA-VA uses a variant of the Monte Carlo method, called Latin Hypercube Sampling or LHS, which better models the tails of the input probability distributions when the number of realizations is small.

#### 11.1.1.2 Weighting of Alternative Conceptual Models

In many subsystems of the overall TSPA system, there are plausible alternative models or assumptions. In some cases these alternatives form a continuum, and sampling from the continuum of assumptions fits naturally within the Monte Carlo framework of sampling from probability distributions. In other cases, the assumptions or models are discrete choices. In particular, some processes are so highly uncertain that there is not enough data to justify developing continuous probability distributions over the postulated ranges of behavior. In other words, a high degree of sampling is unwarranted, and it is better just to look at two or three cases that are thought to encompass (bound) the likely behavior.

There are two possible approaches to incorporating discrete alternative models within the TSPA: weighting all models into one comprehensive Monte Carlo simulation (lumping), or keeping the discrete models separate and performing multiple Monte Carlo simulations for each discrete model (splitting). There are advantages and disadvantages to both approaches. Lumping has the conceptual advantage that a single CCDF can be said to include all the system uncertainty. Splitting can lead to a profusion of cases that makes it difficult to quantify the relative importance of the various discrete assumptions. The main disadvantage of lumping is the concern that cases with poor performance might be diluted within a sea of more favorable cases. In other words, there could be a combination of the discrete assumptions with poor performance that might not be obvious under the lumped approach but that would stand out if that combination were presented separately. Another potential disadvantage of lumping occurs if there is no good justification for the probabilities used—if the weighting of the alternatives is artificial, then the results will be artificial as well.

For this TSPA, a combination of the two approaches is used. In particular, the TSPA-VA “base-case” model can be considered an implementation of the splitting approach, since it is based on a limited range of uncertainty. Based on expert judgement (and to some extent on finite time and resources that can be applied to the VA effort), the TSPA-VA base case is a best estimate as to the more likely ranges of model behavior and parameter ranges. Some alternative models are not included in the base case and some parameter ranges of the included models have been narrowed. The level of uncertainty included in the TSPA-VA base-case model is based on the current level of knowledge regarding the various processes controlling system behavior. In several instances, the range of uncertainty is set quite large to bound possible behavior. Because of this narrowed range of models and parameters, the base-case CCDF is a conditional CCDF (shown in Section 11.4.2), meaning that it is “conditional” on certain models and parameters being held constant or having their variance restricted. (The primary type of CCDF used to portray repository performance is a CCDF of the peak dose-rate occurring within a given time span at a given location [e.g., the peak dose-rate at 20 km [12.4 mi] that occurs at any time during the first 10,000 years]).

Some of the most important processes and parameters (i.e., having the greatest effect on performance or dose rate) not included in the base case also warrant a separate presentation of their uncertainty in the form of several conditional CCDFs based on alternative process models. Alternative models of water seepage into the drift and of fracture-matrix flow in the UZ are treated in this manner (DOE 1998). Also, for design options, such as drip shields and ceramic coatings on the waste packages, there is no reasonable conceptual justification for lumping them

together into a single probability distribution. Therefore, they must be presented as conditional CCDFs—conditional on the given repository and/or waste-package design.

### 11.1.1.3 Uncertainty and the Base Case

Because of the significant amount of uncertainty in most of the component models, the variance associated with most models and parameters can only reasonably be restricted, but not wholly eliminated. Thus, the base case necessarily encompasses much of the underlying uncertainty. It includes: value or parameter uncertainty, conceptual model uncertainty, and future-event uncertainty. Therefore, the base case by itself also represents the “lumping” approach described above. Uncertainty not lumped into the TSPA-VA base case is captured discretely in alternative models, alternative features, and alternative events. These alternatives that have been “split” off of the base case, and their effects on performance are described separately as either alternative conditional CCDFs or, in some cases, as alternative single-realization time histories of performance. Examples of this for the TSPA-VA, with respect to each of the four types of uncertainty, include the following:

- **Parameter uncertainty**—widened parameter ranges for the cladding degradation models
- **Conceptual model uncertainty**—alternative process models for UZ flow and seepage
- **Numerical model uncertainty**—none shown for TSPA-VA
- **Future-event uncertainty**—disruptive events, such as volcanism.

A total “lumped” CCDF, including all of the uncertainty in TSPA-VA, is not presented because of difficulties (i.e., uncertainty) in assigning probabilities to some of the alternatives.

A final type of uncertainty, already mentioned above, but not included in the above four and not a candidate for lumping, is “design” uncertainty. This uncertainty is driven by the uncertainty in the natural-system parameters and processes. It represents the desire to design the safest repository possible within certain cost restrictions. However, the “best” design at any given time (for example, the VA design) may not represent the best design in the future (for example, the license application design) because new knowledge may be acquired based on additional site characterization and additional TSPA analyses. Either of these factors can lead to a new repository and/or waste-package design. This type of uncertainty for the VA is examined in the form of various “design options.”

The 1997 Energy and Water Appropriations Act asks for the “probable behavior of the repository in the Yucca Mountain geological setting.” However, it does not define the word “probable” in this context. Any of the random outcomes in the base-case CCDF, or for that matter any of the random outcomes in the alternative CCDFs, could be considered “probable” since they all have a finite probability. A more useful interpretation of the congressional language would either be “representative” or “most probable.” Regarding the latter, the most probable behavior is clearly the “mode” of a CCDF.<sup>5</sup> Since we do not present the total “lumped” CCDF that includes all

---

<sup>5</sup> In the theory of probability, the “mode” of a distribution is the point with the highest probability or highest likelihood of occurrence.

alternatives (see above), the most probable behavior could be taken as the mode of the base-case CCDF. Other points on the output CCDF are also often chosen as being "representative" of the likely or probable behavior of a stochastic system, including the expected-value (i.e., the mean or average of all dose rates) and the median (i.e., the 50<sup>th</sup> percentile value, above which lie half of the dose rates and below which lie the other half). The median and mean of the peak dose-rate CCDF are given in Section 11.4.2.

The CCDFs of peak dose rate shown in Section 11.4.2 are the most important measure of repository performance since they represent the peak, or highest, dose rate within a given time frame. However, they hardly tell the whole story of repository performance, since they are only a collection of 100 single points from the entire set of 100 complete time histories of repository behavior. To illustrate how the various component and subsystem models interact with one another, it is also useful to display one or more realizations of dose-rate versus time over specific time periods. Perhaps the most useful realization of the input parameters for this purpose is the expected values (means) of all the input parameters. This single realization is useful because its input parameters are time independent (that is, the same values of input parameters can be used regardless of the time span of interest, whether it be 10,000 years, 100,000 years, or 1,000,000 years). This single realization is called the "expected-value realization" in the rest of this document. (It is not the realization of the input parameters that produced the expected value or mean peak dose rate on any of the peak-dose-rate CCDFs because those realizations differ according to the time period being examined.) Other samplings of the input parameters, besides the expected values, are possible, such as the input medians or input modes; however, the input expected-values give a first-order estimate of the mean of the output,<sup>6</sup> whereas choosing the input medians or input modes does not provide an estimate of the output median or mode.

In addition to examining the behavior of the expected-value realization (expected value of all inputs), it is also useful to examine the behavior of realizations that lie close to both tails (i.e., both the upper and lower extreme) of the various input parameters. This is usually done one input parameter at a time (that is, all parameters except one are sampled at their expected values). The parameter of interest is then sampled at either its 5<sup>th</sup> percentile probability or its 95<sup>th</sup> percentile probability.<sup>7</sup> This is useful because the behavior of the various component models and their influence on one another can be quite different than for the expected-value realization. It is also useful to display these more-extreme time histories on the same graph as the expected-value time history because together they give a good indication of the complete range of influence of each of the input parameters on total repository performance during the specified time period, whether it be over the first 10,000 years, 100,000 years, or 1,000,000 years after closure. This type of analysis is presented in DOE (1998).

---

<sup>6</sup> For a linear model, they provide an exact estimate of the output mean. However, for the typical nonlinear models comprising the repository subsystems, they only yield a first-order approximation.

<sup>7</sup> Other samplings are possible, such as the 1<sup>st</sup> and 99<sup>th</sup> percentiles. We have chosen 5<sup>th</sup> and 95<sup>th</sup> as being representative of "extreme" input values.

#### 11.1.1.4 Presentation and Analysis Techniques for Uncertainty

One goal of the TSPA-VA is to evaluate the performance and associated uncertainty for the reference repository design and various design options. Another important goal is to determine the characteristics of the engineered and natural systems that have the most influence on repository performance. This information provides input to the design and site-characterization organizations about additional data that could provide the greatest improvement in confidence about the repository. Beyond these formal goals, there is the simple need to understand the results and make them clear to all interested parties. A number of methods are used to explain the results and quantify the sensitivities.

Total system performance is a function of sensitivity (i.e., if a parameter is varied, how much do the performance measures change?) and uncertainty (i.e., how much variation of a parameter is reasonable?). For example, the TSPA results could be very sensitive to a certain parameter, but the value for this parameter may be exactly known. In the uncertainty analysis techniques described below, a parameter would not be regarded as important. Many parameters in the TSPA-VA analyses do, however, have uncertainty associated with them and do end up with a high ranking for their importance to performance. On the other hand, the level of their ranking can depend on the width of the assigned uncertainty range. Therefore, uncertainty analyses must be carefully interpreted (i.e., the width of the uncertainty ranges must be considered). Most of the important parameters with possibly limited uncertainty ranges in the base case are examined in alternative models that either expand the range of their parameters beyond the expected range of uncertainty or change the weighting of the parameter distribution (DOE 1998).<sup>8</sup>

System performance may also be sensitive to repository design options, but models and parameters for these various options are not assigned any uncertainty. Therefore, even though they can be important, they do not show up in the tables of key parameters based on uncertainty analysis.

The determination of the parameters or components that are most important depends on the particular performance measure being used. This point was demonstrated in the 1993 TSPA (Andrews et al. 1994; Wilson et al. 1994) and the 1995 TSPA (CRWMS M&O 1995). For example, these two TSAs showed that the important parameters are different for 10,000-year peak doses than for 1-million-year peak doses.

Some methods for investigating sensitivity are discussed below:

- **Scatter plots**—Scatter plots are a good qualitative method of looking for sensitivities based on multi-realization simulations of the system. The final results (for example, dose rate) are plotted against the input parameters and visually inspected for trends. If there is a visible trend, it is an indication of sensitivity. The performance measures can

---

<sup>8</sup> The parameter uncertainty ranges established for the base case are usually based on site characterization data and expert judgement. Often times these ranges are expanded beyond the existing data in order to "bound" possible behavior. If the performance is found to be sensitive to the parameter within the base-case range, it is often useful to expand the range to quantify the effect of uncertainty beyond the "expected" base-case range.



also be plotted against various subsystem outputs or surrogate performance measures (e.g., waste-package lifetime) to determine whether that subsystem or performance surrogate is important to performance.

- **Regression analysis**—In regression analysis, a mathematical relationship between the outputs (performance measures) and inputs (model parameters) of a Monte Carlo simulation is developed. Typically, a method called stepwise linear regression is used in which only a subset of the input parameters is used for the regression, with parameters added one at a time based on calculated correlation coefficients. Parameters that have little influence on the performance measure are those that, when added, only marginally change the variance of the output. This method produces a ranking of input parameters according to their impact on the performance and a quantitative measure of the impact (basically, the correlation coefficient for the performance measure versus the input parameter). Note that linear regression only approximates parameter importance ranking for highly nonlinear systems. A more detailed description of regression analysis is presented in Section 11.3.2.2.
- **Differential analysis**—Another quantitative method for ranking important parameters is differential analysis, in which the partial derivatives of the performance measure with respect to the input parameters are calculated to find the amount that performance is affected when one parameter is varied while the others are held constant. A significant drawback of this method is that it is local; the derivatives are calculated about a point in the parameter space and only represent the sensitivity at that point. In contrast, regression analysis of Monte Carlo results is more global; the sensitivities are determined and ranked taking into account the whole parameter space.
- **Alternative models or parameter sets**—A useful but less systematic method of sensitivity analysis is to look at discrete cases; for example, some discrete sets of input parameters (as opposed to a systematic sampling) or some discrete choices of alternative models for a given process or subsystem. This method provides qualitative information about the sensitivity to the changes in assumptions (i.e., do the results change a little or a lot?) but not the same type of quantitative ranking produced by the previous two methods.

## 11.2 TSPA-VA MODEL AND CODE ARCHITECTURE

In this section, the TSPA-VA model is described with emphasis on how the different individual components described in Chapters 2 through 9 are combined for conducting performance-assessment calculations. Along with this, the computer-code architecture, which facilitated the information flow between the different components is also discussed. In the future, the information flow between the different components will be quality assured. The primary codes used in TSPA-VA, along with the information flow amongst the component computer codes, is shown in Figure 11-4. The executive driver program or integrating shell that links all the various component codes is RIP V.5.19.01 (Golder 1998) (see Table 11-4). The RIP code forms the heart of the TSPA-VA code architecture. It ties all the component models, codes, and response surfaces together in a coherent structure and uses a probabilistic sampling algorithm (Monte

Carlo sampling) that allows for consistent sampling of all uncertain parameters in the various component models. Figure 11-4 shows both the codes run prior to the RIP program and the ones run in real time that are coupled to RIP as external callable routines. For the codes that are coupled to RIP, the information between the codes are transferred in real time at every time step, but for those that are run prior to running RIP, the information is abstracted as response surfaces, generally in the form of multidimensional tables.

Because there are inherent uncertainties in predicting physical behavior many thousands of years into the future, and because there is the associated complexity in modeling the different components of the repository system, probabilistic risk analysis is the general approach adopted for conducting total system performance assessment calculations. This often requires simplifications to the detailed underlying process-level models in order to conduct multiple realizations of the complete system involving many components. The RIP driver program is generally flexible enough to incorporate these simplifications as well as to couple more complex process models. The four general ways in which the different components of the total system can be combined using RIP are listed below in the order from most complex to least complex.

- External function calls to detailed process codes
- RIP cells, which are basically equilibrium batch reactors, which, linked in series, can provide a reasonably accurate description of the underlying processes (e.g., engineered-barrier-system transport)
- Response surfaces, which take the form of multidimensional tables representing the results of modeling with detailed process models before running the RIP TSPA code
- Functional or stochastic representations of a component model directly built into the RIP architecture.

The first method—coupling external functions to RIP—enables information transfer in real time at every time step. An example of this in TSPA-VA is the direct-coupling of the FEHMN particle tracker used for modeling transport in the UZ with RIP (see Chapter 7). The direct coupling method greatly facilitates information transfer and traceability. It also facilitates the use of linear regression analysis to analyze the entire system. The transport of radionuclides in the EBS is an example of the RIP cell algorithm, and is modeled by linking a series of mixing cells together, which mathematically is equivalent to a network of finite difference nodes. In the third coupling method—“response surfaces”—most of the computational work for the individual components of the system is done outside RIP, prior to running the actual total system computations. The results from the modeling of these individual components are abstracted as multidimensional tables into RIP. In the future, these multidimensional tables will be quality assured. An example of this method would be the abstraction of the waste-package-degradation modeling, generated by the computer code WAPDEG V.3.07, into RIP in the form of waste-package-degradation time histories (see Chapter 5).

The total system model, which is a combination of all the components of the system with RIP as the integrating shell, is used for conducting both single realizations and multiple realizations of the entire repository system. The results from a single realization run are generally shown as

time histories of dose rate in the biosphere and activity release rate at the downstream boundary of the different components of the system. Multiple realizations yield a probability distribution of dose rate in the biosphere that shows uncertainty in dose rate based on uncertainty in all the component models.

The different components and associated computer codes of the TSPA-VA model are discussed in the following sections and they are generally arranged in the same order of the different chapters of this document. Each section contains a brief description of the subsystem involved, but the discussion is primarily oriented toward how it is implemented within the framework of the total system model and how information is transferred to the other components of the entire system. For detailed discussions of the different components, the reader is referred to the individual chapters.

The different components of the TSPA-VA model to be discussed in the following sections are broadly subdivided into: (1) UZ flow, (2) thermal hydrology, (3) near-field geochemical environment, (4) waste-package degradation, (5) cladding degradation, (6) waste-form degradation and mobilization, (7) EBS transport, (8) UZ transport, (9) SZ flow and transport, and (10) biosphere transport.

### **11.2.1 Unsaturated-Zone Flow**

The three components of the UZ flow model explicitly included in the TSPA-VA model are (a) climate, (b) mountain-scale UZ flow and (c) seepage into the repository emplacement drifts. The methodology used to implement each of these components in the TSPA-VA total system model are described below.

#### **11.2.1.1 Climate**

Climate is assumed to shift in a series of step changes between three different climate states: present-day dry climate, long-term-average climate (about twice the precipitation of dry climate), and superpluvial climate (about three times the precipitation of dry climate) (Chapter 2, Sections 2.2.1 and 2.2.3). Within RIP, the duration of the first dry climate is sampled uniformly between 0 and 10,000 years, with an expected-value of 5,000 years. The duration of the subsequent dry climates is sampled uniformly between 0 and 20,000 years, with an expected-value of 10,000 years.<sup>9</sup> The duration of the long-term-average climate is sampled uniformly between 80,000 and 100,000 years, with an expected-value of 90,000 years. Finally, similar to the dry climate, the superpluvial climate is sampled uniformly between 0 and 20,000 years, with an expected-value of 10,000 years. The calculations begin with the present-day dry climate and then they alternate between dry and long-term-average climates until the long-term-average climate that spans the 250,000-year mark. For the expected-value case, the last 10,000 years of that long-term-average time period is replaced by 10,000 years of superpluvial climate. Then the climate model returns to the alternating dry and long-term-average climates (beginning with dry

---

<sup>9</sup> Thus, the first dry climate duration is based on the assumption that the present-day dry climate period is half way to completion.

directly following the superpluvial) until the long-term-average climate that spans the time of 400,000 years after the first superpluvial. The end of that long-term-average climate is again replaced by a superpluvial climate, and then back to dry, followed by alternating long-term-average and dry climates. These changes in the climate states are implemented as a series of steady-state flow fields in the UZs and SZs (including changes in the water-table elevation) (Chapter 7, Section 7.4.4.2)<sup>10</sup> Also, changes in the climate states result in changes to the seepage flux through the drift, number of waste packages encountering seeps, biosphere dose conversion factors (BDCF), and the waste-package surface temperatures used for the calculation of the waste-form alteration rate. In a multiple-realization run, the duration of the different climate states are sampled from the distributions described above but the same sequence of climate states are followed.

### 11.2.1.2 Mountain-Scale Unsaturated-Zone Flow

TSPA-VA, mountain-scale UZ flow was modeled using the three-dimensional, UZ flow model developed by the YMP using an integrated finite difference computer program named TOUGH2 (Pruess 1991) (for version numbers see Table 2-3 in Chapter 2). Three-dimensional, steady-state flow fields are generated for three different infiltration boundary conditions, using three calibrated hydrogeologic property sets, which are derived with an inverse model, ITOUGH2 (Finsterle et al. 1996) by calibrating the model-predicted liquid saturations to measured liquid saturations in the matrix (see Chapter 2, Section 2.4.3.1.3). The three sets of flow fields generated for the present-day dry conditions are: the base infiltration case with mean fracture alpha, which represents the best guess at current infiltration conditions; the "base infiltration  $\times 3$ " with maximum fracture alpha, which represents the worst-case scenario for current infiltration; and the "base infiltration  $\div 3$ " with minimum fracture alpha, which represents the most optimistic scenario for current conditions (see Chapter 2, Section 2.4.3.1.4). To derive flow fields for the other climate states, these three calibrated property sets were used in the TOUGH2 (for version numbers see Table 2-3 in Chapter 2) computer code to attain steady states at boundary conditions representing precipitation in the two wetter climates. So a total of nine pre-generated flow fields, three for each of the infiltration scenarios are placed in the library of files to be read by FEHMN V.1.2 radionuclide transport calculations in the UZ. All nine resulting flow fields are three-dimensional, with vectors for fracture and matrix flux and for fracture-matrix interflux at each of the approximately 40,000 grid points (actually 80,000 since there are two continua—fracture and matrix).<sup>11</sup>

For any realization, the appropriate flow fields are selected, based on the infiltration scenario being used for that particular realization. The infiltration scenario to be used in any realization is determined within RIP, by sampling a parameter defined as a discrete distribution with probabilities for the three infiltration scenarios. In the TSPA-VA base case, the base infiltration case is given a 60 percent probability, the "base infiltration  $\div 3$ " is given 30 percent and "base

---

<sup>10</sup> Water table rise for the three climates are 0 m, 80m (260 ft), and 120 m (390 ft) for the present day, long-term average, and superpluvial climates, respectively.

<sup>11</sup> The UZ transport model requires only the vectors from the repository horizon down to the water table.

infiltration  $\times 3$ " is given a 10 percent probability. As described in the earlier section on climate, the change in climate is modeled as a series of step changes in the boundary conditions. Based on (a) the infiltration scenario obtained by sampling a parameter within RIP and (b) the climate state, an index is passed to the FEHMN V.1.2 code, and appropriate flow field from the set of nine is selected for radionuclide transport. This change in climate also results in the change of the water-table level, rising by 80 m from dry to long-term-average climate and another 40 m from long-term-average to superpluvial climate. These changes in water-table elevation are based on Sr data from the Calico Hills formation and paleosprings in the vicinity of the site (Chapter 2, Section 2.4.1.1).

### 11.2.1.3 Seepage Into the Drift

Seepage of water into the emplacement drifts is modeled external to RIP, using TOUGH2 TOUGH2 (for version numbers see Table 2-3 in Chapter 2) on a finely discretized grid around the drift. Numerous TOUGH2 simulations of a three-dimensional, heterogeneous fracture continuum surrounding the drifts are carried out using many different infiltration rates and nine combinations of fracture permeability and fracture alpha (see Chapter 2, Section 2.4). The results of the simulations are statistically weighted to develop probability distributions of the seepage fraction (fraction of packages in the drifts that encounter drips) and seepage flux ( $\text{m}^3/\text{yr}$ ) as a function of the percolation flux. These probability distributions of the seepage fraction and seepage flux are input into RIP as beta probability distributions defined with a mean, standard deviation, minimum, and maximum values (see Appendix A for these values). All the parameters used to define the distribution are input in tabular form as a function of the percolation flux.

The repository horizon was discretized into six separate regions based on the infiltration and thermal-hydrologic response. For each of the repository regions, area-weighted percolation flux in the fractures are directly input into RIP for the three infiltration scenarios and also for the three different climate states. The average percolation flux was taken from the steady-state values of percolation predicted by the UZ flow model, TOUGH2 (for version numbers see Table 2.3 in Chapter 2). These percolation fluxes are used to determine the parameters of the distribution, from which the seepage flux and seepage fraction values are sampled for each region. For the six different regions, different seepage flux and seepage fraction values are sampled as a result of the difference in the average percolation flux. When climate changes, again different seepage flux and seepage fraction values are sampled based on the percolation flux in the respective regions. The seepage flux and seepage fraction were given perfect positive correlation, that is, the same random number was sampled for these two parameters. Also, the same random number was used in all climate states, meaning that although seepage changes with climate state (because percolation flux changes), the different seepage values used in different climate states have the same probability. Furthermore, the same random number was used across the six regions within a given realization.

Within RIP, the seepage fraction values are used to determine the number of packages seeing drips. Since it is not computationally efficient to model every distinct waste package, waste packages are grouped according to the waste-form type and repository region. In TSPA-VA, three waste form types are considered and they are: commercial spent nuclear fuel (CSNF), high level radioactive waste (HLW), and DOE spent nuclear fuel (DSNF). This results in eighteen

source term groups, for the three waste-form types and six repository regions. The waste packages grouped into these source term groups are further sub-divided into four subgroups, based on the dripping condition. The four subgroups are: (1) packages that are always exposed to drips (in dry, long-term-average, and superpluvial climates), (2) packages that are exposed to drips only during the long-term-average and superpluvial climates, (3) packages that are exposed to drips only during the superpluvial climates and, (4) the packages that are not subjected to dripping conditions. The number of packages in each of these subgroups is determined by the seepage fraction in the different climate states for each region. The total number of packages within each source term group is multiplied with the seepage fraction in the dry climate to obtain the number of packages in the first subgroup. Similarly, the seepage fractions in the long-term-average and superpluvial climate states are used to determine the number of packages in the second and third subgroups, respectively. The remaining packages out of the total are assigned to the fourth subgroup containing packages that are not exposed to drips during the entire duration of the simulation.

The seepage flux discussed above defines the amount of water seeping into the drift. This flux value is scaled to the patch openings and pit perforations to obtain the volumetric flux ( $\text{m}^3/\text{yr}$ ) flowing through the waste package. The number of patch openings and pit perforations as a function of time are provided by the waste package degradation model, the details of this will be discussed in Section 11.2.4. These patch openings and pit perforations define the surface area of the waste package that is degraded, through which dripping water could enter the waste package and also radionuclides could transport out of the waste package. The surface area available for seepage by patch opening and pit perforations was increased by a "collection" factor to account for the focusing of water dripping on the waste package. This factor is sampled uniformly from 1 to 10, with a mean of 5.5 for the volumetric flux factor through the patch openings, and is sampled uniformly from 0 to 2, with a mean of 1 for the volumetric flux factor through the pit perforations. These volumetric flux values are used to define the advective connection between the waste package and the invert, the details of this will be presented in the section on engineered-barrier-system (EBS) transport. For additional discussion of the "collection" factor see Chapter 6, Section 6.5.2.2.

## **11.2.2 Thermal Hydrology**

In TSPA-VA, thermal-hydrologic calculations are carried out at two scales: at the repository-scale (mountain-scale) and the emplacement drift-scale.

### **11.2.2.1 Repository-Scale Thermal Hydrology**

The results of the repository-scale thermal hydrology were used only at two places in the TSPA-VA calculations:

- Conduction-only models that fed the abstraction methodology for drift-scale thermal hydrologic parameters; these simulations use the NUFT code
- Two-dimensional, thermal-hydrologic models (over an east-west cross section running through about the center of the repository) that provided air mass fraction and gas flux to the near-field-geochemical-environment models; these simulations use the TOUGH2

code on two-dimensional cross sections taken from the three-dimensional, site-scale, UZ flow model.

In both cases, the hydrogeologic property set came from the "base infiltration" flow field from the UZ flow model (see Chapter 2). For the first set of models (three-dimensional, conduction-only), the climate state was irrelevant, since hydrology was not modeled. For the second set of models (two-dimensional, thermal-hydrology), only the long-term-average climate was used. This was appropriate because it is assumed that this climate exists approximately 80 percent of the time. More details on this topic can be found in Chapters 3 and 4.

#### 11.2.2.2 Drift-Scale Thermal Hydrology

Drift-scale, UZ thermal hydrology is modeled with integrated the finite-difference computer program NUFT (Nitao 1998) in one, two, and three dimensions prior to the RIP simulations. (Several versions of NUFT are used and are noted in Table 3-4 of Chapter 4). The drift-scale thermal-hydrology model uses a complicated set of embedded abstractions at different levels of spatial and process detail (e.g., conduction-only versus conduction and convection), as described in Chapter 3. The entire automated set of multi-scale (drift-scale and associated mountain-scale) thermal-hydrologic models takes about a day to run on 12 Unix workstations for each scenario. The results from the drift-scale, thermal-hydrologic modeling are used as input to the waste-package-degradation model, near-field geochemical model, waste-form-degradation model, and for the calculation of diffusive mass transfer through the EBS.

The waste-package-degradation model uses the waste-package surface temperature ( $T_{wp}$ ) and relative humidity at the waste-package surface ( $RH_{wp}$ ) for seven different combinations of package types and heat outputs within six discrete spatial regions of the repository. The output from different waste packages types and heat outputs are used to represent some of the package-to-package variability within each region. The waste-package-degradation model uses each of these output parameters for the long-term-average climate and the three infiltration scenarios ("base infiltration with mean fracture alpha" case, "base infiltration  $\div 3$  with minimum fracture alpha" case, and "base infiltration  $\times 3$  with maximum fracture alpha" case).

The average drift-wall temperature ( $T_{dw}$ ), relative humidity at the drift wall ( $RH_d$ ), and liquid saturation in the invert ( $S_l$ ) in the central-central (CC) region are used as input to the near-field geochemical models (see Section 11.2.3).

Average waste package surface temperature ( $T_{wp}$ ) in each of the six repository regions and for both CSNF and HLW are fed into RIP for waste-form-degradation modeling. The thermal histories of HLW are used for DSNF waste-form-degradation modeling as they both have very similar thermal behavior.

The thermal histories are read into RIP as six different multidimensional tables. Three tables are used for reading CSNF thermal histories and the remaining three are used for reading the HLW waste-package thermal histories. For each waste type, three tables are used to read in the thermal histories for the three infiltration scenarios being considered in the TSPA-VA analyses. Each table contains twelve columns, with the first six representing the thermal profiles in the six different repository regions for the dry climate and the next six columns are for the long-term-

average climate. When the simulation starts with a dry climate, the corresponding thermal histories are read from the table and the simulation switches over to the long-term-average thermal histories when the climate changes to long-term-average climate and these values are used throughout the simulation. For example, in the expected-value base case, for the first 5,000 years of dry climate, the thermal histories corresponding to the dry climate are used as input for the waste-form-degradation models and then the simulation switches over to the long-term-average thermal histories for the remaining period of the simulation. This switching from the steady-state dry-climate thermal histories to the steady-state long-term-average-climate thermal histories is justified in some transient simulations shown in Chapter 3. Also, there is no need to switch back to the dry-climate thermal histories after the first long-term-average climate because the temperature has returned to ambient by that time (approximately 100,000 years).

The liquid saturation in the concrete invert obtained from drift-scale, thermal-hydrologic modeling is also read into RIP for calculating the diffusive transport through the invert. This is done by using the liquid saturation as input to the equation for obtaining the diffusion coefficient in a partially saturated porous medium (Conca, 1990; Conca and Wright, 1992). The liquid saturation is input into RIP directly as constant values, because the invert returns to ambient saturation (99.8 percent) by the time packages begin to fail.

### 11.2.3 Near-Field Geochemical Environment

For the base-case analyses, the near-field geochemical environment is represented by time-dependent distributions of the gas and water compositions that interact with the waste package and waste form inside the drift. The parameters supplied to the RIP analyses are the oxygen fugacity ( $fO_2$ ),<sup>12</sup> the solution pH, the total dissolved carbonate ( $\Sigma CO_3^{2-}$ ), and the ionic strength (I) of the water. The first three parameters are used for waste-form degradation modeling and the last one for colloidal transport in the EBS. These four parameters are derived from considering a more comprehensive 13-component chemical system (see Chapter 4, Sections 4.4 and 4.5). The values represent the time-dependent composition of water entering the drift and reacting with iron-oxide corrosion products, as opposed to water that has reacted with concrete.

These four composition time histories are not smooth functions; they comprise a series of steps. This step-change approximation is based on a simplified representation of the thermal history derived from various thermal-hydrologic models. The temperature, gas flux, and air mass-fraction histories from these thermal-hydrologic models (see Chapter 3, Section 3.5) were approximated as a sequence of steady states, which allowed the near-field environment to be modeled as a sequence of constant-composition states (Chapter 4, Section 4.2.3). In the case of the near-field environment, the width of the discrete time periods was rather large. For each of these discrete time periods, often referred to as "abstracted" time periods, a batch calculation is performed with a geochemical simulator (EQ3/6 V.7.2b; Wolery 1992) to determine the appropriate chemical composition of the groundwater during that time period based on the temperature and air mass fraction from the thermal-hydrology models and on the incoming

---

<sup>12</sup> For an ideal gas, oxygen fugacity is the same as oxygen partial pressure, which is about 0.2 atmospheres at sea level.



composition of the groundwater reacted with iron oxides. The base-case values and abstracted time periods represent the thermal history of the "central" portion of the repository, as opposed to the "edge" portion. The values and time periods were generated using both (1) the air-mass fractions and gas fluxes from the two-dimensional, mountain-scale, thermal-hydrologic results for the center portion of the two-dimensional cross section and (2) the average drift-wall temperature history of the central-central region for the "base-case infiltration" history, derived from three-dimensional drift-scale thermal-hydrologic modeling.<sup>13</sup> The CC region was chosen because the excursions from ambient conditions, in particular the period of boiling, are largest for this region and will bound<sup>14</sup> the effects at the edge portions of the repository where the excursions occur for shorter time periods.<sup>15</sup>

The four chemical composition parameters discussed above were fed into RIP as stochastic distributions for different time intervals. The different time intervals at which the values were abstracted are: Period A (0-200 years), Period B (200-1,000 years), Period C (1,000-2000 years), Period D (2,000-4,000 years), Period E (4,000-10,000 years) and Period F (10,000-100,000 years). The first three periods (A, B and C) represent the boiling periods and the remaining three represent the cooling periods. By 100,000 years, the system is considered to have returned to ambient conditions and the values at 100,000 years are used for the remaining period of the simulation. These values are used as a step function, with the values being kept constant for each of the time periods discussed above.

#### 11.2.4 Waste-Package Degradation

In TSPA-VA, waste package degradation modeling is done using WAPDEG V.3.07 (Waste Package DEgradation) (CRWMS M&O 1998a) (see Chapter 5). WAPDEG V.3.07 is a computer code based on a probabilistic approach, which simulates the degradation of both the corrosion-allowance material (CAM) and the corrosion-resistant material (CRM). The processes modeled for degradation include general corrosion and localized or pitting corrosion. WAPDEG V.3.07 run external to RIP and provides a description of waste-package degradation, which occurs as a function of time and repository location for specific design and thermal hydrologic responses. This information is abstracted into RIP as waste-package failure history, average number of pit perforations per package, and average number of patch openings per package. The waste package failure history defines the number of packages failed as a function of time and is fed into RIP as a cumulative distribution function to define the temporal variability in waste package failure times. Average number of pit perforations per package is used to define the

---

<sup>13</sup> More details of the rather complicated set of models used to derive the near-field geochemical parameters are given in Chapter 4.

<sup>14</sup> "Bound" is always used in the sense of "conservative" (i.e., "bounding" models always predict higher doses).

<sup>15</sup> The multiscale thermal-hydrology models described in Chapter 3 indicate that much of the repository functions as though it is center-like in thermal-hydrologic behavior; however, there is a gradual transition to edge-like behavior as the repository edges are approached. The major difference between the center and edge portions is that shorter abstracted time periods are appropriate for the boiling regime in the edge region as compared to the central portion of the repository. This difference is also true for the two wetter climate states because of the increased cooling capacity of the system.

subsequent degradation of the failed waste package due to penetration of pits. Average number of patch openings per package is used to define the subsequent degradation of the failed waste package due to corrosion patches.

Because it is computationally impractical to model every distinct waste package, the waste packages are broadly grouped according to their inventory and spatial location. As discussed earlier, the repository horizon is divided into six regions and the three waste types included in the TSPA-VA analyses are CSNF, HLW and DSNF. This gives a total of eighteen groups of waste packages or source term groups. Each source-term group is further sub-divided into four subgroups according to the dripping conditions to which the waste packages are exposed. The first subgroup contains packages that are exposed to drips during the dry climate and throughout the period of the simulation, the second subgroup contains packages that are exposed to drips only during the long-term-average and superpluvial climate states, the third subgroup contains waste packages that are exposed to drips only during the superpluvial climate, and the fourth subgroup contains packages that are not exposed to drips. As discussed in the section on seepage, the total number of packages in each of these subgroups is obtained based on the seepage fraction in each region during different climate states. Although seepage behavior through the packages is different for each of these four groups, only two waste-package failure histories are used: packages that are always dripped on and packages that are never dripped on. Chapter 5 has supporting analyses to show why degradation of the CAM and the CRM is sufficiently modeled with only these two conditions. The packages that are never dripped on and the packages dripped on only during the superpluvial climate are modeled with the no-drip failure history from the WAPDEG V.3.07 computer code, and the other two groups are modeled with the always-drip failure history. It is a conservative assumption (i.e., erring on the side of maximum releases) to assume that the long-term-average fraction of packages (i.e., the second subgroup or fraction that is dripped on during long-term-average and superpluvial climates) has the same failure rate during the long-term average climate and the dry climate. On the other hand, a somewhat nonconservative assumption is that the superpluvial fraction of packages (i.e., the third subgroup) fails according to the non-seep failure curve. This assumption is used because these packages are not dripped on at all until at least 250,000 years after repository closure.

The waste-package failure history is used to determine the number of packages failed as a function of time in each subgroup. This calculation is done by multiplying the total number of waste packages in each subgroup with the waste-package failure history provided as a cumulative distribution function. The average number of pit perforations per package is used to define the area on a single failed waste package through which radionuclides could diffuse and advect to the invert below the waste package. Similarly the average number of patch openings per package is also used to define the area available on a single failed waste package through which radionuclides could diffuse and advect to the invert below the waste package. As discussed in Section 11.2.1.3, these average number of pit perforations and patch openings are also used to scale the seepage flux through the failed waste package. Both the number of pit perforations and patch openings are input to RIP for a single failed-waste package and are associated with all the subgroups within each source-term group. These values are scaled up when more packages fail within each subgroup. Also, the waste package degradation results corresponding to the northeast region are used for the packages in all the six regions and for each

of the three different waste types, since all six regions had very similar degradation histories (see Chapter 5).

The waste package degradation analysis for the TSPA-VA base-case analysis includes a set of nine cases to represent a range of the uncertainty in the median corrosion rate and the variability of the corrosion rate among waste packages and patches. Uncertainty and variability are represented by splitting the total variance of the general corrosion rate for Alloy 22 into three different variability and uncertainty combinations: 75 percent variability and 25 percent uncertainty, 50 percent variability and 50 percent uncertainty, and 25 percent variability and 75 percent uncertainty. For each of the variability-uncertainty splits, the median general corrosion rate is sampled from the 5th, 50th and 95th percentiles of the uncertainty variance, respectively. The expected-value base case is the 50 percent variability and 50 percent uncertainty split and the median corrosion rate at the 50th percentile of the uncertainty variance. All these nine cases for the three infiltration scenarios (base infiltration with mean fracture alpha, base infiltration  $\div 3$  with minimum fracture alpha and base case infiltration  $\times 3$  with maximum fracture alpha) are included in the TSPA-VA base case analysis for the dripping packages. For the non-dripping packages, three cases are included representing the three infiltration scenarios with 25 percent variability and 75 percent uncertainty for the corrosion rates. For additional discussion of how uncertainty and variability in waste package degradation is quantified and represented in the TSPA-VA base case analysis see Chapter 5, Sections 5.7.2 and 5.10.3.

The results from the waste-package-degradation analyses are fed into RIP using multidimensional tables. Each of the cases discussed above is fed into RIP using a different multidimensional table. The multidimensional table contains the waste package failure history, average number of pit perforations per package, and average number of patch openings per packages as dependent variables with time as the independent variable.

In addition to corrosion degradation of waste packages, the base case includes the effect of early or "juvenile" waste-package failures by noncorrosion processes such as materials defects, seismic activity, and human-induced factors, such as welding, handling, and transportation. In the base case, juvenile failure is assumed to cause a single patch opening in a commercial spent fuel nuclear fuel package in a dripping environment, in the southeast region. This is implemented within RIP by adding a source-term group in addition to the eighteen source-term groups. The expected-value base case assumes a single juvenile failure at 1,000 years. The probabilistic base case uses a log-uniform distribution for juvenile failures from 0.001 percent to 0.1 percent, all occurring at 1,000 years after closure.

### **11.2.5 Cladding Degradation**

Cladding degradation of CSNF is modeled external to RIP and the results are abstracted into RIP as fraction of cladding failed (exposed waste-form area) with time. The different mechanisms of cladding degradation included in the TSPA-VA base-case analysis are:

- Creep (strain) failure at high temperatures with simultaneous exposure to oxygen
- Juvenile cladding failures (packages emplaced in the repository with cladding already failed)

- Total failure of stainless-steel-clad fuel rods
- Mechanical failure of cladding because of structural failure of the waste package, as a result of rockfall, corrosion, or seismic events after closure
- Long-term corrosion failure.

Creep and juvenile failures are combined with failure of the stainless steel cladding and are defined at a constant value of 1.25 percent, beginning at the time of any waste-package failure. Most of this is because the stainless steel fails. Mechanical failure of cladding is initiated after waste-package failure and is defined as a distribution. This is implemented by defining the maximum and minimum cladding fraction that failed as a function of time. For any realization, the cladding fraction failed due to mechanical failures at a particular time step is determined by a sampling log-uniformly distribution between the maximum and minimum values. Long-term corrosion of zircaloy clad fuel is also initiated after waste-package failure and is modeled using the waste-package-degradation model WAPDEG V.3.0.7. The results are abstracted into RIP as cladding fraction failed versus time with maximum and minimum bounds. Similar to the mechanical failures, the cladding fraction failed due to this mechanism is also determined by sampling log-uniformly between the maximum and minimum values for every time-step.

#### 11.2.6 Waste-Form Degradation and Mobilization

Waste-form degradation is modeled within RIP using dissolution-rate equations for fuel exposed by package and cladding degradation. This is done by coupling external subroutines, which contain the empirical dissolution-rate equations developed from available data and experiments for the three different waste form types: CSNF, high-level radioactive waste (HLW) and DSNF. Within RIP, the input variables are passed to separate external routines for both the CSNF and HLW and the dissolution rate ( $\text{g/m}^2/\text{yr}$ ) is calculated at every time step. For DSNF, the empirical equation for calculating the dissolution rate is specified directly within RIP.

The dissolution rate for CSNF is a function of the temperature (T), total dissolved carbonate, oxygen fugacity, and pH of the water contacting the waste form. There is also some uncertainty in the dissolution-rate model associated with the equation used to fit the experimental data, and this is implemented by defining the coefficients of the equations as stochastic parameters. For T in the rate equations, the average temperature on the waste-package surface is used for the six different repository regions, as calculated by the drift-scale, thermal-hydrology model. Total dissolved carbonate, oxygen fugacity, and pH of the water are obtained from near-field geochemical modeling.

The glass-dissolution rate is a function of the waste-package surface temperature (T) and the pH of the incoming water. The uncertainty in the regression fit of the experimental data is included by defining the coefficients of the equation as stochastic parameters, which are passed as input by RIP to an external function that calculates the dissolution rate.

Metallic-dissolution rate is used for the DSNF, which is modeled using a surrogate radionuclide inventory composed mostly of N-Reactor fuel. The model for metallic spent fuel was taken from the performance assessment calculations of DOE SNF (Duguid et al. 1997, pp. 3-7). The

dissolution rate in  $\text{g/m}^2 \text{ yr}$  is multiplied with the specific surface area of the fuel in  $\text{m}^2/\text{g}$  to obtain the degradation rate of the fuel matrix, which is used to calculate the mass of waste form exposed per time. The degradation rate is also used to calculate the volume of water in contact with the waste form, which is used to calculate the concentration of the dissolved mass. This calculation is described in Section 11.2.7.

The radionuclide inventory for the three waste forms (CSNF, HLW and DSNF) is directly input into RIP within each source term group in Ci/package. The nine radionuclides considered in the TSPA-VA analysis are : C-14, I-129, Np-237, Pa-231, Pu-239, Pu-242, Se-79, Tc-99 and U-234. Since decay chains are not considered in the analysis (see Chapter 6, Section 6.2.2), the specified inventory includes a correction for ingrowth of radionuclides from the parent radionuclides. For example, all of the Am-241 and Pu-241 in the waste is assumed to decay to Np-237 when the waste is emplaced to determine the initial inventory of Np-237.

### 11.2.7 Engineered-Barrier-System Transport

The transport of radionuclides in the EBS is modeled within RIP using a series of mixing cells coupled by advective and diffusive "connections." Mixing cells are equivalent to equilibrium batch reactors and by linking multiple cells together, a fairly accurate description of the underlying processes can be realized. A schematic of the series of mixing cells used to represent the EBS is shown in Figure 11-5. The waste-package and waste form together are represented as a single cell pathway. The concrete invert below the package is assumed to be shaped as a semi-circle around the package and is discretized into three cell pathways to decrease the numerical dispersion. The waste package/waste-form cell pathway is coupled to the first invert cell pathway through two advective and two diffusive connections. The two advective connections represent the water seepage through the failed waste package into the invert through the patch openings and pit perforations, respectively. The two diffusive connections represent the diffusive mass transfer through patch openings and pit perforations of a failed waste package. An advective connection requires the definition of a volumetric flux ( $\text{m}^3/\text{yr}$ ) and a diffusive connection requires a diffusive area ( $\text{m}^2$ ), length of diffusion (m), and diffusion coefficient ( $\text{m}^2/\text{yr}$ ) to calculate the mass transfer rate, in addition to defining the volume of the cell and the properties of the media contained in the cell. The volumetric flux through the two advective connections coupling the waste package with the invert is calculated by scaling the seepage flux into the drift with the available surface area arising from the patch and pit failures.

The pit perforations and the patch openings define the surface area on the package through which diffusive mass transfer could occur and the length of diffusion through the pit perforations is set equal to the thickness of the inner container of the waste package. For the patch openings, it is set equal to half the thickness of the invert. The selection of these diffusion lengths is discussed in Chapter 6, Section 6.5.2.2. For the corrosion-product-filled pit perforations, the diffusion coefficient is calculated using the equation for partially saturated medium (CRWMS M&O 1998c ) for a material with 40 percent porosity and 99.8 percent water saturation equal to that of the concrete invert, obtained from drift-scale thermal hydrology (see Chapter 6, Section 6.5.2.2). Similarly for the diffusive mass transfer through the patch openings, the diffusion coefficient is calculated for the concrete material with 10 percent porosity and 99.8 water saturation. The number of pit perforations and patch openings as a function of time is provided by the waste-package-degradation modeling. The volume of water in the waste-package/waste-form cell

pathway available for mobilization of waste (for computing solubility) at any time step is equal to the volume of water in the pores of the "rind," which is the ingrowing shell of altered fuel being changed into other minerals through contact with gases and liquids that have entered the degraded waste package. This water volume is based on a porosity of 40 percent and water saturation of 100 percent in the rind. The rind volume itself is linearly proportional to the fuel rod volume times the fuel degradation rate times the time since first water contact.

The three cell pathways representing the concrete invert are coupled with both an advective and diffusive connection. The volumetric flux used to define the advective connection is not the same as reduced flux through the packages but is equal to seepage into the drift. The area for diffusive mass transfer is equal to the surface area of the invert and the length of diffusion is equal to half the thickness of the invert. The concrete material used for invert also sorbs some of the radionuclides and this is implemented by defining sorption coefficients ( $K_{ds}$ ) for those sorbing radionuclides within RIP (see Chapter 6).

Colloid-facilitated mobilization and transport of radionuclides in the EBS is modeled for plutonium-239 and plutonium-242, assuming fast reversible attachment. As more colloid data are obtained, colloidal transport of additional radionuclides will be investigated (Chapter 6, Section 6.4.2). Colloid-facilitated mobilization and transport is modeled within RIP by defining various media for the different type of colloids. The colloid concentrations are defined as a function of the ionic strength, which is obtained from the near-field geochemical modeling. The mass of colloids in each of the cell pathways is obtained by multiplying the colloid concentrations with the volume of water in them. There are four types of colloids in the EBS: two natural types, iron-oxides and clays; and two types based on fuel degradation, spent fuel colloids and glass waste colloids. A small fraction of the total mobilized plutonium, which includes both the plutonium in the aqueous phase and reversibly sorbed colloids phases, is assumed to sorb irreversibly to colloids at the edge of the EBS. This treatment allows plutonium to be transported on colloids and is based on field data observed at the location of the Benham Nuclear Detonation at the Nevada Test site. This is done by multiplying the mass flux of plutonium-239 and plutonium-242 from the EBS with the fraction of irreversibly sorbed plutonium on colloids, defined as a log-uniform distribution.

As discussed earlier, because there are computational limitations, waste packages are broadly grouped into eighteen source term groups according to the waste type and the six repository locations. These source term groups are further sub-divided into four subgroups according to the dripping conditions to which the packages are exposed during a simulation. Each of the four cell pathways representing an idealized EBS is associated with each of these subgroups. All the properties for the cell pathways and the connections are defined for a single waste package and these values are scaled up as more packages fail within each subgroup. Further, the release from all the three waste forms in a particular region is combined together before being passed to the UZ transport code. For example, the releases from the CSFN, HLW, and DSNF waste packages in the first repository region are combined using a mixing cell downstream of the third invert cell pathway. The nineteenth source-term group containing the juvenile failed packages is combined with the release from the packages in the southeast region, since the juvenile package is assumed to fail in this region. The release from the six mixing cells representing the six distinct repository regions is passed as input to the FEHMN V. 1.2 particle tracker (see Chapter 7) at every time step.

### 11.2.8 Unsaturated-Zone Transport

In TSPA-VA, UZ radionuclide transport is modeled by directly coupling the three dimensional, dual-permeability, finite-element code FEHMN V.1.2 (Robinson et al. 1997; Zyvoloski et al. 1995) to RIP as an external function (subroutine)(see Chapter 7). The UZ transport model is based on the UZ flow model and uses the same three sets of flow fields for the different infiltration scenarios (base infiltration with mean fracture alpha, base case infiltration  $\times 3$  with minimum fracture alpha, and base-case infiltration  $\times 3$  with maximum fracture alpha) and three climate states. As with the UZ flow, a dual-permeability model is assumed, and transport is modeled with the FEHMN V.1.2 particle tracker in three dimensions.

The mass release from the EBS in each of the six repository regions is passed as input to FEHMN V.1.2 particle tracker for every time step. This mass is spread uniformly over the grid blocks in FEHMN V.1.2 within the corresponding area of the six regions. In addition to the mass flux, the input from RIP also includes the time in years, the flow-field index parameter, and a realization index. The flow field index is used to select the appropriate flow field from the nine flow fields pre-generated using TOUGH2 UZ flow code. Within a time step, the particles are moved by FEHMN V.1.2 as far as they would travel during that time step, based on the steady-state velocity field in the fractures and matrix of the various UZ rock units.

The outflow at the water table is also divided into six distinct regions based in part on the lithology of the geologic units intersecting the water table. These six regions are not related to the six source-term regions at the repository horizon. Mass flux from both the fractures and matrix at the six water-table regions is passed from FEHMN V.1.2 back to RIP at every time step. The mass fluxes from both the fractures and matrix in each of the six regions are then combined together before being passed to the SZ code at every time step. Within a realization, when the climate changes, based on the flow field index a new flow field is selected and the particles are assumed to be instantly traveling with the new velocities. This quasi-steady representation of the flow fields is sufficient for long-term transport calculations and is discussed in Chapter 7, Section 7.4.4. Change in climate also results in the change of the water table elevation. When the water-table elevation rises, the particles in the "lost" vertical distance corresponding to this rise are instantly released in that time step to the water table. Similarly, when the water-table elevation falls, there is a brief time when there are no particles in the new vertical distance. Uncertainty in the transport parameters, which includes sorption coefficients ( $K_{ds}$ ), matrix diffusion coefficients, dispersivity,  $K_c$  values for plutonium colloids, and fracture aperture are included in the UZ transport by pre-generating the entire matrix of the uncertain parameter values using RIP. In a multiple realization case, the appropriate row from an uncertainty matrix with a one-hundred rows is selected based on the realization number passed from RIP. For example, in a simulation with 100 multiple realizations, the realization number passed to FEHMN V.1.2 would be between 1 and 100 and each and every row from the uncertainty matrix would be used over the course of 100 realizations. When more than 100 realizations are run, values from this table will be reused.

### 11.2.9 Saturated-Zone Transport

SZ transport is modeled by one-dimensional, effective-continuum, flow and transport simulations over six streamtubes using the FEHMN V.2.0 computer program (see Chapter 8).

The streamtubes extend from the bottom of the repository at the water table to the 20 km (12.4 mi) distance down-gradient. The locations and directions of the six streamtubes, and the lithology along their flow paths, are determined with a three-dimensional computer model for SZ flow, based on the FEHMN V.2.0 code and the three-dimensional, site-scale geologic framework model (see Chapter 8). The volumetric flux of groundwater through each of the streamtubes was determined at the water table from the UZ flow model. The average specific discharge in the dry climate is assumed to be 0.6 m/yr in all six of the streamtubes, based on the results of the Saturated-Zone Expert Elicitation (CRWMS M&O 1997, Table 3-2). This value combined with the volumetric flux from the UZ is used to determine the cross-sectional area of the streamtubes (see Chapter 8). The output from these one-dimensional SZ transport simulations through the six streamtubes provide concentration breakthrough curves at 20 km (12.4 mi) for unit releases of radionuclides from the UZ. These breakthrough curves reside in files in the RIP runtime directory and are accessed when needed by the SZ\_CONVOLUTE V.1.0 external function (which convolves—i.e., integrates—the real source term with the pre-generated unit breakthrough curves) called by the RIP program (CRWMS M&O 1998b).

The flow and transport simulations to develop the unit breakthrough curves are done outside and prior to the RIP program for each of the nine radionuclides over 100 realizations of uncertain SZ transport parameters. The uncertain parameters used in the one-dimensional transport simulations include effective porosity in the volcanic units and the alluvium unit, distribution coefficients ( $K_d$ s) for sorbing radionuclides in the volcanic and alluvium units; the ratio of the radionuclide mass in aqueous and colloidal forms ( $K_c$ ) for colloid-facilitated transport of plutonium; longitudinal dispersivity; the fraction of flowpath through the alluvium, and the dilution factor used for representing the transverse dispersivity. For the case of 100 realizations, 6 streamtubes, and 11 radionuclides, there are 6,600 files of breakthrough curves.

The input from RIP to SZ\_CONVOLUTE V.1.0 at every time step includes the mass flux at the water table from the UZ transport model at each of the six water table regions, an index for the climate state, and the realization number. Climate change provided to the convolution integral function by the climate index is incorporated into the SZ transport analysis by assuming instantaneous change from one steady-state flow condition to another steady-state condition (see Chapter 8, Sections 8.3.5 and 8.3.6). The velocity and the volumetric flux in each of the streamtubes are scaled when the climate changes. In a multiple realization case, based on the realization number, the appropriate breakthrough curve for the different radionuclide and streamtube are selected. The concentration in  $\text{Ci/m}^3$  (curies per cubic meter) is passed back to RIP from all the six streamtubes.

Before passing the concentrations back to RIP, the convolved concentrations are divided by the dilution factor to account for the transverse dispersion, based on the Saturated-Zone Expert Elicitation (CRWMS M&O 1997, Figure 3-3d). The dilution factor is defined with probability distribution and the same value is used for all the radionuclides, all the six streamtubes, and at all time scales. The actual concentration used to determine the dose rate is based on the concentrations in all six streamtubes. That is, the concentrations for each radionuclide were summed among the six streamtubes. Within RIP, this summed concentration was compared with the maximum undiluted concentration for each radionuclide at every time step. The maximum diluted concentration is used to compute the dose rate when the maximum undiluted



concentration is lower than the summed concentration, otherwise the summed concentration is used (see Chapter 8, Section 8.3.7).

#### **11.2.10 Biosphere Transport**

Biosphere transport is modeled within RIP using biosphere dose-conversion factors that convert SZ radionuclide concentration to individual radiation dose rate. The biosphere dose-conversion factors are developed outside RIP using a computer program named GENII-S V.1.485 (Napier et al. 1988). The dose-conversion factors are determined for an "average individual" living in Amargosa Valley 20 km (12.4 mi) downgradient from the potential repository, who draws water from a well for drinking and irrigation purposes (see Chapter 9). The dose-conversion factors are abstracted into RIP as lognormal distributions for all the nine radionuclides and the three climate states. The dose-conversion factors for all the nine radionuclides and all the three climate states are perfectly positively correlated during the Monte Carlo sampling, by using the same random number for sampling all the distributions. The appropriate dose-conversion factors based on the climate state are used to multiply the SZ concentration to calculate the dose rate in mrem/yr.

### **11.3 UNCERTAINTY/SENSITIVITY ANALYSIS METHODS IN TSPA-VA**

For the TSPA-VA, a probabilistic approach is used for assessing the long-term performance of the Yucca Mountain repository. This approach uses a linked system of deterministic process models to represent the repository and its associated geologic system, and a Monte Carlo technique to propagate parameter uncertainty through to the calculation of maximum radiation doses at the specified location 20 km (12.4 mi) from the repository. A full analysis includes the following:

- A. Selecting imprecisely known model input parameters to be sampled
- B. Constructing probability distribution functions for each of these parameters, incorporating available data and subjective information to capture uncertainty
- C. Generating a sample set by selecting a parameter value from each distribution
- D. Calculating outcomes for the sample set.

Steps 3 and 4 are repeated many times to produce a distribution of peak dose rates that represents the spectrum of repository performance. The distribution of peak dose rates is normally presented as a complementary cumulative distribution function that gives the probability of exceeding a given peak dose rate. The range or spread of peak dose rates represents the amount of uncertainty in the results. In addition to quantifying the uncertainty in the results of the performance assessment, another important component of the probabilistic approach used in the TSPA is the sensitivity analysis. Sensitivity analysis is used to identify the relative importance of uncertain input parameters to the predicted repository performance. This information is useful for selecting and assigning priorities to future modeling, site-characterization, and design activities so that uncertainty in estimates of long-term performance may be decreased.

This section summarizes the uncertainty and sensitivity analysis methods and computational tools used to analyze the probabilistic results obtained from the base-case Monte Carlo simulations. The methods and computational tools are presented in three subsections: Uncertainty Analysis Methods, Sensitivity Analysis Methods, and Sensitivity Analysis Calculations. The Uncertainty Analysis Methods subsection provides a description of how the probabilistic results are obtained and subsequently represented in the form of a complementary cumulative distribution function. In the Sensitivity Analysis Methods subsection, the techniques used to quantify the relative importance of uncertain input parameters on repository performance are discussed. These techniques include scatter plots and linear regression analysis. The Sensitivity Analysis Calculations subsection describes how the sensitivity analyses were performed. Included in this section are descriptions of the computational tools developed for this task.

### 11.3.1 Uncertainty Analysis

The objective of uncertainty analysis in the TSPA is to estimate the complementary cumulative distribution of peak radiation doses at the specified location 20 km (12.4 mi) from the repository. The range or spread of estimated peak dose rates represents the amount of uncertainty in the results. This uncertainty arises from input parameter uncertainty. In this subsection, a brief description of how complementary cumulative distribution functions of peak radiation doses are obtained is presented.

The TSPA results can be symbolically represented by a simple function of the form

$$\text{Dose Rate} = f(x_1, x_2, \dots, x_{nc}, s_1, s_2, \dots, s_{nu}, t),$$

where Dose Rate represents the dose rate to a human at the 20-km boundary as a function of time  $t$ .

The variables  $x_1, x_2, \dots, x_{nc}$  are precisely known input parameters, such as the acceleration of gravity and the density of water, and  $nc$  is the number of such inputs. Variables  $s_1, s_2, \dots, s_{nu}$  are imprecisely known or uncertain parameters, such as corrosion rate and waste-form dissolution rate, and  $nu$  is the number of such parameters. In the TSPA-VA base-case probabilistic calculations,  $nc = 1,006$  and  $nu = 177$ . Note that the 1,006 certain parameters and 177 uncertain parameters include only those that are used within RIP; many additional parameters are used in the various component models such as TOUGH2 and WAPDEG V.3.07. A description of the uncertain parameters is provided in Appendix A. The imprecisely known inputs are the parameters that cause uncertainty in the performance assessment predictions (DTN SNT05070798001.002).

The uncertainty in parameters  $s_1, s_2, \dots, s_{nu}$  is characterized by a sequence of probability distributions

$$D_1, D_2, \dots, D_{nu}, \quad (11-1)$$

where  $D_j$  is the probability distribution for variable  $s_j$ . In some cases, the definitions of these distributions are also accompanied by specifications of correlations that further define the

relations between the  $s_j$ . For the TSPA-VA base case, the seepage parameters for different repository subregions are correlated, seepage and infiltration for different climate states are correlated, diffusion coefficients for different geologic layers in the UZ are correlated, and biosphere dose-conversion factors for different radionuclides are correlated (see Appendix A).

Once distributions  $D_j$  are specified, the next step is to determine the uncertainty in the performance-assessment results that arises from uncertainty in  $s_1, s_2, \dots, s_{nu}$ . First, a sample

$$S_k = [s_{k1}, s_{k2}, \dots, s_{nk,nu}], \quad k = 1, \dots, nk, \quad (11-2)$$

is generated from the specified distributions  $D_1, D_2, \dots, D_{nu}$ , where  $nk$  is the size of the sample, or number of realizations. In the TSPA, this sample is generated using Latin Hypercube sampling and the sample size is  $nk = 100$  for most simulations (the sufficiency of a sample size of 100 is discussed in Section 11.4.2.2). A performance-assessment calculation is then conducted for each sample  $S_k$ , with all precisely known input parameters  $x_1, x_2, \dots, x_{nc}$  held fixed at their known values. The performance-assessment calculations yield a series of curves that show how the dose rate changes with time. These curves are often referred to as dose time histories and can be represented symbolically as

$$(\text{Dose Rate})_k = f(x_1, x_2, \dots, x_{nc}, s_{k1}, s_{k2}, \dots, s_{kn,nu}, t), \quad k = 1, 2, \dots, 100, \quad (11-3)$$

where each  $(\text{Dose Rate})_k, k = 1, 2, \dots, 100$ , is the result of a complete calculation of all the linked TSPA components.

Once the dose history for each realization is obtained, the peak dose rate that occurred during the simulation period for each realization is determined by taking the highest point on each dose-rate history curve. Once a peak dose is obtained for each realization, the next step is to graphically represent the dose results in the form of a complementary cumulative distribution function, which shows the probability (represented on the ordinate axis) that a dose rate is greater than a given value (represented on the abscissa axis) and is constructed by first ordering the peak doses from smallest to largest values, with a weight of  $1/nk = 1/100$  assigned to each peak dose rate. The probability that a dose rate is greater than a specified dose rate,  $D$ , is determined by summing the probabilities associated with all dose rates larger than the specified one. That is,

$$\text{Prob}(\text{Dose Rate} > D) = \sum_{d=1}^{100} \delta_d / 100 \quad (11-4)$$

where the sum on the right is taken over all peak dose rates and  $\delta_d = 1$  if the dose rate is greater than  $D$  and  $\delta_d = 0$  if the dose rate is less than  $D$ .

One way to characterize the uncertainty represented by the complementary cumulative distribution function is with the mean value and the coefficient of variation, which is the variance normalized by the mean. These quantities are estimated by

$$E(\text{DoseRate}) = \sum_{k=1}^{100} (\text{Dose Rate})_k / 100 \quad (11-5)$$

and

$$CV(Dose Rate) = \left[ \sum_{k=1}^{100} \frac{[(Dose Rate)_k - E(Dose Rate)]^2}{(99)} \right]^{1/2} / E(Dose Rate) \quad (11-6)$$

respectively.

### 11.3.2 Sensitivity Analysis Methods

The primary objective of sensitivity analysis is to identify those uncertain parameters that have a strong influence on the repository performance measures and to quantify the strength of their influence. A simple tool for sensitivity analysis is the scatter plot, which is a plot of sampled numerical values of an uncertain variable, or independent variable, used in the computations versus the calculated results such as peak dose rate, or dependent variable. Scatter plots are invaluable for identifying a relationship between variables, but they do not quantify the intensity of that relationship. In the TSPA, multiple linear regression modeling is used to quantify relationships between dependent and independent variables. By using a regression model, it is possible to identify variables that contribute most to the calculated uncertainty in the peak-dose rates.

For the TSPA, the primary technique for regression modeling is linear stepwise regression. In the stepwise approach, a sequence of regression models is constructed starting with a single selected input parameter, and including one additional input variable at each successive step until all significant input variables have been included in the model. This approach avoids having to treat all of the independent uncertain variables simultaneously in a single model. A good discussion of multiple linear regression modeling and other sensitivity-analysis techniques, and their application to the performance assessment of the Waste Isolation Pilot Plant, is given by Helton (1993) and Helton et al. (1998, Section 6.10).

#### 11.3.2.1 Scatter Plots

Scatter plots are plots of sampled numerical values of input variables used in a computation versus the output results calculated using those numerical values for the input variables. Recall that the TSPA base case model is characterized by  $n_u$  uncertain input variables  $s_1, \dots, s_{n_u}$ , where  $s_1$  might be the solubility in groundwater of an inventoried radioisotope,  $s_2$  might be the partition coefficient for that isotope in the low permeability zeolitic layers in the UZ, and so on. In the TSPA Monte Carlo simulations, the RIP Latin hypercube sampling module assigns to each uncertain parameter  $s_j$  a set of  $n_k = 100$  numerical values that span the parameter's entire range of plausible values. The TSPA base-case model is then executed 100 times, one simulation for each different input variable vector, and 100 different results  $Y_i$ ,  $i = 1, 2, \dots, 100$  are obtained. A plot of the 100 calculated values of  $Y_i$  against all 100 sampled values of, say, the  $j^{\text{th}}$  input variable,  $s_j$ , is called a scatter plot of  $Y$  versus  $s_j$ .

If little or no relationship exists between the sampled values of the selected input variable and the corresponding calculated results, their scatter plot will resemble a random distribution of points. Alternatively, the existence of a well-defined relationship between the sampled values of an

input variable and their corresponding calculated results will produce an organized distribution or clustering of the points in some sort of recognizable pattern.

Finally, scatter plots are especially effective in revealing nonlinear dependencies, threshold behaviors, variable interactions, and other dependencies that are invaluable in understanding model behaviors and sensitivities. However, scatter plots are basically qualitative in nature, and quantitative measures are preferred for performance assessments. A quantitative approach to sensitivity analysis is provided by linear regression analysis.

### 11.3.2.2 Linear Regression Analysis

Sensitivity analyses performed on Latin hypercube sampled data are based on the construction of linear regression models that approximate the behavior of output from the TSPA-VA model. As described previously, the TSPA-VA base case model is run with 100 different Latin hypercube-sampled sets of uncertain input vectors. Each input vector (or realization) is numerically different from every other input vector and produces a family of 100 different output results  $Y_i$ . These data can be fit to a regression model of the form

$$\hat{Y} = b_0 + \sum_{j=1}^P b_j S_j, \quad (11-7)$$

where the method of least squares is applied to determine the coefficients  $b_j$ , which are called "ordinary regression coefficients." This equation represents the line<sup>16</sup> that best fits the scatter-plot data in the sense that the sum of the squared differences between the actual scatter-plot data and the values given by the regression line are minimized for the chosen coefficients,  $b_j$ . The ordinary regression coefficients may be thought of as the partial derivatives of the regression model with respect to the input variables. However, these ordinary regression coefficients are dimensional quantities and their numerical values are strongly dependent on the units in which the variables are expressed. For example, if  $Y$  is peak dose rate and  $s_3$  is a permeability value, then the numerical value of  $b_3$  would increase by four orders of magnitude if the units of  $s_3$  were changed from  $m^2$  to  $cm^2$ . Moreover, the different elements of set  $b_j$  (i.e., for different values of  $j$ ) have different dimensions from one another. Therefore, the elements of  $b_j$  cannot be directly compared to one another. Consequently, the elements of  $b_j$  do not provide satisfactory direct measures of the relative importance of the different input variables. To achieve a direct comparison between regression coefficients, the input variables must be transformed linearly to form new variables called "standardized variables."

Standardized (dimensionless) variables are centered on the means of their samples and normalized by the standard deviations of their samples. Standardized variables, denoted by an asterisk, can be expressed as  $s_j^* = (s_j - \bar{s})/\sigma_x$ , where  $\bar{s}$  and  $\sigma_x$  are the mean and standard deviation, respectively, for each sample variable  $s_j$ . In terms of standardized variables, the previous regression model reduces to the standardized form,

---

<sup>16</sup> If  $P = 1$  (i.e., there are two regression coefficients,  $b_0$  and  $b_1$ ), the equation represents a line. If  $P = 2$ , the equation represents a plane. For  $P = 3$ , a space having more than three dimensions is required to plot the equation.

$$\hat{Y}^* = \sum_{j=1}^P b_j^* S_j^* \quad (11-8)$$

The coefficients,  $b_j^*$ , for  $j = 1, \dots, nu$ , are standardized regression coefficients (SRCs). These coefficients are dimensionless and vary over approximately the same range of numerical values. Therefore, they can be compared one to each other to provide a direct quantitative measure of the relative importance of the various uncertain input variables, provided the input variables are statistically independent. Thus, if  $b_3^*$  is numerically greater than  $b_4^*$ , then  $Y$  is more sensitive to variations in  $s_3$  than it is to variations in  $s_4$ . The reliability of such results is conditional on the degree to which the actual relationship between  $Y$  and the  $s_1, \dots, s_{nu}$  is described by the regression model, which is assumed to be linear in this analysis.

Coefficients of determination are useful quantitative measures of how well the relationship between TSPA outputs and inputs are described by the regression model. The coefficient of determination is defined as:

$$R_y^2 = \sum_{i=1}^N (\hat{Y}_i - \bar{Y})^2 / \sum_{i=1}^N (Y_i - \bar{Y})^2 \quad (11-9)$$

$R_y^2$  varies between 0 and 1 and measures the fraction of the variation in  $Y$  attributable to regression on the  $s$ 's. An  $R^2$  value near 1 indicates a good fit, meaning that the model is accounting for most of the uncertainty in the performance measure being analyzed. Conversely, an  $R^2$  near zero indicates that the regression model is not very successful in accounting for the uncertainty in the performance measure.

To avoid poor linear fits with nonlinear data, regression analyses were performed on rank-transformed data. Rank-transformed data means that the actual data values of both outputs and inputs are replaced with their corresponding ranks; that is, the smallest value for a given variable is assigned the value of 1, and the next largest value is assigned a value of 2, and so on up to the largest value.

### 11.3.2.3 Stepwise Regression Modeling

Because of the large number of uncertain parameters in the TSPA-VA, it is more efficient to perform regression analysis in a stepwise fashion, rather than treating all the independent variables in a single model. In the stepwise approach (see Helton et al. 1998, Section 6.10), a sequence of regression models is constructed, starting with a single selected input parameter, and including one additional input variable at each successive step until all significant input variables have been included in the model. At each step, tests are made to ensure that the computed regression coefficients correspond to a true underlying linear model. The probability that these regression coefficients are obtained merely by chance, when there is no linear model (i.e., when the regression coefficient is truly zero), is set to a low value. The "t-test" is used to implement this criterion. This test is applied to all variables entering the regression. Further, the test is applied to ensure that the variables already in regression remain significant after a new variable enters. If input variables are correlated, the possibility does exist that a variable selected in a

previous step may be dropped in a later step. In this study, the probability levels (called  $\alpha$ -levels) for the entering variables have been set at 0.02 and for the departing variables at 0.05. When there are no new variables to enter the regression at the specified  $\alpha$ -levels, the stepwise procedure terminates.

The largest sample correlation coefficient identifies the first input parameter to be added to the regression model in the stepwise process. Correlation coefficients measure the strength of the linear relationship between two variables, and are closely related to SRCs. The sample correlation coefficient is based on all the sampled values of the  $j^{\text{th}}$  input parameter and all the calculated results that correspond to those values, that is,

$$r_{yj} = \frac{\sum_{i=1}^N s_{ij} Y_i - \sum_{i=1}^N s_{ij} \sum_{i=1}^N Y_i / N}{\left[ \left( \sum_{i=1}^N s_{ij}^2 - \left( \sum_{i=1}^N s_{ij} \right)^2 / N \right) \left( \sum_{i=1}^N Y_i^2 - \left( \sum_{i=1}^N Y_i \right)^2 / N \right) \right]^{1/2}} \quad (11-10)$$

The value of  $r_{yj}$  can vary between positive one and negative one. When  $r_{yj}$  is close to positive one, this indicates a positive linear relationship exists between the input variable  $s_j$  and the calculated result  $Y$ . When  $r_{yj}$  is close to negative one, this indicates that a negative linear relationship exists between the input variable  $s_j$  and the calculated result  $Y$ . Values of  $r_{yj}$  close to zero indicate that no linear relationship exists between the input variable  $s_j$  and the calculated result  $Y$ .

The largest of the  $r_{yj}$  (in absolute value) over  $j = 1, \dots, nu$ , serves to identify the input variable having the strongest linear relationship with  $Y$ . This variable is used as a starting point on which to construct a stepwise regression. The second regression model contains the two input variables that have the largest impact on the output variable. That is, the input variable from the first step plus whichever of the remaining variables that produces a two-variable model with the largest gain in  $R^2$ . Additional models in sequence are defined in the same manner until a point is reached at which further models are unable to meaningfully increase the amount of uncertainty in the output variable that can be accounted for. Also, at each step of the stepwise regression process, the possibility exists for an already selected variable to be dropped out if it no longer has a significant impact on the amount of uncertainty in the output variable; this only occurs when correlations exist between input variables.

Several aspects of stepwise regression help quantify the importance of individual input variables (Helton et al. 1998, Section 6.10.5). The order in which variables are selected in the stepwise procedure described above provides an indication of their importance, with the most important variable selected first, and next most important variable selected second, and so on. The  $R^2$  values at successive steps of the analysis also provide a measure of variable importance by indicating how much of the uncertainty in the dependent variable can be accounted for by variables selected through each step. Moreover, when input variables are uncorrelated, differences in  $R^2$  values for the regression models constructed at successive steps equals the fraction of total uncertainty in the output variable that can be accounted for by the individual input variables added at each step. The absolute values of the SRCs in the regression models

also provide an indication of importance. Finally, the sign of an SRC indicates whether the input and output variables tend to increase and decrease with each other (a positive coefficient), or tend to move in opposite directions (a negative coefficient).

In Yucca Mountain TSPA applications, correlations do exist between input variables. As a consequence, the order in which variables are selected and the absolute values of the SRCs do not in general indicate the order of variable importance. Note that a general indicator of variable importance is the fraction of output variance that is attributable to the particular input variable under consideration. That is, the partial correlation coefficient (PCC) characterizes the strength of the linear relationship between two variables; after the linear effects of the other variables in the analysis have been removed (Helton et al. 1998, Section 6.10.4). As a result, PCCs tend to exclude the effects of other variables, whereas SRCs do not. The SRC simply characterizes the effect on the output variable that results from perturbing an input variable by a fixed fraction of its standard deviation. However, when input variables are uncorrelated, the order of variable importance as given by the absolute value of SRCs is the same as that given by the absolute value of the PCCs. Partial correlation coefficients are used in this study as a measure of variable importance.

### 11.3.3 Sensitivity Analysis Calculations

This subsection gives an overview of the steps involved in the sensitivity analysis calculations and the computational tools used to perform the calculations.

The sensitivity analysis consisted of three steps:

- A. Constructing data files containing the sampled uncertain input parameter values (independent variables) and output performance measures (dependent variables) such as peak dose and radionuclide releases
- B. Using the code PRESATool Version 1.5 (hereafter referred to as PRESATool) to read these files and generate the input files for the sensitivity analysis code SATool Version 1.2
- C. Using SATool Version 1.2 (hereafter referred to as SATool) to perform multiple linear regression analysis and provide an importance ranking of the independent variables.

These three steps and the flow of information between them are described next. The data files in step 1 are constructed using RIP Version 5.19.01 to extract sampled input parameter values and selected output performance measures from the detailed RIP output files. Detailed RIP output files were then generated for each multiple realization TSPA simulation period (i.e., 10,000-, 100,000-, and 1,000,000-year simulation periods). The output performance measures analyzed in the TSPA-VA sensitivity analysis include:

- Peak radiation dose rate (mrem/yr) at a specified location of 20 km (12.4 mi) from the repository



- Total radionuclide releases (Ci/yr) from the EBS to the UZ
- Total radionuclide releases (Ci/yr) from the UZ to the SZ.

In practice, once the data files containing the sampling and output performance data in step 1 are constructed, steps 2 and 3 are implemented by executing the codes PRESATool and SATool in sequence using script files (files containing commands for executing the codes). Two final output files are provided by SATool; One file gives detailed output of the sensitivity analysis and one file summarizes the importance ranking of input variables in tabular form. The specific codes, output and input files, and script files used to complete the three sensitivity analysis steps are stored in the YMP Technical Data Base (DTN SNT05070798001.001). Brief descriptions of PRESATool Version 1.5 and SATool Version 1.2 are provided below.

PRESATool has been designed to read RIP output files and associated user-specified input control files and generate two input files for SATool. One input file contains control parameters for the execution of SATool; another file contains the independent and dependent variable values for each realization in a Monte Carlo simulation. Dependent variables can be analyzed at the final simulation time (such as final peak dose) or for a sequence of output times (such as every 1,000 years). PRESATool also averages uncertain region-dependent repository parameters (i.e., fraction of packages with seeps, percolation flux, and seepage flux) over the six repository regions. This averaging is performed by weighting each region-dependent repository parameter by the ratio of the corresponding repository region footprint area to the total footprint area of the repository and summing the weighted contributions from all regions to produce an average uncertain parameter for the entire repository. All averaged repository parameters are treated as independent variables in the regression analysis.

SATool is the code used to conduct sensitivity analyses and provide importance ranking of the uncertain input variables in the TSPA Monte Carlo simulations. SATool uses stepwise regression for identifying the linear regression model and is an enhanced version of the code STEPWISE (Iman et al. 1980). Enhancements implemented in SATool include the calculation of PCCs, increased array dimensions for processing large numbers of independent and dependent variables, and improved presentation of regression analysis results. In SATool, PCCs are calculated directly from  $R^2$ -deletes. These latter quantities represent the  $R^2$  a regression model will have after the corresponding input variable is removed from the model. SATool computes the PCC for input variable  $i$  using  $R^2$ -deletes in the following relationship

$$PCC_i^2 = \frac{R^2 - R_{delete\ i}^2}{1 - R_{delete\ i}^2} \quad (11-11)$$

which can be derived from Equation 3 in RamaRao et al. (1998). The sign on a PCC is the same as the corresponding SRC.

The second importance indicator used in the TSPA-VA sensitivity analysis is  $R^2$ -loss.  $R^2$ -loss represents the loss in  $R^2$  of the current  $n$ -variable regression model if the variable of concern is dropped from the regression model, creating a model with  $n-1$  variables, where  $n$  is the total number of variables in the final regression model. That is

$$R^2_{loss\ i} = R^2 - R^2_{delete\ i} \quad (11-12)$$

Therefore, a high value of  $R^2$ -loss indicates that the removed variable is important.

Finally, SATOOL provides two output files, detailed and summary output files. The detailed output file contains information such as the mean and standard deviation of each input distribution, sum of squares and correlation matrices, and regression results and importance ranking at each step in the stepwise regression process. The summary output file contains the regression results and importance ranking at each step in the stepwise regression process.

The two computer codes PRESATOOL and SATOOL do the bulk of the calculations and data processing for the sensitivity analysis. In addition to these codes, several auxiliary codes are used in the sensitivity analysis (see Table 11-4). These auxiliary codes are used for processing RIP output to make, for example, time-dependent plots of partial correlation coefficients and scatter plots. These auxiliary codes and their input and output files are stored in a Performance Assessment dataset (DTN SNT05070798001.001) and are controlled under Sandia National Laboratories Yucca Mountain Project's configuration management system.

#### 11.4 SUMMARY OF TSPA-VA RESULTS

The previous chapters in this document have shown the complexity of the repository system, both the engineered and natural barriers, and the resulting need to break the system into various components in order to analyze repository performance. In this chapter, sections 11.1 and 11.2 describe the specific components or subsystems used in TSPA models, the rationale for choosing these specific components (how they correlate to specific physical-chemical processes and to location within the overall system, and how they are coupled to one another), and the specific methodology used to incorporate and analyze these components in the overall total system performance model. Chapters 2 through 9 give detailed descriptions of each of the key component models: the conceptual basis of these models as determined by experimental data, how to implement these conceptual models into the overall TSPA analyses (including model abstractions or simplifications that are necessary in some instances), the range of uncertainty underlying these component models and their corresponding data, and finally some key results of the component models, that is, how well the models fit available data and how the range of uncertainty in available data leads to a range of predictions of key model output parameters (e.g., groundwater flux).

Having shown in previous sections the necessity of breaking the total system into components and the details of modeling each component, it is now appropriate to describe the results of recombining all the component models into one integrated total system performance model—specifically the predictions of this overall model with respect to both total system performance (i.e., dose rate at the accessible environment) and to subsystem performance of the various components (e.g., performance of the SZ by itself). A key point is that the assessments will be based on the calculated source term, that is, the predicted radionuclide releases from the repository as the waste packages and waste forms degrade with time. This is a bit different from some of the earlier results (e.g., in Chapters 7 and 8), which were based on an idealized source term.

The phrase "base case" has already been defined in more general terms in Section 11.1 as it relates to uncertainty. However, in this section, "base case" is examined more specifically as it defines the predictions from the various component models of the TSPA. The phrase "base case" might also be termed the "baseline" case, where baseline is used in the sense of "likely" rather than as "initial," implying that the "base case" encompasses some of the possible uncertainty regarding predictions of system performance, but not all. For example, consider the fourth type of uncertainty listed in Section 11.1.1.1 regarding features, events, and processes: uncertainty about future events. The TSPA-VA base case encompasses some uncertainty related to climate-change events, but no uncertainty related to volcanism events. In addition, consider the second type of uncertainty, conceptual model uncertainty. The TSPA-VA base case does not include the dual permeability model (DKM)/Weeps model discussed in Chapter 2, but does include the DKM model. These are a couple of examples of how the base case represents a narrowed range of uncertainty in comparison to the entire space of possible outcomes. However, because of the still remaining uncertainty in all of the component models and future scenarios (features, events, and processes), the base case necessarily encompasses multiple outcomes (i.e., realizations) for the future repository behavior. The intent of Section 11.4 is to quantify the range of possible outcomes of overall system behavior for the TSPA-VA base case and to describe the key parameters of the component models that are most responsible for the performance variation across this range of system behavior (see Section 11.4.2). Before describing this entire range of overall base-case behavior, that is, the probability distribution of dose in the biosphere at 20 km (12.4 mi) downgradient of the repository, a single realization of repository behavior is examined to illustrate in detail how the behavior of the various components influences both the behavior of the dose and the behavior of other components (see Section 11.4.1). This will lead to a more thorough understanding of why the repository behaves as it does. This single realization is the realization that chooses the expected value of all the stochastic input parameters.

#### **11.4.1 Deterministic Results of the Base Case**

The single realization described in this section is the outcome of sampling all uncertain input parameters in the TSPA-VA component models at the expected value of their ranges (i.e., at their mean or average value). The intent is to show how total system behavior (i.e., individual dose rate) is influenced by the various component or subsystem models and parameters. The method is to compare time history plots of key subsystem parameters (e.g., waste-package failure history) with the time history plots of both dose rate and release rate at various system boundaries (e.g., the bottom boundary of the UZ—the water table).

Figure 11-6 illustrates the dose rate versus time from all biosphere dose pathways to an average adult (see Chapter 9) residing 20 km (12 mi) downgradient of the repository, for the expected-value simulation. The three graphs in this figure correspond to three different time frames:

- The first 10,000 years after repository closure.
- The first 100,000 years after repository closure.
- The first 1 million years after repository closure, which is the likely maximum geologically stable time period according to the National Research Council panel on

Yucca Mountain performance standards (National Academy of Sciences/National Research Council 1995, p. 72).

The shape and timing of various dose histories in these plots is explained in subsequent figures in this section. Note that the dose histories in Figure 11-6 are computed using three different simulations (10,000-yr, 100,000-yr, and 1,000,000-yr simulations), each with different time-step sizes. Key points about the three plots in Figure 11-6 are the following:

- Within the first 10,000 years, the only radionuclides to reach the biosphere are the nonsorbing radionuclides with high inventories, Tc-99 and I-129, and the total peak dose rate is about 0.04 mrem/yr.
- Within the first 100,000 years, the weakly sorbing radionuclide Np-237 begins to dominate doses in the biosphere at about 50,000 years, with the total dose rate reaching about 5 mrem/yr.
- Within the first 1 million years, neptunium-237 continues to be the major contributor to peak dose rate, which reaches a maximum of about 300 mrem/yr at about 300,000 years after closure of the repository, just following the first climatic superpluvial period.<sup>17</sup> The radionuclide Pu-242 is also important during the million-year time frame and has two peaks at about 320,000 years and 720,000 years, closely following the two superpluvial periods. There are regularly spaced spikes in all the dose rate curves (more pronounced for nonsorbing radionuclides such as Tc-99 and I-129) corresponding to the assumed climate model for the expected-value base-case simulation. As described below, these spikes are a result of assumed abrupt changes in water-table elevation and seepage through the packages.

#### 11.4.1.1 Ten-Thousand-Year Dose Rates

Within the first 10,000 years after closure, Tc-99 and I-129 are the dominant radionuclides to reach the biosphere. The majority of Tc-99 and I-129 are emplaced in the CSFN packages. Following are three important qualities of these two radionuclides:

- High solubility in the Yucca Mountain pore water seeping into the waste packages,<sup>18</sup> which allows rapid release from the waste packages and the EBS compared to releases of the actinide elements, that is, uranium, neptunium, curium, and americium

---

<sup>17</sup> This dose rate is comparable to the annual mean background radiation in the United States from natural sources (NCRP 1987, p. 149; National Research Council 1990, p. 19). The dose rate shown in Figure 11.4-1 reaches a peak after the superpluvial period because of a sorption delay affecting neptunium-237 transport in the SZ. Also, as discussed in Chapter 6 of this document, the predicted total dose rate of 300 mrem/yr would perhaps increase by 15 to 20 percent if the daughter products of neptunium-237 (uranium-233 and thorium-229) had been included in the model.

<sup>18</sup> The composition of the water seeping into the waste packages may be altered from ambient (i.e., pre-repository) conditions because of thermal-chemical processes, including evaporation and recirculation during the early high-temperature period and chemical reaction with the emplaced in-drift, waste-package, and waste-form materials.

- Negligible sorption onto the tuff rock matrix in the natural barriers, which allows relatively rapid transport through the natural system compared to other, more chemically reactive, elements<sup>19</sup>
- Relatively slow decay compared to the 10,000-year time span<sup>20</sup>.

Because both Tc-99 and I-129 behave similarly with respect to these three key attributes, only the movement of Tc-99 needs to be tracked through the system to explain the behavior of both ions, and the behavior of the total dose rate within 10,000 years.

Figure 11-7 through Figure 11-9, discussed in detail in this section, show the primary causes for the shape and timing of the 10,000-year dose rate graphs for Tc-99 and I-129. Two primary sets of plots are shown:

- Time histories of activity release and radionuclide concentrations at the downgradient boundaries of various parts of the natural and engineered barriers (e.g., EBS, UZ, and SZ)
- Time histories of key subsystem parameters.

Figure 11-7 shows the performance of the EBS. It is evident from Figure 11-7 that the initial releases of Tc-99 (and also I-129) from the waste packages and the EBS are caused by the first package failure at 1,000 years, which is an assumed juvenile, or early, failure arising from possible manufacturing defects, rockfall, or seismic activity. This failure is assumed to occur in the southeast repository region, the largest in area of the six regions. The small initial peak and oscillation in release from the EBS in the southeast region at about 1,000 years is caused by the immediate dissolution of the gap fraction and subsequent release from the single juvenile-failure package. The gap fraction is the 2 percent of the total Tc-99 inventory residing in very soluble form in the gap between the fuel matrix and the cladding.

After the initial juvenile failure at 1,000 years, the first corrosion failures occur at about 4,100 years and 4,200 years (the first one in the southeast region and second one in the central-central region), indicated by the bar heights equal to 1 in the histogram plot of package failures. After that, more packages fail by corrosion in all the various regions starting at 5,000 years. Besides this waste-package failure history, the other key event influencing performance in the 10,000-year time frame is the abrupt climatic change from current dry conditions to the relatively

---

Thus, the use of ambient pore-water solubility in the radionuclide mobilization model in TSPA-VA is an approximation—see Chapter 6, Sections 4.2.3.1.2 and 4.2.1.1.2 for clarification of this modeling assumption.

<sup>19</sup> Both technetium and iodine are assumed to be dissolved in the pore water in their anionic, oxidized forms as pertechnetate ( $\text{TcO}_4^-$ ) and iodide ( $\text{I}^-$ ). Under ambient or chemically unaltered conditions in Yucca Mountain, anions have a low affinity for sorption onto the volcanic tuff rocks, which implies that they can travel more rapidly through the UZ than other radionuclides that are in a cationic, or positively charged, state in the oxidized groundwater. Furthermore, pertechnetate and iodide have a lower potential for incorporation into minerals via precipitation than some other elements, such as the actinide elements, particularly under oxidizing conditions.

<sup>20</sup> Technetium-99 has a half life of about 213,000 years and iodine-129 about 15,700,000 years.

wetter long-term-average climate, occurring at 5,000 years in this expected-value realization. This climatic change is evident in both the waste-package and EBS mass-release graphs and causes the abrupt peak in releases at 5,100 years. However, this mass-release peak originates almost solely from the single juvenile-failure package and not from the two corrosion-failed packages.<sup>21</sup> For example, the advective/diffusive release plot shows that the two corrosion-failed packages at 4,100 and 4,200 years have a negligible influence on either total<sup>22</sup> advective or total diffusive mass-release curves prior to the climate change at 5,000 years.<sup>23</sup> This lack of influence is a result of the very small initial patch area per package, shown graphically in Figure 11-7. This small area means a low diffusive flux out of the corrosion-failed packages and a low seepage flux into the corrosion-failed packages. The latter causes low advective releases during the dry climate (Figure 11-7).<sup>24</sup> (The seepage flux into the drift is the same for both the juvenile package and the corrosion packages, but the seepage into and through the packages is different because of the different patch area.) The single juvenile-failure package was assumed to have a patch area of 0.031 m<sup>2</sup> (see Chapter 6, Section 6.5.2).

At 5,000 years, the climate becomes wetter and the seepage flux through both the juvenile-failure package and the corrosion-failed packages abruptly increases, as shown on the plot of seepage flux. This increase produces a burst of Tc-99 release from the repository at 5,000 years, shown by the peak in the Tc-99 advection curve. The diffusive release curve drops off during the long-term-average climate because the removal of Tc-99 by advection decreases the concentration in the waste package. The burst in Tc-99 release at 5,000 years is caused almost solely by the greater flushing of the juvenile-failure package, with only a negligible contribution from the corrosion-failed packages. The contribution from the corrosion-failed packages is very small because the patch area and seepage flux are low enough that the solubility limit for Tc-99 becomes important for those packages.

---

<sup>21</sup> The juvenile-failure package has the same clad failure fraction initially (about 1.25 percent) as the corrosion-failed packages.

<sup>22</sup> "Total" as used here means the total releases from all waste packages in the entire repository.

<sup>23</sup> During the dry climate in the first 5,000 years, the technetium-99 releases from advection and diffusion are about the same from the juvenile-failure package and add up to the total release curve from the engineered barrier system. Later, in the 100,000-year and 1 million year time frames (see Figure 11.4-5 and Figure 11.4-10), diffusion dominates over advection by about a factor of 10 for technetium-99 releases during the dry climate periods. This is because technetium-99 is not released by advection from the package at nearly as high a rate during the dry climate compared to the long-term-average climate. Therefore, a higher concentration of technetium-99 builds up in the waste package during the dry climate, producing a much higher concentration gradient from the inside to the outside of the package. This concentration gradient is the force that produces diffusive releases. However, at very early times, from 1,000 to 5,000 years, the patch area on the single juvenile-failure package is too small to allow diffusive releases to dominate advective releases (compared to the larger patch area available on corrosion-failed packages at later times).

<sup>24</sup> On the seepage flux plot, the red line indicates the average seepage flux through the packages, averaged over all six repository regions. The six gray lines (hard to see individually because they overlap) are the seepages into the six individual regions. Similarly, for the seepage into the drift, the blue line represents an areal average over the regions.

Figure 11-7 shows the major factors controlling the 10,000-year repository performance. These factors are related to the EBS, primarily waste-package performance and seepage. Some additional contribution to performance is gained within the natural geologic setting (that is, the barriers of the unsaturated and SZs), but primarily only during the dry climate up to 5,000 years. This additional performance is caused by delay in transport because of slow liquid flow through the 300 m of UZ between the repository and the water table. It is also caused by the relatively long (20 km, or 12.4 mi) travel distance in the SZ—from the repository footprint at the water table to the water-withdrawal location. On the other hand, in the long-term-average climate, the delay because of travel time in the UZ is greatly reduced by the higher overall infiltration flux, from an average of about 7 mm/yr to an average of 40 mm/yr (see Chapter 2, Section 2.4). The delay is also influenced by the increase in proportion of the UZ travel path associated with fracture flow and the much greater proportion of fracture flow (compared to matrix flow). The delay during the long-term-average climate is only about 300 years, based on the 50 percent point of the breakthrough curve.

Figure 11-8 shows the effect of the UZ on Tc-99 activity releases. The fast transport of nonsorbing radionuclides is apparent. However, comparing the total activity release from the EBS with the total activity release from the bottom of the UZ does not provide a measure of the Tc-99 travel time through the UZ because the EBS releases have been occurring only over a 4,000-year period prior to the switch to long-term-average climate. Thus, the full time needed for completely traversing the 300 m of UZ during a dry climate is not realized before the switch to long-term-average climate. This is shown in the pulse-release, breakthrough-curve plot shown in Figure 11-8 for the three climate states. The 50 percent point on the breakthrough curves requires about 6,000 years in the dry climate and 300 years in the long-term-average climate. Another point with regard to these activity release plots is that the sharp peak in the total UZ release curve at 5,100 years is *not* caused by the transport of the sharp peak in the total EBS release curve. Rather, it is caused by a rapid (modeled as instantaneous) 80-m rise in the water table when the climate changes from dry to long-term-average. This rise causes an instantaneous burst of Tc-99 into the SZ from the 80 m of UZ pore water, which produces the activity-release peak at the base of the UZ.<sup>25</sup>

Examination of the EBS release plot in 11-8 also reveals that during the period from 5,000 to 10,000 years, packages have failed by corrosion in all six repository regions. The failures can be seen in the curves for the six individual regions as they begin to appear at various times corresponding to initial corrosion failures of packages in the various regions. The southwest region, being the smallest and driest region, has the longest delay in initial failures, with the release curve appearing just before 10,000 years.

Further comparison of the EBS release plot with the UZ release plots reveals some of the behavior of the UZ between the repository and the water table. The initial juvenile failure of a waste package has occurred in the southeast repository region, which approximately overlies regions 2, 4, and 5 at the water table. Therefore, during the period of release from the juvenile-

---

<sup>25</sup> The sharp peak in the engineered-barrier-system curve at 5,200 years is transported through the UZ and appears in the UZ release curves as a subdued peak at about 5,600 years.

failure package (1,000 to 5,000 years), the radionuclide mass arrives at the water table only in SZ regions 2, 4, and 5. This arrival location is also because of the generally southeasterly direction of lateral diversion in the UZ as described in Chapter 7.

Similarly to the UZ, the SZ provides its best performance during the dry climate periods that occur approximately every 90,000 years on average. During these dry periods, the delay in the SZ for nonsorbing radionuclides such as Tc-99 and I-129 is about 1,000 years. During the long-term-average climate, the delay is only equal to  $1000/5.44 = 184$  years, where 5.44 is the flux multiplier used for the long-term-average climate relative to the dry climate (Chapter 8).<sup>26</sup> The performance of the SZ during the first 10,000 years after closure is illustrated in Figure 11-9, which compares activity releases at the base of the UZ, or entry to the SZ, to activity releases at the end of the SZ, at 20 km (12.4 mi). Seeing the time delay in either the dry or long-term-average climate from these two activity release figures is difficult. However, comparing the temporal location of the water-table-rise peak on the UZ Tc-99 breakthrough curve (Tc-99 concentration at the water table) with the location on the SZ Tc-99 breakthrough curve (Tc-99 concentration at 20 km) indicates that the peak is delayed by at least the expected 184-year travel time in the long-term-average climate. In the dry climate, all that can be compared is the temporal location of a specific value of the activity release rate (e.g., the  $10^{-4}$  Ci/yr rate). This location is at about 3,600 years on the UZ release plot and about 4,700 years on the SZ release plot, which demonstrates the approximate 1,000-year delay during the dry climate (shown in Figure 11-9 by the Tc-99 breakthrough curve, for a constant-concentration source).

The other key feature of SZ performance is the dilution it provides because of plume dispersion. This dilution is illustrated on Figure 11-9 by the two concentration plots, one at the beginning of the SZ for the six regions, or streamtubes, and one at the end where a single concentration value is chosen for determining dose rate. An explanation of how this single concentration is chosen has been given previously in Section 11.2.9. Here the explanation is briefly summarized with the plot of effective dilution factor shown in Figure 11-9. In particular, the dilution factor range of 1 to 100 was based on the SZ Expert Elicitation (CRWMS M&O 1997, Figure 3-3d), which assumed a plume dimension of approximately the size of *each* of the streamtubes in the TSPA-VA SZ model. In this model, there are six SZ streamtubes adjacent to one another. As described in Section 11.2.9, the concentrations for each radionuclide were summed among the six streamtubes. This sum was compared to the maximum undiluted concentration for that radionuclide from among the six streamtubes. Note that the maximum undiluted concentration is the concentration at the UZ/water table interface. For example, see the Tc concentration at the water table plot in Figure 11-9. If the sum of concentrations from the six streamtubes exceeded the maximum undiluted concentration, then the maximum undiluted concentration was used as the simulated concentration at that time step for that radionuclide. Conversely, if the sum of the concentrations was less than the maximum undiluted concentration, the sum was used as the concentration at that time step. In the expected value case, which assumes a median dilution factor of 10 in *each* individual streamtube (see Chapter 8, Section 8.4.2), the latter condition occurred. However, in this case, the summed concentration resulted in an effective dilution factor of only four, as shown by comparing the concentration plots at the beginning and end of the SZ

---

<sup>26</sup> The superpluvial climate flux multiplier is 14.7.



at 10,000 years (i.e., Tc-99 concentration at the water table versus Tc-99 concentration at 20 km). The cumulative distribution function plot for the effective dilution factor can also be examined, and it shows that the median probability of 0.5 corresponds to a dilution factor of four.

A final summary point about the 10,000-year dose rates is that only nonsorbing radionuclides such as Tc-99 and I-129 reach the biosphere because most of the other radionuclides react to some degree with the tuffaceous rocks in the geosphere. These radionuclides are delayed enough by these reactions that they do not reach the biosphere during the first 10,000 years after repository closure.

#### 11.4.1.2 One-Hundred-Thousand-Year Dose Rates

Within the first 100,000 years after closure, Tc-99 and Np-237 are the dominant radionuclides to reach the biosphere; Tc-99 dominates dose rates up until about 50,000 years, after which Np-237 finally reaches the biosphere and dominates thereafter. The majority of these radionuclides are from CSFN packages. The three important qualities about Tc-99 were pointed out in the previous section: high solubility in Yucca Mountain porewater, no sorption on the volcanic tuffs, and relatively slow decay. Following are three key qualities about Np-237:

- Relatively low solubility in the porewater seeping into the waste packages,<sup>27</sup> implying that Np-237 mass release from failed waste packages is "solubility-limited" until the failed inventory is nearly depleted. In other words, the Np-237 release rate from the packages will be linearly proportional to the liquid flow rate through the failed packages.
- Weak, but nonzero, sorption onto the tuff rock matrix in the natural barriers, which means a lower transport rate through the unsaturated and SZ than for Tc-99 (about a factor of 20 to 80 times slower in the rock matrix, but the same through fractures). However, the Np-237 transport rate is still relatively rapid compared to more chemically reactive elements.<sup>28</sup>
- Relatively slow decay compared to the 100,000-year time span.<sup>29</sup>

In the following discussion, mainly the behavior of these two key radionuclides, Tc-99 and Np-237, is discussed, but the behavior of Pu-239 is also discussed. There is also a large inventory of Pu-239, but the radionuclide has a much higher sorption than neptunium, implying much slower transport through rock matrix. However, because Pu-239 has been observed in

---

<sup>27</sup> As with technetium-99, the solubility used for neptunium-237 is the "ambient" solubility in pre-repository pore water.

<sup>28</sup> Because the pore waters are assumed to be oxidizing, neptunium is thought to be present in ionic form mainly in the  $\text{Np}^{+5}$  oxidation state, as the  $\text{NpO}_2^+$  ion at ambient pH levels (below 8) (see Chapter 7, Section 7.6.2 and Chapter 6, Section 6.1.2.3).

<sup>29</sup> Neptunium-237 has a half life of about 2,140,000 years. The sources of colloidal Pu-239 are past underground nuclear detonations.

colloidal form in recent measurements at the Nevada Test Site, it is important to consider the possible future behavior of colloidal Pu-239 at Yucca Mountain.<sup>30</sup>

Figures 11-10 through 11-14, discussed in detail in this section, show the primary causes for the shape and timing of the 100,000-year Tc-99 and Np-237 dose rate graphs. As in the previous section, two primary sets of plots are displayed: time histories of activity release or concentration at the downgradient boundary of various parts of the natural and engineered barriers (i.e., EBS, UZ, and SZ); and time histories of key subsystem parameters. Figure 11-10 portrays the 100,000-year performance of the EBS. Similarly to the 10,000-year performance, the key factors are climate change and waste-package failure history. Consider first the waste-package and engineered-barrier-system releases of Tc-99 and also its dose rate in the biosphere. All three of these time histories mirror the jagged nature of the instantaneous waste-package failure history. This instantaneous failure curve is a histogram of package failures, with the interval size being equal to the time step size of 333 years.<sup>31</sup> Ten or 11 packages are about the most that fail (by patch penetration) in any 333-year period. The reason that the release-rate curves and dose curve for Tc-99 mirror the package failure rate is that Tc-99 is not solubility limited at the values of seepage flux flowing through the packages after 10,000 years. Therefore, Tc-99 is flushed very rapidly from a failed package. As package inventories become available for release via the failure histogram, their inventories of Tc-99 are almost instantaneously released, which causes this mirroring of releases with package failures.

The releases of Np-237 are different from Tc-99 releases because of Np-237's low solubility. Low solubility causes the shape of the Np-237 release curve to be relatively smooth and controlled by two features: the flow rate of water through the packages and the cumulative amount of failed packages or inventory. The cause and effect of the first feature, seepage flux, is evident when the climate changes from long-term-average to dry at 95,000 years. When the dry climate is reestablished, advective releases of Np-237 are dramatically reduced because of the linear proportionality between flow rate and mass release for radionuclides that have reached their solubility limit in the water seeping through the waste packages. Furthermore, the Np-237 diffusive releases do not abruptly change with the switch from long-term-average climate to dry climate at 95,000 years, because the accompanying change in seepage flux does not change the Np-237 concentration in the packages, which is the driving force behind diffusion.<sup>32</sup> In the dry climate, the Tc-99 advective release rate also drops by about the same factor as the Np-237 release rate. The lower release rate gives the appearance that Tc-99 is also solubility limited. However, this is not the case, as shown by the significant increase in diffusive releases for Tc-99 during the dry climate. The explanation for this phenomenon is found in the "seepage fraction" plot shown in Figure 11-10, which shows the fraction of all packages that are exposed to seeps in each of the six repository regions, plus the average over the regions. This average fraction drops

---

<sup>30</sup> Plutonium-239 has a relatively short half life of about 24,000 years.

<sup>31</sup> If divided by the total number of packages, this instantaneous failure history becomes a probability density function (pdf) for waste-package failure as a function of time.

<sup>32</sup> This, in fact, is the key point about reaching a solubility limit: that the amount of water or water flow present does not alter the concentration (mass/volume) of the radionuclide in solution.

from about 0.27 to 0.045 with the switch to dry climate; however, the packages keep failing at about the same rate during the dry climate,<sup>33</sup> continually exposing Tc-99 inventory to contact with water, but in this case stagnant or nonflowing water. Because of the very high solubility of Tc-99 (0.34 g/m<sup>3</sup> or  $1.43 \times 10^{-6}$  M for this expected-value realization), the concentration of Tc-99 is very high in these failed packages because flowing water is not removing the inventory. A much higher concentration gradient is created between the inside and outside of the packages, causing a much higher diffusive mass release. [As discussed in the next section regarding million-year releases, when the climate goes back from dry to long-term-average, a burst of Tc-99 is released. This burst represents the Tc-99 that has built up during the long-term-average climate within the fraction of packages that are not dripped on during the dry period, even though they have failed by corrosion. When this incremental fraction of packages (about 0.225) is suddenly dripped on again during the new long-term-average climate, all of the Tc-99 is abruptly transported away. This Tc-99 available for rapid transport has accumulated during the dry climate because the CSFN degradation rate is very high. All of the Tc-99 available from this degradation is present in a highly soluble form that can dissolve at a very high concentration in the newly available flowing water during the long-term-average climate.]

The second factor controlling the Np-237 release is the cumulative amount of inventory exposed, shown in Figure 11-10 for the three inventory types: CSFN, DSNF, and high-level radioactive waste. For the latter two, the cumulative inventory exposed curve is found by multiplying the cumulative failed-package curve by the inventory per package.<sup>34</sup> However, for CSFN there is a second barrier to consider: the zircaloy fuel cladding.<sup>35</sup> During the first 100,000 years, this cladding is considered to be very robust in the base-case, expected-value realization. At most only about 3 percent of the cladding will fail by various mechanisms by 100,000 years (see Chapter 6, Section 6.3.1), meaning that to obtain the cumulative exposed inventory in CSFN, the cumulative package-failure history must be multiplied by both the

---

<sup>33</sup> The fact that packages keep failing at the same rate during the dry climate is a conservative assumption. Within the RIP model, there are four environmental package groupings: packages that are never dripped on (55 percent of all packages, in the expected-value base case); packages that are dripped on during all climates (4.5 percent); packages that are dripped on only during the long-term-average and superpluvial climates (22.5 percent); and packages that are dripped on only during the superpluvial climates (18 percent). However, only two of these groupings are represented in the waste-package degradation model: packages that are dripped on from time zero to 1 million years, and packages that are never dripped on. It is thus a conservative assumption (i.e., erring on the side of maximum releases) to assume that the long-term-average fraction of packages (i.e., the fraction that is dripped on during long-term-average and superpluvial climates) has the same failure rate during the long-term average climate and the dry climate. On the other hand, a somewhat nonconservative assumption is that the superpluvial fraction of packages fails according to the non-seep failure curve. This assumption is used because these packages are not dripped on at all until at least 250,000 years after repository closure (see Chapter 6, Section 6.5).

<sup>34</sup> The average neptunium-237 inventory per package is 11.4 Ci/pkg for CSNF, 0.735 Ci/pkg for high-level radioactive waste, and 0.153 Ci/pkg for DOE spent nuclear fuel.

<sup>35</sup> Some of the inventory of DOE spent nuclear fuel has intact cladding (such as Naval fuel and about 50 percent of N-reactor fuel); however, it is conservatively assumed in TSPA-VA that all the DOE spent fuel cladding is failed at emplacement. This assumption is made in order to bound the effect of DOE spent fuel on repository performance.

Np-237 inventory per package and by the clad failure fraction.<sup>36</sup> In Figure 11-10 the Np-237 cumulative inventory-exposed history has the same shape as both the waste-package and engineered-barrier-system release histories. On the other hand, the seepage flux into the packages also has the same steadily increasing curve (ignoring the climate change at 95,000 years), which is caused by the steadily growing patch area curve. It appears that both, seepage flux and cumulative-inventory exposure are responsible for the shape of the Np-237 release curve. The steadily increasing cumulative-inventory curve means that more packages, seepage, and inventory are becoming available with time for transport of more Np-237 away from the entire repository.

Figure 11-11 shows the performance of the waste package and EBS for the three inventory types: CSFN, DSNF, and high-level radioactive waste. One implication from this figure, especially when the Tc-99 cumulative inventory exposure curves are compared, is that the exposed DSNF inventory is nearly as large as the exposed CSFN inventory at 100,000 years—the ratio of DOE inventory to commercial inventory is about 0.4. Also, this ratio is roughly maintained when translated to releases from the waste packages, because the dissolution rates for DSNF and CSFN are comparable for most of the 100,000 years, as shown in Figure 11-11. In contrast, the exposed Tc-99 high-level radioactive waste inventory is about twice as much as the exposed CSFN inventory. However, the Tc-99 high-level-waste activity released is about five times lower than the commercial-spent-nuclear-fuel activity released because the high-level-waste degradation rate is lower than the commercial and DSNF degradation rates. The exposed Np-237 inventory and its activity released from the EBS has a similar relationship to that of Tc-99 because of fuel-degradation rate.

Returning to Figure 11-10, another point about the engineered-barrier-system behavior is the Pu-239 release curve. The radionuclide Pu-239 is another actinide that is solubility limited in ambient Yucca Mountain pore waters. Therefore, its release behavior from the waste package and EBS should be similar to Np-237, which is exactly the behavior shown in Figure 11-10. However, as discussed in Chapter 6, colloidal transport of Pu-239 is also included in the TSPA-VA model, so the shape of the engineered-barrier-system release curve for Pu-239 might be expected to be different from the Np-237 release curve. It is not different because in the TSPA-VA model the fraction of *irreversible* colloids (unaffected by interaction with rock matrix or fractures anywhere in the system) is at most only  $1 \times 10^{-4}$  times the concentration of reversible colloids (and only  $1 \times 10^{-7}$  for the expected-value base-case realization being described here). Furthermore, since the *reversible* colloid concentration is linearly proportional to the dissolved aqueous concentration (see Chapter 6), it is necessarily true that the shape of the Pu-239 release curve is the same with or without colloids. Also, for the expected-value base case the proportionality factor,  $K_c$  (the ratio of plutonium mass on colloids to plutonium mass dissolved in the aqueous phase), is only about 0.33, so the Pu-239 release curve must be dominated by dissolved Pu-239, not colloidal Pu-239.

---

<sup>36</sup> This maximum fraction of 3 percent clad failure over 100,000 years is a combination of creep failure, stainless-steel-rod failure, zircaloy corrosion failure, and mechanical failure.

Figure 11-10 also shows the performance of the EBS, specifically the concrete invert. Although a pulse-release breakthrough curve is not shown, a comparison of total Np-237 releases from the EBS with advective Np-237 releases from the waste package indicates that there is a transport delay of Np-237 in the invert. The Np-237 distribution coefficient ( $K_d$ ) in the invert is about 100 ml/g (and the plutonium  $K_d$  is about 600 ml/g). This  $K_d$  for neptunium makes invert travel time in the dry climate very slow (on the order of 100,000 years through the 1 m of invert), while in the long-term-average climate the travel time is about 7,500 years. Therefore, because there is a climate change at 5,000 years after closure, the effective travel time of Np-237 through the invert is about  $(5,000 + 7,500 =) 12,500$  years. (The neptunium moves only a negligible distance during the 5,000 years of dry climate).

Figure 11-12 shows the performance of the UZ, base-case model over the 100,000-year time span, during which the long-term-average climate predominates. In Chapter 2 the UZ expected-value long-term-average base case was explained as having an average of about 40 mm per year percolation through the UZ at the repository horizon. Part of this flow is diverted laterally by the perched-water zone beneath the northern portions of the repository. The net effect of the diversion, and also sorption of the radionuclides onto the rock matrix, is shown in the UZ activity-release plot in Figure 11-12. This plot represents the summed activity release over all six regions at the water table for the three indicated radionuclides. Comparison of the engineered-barrier-system and UZ release rates shows that the UZ has little delaying effect on the transport of the nonsorbing Tc-99. For the weakly sorbing Np-237, the UZ appears to delay its movement by about several thousand years. For the strongly sorbing Pu-239, the UZ delays its releases by tens of thousands of years.<sup>37</sup> (Using the 50 percent point on the pulse-release breakthrough curves as the metric to gauge travel time, Tc-99 delay is 300 years, Np-237 delay is 20,000 years, and Pu-242 delay is apparently greater than 1 million years. Pu-242 breakthrough is shown in the plot because Pu-239 has a very short half-life of 24,000 years, while Pu-242 has a half-life of about 387,000 years. However, even with this half-life, the 50-percent-breakthrough metric is in error because the normalization factor for the plot is the initial number of particles, many of which have decayed before traversing the entire UZ. The exact amount of error can be determined only by simulating Pu-242 or Pu-239 transport without decay, that is, taking into account sorption, but not decay.)

Figure 11-13 shows the performance of the SZ over the 100,000-year time span for this expected-value base case realization. Shown are two sets of plots; release rate graphs at both the base of the UZ and the 20-km (12-mi) distance in the SZ, and concentration plots at the water table beneath the repository and at the 20-km (12-mi) distance. Also shown again (see Figure 11-9) are the SZ, generic breakthrough curves and the dilution-factor cumulative-distribution functions. The SZ demonstrates similar behavior to the UZ for the three radionuclides; Tc-99 is only slightly delayed, Np-237 is moderately delayed, and Pu-239 is strongly delayed. Based on the breakthrough curves shown, the delay of the 50 percent concentration point is about 50,000 years for Np-237 and about 110,000 years for Pu-239.

---

<sup>37</sup> The plutonium-239 release curve is erratic at the base of the UZ. This nonphysical behavior is caused by the discrete nature of the particle tracking model when releases are very low, resulting in the observance of individual particles passing out of the domain.

Finally, as with the 10,000-year Tc-99 transport discussed in Section 11.4.1.1, Np-237 transport through the six stream tubes similarly experiences an effective dilution factor of about four when sampled in a well-withdrawal scenario at 20 km (12.4 mi).

Figure 11-14 illustrates how the relative concentrations of the three radionuclides in the groundwater translate to relatively different doses as a result of the differing biosphere, dose-conversion factors. In particular, the biosphere, dose-conversion factors (mrem/yr per Ci/m<sup>3</sup>) of Np-237 and Pu-239 are about 1000 times higher than the Tc-99 biosphere dose-conversion factor. This implies that although the Np-237 activity concentration in the groundwater (Ci/m<sup>3</sup>) is much lower than Tc-99, its dose rate is about 10 times higher because of larger impact on the human body.<sup>38</sup> Similarly, although the Pu-239 activity concentration in the SZ is very low at 100,000 years ( $1 \times 10^{-12}$  Ci/m<sup>3</sup> or 0.001 pCi/liter), its dose reaches several  $\mu$ mrem/yr because of its relatively high biosphere dose-conversion factor.

The final plot in Figure 11-14 shows the small effect of including a model for irreversible sorption of Pu-239 onto colloids, where the ratio of the irreversible fraction to the reversible fraction is  $1 \times 10^{-7}$  in the base-case, expected-value realization. This model accounts for the early breakthrough of plutonium colloids observed in the Benham test. The scale on this plot is not low enough to show the first breakthrough of these irreversible colloids at the 20-km (12-mi) boundary. However, examining the modeling results shows a first breakthrough at about 1,500 years, which represents the very fast fracture transport through the natural system of the releases from the juvenile-failure package that fails at 1,000 years.

#### 11.4.1.3 One-Million-Year Dose Rates

Within the first 1 million years after closure, Tc-99 and Np-237 are the dominant radionuclides to reach the biosphere; Tc-99 dominates dose rates up until about 50,000 years, after which Np-237 reaches the biosphere in appreciable amounts and dominates thereafter. After a long period of delay in the natural barriers, Pu-242 finally appears at the biosphere in appreciable amounts beginning at about 200,000 years and then remains as the second most important radionuclide, after Np-237, for the remainder of the million-year period. In the two superpluvial periods that occur, Pu-242 has a relatively sharp peak that contributes about the same as Np-237 to the total peak dose during those climatic periods. There are relatively large inventories of all three radionuclides (Tc-99, Np-237, and Pu-242) in the CSFN packages. The key qualities of Tc-99 and Np-237 have already been discussed at the beginning of Sections 11.4.1.1 and 11.4.1.2. For the million-year performance period, their behavior is again used to explain the performance of the repository system and subsystems. In addition, the behavior of the rather long-lived Pu-242 is used to explain the behavior of strongly sorbing radionuclides during the 1 million year period.<sup>39</sup>

---

<sup>38</sup> The mass concentrations (g/m<sup>3</sup>) for technetium-99 and neptunium-237 are actually much closer to each other than are their activity concentrations, about  $7 \times 10^{-6}$  g/m<sup>3</sup> and  $1 \times 10^{-6}$  g/m<sup>3</sup> respectively; however, the specific activity (Ci/g) of neptunium-237 is much lower than that of technetium-99.

<sup>39</sup> Plutonium-242 has a half life of about 387,000 years.

Figures 11-15 through 11-18, discussed in detail in this section, show the primary causes for the shape and timing of the 1-million-year dose rate graphs. Figure 11-15 shows the 1-million-year performance of the EBS. Again, the key factors are climate change and waste-package failure history. In contrast to the 10,000-year and 100,000-year time spans, however, an additional parameter is necessary to explain the shape of the curves after 200,000 years: cladding failure rate. This parameter is discussed in detail below.

As in the 100,000-year time span, the jaggedness of the instantaneous package-failure history explains the jagged appearance of the graphs for Tc-99 waste-package releases and biosphere dose rates—for the identical reason, namely, that Tc-99 is a “release-rate-limited” radionuclide. That is, the radionuclide has such a high solubility that its release is limited by the rate at which packages fail, not the rate at which water moves it out of the packages. The instantaneous package failure history shown in Figure 11-15 is a histogram of package failures, with the interval size being equal to the time step size of 1,000 years. Because this time step is larger than for the 100,000-year simulation, some of the peaks on the histogram are larger than the 100,000-year package-failure histogram in Figure 11-10. Instead of 10 packages being the maximum in any interval, there are up to 30 or more in an interval.

Another feature of the waste-package failure history is the failure of the no-drip packages beginning at about 730,000 years. This is the group of packages discussed earlier that are never dripped on; about 55 percent of the total packages in the repository. Because they are never dripped on, their corrosion rate is much lower than for dripped-on packages and, therefore, they do not begin to fail until a very long time after emplacement. Even when they do fail, there is no flowing water to sweep out the inventory, so the only release mechanism is diffusive transport. This effect is shown on the Tc-99 diffusive release curve and slightly evident on the Np-237 release curve; however, the effect of these no-drip packages is barely discernable on the dose rate curve in the biosphere.

As with the 100,000-year time histories discussed in Section 11.4.1.2, Np-237 releases are different from Tc-99 releases because of Np-237's low solubility, at least for the first 200,000 years. However, after 200,000 years Np-237 actually switches from being a solubility-limited radionuclide to being a release-rate limited radionuclide—limited by the cladding failure rate. A number of the plots on Figure 11-15 explain this effect. First, after about 200,000 years the seepage flux through the packages is very high—high enough to sweep out all of the released Np-237, even though it has a very low solubility in the flowing water. Second, the CSFN, cumulative, package-failure curve flattens out at about 200,000 years, showing that very few additional CSFN packages fail for the remainder of the 1 million years. However, the combined CSFN, cumulative package-cladding, failure curve (the integrated or “convolved” product of package failures with cladding failures) continues to increase after 200,000 years, indicating that more inventory is being exposed. However, the rate at which this cumulative, package-cladding, failure curve increases is declining with time after 200,000 years. This effect is evident on the instantaneous “CSFN inventory exposure rate” curve, which represents the rate at which inventory is exposed to transport as a function of time (where the inventory is represented as a

fraction of the entire repository inventory).<sup>40</sup> This inventory exposure curve mirrors the shape of the Np-237 advective-release curve between 200,000 years and 1 million years, and also the shape of the Np-237 dose-rate curve. This implies that Np-237 is no longer solubility-limited after about 200,000 years, but is "cladding-release-rate" limited. In other words, the release rate or exposure rate of Np-237 by failing cladding is slow enough and the seepage flux is high enough that the low solubility of Np-237 no longer limits its release from the waste package. This effect is also shown on the diffusive release curve for Np-237, which looks very much like the Tc-99 diffusive release curve after 200,000 years. In particular, during the dry climate states, the diffusion releases of both Np-237 and Tc-99 attain the same rate as the long-term-average advective release rate. This is because the concentrations of both radionuclides build up during the dry climate (i.e., neither were solubility limited during the long-term average climate, so both of their concentrations in the waste packages build up during the dry climate, causing an increased diffusive flux). On the Np-237 release plot, this behavior is evident in the dry climate states after 200,000 years. However, in the two dry climate states before 200,000 years, Np-237 is solubility limited and its diffusive release curve shows no abrupt changes when the dry climate is established. Also, before 200,000 years, the Np-237 release curve shows a sharper rise and peak than the CSFN inventory exposure curve because the Np-237 release follows the package-failure cumulative distribution function up until that point. The Tc-99 release rate curves also follow the CSFN inventory exposure curve at all times, as is expected for a radionuclide that is not solubility limited.<sup>41</sup>

Figure 11-16 shows the relative contributions to EBS releases from the three main inventory types over the million-year time frame. Following are the important points about this figure:

- DSNF is the second highest contributor to Np-237 and Tc-99 releases during the first 200,000 years. Commercial spent nuclear fuel is the highest contributor. After that time, the DSNF release begins to decrease because very few DSNF packages fail after 200,000 years. (Individual package failure is readily discernible on the plot.)
- High-level radioactive waste never contributes very much to Np-237 and Tc-99 releases compared to CSFN.

For performance over the 1-million-year period, the relatively short delay in travel time in the UZ is short relative to the time period of concern and is of very little consequence, so no figures are shown for it. For additional discussion on the impact of UZ travel times on peak-dose rates see Section 11.4.2.1. On the other hand, the SZ is important because of dilution, which proves to

<sup>40</sup> This inventory exposure rate curve is the derivative of the cumulative package-cladding failure curve normalized to (i.e., divided by) the total number of commercial spent fuel packages.

<sup>41</sup> An unusual feature of the Np-237 diffusive release curve is the series of gaps that appear in the curve each time the climate switches from dry to long-term-average, and also when the climate switches from long-term-average to the second superpluvial at about 730,000 years. The gaps are caused by the negative diffusion rate at these points, which cannot be plotted on a log scale. Apparently, when an abrupt change to a wetter climate occurs, Np-237 is rapidly flushed from the waste package, causing near zero concentration in the waste package and allowing "backwards" diffusion from the invert into the package. Although not shown in this document, the comparable advective and diffusive releases from the engineered barrier system do not exhibit these negative diffusion rates.



be the second most important uncertainty (see Section 11.4.2.3).<sup>42</sup> Figure 11-17 shows how dilution in the SZ affects concentration, specifically Np-237, and how the BDCFs for the various radionuclides are used to convert SZ concentrations to dose rates.

#### **11.4.1.4 Cumulative Activity Releases from the Repository and the Engineered Barrier System**

Another way of examining repository performance is by looking at cumulative activity release (Curies) versus time at the edge of the EBS compared to the cumulative activity release in the SZ at 20 km (12.4 mi). First, this method is another means of comparing natural system performance with engineered system performance. Second, the method illustrates the large fraction of the total radioactivity that is actually retained in the repository system at various times. The expected differences in the engineered-barrier-system and SZ cumulative release curves are because of retardation (sorption) and decay. If radionuclides did not decay, eventually the EBS and SZ cumulative curves would become equal. Figure 11-18 shows cumulative fractional activity releases of Tc-99, Np-237, Pu-239, and Pu-242 at these two spatial locations for the time frames of 10,000 years, 100,000 years, and 1 million years. Cumulative fractional release for any radionuclide at a given spatial location and a given time is defined as the cumulative activity that has traveled past that spatial location divided by the initial inventory emplaced for that radionuclide. In the 10,000-year time frame, nearly all the Tc-99 radioactivity is retained in the repository—less than 0.001 percent has been released from either the EBS or the SZ.<sup>43</sup> After 100,000 years, less than 0.2 percent of the Tc-99 has been released from the repository system (SZ at 20 km) and less than 0.02 percent of the Np-237 has been released. The amount of Pu-239 released beyond 20 km (12.4 mi) in the SZ does not appear on this graph but is slightly less than  $1 \times 10^{-9}$  percent. At 1 million years, about 1 percent of the Tc-99, 2 percent of the Np-237, and 0.4 percent of the Pu-242 activities have reached the 20-km (12-m) boundary. Much of the 99 percent of the Tc-99 that is never released is a result of radioactive decay throughout the repository system.

#### **11.4.1.5 Summary**

The purpose of this section has been to demonstrate the influence of the various subsystem and component processes on the overall system performance. The illustrative realization used for this purpose is the “expected-value” realization, that is, the realization that chooses the expected value of all input parameters. The behavior of this realization cannot necessarily be considered to represent the overall mean behavior of the repository, as determined by multiple realization simulations, because of the nonlinear behavior of the models and processes. However, as will be seen in Section 11.4.2.3, this expected-value realization does lie near the central tendency of the overall probability distribution—generally somewhere between the median and the mean.

---

<sup>42</sup> The Np-237 biosphere dose conversion factor is the third most important uncertainty in the million-year time frame.

<sup>43</sup> The percent of Np-237, Pu-239, and Pu-242 released is negligible.

Based on the analysis in this section, nonsorbing radionuclides, such as Tc-99, dominate peak dose rates at "early" times, perhaps up to 50,000 years after repository closure. After that the weakly sorbing Np-237 controls peak dose rates, with some additional contribution from Pu-242.

During the 10,000-year time frame, the key factors controlling repository behavior are the failure of the single juvenile (or early) failed package and the few (about 17) corrosion-failed packages, and the climate change at 5,000 years. The main factor affecting releases from the waste packages is the seepage of water into the waste packages, which is controlled by the corroded pit and patch area. During this time frame the seepage flux into the corrosion-failure packages is low enough that Tc-99 releases become solubility-limited in those packages. During this 10,000-year span after closure, travel time in the UZ and SZ during the dry climate state is also long enough to enhance performance.

During the 100,000-year time span, the major factors controlling performance are the instantaneous waste-package failure rate (controls Tc-99 releases), the cumulative waste-package and cladding failures (controls Np-237 releases), the fraction of packages encountering seeps, and the seepage rate into the packages. The seepage rate is important because neptunium release is solubility limited, so the absolute amount of Np-237 escaping any package is linearly proportional to the seepage flowing through the package.

During the 1-million-year time span after closure, the major factors controlling performance are the combined cumulative package and cladding failures, and the superpluvial climate change. The latter causes the peak in the total and neptunium dose-rate curves at about 300,000 years.

Dilution in the SZ is important at all time frames (see Sections 11.4.2.3 and 11.4.2.4), but because its values are orders of magnitude lower than those used in earlier analyses (see Chapter 8, Section 8.4.2), it does not play as large a role as in previous TSPAs (for example, see CRWMS M&O 1995, Section 9.3.7). Also, sorption in the unsaturated and SZs is important for all of the strongly sorbing radionuclides, such as plutonium, and provides a very long delay (up to hundreds of thousands of years) in transport to the 20-km (12-mi) boundary.

Commercial spent nuclear fuel dominates technetium and neptunium releases, but DSNF releases are not insignificant and comprise about 25 percent of the total.

A summary of input and output files, plot file names (SigmaPlot), and DTNs associated with the TSPA-VA figures 11-6 to 11-19 is provided in Table 11-1.

#### **11.4.2 Probabilistic Results of the Base Case**

This section summarizes the probabilistic results obtained from the base-case Monte Carlo simulations, focusing on the calculated peak-dose rates to a human located 20 km (12.4 mi) from the repository. Dose rates are presented in the form of complementary cumulative distribution functions for three periods: 10,000 years, 100,000 years, and 1 million years. Factors are also discussed that cause uncertainty in the calculated peak-dose rates. Auxiliary results are provided about which radionuclides contribute most to dose and the range in times at which peak-dose rates occur. In Section 11.4.2.3, the contributions of individual parameters to uncertainty in peak-dose rates are discussed. Uncertain parameters that are most important to subsystems, such

as radionuclide releases from the EBS or from the UZ, can also be analyzed, and one example is briefly discussed. In Section 11.4.2.4, the impact of seepage and waste package parameter uncertainty ranges on sensitivity analysis results is evaluated for the 100,000-year simulation period. This evaluation is based on replacing seepage and waste package parameters with their expected values, conducting another set of 100 probabilistic simulations, and performing a new sensitivity analysis. For information on the methods used for probabilistic analysis, see Section 11.3.

#### 11.4.2.1 Uncertainty Analysis Results

Dose-rate histories for the 100,000-year simulation period are presented at the top of Figure 11-19. As noted in the figure caption, 20 realizations in the 100,000-year simulation period did not produce a dose. Also, in the 10,000-year simulation period, 27 realizations have zero dose, and in the 1-million-year simulation all realizations produced a dose. For illustration, four selected realizations are highlighted; they will be discussed in more detail later in this section. Figure 11-19 shows that the majority of dose rates tend to rise quickly between 3,000 and 10,000 years. A few realizations begin to produce doses in the 20,000- to 30,000-year time interval, with one realization not having any dose until after 90,000 years. In general, four types of behavior through time are shown:

- After the initial steep rise, many of the realizations show a steady increase in dose rate with time that continues throughout the simulation period. This type of behavior reflects significant numbers of waste-package failures over time because of corrosion in combination with relatively large fraction of waste packages contacted by seeps.
- Other realizations reach their peak early, and their dose rate gradually decreases with time over the simulation period. This type of behavior reflects the impact of juvenile waste-package failures, a lower number of waste-package failures because of corrosion, and a lower fraction of waste packages contacted by seeps.
- In some realizations, the curves dose rate remain relatively flat with time after the initial rise. This behavior is caused by juvenile failures in combination with a small number of corrosion-induced waste-package failures that are spread over the simulation period.
- In some realizations, dose rate tends to alternately increase and decrease throughout the simulation period. This behavior is caused primarily by a combination of low seepage fraction and discrete waste-package failures well separated in time, with a waste-package failure roughly coinciding with each dose-rate peak on the history curve.

The distributions of peak-dose rates to an individual located at 20 km (12.4 mi) from the repository are presented at the bottom of Figure 11-19 for the 10,000-, 100,000-, and 1-million-year simulation periods. Peak-dose rate is defined as the maximum dose rate that occurs for a given curve during the entire simulation period. This definition is illustrated by indicating the maxima of the four selected realizations and showing where they fall on the 100,000-year complementary cumulative distribution function. All realizations are weighted equally, so the lowest probability shown on the curves is 1/100. The median and mean peak-dose-rate values are also shown for each simulation period. The figure shows that peak-dose rates continue to

increase as time increases. However, the 100,000-year curve shows about a factor of 100 increase in dose rates over the 10,000-year curve, whereas the 1-million-year curve shows only a factor of five to ten increase in dose rates over the 100,000-year curve.

Figure 11-20 presents the average radionuclide contribution to the peak-dose rate. Average contributions are determined by calculating the relative individual radionuclide contributions to the peak-dose rate for each realization and averaging the relative contributions across all realizations. In the 10,000-year simulation period (see the top of Figure 11-20), contributions to peak-dose rate are dominated by Tc-99 and I-129, with a small contribution from C-14. Contributions from C-14 in the gaseous phase are not considered. In addition, 27 percent of the realizations have zero calculated dose. In the 100,000-year period (see the middle chart), contributions to peak-dose rate are dominated by Tc-99, Np-237, and I-129, with 20 percent of the realizations having zero dose. Two percent of the realizations are dominated by Pu-239. Over 1 million years (see the bottom chart), most peak-dose rates are dominated by Np-237, with a small number being dominated by I-129, Pu-239, or Pu-242 (Pu-239 and Pu-242 are lumped together in the chart); Tc-99 makes a small contribution to the peak dose rate but is never dominant in any realization.

In general, Tc-99 and I-129 are significant contributors to dose because of the following characteristics:

- Large inventories
- Long half-lives (although Tc-99 starts to decay significantly after 100,000 years)
- Highly solubilities
- No retardation during transport.

C-14 is highly soluble, and is unretarded during transport, but its half-life is so short (5,700 years) that it is a significant contributor for only the 10,000-year period. Np-237 has a large inventory and long half-life; however, it is released more slowly from the waste and travels more slowly because of retardation by adsorption. As a consequence, Np-237 is not a significant contributor to dose until after 10,000 years. Plutonium (represented by Pu-239 and Pu-242) has a very large inventory but normally is released very slowly from the waste because of low solubility and travels very slowly because of high adsorption. These two factors can both potentially be reversed because of colloidal mobilization and transport. With the models and assumptions in the TSPA-VA base case, plutonium is very mobile in colloidal form a small percent of the time. Pu-239 has the greater inventory, but it has a half-life of only 24,000 years so it is important only for the first 100,000 years or so.

The timing of the peak dose rates varies for each of the three simulation periods. Figure 11-21 presents scatter plots of the peak dose rate and the time at which peak dose rate occurs for each simulation period. In the plots, each symbol represents a single realization. The scatter plot of 10,000-year peak-dose times (see the top of Figure 11-21) shows that doses do not occur before 3,000 years and that peak dose rates are spread relatively uniformly throughout the remaining 7,000 years. Regression analyses on peak-dose times found that realizations having later peak times tend to have more waste packages in contact with seeps (and therefore more corrosion failures). Juvenile waste-package failures may lead to early releases, whereas later releases and doses are generally controlled by waste-package failures that occur because of corrosion.

Regression analyses on peak-dose times also found that later-peak-dose realizations tended to have lower net infiltration rate and, therefore, longer UZ travel times. Thirty-one realizations reach an apparent peak dose rate at 10,000 years, as indicated by the numerous symbols along the vertical line at 10,000 years; these realizations have not reached a true peak and will continue to increase if the simulation time is extended.

As shown in the middle plot of Figure 11-21, the peak-dose times in the 100,000-year period are clustered in two areas, with few points in between. Before 30,000 years, 16 percent of the realizations have their peak dose rate, and 56 percent of the realizations have their peak after 70,000 years, plus 20 percent with zero dose for the whole period. A closer examination of individual realizations showed that many of the early peak-dose rates, and especially those before 10,000 years, have only juvenile waste-package failures and no corrosion failures for the first 100,000 years. The peak-dose rates before 10,000 years are all very low, less than 0.1 mrem/year. For the 100,000-year period, peak-dose times are influenced by the number of packages in contact with seepage water and by waste-package corrosion rate. Peak-dose times again tend to increase as both the number of packages in contact with seepage increases and the number of package failures increases. The two are closely related. However, as determined from regression analysis of peak-dose times, percolation flux through the UZ and the resulting effect on travel time have less of an influence on peak-dose time in this longer simulation period. Again, several realizations reach an apparent peak-dose rate at 100,000 years, indicating that these realizations have not reached an actual peak during the 100,000-year simulation period.

The clustering of peak-dose rates in particular time periods is even more pronounced in the 1-million-year simulation, as shown in the bottom plot of Figure 11-21, with 39 percent of the peaks occurring prior to 400,000 years and 57 percent occurring after 700,000 years. This behavior is mainly because of the climate model, with most of the peak-dose rates associated with superpluvial climates. The figure shows two distinct clusters of points: one cluster at about 330,000 years and the other at about 780,000 years. These times correspond to the two superpluvial climates, with the scatter in peak-dose time largely because of the scatter in the sampled time of the superpluvial climates.

As for the 10,000-year and 100,000-year periods, waste-package corrosion rate and seepage fraction influence peak-dose times, but here the relationship is reversed, with higher corrosion rates and more seepage tending to produce earlier peak dose rates. This difference can be explained as follows. Waste-package failures and dose rates are still increasing at 100,000 years in most realizations; realizations with higher waste-package failure rates, influenced both by Alloy 22 (ASTM B 575 N06022) corrosion rate and the fraction of waste packages contacted by seeps, tend to have dose rates increasing faster as well, so their 100,000-year peak is at the end of the period. Regression analysis of peak-dose times and examination of these realizations show that they tend to have their 1 million-year peak-dose rates at the earlier superpluvial. However, realizations with low corrosion-failure rates because of low sampled Alloy 22 corrosion rate or low seepage fraction, tend to have their 10,000-year and 100,000-year peak-dose rates early because of juvenile waste-package failures. These realizations then achieve their 1-million-year peak-dose rates late in the period (or even after 1 million years), after they finally have significant numbers of corrosion-failed waste packages.

To further illustrate some of the key processes that affect calculated dose rates and their peak times, five realizations were selected for more detailed discussion for the 100,000-year and 1-million-year simulation periods. The five realizations were chosen to have a spread of peak-dose rates and peak-dose times and, therefore, a variety of different behaviors. The selected realizations are indicated with different colors in Figure 11-21, and their time histories are highlighted with the same colors in Figure 11-19 (except for the blue realization, which does not appear in Figure 11-19 because it has zero dose for the 100,000-year period).

Additional information is given in Figure 11-22, which shows the number of failed waste packages over time for the selected realizations, for the 100,000-year simulation. There are only four curves because one of the selected realizations has no waste-package failures for the first 100,000 years. In Figure 11-22, the pink and blue realizations have one juvenile waste-package failure, the cyan realization has two juvenile failures, and the red realization has no juvenile failures. The blue realization has no additional waste-package failures for the rest of the 100,000-year period, the pink realization has a small number of additional failures, and the red and cyan realizations have many corrosion failures. These numbers of waste-package failures are strongly reflected in the relative dose rates in Figure 11-19. The blue realization has a low dose rate throughout the entire period, the pink realization is higher, and the red and cyan realizations are higher yet. However, the number of waste-package failures is not the only determinant of dose, because the red realization has the highest dose rate even though the cyan realization has more waste-package failures. The primary reason that the red realization has such a high peak-dose rate even though it does not have the greatest number of waste-package failures is that it is one of the realizations with highly mobile plutonium colloids; 97 percent of its peak-dose rate is from Pu-239. The significant falloff in dose rate after 100,000 years in that realization is because of Pu-239 decay.

The dose-rate-history curves for the five selected realizations are shown in Figure 11-23 for the 1-million-year simulation period. One feature that stands out in that figure is the regularly spaced spikes on the curves. These spikes are caused by the climate changes that occur roughly every 100,000 years. The most extreme climate changes occur at the superpluvials, which happen at approximately 300,000 years and 700,000 years. The spikes at those times are larger than the other climate-change spikes, leading to the predominance of those times in the peak-time scatter plot (Figure 11-21, bottom). The climate history for one of the realizations is shown in Figure 11-24, to show that the spikes in the dose-rate curves line up with the times of climate changes. However, the climate changes are at slightly different times in different realizations.

Figure 11-25 shows the number of failed waste packages over time for the five selected realizations. The dark green realization has no waste-package failures for nearly 200,000 years, which is reflected in the dose-rate curve in Figure 11-23. The blue realization has no waste package-failures other than one juvenile failure until almost 700,000 years. Figure 11-25 shows that three realizations have an increase of waste-package failures starting at about 700,000 years. In fact, the red and cyan realizations have a similar increase in the number of failures but it cannot be seen on the log scale because they already have so many waste-package failures. The explanation for this behavior is that around 700,000 years the waste packages with no seeps dripping on them start failing. Until that time, only waste packages contacted by seeps have failed. Because the waste packages failing after 700,000 years are dry, the failures are not reflected in significantly increased dose rates in some cases (Figure 11-23). Dry waste packages

have lower rates of release (diffusive only) than wet ones (diffusive plus advective). The fraction of waste packages contacted by seeps is reflected directly in the waste-package failure curves. For example, the cyan realization has a seepage fraction for the long-term average climate of 95 percent, which allows almost all of the waste packages to fail within 300,000 years. The number of failed packages is over 10,000. The red realization has a seepage fraction for the long-term-average climate of about 36 percent, so only about a third of the waste packages fail before 300,000 years in that realization. The other three selected realizations all have seepage fraction less than one percent for the long-term-average climate, so less than one percent of the waste packages fail in those realizations, until the dry ones start failing at late times.

#### 11.4.2.2 Precision of the Base Case CCDFs

The number of realizations to use in a Monte Carlo simulation is a significant issue in terms of reliable analyses and proper allocation of resources. Therefore, the number of runs required to reliably predict peak-dose rates was examined. To verify whether 100 realizations are sufficient, the 10,000-year and 100,000-year, base-case simulations were repeated with 1,000 and 300 realizations, respectively. The resulting distributions of peak individual dose rates are compared with the 100-realization base-case results in Figure 11-26—the distributions for each time period nearly overlay. The 100-realization, distributions do not go below a probability of 0.01 because each predicted dose rate has a probability of occurrence of 1/100, or 0.01. Similarly, the 1,000- and 300-realization distributions display minimum probabilities of 0.001 and 0.003, respectively. In Figure 11-26, peak-dose rates do continue to increase as probability decreases. Increased dose rates at these low probabilities are caused by combinations of extreme uncertain parameter values that are sampled from the tails of the parameter probability distributions. However, 100 realizations appear to provide a good compromise between cost and precision.

#### 11.4.2.3 Sensitivity Analysis Results

Sensitivity-analysis results are presented for 10,000-year, peak-dose rates at the top of Figure 11-27. Parameters most important to uncertainty in peak-dose rates are depicted in bar-chart form with the most important parameter represented by the largest bar, the next most important variable represented by the next largest bar and so on. The important variables are as follows:

- A. Fraction of waste packages contacted by seepage water

$$(R^2\text{-loss} = 0.18; \text{partial rank correlation coefficient} = 0.68)$$

- B. Mean corrosion rate of Alloy 22

$$(R^2\text{-loss} = 0.13; \text{partial rank correlation coefficient} = 0.62)$$

- C. Number of juvenile waste-package failures

$$(R^2\text{-loss} = 0.11; \text{partial rank correlation coefficient} = 0.60)$$

#### D. Saturated-zone dilution factor

( $R^2$ -loss = 0.04; partial rank correlation coefficient = -0.42)

The regression model from which these results are drawn has a total of ten input variables with a total  $R^2$  of approximately 0.80. While a higher  $R^2$  would be desirable, it is considered adequate for the purpose of inferring the importance of the dominant input variables.

Regression results for the 100,000-year peak dose rates are presented next, in the middle chart of Figure 11-27. The important variables are as follows:

- A. Fraction of waste packages contacted by seepage water  
( $R^2$ -loss = 0.29; partial rank correlation coefficient = 0.77)
- B. Mean corrosion rate of Alloy 22  
( $R^2$ -loss = 0.20; partial rank correlation coefficient = 0.70)
- C. Variability of the Alloy 22 corrosion rate  
( $R^2$ -loss = 0.06; partial rank correlation coefficient = 0.49)

The regression model for this case also has ten variables and an  $R^2$  of 0.80.

Peak-dose-rate regression results for a 1,000,000-year period are presented in the bottom chart of Figure 11-27. The important variables are as follows:

- A. Fraction of waste packages contacted by seepage water  
( $R^2$ -loss = 0.51; partial rank correlation coefficient = 0.86)
- B. Saturated-zone dilution factor  
( $R^2$ -loss = 0.09; partial rank correlation coefficient = -0.56)
- C. Biosphere dose-conversion factors  
( $R^2$ -loss = 0.07; partial rank correlation coefficient = 0.51)
- D. Mean corrosion rate of Alloy 22  
( $R^2$ -loss = 0.04; partial rank correlation coefficient = 0.41)

The regression model for this case has ten variables and a final  $R^2$  of 0.82.

For peak-dose rates, the fraction of waste packages contacted by seepage water is the most important parameter in each of the three simulation periods, and its effect becomes more dominant over time. The positive effect indicated for this variable by its positive partial rank correlation coefficient happens because an increase in the number of waste packages contacted by water leads to an increase in radionuclide releases from the repository. The reason for the great importance of seepage fraction is two-fold. First, it has a direct effect on the number of waste packages that fail, as discussed in Section 11.4.2.1; and second, it has a very large uncertainty. Other parameters either have less impact on dose rate or less uncertainty.



The second most important variable in the 10,000-year and 100,000-year cases is the mean corrosion rate for Alloy 22, the inner barrier in the reference-design waste package. The positive effect for this parameter arises because increasing the Alloy 22 corrosion rate produces earlier waste-package failures and, therefore, more of the waste packages fail and release radionuclides within 10,000 years or 100,000 years. The corrosion rate for Alloy 22, however, is less important in the 1-million-year simulation period as indicated by its relatively low  $R^2$ -loss value in the bottom chart of Figure 11-27. This reduced importance is because the majority of the wet waste packages fail during the 1-million-year period, even for low Alloy 22 corrosion rates; failures of dry waste packages are only starting to be a factor near the end of the million-year period (see the discussion in Section 11.4.2.1). As a consequence, waste-package parameters appear to become less important in this longer simulation period because the quantities of radionuclides released from the repository are primarily controlled by the inventory, the fraction of waste packages in contact with seepage water, and the seepage flow rate into the waste packages.

The second most important variable in the 1-million-year case is the SZ dilution factor. This factor accounts for the reduction in radionuclide concentrations caused by transverse dispersion that occurs during transport through the SZ. The negative effect indicated for this variable (partial rank correlation coefficient = -0.56) is caused by the fact that, as dilution during transport increases, peak radionuclide concentrations at the 20-km (12.4-mi) distance decrease and, consequently, peak-dose rates decrease.

The third most important variables in the 10,000-year and 100,000-year simulation periods are the number of juvenile waste-package failures and variability in the inner-barrier Alloy 22 corrosion rate, respectively. Both of these waste-package variables have a positive effect on peak-dose rates because, as noted previously for increased Alloy 22 corrosion rates, they lead to earlier waste-package failures and, therefore, increased radionuclide releases from the repository during the given time period. The third most important variable for the 1-million-year simulation period is the biosphere dose-conversion factor. Note that the biosphere dose-conversion factors for all radionuclides were correlated for the TSPA base case; that is, they are all either low or high together, rather than allowing one radionuclide to be high while another is low.

Examination of scatter plots provides an additional way to visualize the effects of uncertain variables on peak dose rates. Two important parameters discussed above are fraction of waste packages contacted by seepage water and Alloy 22 mean corrosion rate. Scatter plots for these two parameters are shown in Figure 11-28 and Figure 11-29 for the 100,000-year simulation period. Although there is a lot of scatter in the values, a pattern of higher dose rates for higher parameter values is clearly discernable in both scatter plots. As suggested by the regression-analysis results discussed above, the relationship between fraction of waste packages contacted by seepage water and peak-dose rate is even more well defined for the 1 million-year simulation period, as shown in Figure 11-30. This strong relationship is reflected in the high  $R^2$ -loss value of 0.51 as compared to the  $R^2$ -loss value of 0.29 in the 100,000-year simulation period.

Dose rates are actually time-dependent quantities. As described in Section 11.3, a peak-dose rate represents the highest dose rate that occurred during the simulation period for a given realization. The sensitivity analysis results presented thus far are for the peak-dose rate only and, therefore,

do not give explicit information about how parameter importance changes with time, although some insight is gained about changes with time by considering three different periods. To examine how parameter importance changes with time, regression analyses were performed on dose rates at selected simulation times. The resulting values of partial rank correlation coefficients plotted as a function of time are presented in Figure 11-31. This figure shows that the number of juvenile waste-package failures is the dominant variable at early times. However, over the long term, the importance of early releases decreases as more waste packages fail. The fraction of waste packages contacted by seepage water begins to increase in importance at around 5,000 years and becomes the dominant variable after approximately 8,000 years. The Alloy 22 corrosion rate begins to increase in importance at around 5,000 years and remains important throughout the 1-million-year time period, with its importance decreasing somewhat after 400,000 years. Biosphere dose-conversion factors increase in importance at late times. The SZ dilution factor appears in the time-dependent regression model with a negative partial rank correlation coefficient because of its role in reducing radionuclide concentrations and dose rates. Some of the other variables also have small negative partial rank correlation coefficients before 5,000 years. These small negative values are probably spurious (that is, arising simply because of chance correlations among the randomly sampled variables) because they correspond to  $R^2$ -loss values smaller than 0.005 and because it is unlikely that these variables have a negative effect on dose rate. Note that the values plotted in Figure 11-31 do not correspond to the values listed earlier because the ones in the figure are for correlations with dose rate at particular times, whereas the earlier ones were for correlations with the peak-dose rate over a period of time.

Regression analyses have also been performed for intermediate performance measures, including radionuclide releases from the EBS to the UZ and from the UZ to the SZ. These performance measures are also time-dependent and can be presented in the same way that the time-dependent dose rates were presented. Analyzing intermediate performance measures is useful for isolating individual components of the total system and assessing the importance of variables among the smaller corresponding set of uncertain parameters. As an example, results are presented for releases from the EBS to the UZ in Table 11-5. Results for releases from the UZ to the SZ are similar because they are not strongly influenced by uncertain UZ transport parameters. The results shown in Table 11-5 are for the specific simulation time of 1 million years. Results for EBS releases and UZ releases at other times may be found in the YMP Technical Data Base (DTN SNT05070798001.001). Again, the dominant variable is the fraction of waste packages contacted by seepage water. The second and fourth variables, the number of cladding failures because of corrosion and the fraction of plutonium colloids transported with irreversible sorption, did not appear to have a significant effect on dose rate but are important to releases from the EBS.

#### 11.4.2.4 Impact of Parameter Uncertainty Ranges on Sensitivity Analyses

Sensitivity analyses based on linear regression must be carefully interpreted. More specifically, a regression-based sensitivity analysis will not give an uncertain variable a high importance ranking if its sample input values do not produce a relatively wide range of calculated output values. In other words, a parameter will not be assigned a high importance ranking unless it accounts for a large fraction of the variance in the output measure being analyzed. Therefore, in practice, the magnitude of peak dose rate may be strongly affected by a certain parameter, but if the range of uncertainty associated with that parameter is relatively small, this parameter may not

be found to be important. As an example, neptunium solubility was not found to be an important variable in the above analysis, but because Np-237 often dominates the calculated dose rates (see Figure 11-6) neptunium solubility does significantly influence total peak dose rate. The reason neptunium solubility did not show up as an important variable in the regression-based sensitivity analysis is largely due to the wide uncertainty ranges associated with seepage fraction and waste-package corrosion.

One approach to understanding the effects of parameters that have very wide uncertainty ranges is to perform sensitivity analyses in steps. That is, an initial regression analysis is performed, such as the one presented in Section 11.4.2.3, and important uncertain parameters are identified. In the second step, single values, such as mean or median values, are assigned to some or all of the important uncertain parameters identified in the first step and the analysis is repeated. By assigning single values to uncertain parameters identified in the first step, important parameters with less uncertainty may be identified.

The phased approach to sensitivity analysis described above was conducted to see if neptunium solubility would become an important variable once important parameters identified in the initial sensitivity analysis were assigned single deterministic values. In this TSPA simulation, the expected UZ-flow case (base infiltration map) was used. The following parameters corresponding to the base-case infiltration value were assigned single values:

- A. Seepage fraction and seep flow rate were assigned their expected values
- B. Waste-package degradation profiles for 50 percent variability and 50 percent uncertainty, resulting in an expected-value Alloy 22 corrosion rate.

To evaluate the differences between this modified parameter case and the base case, 100 simulations were conducted for the 100,000-year simulation period. The dose-rate histories for the two cases are compared in Figure 11-32. The dose histories in the modified parameter case show a much narrower spread of dose rates, as expected, since uncertainty in seepage fraction, corrosion rate, and infiltration are not present. Note that in the base case, 20 realizations did not produce a dose. In the modified parameter case all realizations produced a dose. Also, waste-package failures do not occur after 11,000 years in the modified parameter whereas in the base case many waste packages fail at later times. The distributions of peak dose rates to an individual located at 20 km (12.4 mi) from the repository are compared in Figure 11-32. The modified parameter case displays a reduction in uncertainty as expected, with an increase in high-probability low-peak-dose rates and a decrease in low-probability high-peak-dose-rates. Note that if this process of assigning expected values to important variables and conducting simulations were repeated a number of times, the distribution of peak-dose rates would continue to steepen and converge towards a vertical line located at the expected-value dose rate of about 5 mrem per year.

Regression-based sensitivity-analysis results are presented for 100,000-year peak-dose rates in Figure 11-34. Parameters most important to uncertainty in peak-dose rates are depicted in bar-chart form with the most important parameter represented by the largest bar, the next most important variable represented by the next largest bar and so on. The important variables are as follows:

- A. Solubility of neptunium  
( $R^2$ -loss = 0.33; partial rank correlation coefficient = 0.81)
- B. Saturated-zone dilution factor  
( $R^2$ -loss = 0.20; partial rank correlation coefficient = -0.73)
- C. Biosphere dose conversion factor  
( $R^2$ -loss = 0.16; partial rank correlation coefficient = 0.69)
- D. Fraction of SZ flow path in the alluvium  
( $R^2$ -loss = 0.12; partial rank correlation coefficient = -0.64)

The regression model from which these results are drawn has a total of seven input variables with a total  $R^2$  of approximately 0.82.

For peak-dose rates, neptunium solubility is the most important parameter. The positive effect indicated for this variable by its positive partial rank correlation coefficient happens because an increase in solubility leads to an increase in radionuclide releases from the repository. The second most important variable is the SZ dilution factor. The third most important variable is the biosphere dose-conversion factor. The fourth most important variable is the fraction of SZ flow path in the alluvium. The negative effect indicated for this variable (partial rank correlation coefficient of -0.64) is caused by the higher neptunium sorption of the alluvium relative to the volcanic units and resulting lower peak-dose rates.

#### 11.4.2.5 Summary

The Monte Carlo method is used to propagate parameter uncertainty through to the resulting uncertainty in peak-dose rate to an individual. The uncertainty in calculated peak dose rates is quantified by the complementary cumulative distribution function. The range or spread of peak-dose rates in each distribution represents the amount of uncertainty in the results. Some statistics of the calculated peak dose rates for each base case simulation period are summarized in Table 11-6.

As shown, the peak-dose rates are found to increase substantially with increasing simulation time. However, the coefficient of variation, or standard deviation divided by mean, indicates that relative uncertainty in the calculated dose rates does not increase appreciably in the longer simulation periods (that is, uncertainty in dose rate increases and average dose rate increases, but their ratio does not).

The times at which peak-dose rates occur were examined and found to be influenced by a number of factors, including the fraction of waste packages contacted by seepage water, Alloy 22 corrosion rate, net infiltration rate, juvenile waste-package failures, and seepage flux into the waste packages. Very early dose-rate peaks are associated with juvenile waste-package failures, and late dose-rate peaks are associated with superpluvial climates.

The sensitivity-analysis results indicate that the uncertainty in calculated peak-dose rates in all three simulation periods is primarily dominated by the fraction of packages in contact with

seepage water. Waste-package corrosion rate is also an important contributor to uncertainty in peak dose rates. In particular, the mean Alloy 22 corrosion rate is an important contributor to uncertainty, but to a lesser extent than the fraction of waste packages contacted by seepage water, particularly in the 1-million-year period. In the 1-million-year simulation, the SZ dilution factor and biosphere dose-conversion factors were found to be slightly more important than the mean Alloy 22 corrosion rate. Sensitivity analysis results also indicate that neptunium solubility is an important contributor to uncertainty in peak dose rates once uncertainties in seepage and waste package parameters are reduced or removed.

The other key information in this chapter that is not included in DOE (1998) is contained in Tables 11-1, 11-2, and 11-3, which identify all the electronic data files necessary to reproduce the dose rate results in the figures of Sections 4 and 5 of Volume 3, Draft B, of DOE (1998), including the total-system-model computer codes, and their associated input and output files. Included are DTNs which identifies a location in the YMP Technical Database that contains these electronic files. Table 11- also refers to two figures (11-33 and 11-34) that are not in DOE (1998).

## **11.5 SUMMARY OF PERFORMANCE ASSESSMENT WORK REQUIRED BETWEEN THE VIABILITY ASSESSMENT AND THE SITE RECOMMENDATION AND LICENSE APPLICATION**

The objective of the TSPA-VA was to conduct and document "a total system performance assessment based upon the design concept and the scientific data and analysis available by September 30, 1998, describing the probable behavior of the repository in the Yucca Mountain geological setting relative to the overall system performance standards" (Energy and Water Development Appropriations Act 1997). This document contains descriptions of the design concept and the scientific data and analyses upon which the TSPA-VA have been based. The results of these analyses have been presented in this chapter as well as Volume 3 of DOE (1998).

In examining and summarizing results describing the "probable" behavior of the Yucca Mountain repository system, it is important to understand that the evaluations are indicators of the postclosure performance of the proposed repository. Although every attempt has been made to incorporate the most current understanding of key processes affecting the long-term behavior of Yucca Mountain, such projections are uncertain. Although many of these uncertainties will still remain at the time of the license application, DOE will reduce the significant uncertainties sufficiently and modify the design as appropriate to provide reasonable assurance that postclosure performance objectives will be met. The uncertainty is a result of several factors:

- *The time periods are long.* The period for the quantitative analyses extends to 10,000 years and beyond. Over these long periods, there is uncertainty in the definition of likely future environments. This period is also long compared to available information about a number of principal factors affecting repository performance such as the degradation rates of corrosion-resistant metals.
- *The site is heterogeneous.* Water movement in the unsaturated and SZs at Yucca Mountain is expected to vary with location because of the heterogeneous nature of the

fractured rocks. Precisely defining the flow paths and geochemical interactions along the flow paths is not possible.

- *The system is coupled.* Coupled interactions are expected to occur near the emplaced wastes. These interactions include thermal, chemical, hydrologic, and mechanical processes that can influence one another. For example, the chemical alteration of the rock caused by a temperature increase may cause the hydrologic properties of the rock to change. It is difficult to predict the magnitude and extent of these changes with precision.
- *Future populations are unknown.* It is not possible to reasonably forecast changes in human activities. Therefore, the doses calculated are based on the activities of the present-day population in the region around Yucca Mountain. This assumption, which is consistent with internationally accepted recommendations, implies that the doses represent the range of likely performance of a repository for a hypothetical population.

Although these uncertainties are recognized in the analyses and interpretation of results, they do not detract from the goal of objectively evaluating how the system is likely to perform.

The TSPA-VA analyses represent a significant improvement over previous TSPA iterations. The planned work for the TSPA for the site recommendation and license application will focus on reducing the remaining uncertainties for key principal factors affecting the long-term performance of the repository. Planned work will also evaluate approaches for achieving defense in depth and margin. This work will support the evaluation of alternative designs, design features, and design options. Finally, the planned work addresses key technical issues identified by the Nuclear Regulatory Commission.

The planned work is organized into the following categories:

- Model abstractions
- TSPA analyses
- Design support.

#### **11.5.1 Model Abstractions**

Because of the overall uncertainty and complexity of the repository system, the process models used in TSPA analyses must be simplified to reproduce and bound the underlying detailed process model. This simplification or abstraction retains the basic form of the process model. These model abstractions are required to maximize the use of finite computational resources while maintaining a sufficient range of sensitivity and uncertainty analyses. Once the abstracted models are developed, they are used for a performance assessment of the repository/geologic system.

Work planned to complete the abstraction process is organized into the following six categories:

- UZ flow and transport
- Near-field environment

- Waste-package degradation
- Waste-form degradation and engineered-barrier-system transport
- SZ flow and transport and biosphere uptake
- Disruptive events.

These components are then combined to assess the expected behavior of the system. The combined components include alternative conceptual models, variability and uncertainty in parameters and processes, and a sufficient level of detail to represent the aspects of each process important to performance.

The first step in the process of model abstraction is to identify uncertainties in the TSPA-VA and each supporting model. This effort will consider comments from the expert elicitations completed for the VA, comments from the TSPA-VA Peer Review Panel, and comments from organizations such as the Nuclear Regulatory Commission and the Nuclear Waste Technical Review Board. Model enhancements will be defined along with approaches to addressing the identified uncertainties and approaches to treating defense-in-depth and margin for each of the models.

All of this work addresses the Nuclear Regulatory Commission key technical issue on the TSPA and technical integration. Specifically, the model abstractions will provide part of the technical basis to address the following subissue of this key technical issue: Are the major components of the DOE TSPA methodology (i.e., model abstractions; probability and consequences of relevant features, events, and processes; parameter and model uncertainties; and bounding assumptions) sufficiently comprehensive to provide a defensible safety case?

**Unsaturated Zone Flow and Transport** - This activity will refine the abstractions of process models for climate, infiltration, percolation, ambient seepage, and transport through the UZ. The primary focus will be placed on transport through the UZ. New information from studies of UZ flow and transport processes and updated process models will be evaluated. This activity will develop and document the technical basis for the refined abstractions that will be used in TSPA for the site recommendation and license application.

The work contributes to addressing Nuclear Regulatory Commission key technical issues on unsaturated and saturated flow, and radionuclide transport under isothermal conditions.

**Near-Field Environment** - This activity refines the abstraction of process models for thermal hydrology, ambient geochemistry, and near-field environment. Results from field thermal tests and laboratory tests and updated processes models will be evaluated. Process modeling will assess design options and features, such as dripshields, backfill, and Richards' barriers to evaluate their contribution to performance. The effects of heating and excavation on flow, dryout by ventilation, and water diversion by line loading will also be evaluated. The results of these abstractions will also address seepage into drifts, dripping onto waste packages, humidity and temperature at the waste package, and chemistry on the waste package. The results of this work will be documented to provide the technical basis for processes in the near-field environment for the TSPA for the site recommendation and license application.

The work contributes to addressing Nuclear Regulatory Commission key technical issues on thermal effects on flow and evolution of the near-field environment.

**Waste-Package Degradation** - This activity will refine the abstraction of the process models for waste-package degradation. New data from the waste-package materials testing program, results of material selection for the initial waste package for site recommendation and the license application, and the evaluation of design features will be used to update the abstraction of waste-package degradation processes. The work will be documented as part of the technical basis for TSPA for the site recommendation and license application.

This work contributes to addressing the Nuclear Regulatory Commission key technical issue on container life and source term.

**Waste-Form Degradation and Engineered-Barrier-System Transport** - This activity will refine the abstraction of process models for cladding degradation, waste form integrity, colloid formation and stability, and solubility and transport through the EBS. The work will focus on the evaluation and abstraction of the updated process models for cladding degradation, colloid formation, and studies of solubility. The work will be documented as part of the technical basis of the TSPA for the site recommendation and license application.

This work contributes to addressing the Nuclear Regulatory Commission key technical issue on container life and source term.

**Saturated-Zone Flow and Transport and Biosphere** - This activity will refine the abstraction of process models for transport through the SZ and the biosphere. New site data on hydraulic parameters from testing at the C-well complex, on SZ hydrochemistry, and results of testing in wells in the Amargosa Valley and Nevada Test Site and updated process models for SZ flow and transport will be evaluated. Additional environmental data and the updated biosphere process model will also be evaluated. This work will provide the technical basis for the updated abstraction of SZ flow and transport and biosphere processes for TSPA for the site recommendation and license application.

This work contributes to addressing Nuclear Regulatory Commission key technical issues on unsaturated- and SZ flow and radionuclide transport under isothermal conditions by providing refined model abstractions.

**Disruptive Events** - Previous work has identified four disruptive events that might effect the long-term performance of the repository; volcanic activity, earthquakes, inadvertent human intrusion, and nuclear criticality.

Studies of volcanoes and earthquakes have reached a level of maturity for which only limited new information is required. The remaining work will focus on completing any refinements to the hazard analyses that are required to provide a documented technical basis of the effect of these disruptive events on the performance of the repository system. This work contributes to addressing the Nuclear Regulatory Commission key technical issues of igneous activity and structural deformation and seismicity by documenting the hazard associated with these disruptive events.



Based on guidance from the Environmental Protection Agency and the National Academy of Science, models will be developed to evaluate the consequences of inadvertent human intrusion at the Yucca Mountain site. These models will evaluate direct and indirect effects from drilling on the transport of radionuclides to the SZ and ground surface. The performance assessment will use scenarios that have the potential for either high consequences or high relative probabilities of occurrence and develop model parameter distributions that reflect the variabilities and uncertainties in the conceptual models and data. This work will provide the technical basis for the assessment of inadvertent human intrusion.

Nuclear criticality could occur if the engineered control measures in the waste package fail or if fissile material in the waste forms a critical configuration in the surrounding rock. Work is required to refine the consequences of potential criticalities and to document the technical basis for the assessment of this potentially disruptive event.

### **11.5.2 Total System Performance Assessment Analyses**

Once the model abstractions have been refined, they must be appropriately linked for the assessment of system performance. The TSPA analyses will then be completed to evaluate the expected behavior of the repository system. A wide range of sensitivity and uncertainty analyses will also be conducted to evaluate the significance of the uncertainties in parameters and conceptual models. The sensitivity and uncertainty analyses will help to identify the key site and design features of the repository system that have the greatest impact on repository performance.

Before the TSPA analyses start, the assumptions to be used in the analyses will be defined and justified. These assumptions include the following:

- The basis for which scenarios will be considered in the TSPA analyses for site recommendation and license application
- The basis for which alternative conceptual models and parameters from the abstraction activities will be considered in the TSPA analyses for site recommendation and license application
- The basis for which designs (both repository and waste package) will be considered in the TSPA analyses for site recommendation and license application
- The basis for refining the base case from which all sensitivities will be conducted

These assumptions will define the range of analyses that will be conducted for the TSPA for the site recommendation and license application. The base case will be constructed from a composite of the scenarios refined from the TSPA-VA. It will include the base hydrologic scenarios and some perturbations on the base case (e.g., climate change). The base case will attempt to incorporate alternative conceptual models for degradation of the waste package, dissolution of the waste form, transport through the near field and the EBS, and aqueous transport in the unsaturated and SZs.

As part of the development of the TSPA for site recommendation and license application, evaluations of various design alternatives, features, and options will be conducted in support of development of the technical basis for selecting the initial site recommendation and license application design. These evaluations will build on the analyses of the VA reference design, design options and design alternatives that were evaluated in TSPA-VA analyses and in support of the draft environmental impact statement. The focus of the work will be to evaluate a reasonable range of uncertainty in the design features included in the options and alternatives study and to couple this uncertainty analysis with reasonably bounded uncertainty in the natural system that may be compensated by these design enhancements. In some cases, this work may require additional abstractions of process models from the scientific program and from studies of the waste package and EBS. These analyses will also contribute to the evaluation of defense-in-depth and design margin.

The models for TSPA analyses will be derived from the abstractions of the process models. Stochastic techniques will be used for the analyses to produce results based on a variety of model inputs. If required, alternative numerical representations of processes will be used. The results will be presented as distribution functions showing probability versus effect (e.g., dose, release, or other risk measures). The activities required in this effort include:

- Integrate all features, processes, and events developed in various abstraction activities into a defensible representation of those features, processes, and events that are most important
- Combine all relevant abstracted model results, relevant simplified process models, relevant design information, and TSPA-specific assumptions into the selected TSPA software
- Determine performance for the base-case set of parameters and evaluate the impact of alternative parameter probability distribution functions
- Review and revise the base-case results, as appropriate.

Once the base case has been completed satisfactorily, a range of sensitivity and uncertainty analyses will be conducted to evaluate the impact of parameter uncertainty, conceptual uncertainty, and scenario uncertainty. The impact on design alternatives will also be evaluated. The required activities include the following:

- Generate complementary CCDFs, which define the probability of the resulting performance, to evaluate parameter uncertainty. CCDFs will not be generated for all conceptual and scenario uncertainties or design alternatives; however, a select group focusing on the most significant processes or uncertainties will be evaluated.
- Analyze process sensitivity to define the key parameters that impact the total system performance.
- Use CCDFs to evaluate uncertainty in those cases where parameter sensitivity is not evaluated explicitly.

- Review the sensitivity analyses with the site and design organizations before the analyses are documented in the TSPA for the site recommendation and license application to identify key uncertainties in site and design-related processes, models, and parameters that significantly impact performance.
- Prioritize the focus of the sensitivity analyses. This focus will be based on the importance of the model as identified in the TSPA for the site recommendation and license application and the repository safety strategy available at the time of the analyses.

Results of the TSPA for the site recommendation and license application to assess compliance of the potential repository system at Yucca Mountain will be interpreted and documented. This activity will include the following steps:

- Document the base-case assessment of postclosure performance in sufficient detail to understand how all the elements in the TSPA analysis have been combined. Document the full suite of sensitivity analyses so the significance of alternative assumptions can be evaluated to increase confidence in the overall analysis.
- Choose a reasonably conservative reference case.
- Conduct sensitivity analyses to describe the impact of the conservative assumptions.
- Investigate possible low-likelihood models, or parameter values, to illustrate the potential impact of such unlikely assumptions on performance.
- Describe the implications of these results for performance confirmation and design and recommend testing and design modifications that could reduce uncertainty or enhance performance.
- Complete a technical, regulatory, and management review of the TSPA for the site recommendation and license application document to ensure its suitability for licensing and revise the document, as appropriate.

Using appropriate degrees of detail and illustration, summary documents for scientific and public audiences will be developed. Visualization techniques for displaying the analysis and results on the World Wide Web, including hypertext versions of regulatory, scientific community, and public documents will also be developed.

The completion of TSPA for the site recommendation and license application will support addressing the Nuclear Regulatory Commission key technical uncertainty on the TSPA and technical integration by documenting the methodology for implementing TSPA analyses and documenting the TSPA analyses. This work specifically addresses the following sub-issue of this key technical issue: Are the major components of the DOE TSPA methodology (i.e., model abstractions; probability and consequences of the relevant features, events, and processes; parameter and model uncertainties; and bounding assumptions) sufficiently comprehensive to provide a defensible safety case?

### 11.5.3 Design Support

This work will continue the quantitative evaluation of design alternatives, features, and options to support development of the technical basis for selecting the initial site recommendation and license application design. The evaluations will build on the TSPA-VA analyses of the VA reference design, design options and design alternatives that were evaluated in TSPA analyses supporting the draft environmental impact statement. The focus of the work will be to evaluate a reasonable estimate of uncertainty in the design features included in the options and alternatives study and to couple this uncertainty analysis with reasonably bounded uncertainty in the natural system that may be compensated for by these design enhancements. This will require additional abstractions of process models from the scientific program and from studies of the waste package and EBS. These analyses contribute to the evaluation of defense-in-depth and design margin.

The analysis will focus on key functions of the repository system; keeping water off the waste packages, increasing waste package lifetime, limiting the rate of release of radionuclides from breached waste packages, and reducing concentrations of radionuclides in groundwater during transport away from the waste packages.

### 11.5.4 Concluding Remarks

The current assessment of expected repository performance is summarized in Volume 3 of the VA document. The probable performance has been described in the context of how the four elements of the repository safety strategy work in concert to first minimize the contact of water with the waste and then reduce the concentration of any radionuclides that are released from the engineered barriers.

The Yucca Mountain site provides favorable features for limiting the contact of water with the waste. Its location in an arid region and the nature of the site itself limit the amount of water that can reach the repository. The site provides a thick UZ where the waste can be placed deep below the surface and well above the water table; the waste packages would therefore be protected from changes in conditions at the surface while still being kept well away from the water table. The site would therefore provide predictable and stable environments for design of engineered barriers that can further limit the exposure of waste to water.

Performance assessment and design studies indicate that there are a number of options for the design to keep water away from the waste (see Chapter 5, Section 5.12.5). They indicate for example that the highly corrosion-resistant inner container and the thick steel outer container of the reference design of this VA each provide effective barriers against water. Although there are some issues that must still be addressed, the estimates indicate that robust waste packages could be designed to remain intact for hundreds of thousands of years in the repository environments. The studies also indicate that the spent fuel cladding would likely provide an additional barrier to water contacting the waste, even if the outer and inner waste-package barriers were to be breached.

The postclosure safety case will also explicitly consider processes and events that could disrupt a repository at the Yucca Mountain site. These include disruptive natural processes (seismicity and volcanism), potential human intrusion associated with exploration for natural resources, and

nuclear criticality. In each of these disruptive scenarios, the analyses presented in Chapter 10 indicate there is no substantial increase in the risk to long-term public health or safety.

The TSPA-VA also finds that the engineered system in the reference design has considerable impact on repository performance for a long period, on the order of several hundred thousand years. For very long periods of time, however, the natural system dominates performance. The TSPA-VA shows that some factors and how they are modeled can have especially important influences on performance: for example, the corrosion characteristics of Alloy 22, the dilution of radionuclides in the transport pathways, and the transport of radionuclides as colloids. The TSPA-VA reinforces some ideas about performance; for example, that it is important to isolate waste from advective liquid flow and that, for a dose-based standard, the rate of releases of radionuclides from a repository and the dilution in the environment are important. And finally, the TSPA-VA points out areas where improvements could be made to the TSPA models and data, including the most important uncertainties that could be reduced and the most important assumptions that could be addressed in the future.

## 11.6 REFERENCES

- Andrews, R. W., T. F. Dale, and J. A. McNeish, 1994. *Total System Performance Assessment - 1993: An Evaluation of the Potential Yucca Mountain Repository*. B00000000-01717-2200-00099, REV 01. Las Vegas, Nevada: INTERA. NNA.19940406.0158
- Conca, J. L., 1990. "Diffusion Barrier Transport Properties of Unsaturated Paintbrush Tuff Rubble Backfill," High Level Radioactive Waste Management Conference, Las Vegas, Nevada, pp. 394-401. [MICROFLIM]
- Conca, J. L., and J. Wright, 1992. "Diffusion and Flow in Gravel, Soil, and Whole Rock," Applied Hydrogeology, Vol. 1, pp. 5-24. 224081
- CRWMS M&O. 1995. *Total System Performance Assessment-1995: An Evaluation of the Potential Yucca Mountain Repository*. B00000000-01717-2200-00136 REV 01. Las Vegas, Nevada: TRW Environmental Safety Systems. MOL.19960724.0188.
- CRWMS M&O. 1997. *Saturated Zone Flow and Transport Model Expert Elicitation Project*. San Francisco, California: Geomatrix Consultants, Inc for TRW Environmental Safety Systems, Las Vegas, Nevada. MOL.19980224.0353.
- CRWMS M&O 1998a. *Software Routine Report for WAPDEG (Version 3.07)*, CSCI: 30048 v 3.07, DI: 30048-2999, Rev 01, MI: 30048-M04-001, Rev. 01, SCR: LSCR 170.
- CRWMS M&O 1998b. *Software Routine Report for SZ\_CONVOLUTE*, DI 30038-2999, REV 00, VA Trace Code VA6-WFMD. PLACE: PUBLISHER.
- DOE (U.S. Department of Energy), 1998. *Viability Assessment of a Repository at Yucca Mountain*. DOE/RW/XX-XXXX, 5 Volumes. Washington, D.C.: U.S. Government Printing Office.
- Duguid, J.O.; McNeish, J.A.; Vallikat, V.; Cresap, D.; and Erb, N.J. 1997. *Total System Performance Assessment Sensitivity Studies of U.S. Department of Energy Spent Nuclear Fuel*. A00000000-01717-5705-00017 REV 01. Prepared for National Spent Nuclear Fuel Program, U.S. Department of Energy, Idaho Operations Office, Idaho Falls, Idaho. Las Vegas, Nevada: Author. CATALOG NUMBER. On Order.
- Finsterle, S., Pruess, K., and Fraser, P. ITOUGH2 Software Qualification, LBNL-39489, UC-800, 1996. MOL.19970619.0040
- Golder, 1998, RIP Theory Manual and User's Guide, Golder Associates Inc., March 1998. [ON ORDER]
- Helton, J.C. 1993. "Uncertainty and Sensitivity Analysis Techniques for Use in Performance Assessment for Radioactive Waste Disposal." *Reliability Engineering & System Safety*, 42 (2-3), 327-367. [Barking, Essex, England]: Elsevier Applied Science Publishers; New York, New York: Distributed by Elsevier Science. 237878

Helton, J.C.; Bean, J.E.; Berglund, J.W.; Davis, F.J.; Economy, K.; Garner, J.W.; Johnson, J.D.; MacKinnon, R.J.; Miller, J.; O'Brien, D.G.; Ramsey, J.L.; Schreiber, J.D.; Shinta, A.; Smith, L.N.; Stoelzel, D.M.; Stockman, C.; and Vaughn, P. 1998. *Uncertainty and Sensitivity Analysis Results Obtained in the 1996 Performance Assessment for the Waste Isolation Pilot Plant*. SAND98-0365. Albuquerque, New Mexico: Sandia National Laboratories.

Iman, R.L.; Davenport, J.M.; Frost, E.L.; and Shortencarier, M.J. 1980. *Stepwise Regression With PRESS and Rank Regression (Program User's Guide)*. SAND79-1472. Albuquerque, New Mexico: Sandia National Laboratories.

Napier, B.A., Peloquin, R.A., Strenge, D.L., and Ramsdell, J.V. 1988. "GENII- The Hanford Environmental Radiation Dosimetry Software System Volume 1: Conceptual Representation" PNL-6584 Vol. 1 1988. 206898

National Academy of Sciences/National Research Council. 1995. *Technical Bases for Yucca Mountain Standards*. Committee on Technical Bases for Yucca Mountain Standards, Board on Radioactive Waste Management. Washington, D.C.: National Academy Press. 205 pp. 104273. 217588

National Research Council, 1990. *Health Effects of Exposure to Low Levels of Ionizing Radiation, Beir V*. Committee on the Biological Effects of Ionizing Radiations, Board on Radiation Effects Research, Commission on Life Sciences. Washington, DC: National Academy Press. 2845

NCRP, 1987. *Exposure of the Population in the United States and Canada from Natural Background Radiation*, NCRP Report No. 94, National Council on Radiation Protection and Measurements, Bethesda, MD 20814. 101308

Nitao, J., 1996. Reference Manual for the NUFT Flow and Transport Code. Earth Sciences Department, Lawrence Livermore National Laboratory, March 20, 1996. [ON ORDER]

Pruess, K., TOUGH2 - A general-purpose numerical simulator for multiphase fluid and heat flow, Technical Report LBL-29400, Lawrence Berkeley National Laboratory, 1991. NNA.19940202.0088

RamaRao, B.S.; Mishra, S.; Sevougian, S.D.; and Andrews, R.W. 1998. "Uncertainty Importance of Correlated Variables in the Probabilistic Performance Assessment of a Nuclear Waste Repository." *SAMO 98: Second International Symposium on Sensitivity Analysis of Model Output, Venice, Italy, April 19-22, 1998*. Las Vegas, Nevada: Civilian Radioactive Waste Management System, Management and Operating Contractor. MOL.19980514.0024.

Robinson, B. A., A. V. Wolfsberg, H. S. Viswanathan, G. Y. Bussod, C. W. Gable, A. Meijer, The Site-Scale Unsaturated Zone Transport Model of Yucca Mountain, Los Alamos National Laboratory YMP Milestone SP25BM3, 1997. MOL.19980203.0570

Wilson, M.L., J.H. Gauthier, R.W. Barnard, G.E. Barr, H.A. Dockery, E. Dunn, R.R. Eaton, D.C. Guerin, N. Lu, M.J. Martinez, R. Nilson, C.A. Rautman, T.H. Robey, B. Ross, E.E. Ryder, A. R.

Schenker, S.A. Shannon, L.H. Skinner, W.G. Halsey, J. Gansemer, L.C. Lewis, A.D. Lamont, I.R. Triay, A. Meijer, and D.E. Morris, 1994. *Total-System Performance Assessment for Yucca Mountain- SNL Second Iteration (TSPA-1993)*," SAND93-2675, Sandia National Laboratories, Albuquerque, NM. NNA.19940112.0123

Wolery, T. J., 1992. EQ3/6, A Software Package for Geochemical Modeling of Aqueous Systems, *UCRL-MA-110662*, Lawrence Livermore National Laboratory, Livermore, CA, September 14, 1992. NNA.19921023.0028

Zyvoloski, A. G., B. A. Robinson, Z. A. Dash, and L. L. Trease, 1996. Models and Methods Summary for the FEHM Application, Technical Report LA-UR-94-3787, Rev. 1, Los Alamos National Laboratory, October 23, 1996. 222337



**Basket**

## **APPENDIX A**

### **DESCRIPTION OF TSPA-VA BASE CASE UNCERTAIN PARAMETERS**

INTENTIONALLY LEFT BLANK

## APPENDIX A

### DESCRIPTION OF TSPA-VA BASE CASE UNCERTAIN PARAMETERS

The purpose of this appendix is to document the uncertain input parameters used within RIP and FEHM in the Total System Performance Assessment-Viability Assessment (DTN MO9807MWDRIP00.000). The description and analysis of the uncertain parameters are summarized in an Excel spreadsheet containing 177 parameters (DTN SNT05070798001.002). The parameters are listed alphabetically by series. Information documented for each uncertain parameter includes:

- A. Variable name (column A)
- B. Variable description (column B)
- C. Code the parameter is used in (column C)
- D. Calculation or process parameter is used in (column D)
- E. Probability distribution specified as input (column E)
- F. Mean, standard deviation, minimum and maximum of the specified distribution (columns F, G, H, and I, respectively).
- G. Name of the correlated variable, if specified (column J)
- H. Correlation coefficient specified (column K)
- I. Graphical comparison of the frequency distribution of the samples generated as input to the TSPA-VA and the continuous distribution fit to the samples (column L)
- J. Graphical comparison of the cumulative distribution of the samples generated as input to the TSPA-VA and the continuous distribution fit to the samples (column M)
- K. Scatter plot of correlated variable pairs sampled in the TSPA-VA (column N)
- L. Rank order (column O) and linear correlation coefficients (column P)
- M. Box plots displaying the range of sampled values (column Q)
- N. Graphical comparison of the frequency distribution of the log of the samples generated as input to the TSPA-VA and the continuous distribution fit to the log of the samples for log probability distributions (column R)

The commercial software package Crystal Ball Version 4.0e was used to calculate the goodness-of-fit of the random samples for each uncertain parameter to a number of continuous distributions. Three tests for goodness-of-fit were performed: the Chi-square, the Kolmogorov-Smirnov, and the Anderson-Darling. The distribution with the best overall fit, consistent with

the requested distribution, is compared to the output. For all practical purposes, the distribution requested can be fit with a high degree of correspondence to the distribution of samples generated in the Viability Assessment.

The goodness-of-fit tests are sets of mathematical tests performed to find the fit between a standard probability distribution and the distribution of a set of data. The Chi-square test is the most common of the goodness-of-fit tests. It gauges the general accuracy of the fit. The test breaks down the distribution into areas of equal probability and compares the data points within each area to the number of expected data points. The Kolomogorov-Smirnov test is a measure of the largest vertical distance between two cumulative distributions. The Anderson-Darling test weights the differences between two distributions at their tails greater than their mid-ranges

Where a correlation coefficient is specified, a scatter diagram of the dependent variable versus the independent variable is provided. Both linear (column P) and rank (column O) correlation coefficients are calculated as a measure of the degree of correlation. For some uncertain parameters, a probability distribution of the log of the parameter is defined. In these cases, a goodness-of-fit test is conducted on the logs of the sampled values.

A		B	C	D	E	F	G	H	I	J	K	L	M
Parameter Name		Description	Code	Use in the Calculation and/or Process Model	Distribution Type	Mean	Std Dev	Minimum	Maximum	Correlated To	Correlation Coefficient	Frequency Distribution of TSPA-VA Output (1)	Cumulative Distribution of TSPA-VA Output
1	AFLTA1	Sampled fraction of packages with seeps, long term average, Region-1	RIP	Waste package	beta	FMHL1	FSDL1	0.0	1.0	SFDRY1	1.0		
2		30 simulations				0.168	0.283						
3		60 simulations				0.291	0.359						
4		10 simulations				0.489	0.414						
5													
6													
7													
8													
9	AFLTA2	Sampled fraction of packages with seeps, long term average, Region-2	RIP	Waste package	beta	FMHL2	FSDL2	0.0	1.0	SFDRY1	1.0		
10		30 simulations				0.066	0.112						
11		60 simulations				0.232	0.323						
12		10 simulations				0.429	0.423						
13													
14													
15													
16													
17	AFLTA3	Sampled fraction of packages with seeps, long term average, Region-3	RIP	Waste package	beta	FMHL3	FSDL3	0.0	1.0	SFDRY1	1.0		
18		30 simulations				0.085	0.144						
19		60 simulations				0.243	0.329						
20		10 simulations				0.439	0.423						
21													
22													
23													
24													
25	AFLTA4	Sampled fraction of packages with seeps, long term average, Region-4	RIP	Waste package	beta	FMHL4	FSDL4	0.0	1.0	SFDRY1	1.0		
26		30 simulations				0.175	0.288						
27		60 simulations				0.314	0.373						
28		10 simulations				0.511	0.41						
29													
30													
31													
32													
33	AFLTA5	Sampled fraction of packages with seeps, long term average, Region-5	RIP	Waste package	beta	FMHL5	FSDL5	0.0	1.0	SFDRY1	1.0		
34		30 simulations				0.0759	0.129						
35		60 simulations				0.283	0.328						
36		10 simulations				0.435	0.422						
37													
38													
39													
40													
41	AFLTA6	Sampled fraction of packages with seeps, long term average, Region-6	RIP	Waste package	beta	FMHL6	FSDL6	0.0	1.0	SFDRY1	1.0		
42		30 simulations				0.18	0.291						
43		60 simulations				0.328	0.381						
44		10 simulations				0.525	0.408						
45													
46													
47													
48													
49													

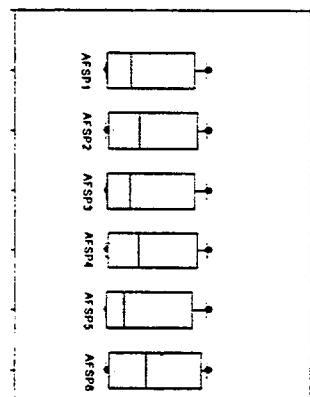
	N	O	P	Q	R
	Scatter Plot	Rank Correlation	Linear Correlation	Series Analysis (2)	Distribution of the logs of the sampled values
1		0.934	0.695		
2					
3					
4					
5					
6					
7					
8					
9					
10		0.94	0.875		
11					
12					
13					
14					
15					
16					
17					
18		0.938	0.848		
19					
20					
21					
22					
23					
24					
25					
26		0.936	0.683		
27					
28					
29					
30					
31					
32					
33					
34		0.939	0.861		
35					
36					
37					
38					
39					
40					
41					
42		0.936	0.875		
43					
44					
45					
46					
47					
48					
49					

note: The parameters FMNL and FSDL, 1 through 6, are defined as the mean and standard deviation of AFLTA, 1 through 6, respectively.

The specification of the input distribution as a function of three different sets of mean and standard deviation and the unequal sampling frequency generated ensemble statistics strongly skewed to the right.

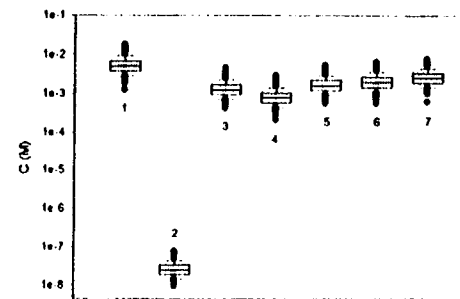
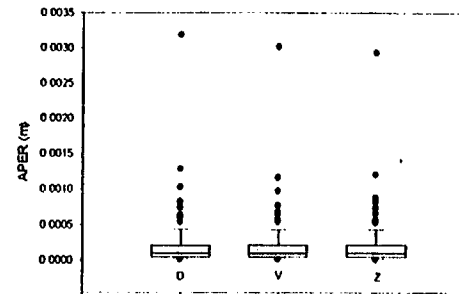
1	A	B	C	D	E	F	G	H	I	J	K	L	M
	Parameter Name	Description	Code	Use in the Calculation and/or Process Model	Distribution Type	Mean	Std Dev	Minimum	Maximum	Correlated To	Correlation Coefficient	Frequency Distribution of TSPA-VA Output (1)	Cumulative Distribution of TSPA-VA Output
50	AFSP1	Sampled fraction of packages with seeps, super phivial, Region 1	RIP	Waste package	beta	FMNS1	FSDS1	0.0	1.0	SFDRY1	1.0	Frequency Comparison	Cumulative Comparison
51		30 simulations				0.242	0.329						
52		60 simulations				0.441	0.421						
53		10 simulations				0.636	0.394						
54													
55													
56													
57	AFSP2	Sampled fraction of packages with seeps, super phivial, Region 2	RIP	Waste package	beta	FMNS2	FSDS2	0.0	1.0	SFDRY1	1.0	Frequency Comparison	Cumulative Comparison
58		30 simulations				0.269	0.346						
59		60 simulations				0.468	0.417						
60		10 simulations				0.671	0.392						
61													
62													
63													
64													
65	AFSP3	Sampled fraction of packages with seeps, super phivial, Region 3	RIP	Waste package	beta	FMNS3	FSDS3	0.0	1.0	SFDRY1	1.0	Frequency Comparison	Cumulative Comparison
66		30 simulations				0.237	0.326						
67		60 simulations				0.435	0.422						
68		10 simulations				0.632	0.395						
69													
70													
71													
72													
73	AFSP4	Sampled fraction of packages with seeps, super phivial, Region 4	RIP	Waste package	beta	FMNS4	FSDS4	0.0	1.0	SFDRY1	1.0	Frequency Comparison	Cumulative Comparison
74		30 simulations				0.266	0.343						
75		60 simulations				0.465	0.417						
76		10 simulations				0.668	0.392						
77													
78													
79													
80													
81	AFSP5	Sampled fraction of packages with seeps, super phivial, Region 5	RIP	Waste package	beta	FMNS5	FSDS5	0.0	1.0	SFDRY1	1.0	Frequency Comparison	Cumulative Comparison
82		30 simulations				0.215	0.312						
83		60 simulations				0.413	0.425						
84		10 simulations				0.604	0.397						
85													
86													
87													
88													
89	AFSP6	Sampled fraction of packages with seeps, super phivial, Region 6	RIP	Waste package	beta	FMNS6	FSDS6	0.0	1.0	SFDRY1	1.0	Frequency Comparison	Cumulative Comparison
90		30 simulations				0.291	0.359						
91		60 simulations				0.49	0.414						
92		10 simulations				0.698	0.39						
93													
94													
95													
96													
97													



N		O		P		Q		R	
Scatter Plot		Rank Correlation		Linear Correlation		Series Analysis (2)		Distribution of the log of the sampled values	
50		0.945		0.938		<div><p>AFSP</p><p>note: The parameters FAMS and FSDS, 1 through 6, are derived as the mean and standard deviation of AFSP, 1 through 6, respectively.</p><p>The specification of the input distribution as a function of three different sets of mean and standard deviation and the unequal sampling frequency generated ensemble statistics strongly skewed to the right.</p></div>			
51									
52									
53									
54									
55									
56		0.95		0.945					
57									
58									
59									
60									
61									
62									
63									
64									
65		0.947		0.933					
66									
67									
68									
69									
70									
71									
72		0.95		0.967					
73									
74									
75									
76									
77									
78									
79									
80									
81		0.94		0.911					
82									
83									
84									
85									
86									
87									
88									
89		0.949		0.945					
90									
91									
92									
93									
94									
95									
96									
97									

A		B	C	D	E	F	G	H	I	J	K	L	M
Parameter Name		Description	Code	Use in the Calculation and/or Process Model	Distribution Type	Mean	Std Dev	Minimum	Maximum	Correlated To	Correlation Coefficient	Frequency Distribution of TSPA-VA Output (1)	Cumulative Distribution of TSPA-VA Output
98	APERD	Sampled fracture aperture (m) over long term	FE1RU(UZ)	Unsaturated zone flow and transport	lognormal	1.44E-04	3.70E-04	0.0	1.0	STDRV1	1.0	Frequency Comparison	Cumulative Comparison
99													
100													
101													
102													
103													
104													
105													
106	APERV	Fracture aperture (m), vitric	FE1VM(UZ)	Unsaturated zone flow and transport	lognormal	1.94E-04	3.72E-04					Frequency Comparison	Cumulative Comparison
107													
108													
109													
110													
111													
112													
113	APERZ	Fracture aperture (m), zeolitic	FE1MZ(UZ)	Unsaturated zone flow and transport	lognormal	1.94E-04	3.72E-04					Frequency Comparison	Cumulative Comparison
114													
115													
116													
117													
118													
119													
120													
121	C1	Carbonate concentration of repository water (M) from 0 - 200 years	RIP	Geochemical environment	lognormal	5.60E-03	2.70E-03					Frequency Comparison	Cumulative Comparison
122													
123													
124													
125													
126													
127													
128													
129	C2	Carbonate concentration of repository water (M) from 200 - 1,000 years	RIP	Geochemical environment	lognormal	2.80E-08	1.30E-08					Frequency Comparison	Cumulative Comparison
130													
131													
132													
133													
134													
135													
136													
137	C3	Carbonate concentration of repository water (M) from 1,000 - 2,000 years	RIP	Geochemical environment	lognormal	1.40E-03	6.70E-04					Frequency Comparison	Cumulative Comparison
138													
139													
140													
141													
142													
143													
144													
145													

	N Scatter Plot	O Rank Correlation	P Linear Correlation	Q Series Analysis (2)	R Distribution of the logs of the sampled values
1		0.934	0.695		
98					
99					
100					
101					
102					
103					
104					
105					
106					
107					
108					
109					
110					
111					
112					
113					
114					
115					
116					
117					
118					
119					
120					
121					
122					
123					
124					
125					
126					
127					
128					
129					
130					
131					
132					
133					
134					
135					
136					
137					
138					
139					
140					
141					
142					
143					
144					
145					



A	B	C	D	E	F	G	H	I	J	K	L	M
Parameter Name	Description	Code	Use in the Calculation and/or Process Model	Distribution Type	Mean	Std Dev	Minimum	Maximum	Correlated to	Correlation Coefficient	Frequency Distribution of ISPA VA Output (1)	Cumulative Distribution of ISPA VA Output
1												
146	At LEV1											
147	Global concentration of polystyrene in the air (mg/m <sup>3</sup> )											
148	2,000 - 4,000 years	RIP	Global chemical environment	lognormal	6.0E-04	4.2E-04	0.0	1.0			Frequency Distribution	Cumulative Distribution
149												
150												
151												
152												
153												
154												
155												
156												
157												
158												
159												
160												
161												
162												
163												
164												
165												
166												
167												
168												
169												
170												
171												
172												
173												
174												
175												
176												
177												
178												
179												
180												
181												
182												
183												
184												
185												
186												
187												
188												
189												
190												
191												
192												
193												

1	Scatter Plot				
146					
147					
148					
149					
150					
151					
152					
153					
154					
155					
156					
157					
158					
159					
160					
161					
162					
163					
164					
165					
166					
167					
168					
169					
170					
171					
172					
173					
174					
175					
176					
177					
178					
179					
180					
181					
182					
183					
184					
185					
186					
187					
188					
189					
190					
191					
192					
193					



N	SARF PM	Rank Condition	Linear Condition	SARF Analysis (2)	Distribution of the log of the sampled values
1		0.534	0.535		
184					
185					
186					
187					
188					
189					
190					
191					
192					
193					
194					
195					
196					
197					
198					
199					
200					
201					
202					
203					
204					
205					
206					
207					
208					
209					
210					
211					
212					
213					
214					
215					
216					
217					
218					
219					
220					
221					
222					
223					
224					
225					
226					
227					
228					
229					
230					
231					
232					
233					
234					
235					
236					
237					
238					
239					
240					
241					

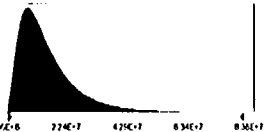
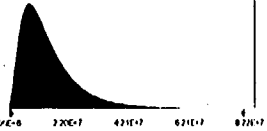
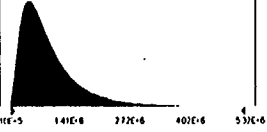
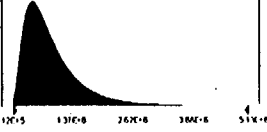
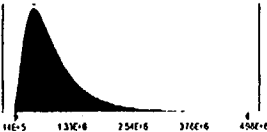
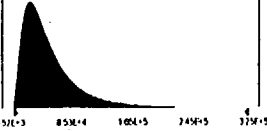
A		B	C	D	E	F	G	H	I	J	K	L	M
Parameter Name		Description	Code	Use in the Calculation and/or Process Model	Distribution Type	Mean	Std Dev	Minimum	Maximum	Correlated To	Correlation Coefficient	Frequency Distribution of TSPA-VA Output (1)	Cumulative Distribution of TSPA-VA Output
242	DFIL	Dose conversion factor (mrem/yr/(gm/m <sup>3</sup> )) for I126, super term average climate	RIP	Accessible environment	lognormal	6.24E+04	7.58E+04	0.0	1.0	DFCD	1.0	Frequency Comparison	Cumulative Comparison
243													
244													
245													
246													
247													
248													
249	DFIS	Dose conversion factor (mrem/yr/(gm/m <sup>3</sup> )) for I126, super physical climate	RIP	Accessible environment	lognormal	6.09E+04	7.77E+04			DFCD	1.0	Frequency Comparison	Cumulative Comparison
250													
251													
252													
253													
254													
255													
256													
257	DFNP	Dose conversion factor (mrem/yr/(gm/m <sup>3</sup> )) for Np237, dry climate	RIP	Accessible environment	lognormal	4.63E+06	3.19E+06			DFCD	1.0	Frequency Comparison	Cumulative Comparison
258													
259													
260													
261													
262													
263													
264													
265	DFNP	Dose conversion factor (mrem/yr/(gm/m <sup>3</sup> )) for Np237, long term average climate	RIP	Accessible environment	lognormal	4.60E+06	3.15E+06			DFCD	1.0	Frequency Comparison	Cumulative Comparison
266													
267													
268													
269													
270													
271													
272													
273	DFNP	Dose conversion factor (mrem/yr/(gm/m <sup>3</sup> )) for Np237, super physical climate	RIP	Accessible environment	lognormal	4.56E+06	3.08E+06			DFCD	1.0	Frequency Comparison	Cumulative Comparison
274													
275													
276													
277													
278													
279													
280													
281	DFPD	Dose conversion factor (mrem/yr/(gm/m <sup>3</sup> )) for Pa231, dry climate	RIP	Accessible environment	lognormal	6.67E+06	4.51E+06			DFCD	1.0	Frequency Comparison	Cumulative Comparison
282													
283													
284													
285													
286													
287													
288													
289													

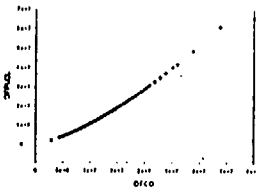
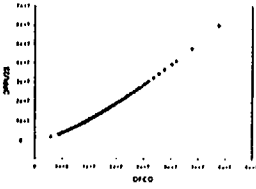
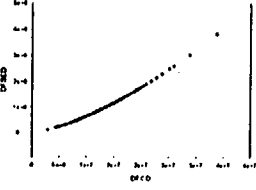
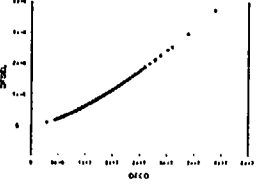
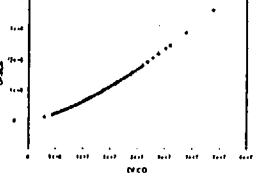
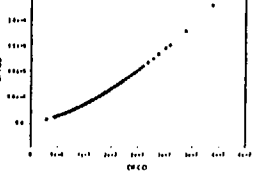


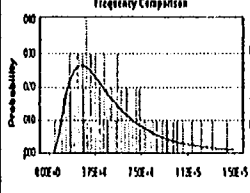
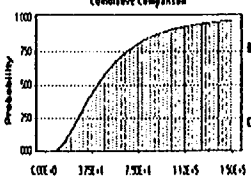
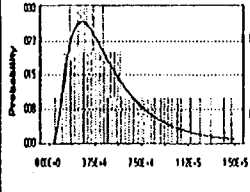
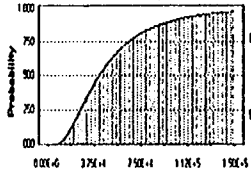
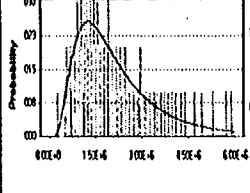
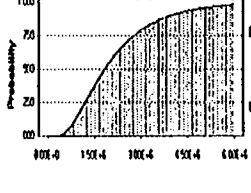
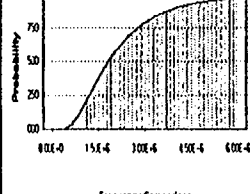
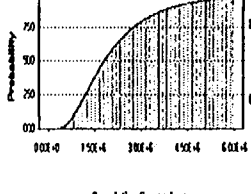
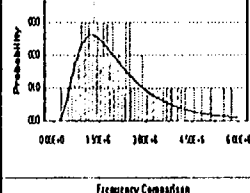
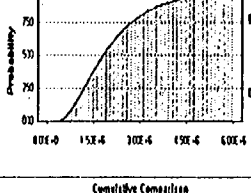
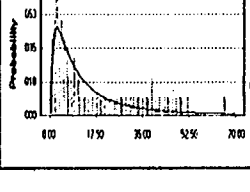
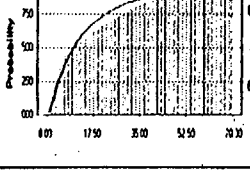
[illegible]

Parameter Name	Description	Code	Use in the Calculation and/or Process Model	Distribution Type	Mean	Std Dev	Minimum	Maximum	Correlation Coefficient	Correlation To	Frequency Distribution of TSA VA Output (s)	Cumulative Distribution of TSA VA Output
DFPAL	Dose conversion factor (microgramm) for Pu239, long term average climate	RIP	Accessible environment	lognormal	6.6E+06	4.6E+06	0.0	1.0	0.5681	1.0		
DFPAS	Dose conversion factor (microgramm) for Pu239, super physical climate	RIP	Accessible environment	lognormal	6.49E+06	4.34E+06	0.0	1.0	0.5681	1.0		
DFPUD	Dose conversion factor (microgramm) for Pu239, dry climate	RIP	Accessible environment	lognormal	2.74E+06	1.91E+06	0.0	1.0	0.5681	1.0		
DFPUL	Dose conversion factor (microgramm) for Pu239, long term average climate	RIP	Accessible environment	lognormal	2.72E+06	1.89E+06	0.0	1.0	0.5681	1.0		
DFPUS	Dose conversion factor (microgramm) for Pu239, super physical climate	RIP	Accessible environment	lognormal	2.70E+06	1.85E+06	0.0	1.0	0.5681	1.0		
DFPZO	Dose conversion factor (microgramm) for Pu239, dry climate	RIP	Accessible environment	lognormal	1.52E+07	1.09E+07	0.0	1.0	0.5681	1.0		
DFPAL	Dose conversion factor (microgramm) for Pu239, long term average climate	RIP	Accessible environment	lognormal	6.6E+06	4.6E+06	0.0	1.0	0.5681	1.0		
DFPAS	Dose conversion factor (microgramm) for Pu239, super physical climate	RIP	Accessible environment	lognormal	6.49E+06	4.34E+06	0.0	1.0	0.5681	1.0		
DFPUD	Dose conversion factor (microgramm) for Pu239, dry climate	RIP	Accessible environment	lognormal	2.74E+06	1.91E+06	0.0	1.0	0.5681	1.0		
DFPUL	Dose conversion factor (microgramm) for Pu239, long term average climate	RIP	Accessible environment	lognormal	2.72E+06	1.89E+06	0.0	1.0	0.5681	1.0		
DFPUS	Dose conversion factor (microgramm) for Pu239, super physical climate	RIP	Accessible environment	lognormal	2.70E+06	1.85E+06	0.0	1.0	0.5681	1.0		
DFPZO	Dose conversion factor (microgramm) for Pu239, dry climate	RIP	Accessible environment	lognormal	1.52E+07	1.09E+07	0.0	1.0	0.5681	1.0		

	H Scatter Plot	O Rank Correlation	P Linear Correlation	Q Series Analysis (2)	R Distribution of the logs of the sampled values
290		0.814	0.99		
291					
292					
293					
294					
295					
296					
297					
298		1	0.99		
299					
300					
301					
302					
303					
304					
305					
306		1	0.99		
307					
308					
309					
310					
311					
312					
313					
314		1	0.99		
315					
316					
317					
318					
319					
320					
321		1	0.99		
322					
323					
324					
325					
326					
327					
328					
329		1	0.99		
330					
331					
332					
333					
334					
335					
336					
337					

A		B	C	D	E	F	G	H	I	J	K	L	M
Parameter Name		Description	Code	Use in the Calculation and/or Process Model	Distribution Type	Mean	Std Dev	Minimum	Maximum	Correlated To	Correlation Coefficient	Frequency Distribution of TSPA-VA Output (1)	Cumulative Distribution of TSPA-VA Output
338	DFPUL	Dose conversion factor (mrem/yr/(gm/m <sup>3</sup> )) for Pu242, long term average climate	RIP	Accessible environment	lognormal	1.58E+07	1.68E+07	0.0	1.0	56P001	1.0	Frequency Comparison	Cumulative Comparison
339													
340													
341													
342													
343													
344													
345	DFPU2S	Dose conversion factor (mrem/yr/(gm/m <sup>3</sup> )) for Pu242, super phical climate	RIP	Accessible environment	lognormal	1.54E+07	1.06E+07			DFCD	1.0	Frequency Comparison	Cumulative Comparison
346													
347													
348													
349													
350													
351													
352													
353	DFSED	Dose conversion factor (mrem/yr/(gm/m <sup>3</sup> )) for Se79, dry climate	RIP	Accessible environment	lognormal	9.46E+05	6.80E+05			DFCD	1.0	Frequency Comparison	Cumulative Comparison
354													
355													
356													
357													
358													
359													
360													
361	DFSEL	Dose conversion factor (mrem/yr/(gm/m <sup>3</sup> )) for Se79, long term average climate	RIP	Accessible environment	lognormal	9.30E+05	6.58E+05			DFCD	1.0	Frequency Comparison	Cumulative Comparison
362													
363													
364													
365													
366													
367													
368													
369	DFSES	Dose conversion factor (mrem/yr/(gm/m <sup>3</sup> )) for Se79, super phical climate	RIP	Accessible environment	lognormal	9.18E+05	6.40E+05			DFCD	1.0	Frequency Comparison	Cumulative Comparison
370													
371													
372													
373													
374													
375													
376													
377	DFTEC	Dose conversion factor (mrem/yr/(gm/m <sup>3</sup> )) for Te99, dry climate	RIP	Accessible environment	lognormal	5.33E+04	4.08E+04			DFCD	1.0	Frequency Comparison	Cumulative Comparison
378													
379													
380													
381													
382													
383													
384													
385													

I	H		O		P		Q		R	
	Scatter Plot		Rank Correlation		Linear Correlation		Series Analysis (I)		Distribution of the logs of the sampled values	
338			0.914		0.999					
339										
340										
341										
342										
343										
344										
345										
346			1		0.99					
347										
348										
349										
350										
351										
352										
353										
354			1		0.99					
355										
356										
357										
358										
359										
360										
361										
362			1		0.99					
363										
364										
365										
366										
367										
368										
369										
370			1		0.99					
371										
372										
373										
374										
375										
376										
377										
378			1		0.99					
379										
380										
381										
382										
383										
384										
385										

A		B	C	D	E	F	G	H	I	J	K	L	M
Parameter Name		Description	Code	Use in the Calculation and/or Process Model	Distribution Type	Mean	Std Dev	Minimum	Maximum	Correlated To	Correlation Coefficient	Frequency Distribution of TSPA-VA Output (1)	Cumulative Distribution of TSPA-VA Output
386	DF TOL	Dose conversion factor (mrem/yr/(gm/m <sup>3</sup> )) for Tc99, long term average climate	RIP	Accessible environment	lognormal	5.79E+4	1.69E+4	0.0	1.0	DFCD	1.0		
387		DF TOL											
388													
389													
390													
391													
392													
393													
394	DF TCS	Dose conversion factor (mrem/yr/(gm/m <sup>3</sup> )) for Tc99, super pluvial climate	RIP	Accessible environment	lognormal	5.24E+04	3.95E+04			DFCD	1.0		
395		DF TCS											
396													
397													
398													
399													
400													
401	DF UD	Dose conversion factor (mrem/yr/(gm/m <sup>3</sup> )) for U234, dry climate	RIP	Accessible environment	lognormal	2.24E+06	1.53E+06			DFCD	1.0		
402		DF UD											
403													
404													
405													
406													
407													
408													
409	DF UL	Dose conversion factor (mrem/yr/(gm/m <sup>3</sup> )) for U234, long term average climate	RIP	Accessible environment	lognormal	2.22E+06	1.51E+06			DFCD	1.0		
410		DF UL											
411													
412													
413													
414													
415													
416													
417	DF US	Dose conversion factor (mrem/yr/(gm/m <sup>3</sup> )) for U234, super pluvial climate	RIP	Accessible environment	lognormal	2.20E+06	1.48E+06			DFCD	1.0		
418		DF US											
419													
420													
421													
422													
423													
424													
425	DILUT	Diffusion Factor	FEHM (57)	Saturated zone flow and transport	cumulative	10 (median)		1.0	100.0				
426													
427													
428													
429													
430													
431													
432													
433													

	N Scatter Plot	O Rank Correlation	P Linear Correlation	Q Series Analysis (7)	R Distribution of the logs of the sampled values
386		0.914	0.999		
387					
388					
389					
390					
391		1	0.99		
392					
393					
394					
395					
396		1	0.99		
397					
398					
399					
400					
401		1	0.99		
402					
403					
404					
405					
406		1	0.99		
407					
408					
409					
410					
411		1	0.99		
412					
413					
414					
415					
416		1	0.99		
417					
418					
419					
420					
421					
422					
423					
424					
425					
426					
427					
428					
429					
430					
431					
432					
433					

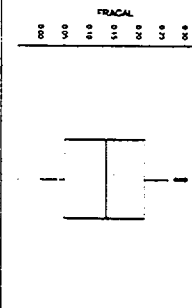
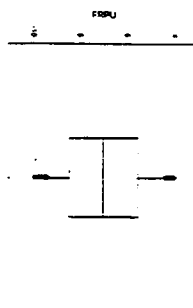
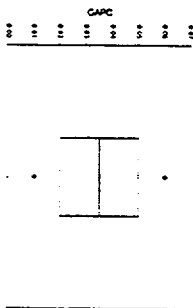
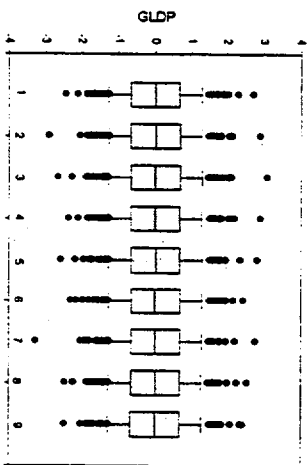
i	Parameter Name	B Description	C Code	D Use in the Calculation and/or Process Model	E Distribution Type	F Mean	G Std Dev	H Minimum	I Maximum	J Correlated to	K Correlation Coefficient	L Frequency Distribution of TSPA-VIA Output (1)		M Cumulative Distribution of TSPA-VIA Output	
												Frequency Cumulative	Cumulative Cumulative	Frequency Cumulative	Cumulative Cumulative
434	DISMAT	Sampled fractional low temperature peaks, long term	FE100(UZ)	Unsaturation flow and transport	normal	1400.1	783.1	0.0	1.0	3FORV1	1.0				
435															
436															
437															
438															
439															
440															
441															
442															
443															
444															
445															
446															
447															
448															
449															
450	DIS1F	Distribution for pore sizes	RIP	White pore size	uniform			-5.0	-3.0						
451															
452															
453															
454															
455															
456															
457	DRY1	Duration of current dry climate (years)	RIP	Boundary condition	uniform			0.0	10000.0						
458															
459															
460															
461															
462															
463															
464															
465	DRY2	Duration of future dry climate (years)	RIP	Boundary condition	uniform			0.0	20000.0						
466															
467															
468															
469															
470															
471															
472															
473	EDCH1	Effective diffusion coefficient, model parameter	RIP	Flow and transport	normal	0.0	1.0								
474															
475															
476															
477															
478															
479															
480															
481															



	H Scatter Plot	O Rank Correlation	P Linear Correlation	Q Series Analysis (?)	R Distribution of the logs of the sampled values
434		0.934	0.895		
435					
436					
437					
438					
439					
440					
441					
442					
443					
444					
445					
446					
447					
448					
449					
450					
451					
452					
453					
454					
455					
456					
457					
458					
459					
460					
461					
462					
463					
464					
465					
466					
467					
468					
469					
470					
471					
472					
473					
474					
475					
476					
477					
478					
479					
480					
481					

	A	B	C	D	E	F	G	H	I	J	K	L	M
	Parameter Name	Description	Code	Use in the Calculation and/or Process Model	Distribution Type	Mean	Std Dev	Minimum	Maximum	Correlated To	Correlation Coefficient	Frequency Distribution of TSPA-VA Output (1)	Cumulative Distribution of TSPA-VA Output
482	FRACAL	Sampled hydraulic conductivity with a long term	FE(RUP)SZ	Saturated zone transport	uniform(0 0)	FMILL	FSOLL	0 0	0 0	SFDV1	1 0	Frequency Comparison	Cumulative Comparison
483		FRACAL			0 0 (0 1)								
484													
485													
486													
487													
488													
489													
490	FRPU	Fraction of Pu colloids transported with irreversible solubility	RIP	Unsaturated zone transport	uniform			-10	-4			Frequency Comparison	Cumulative Comparison
491		FRPU											
492													
493													
494													
495													
496													
497	GAFC	C-14 gap fraction	RIP	Waste package	uniform			0 0125	0 0575			Frequency Comparison	Cumulative Comparison
498		GAFC											
499													
500													
501													
502													
503													
504													
505													
506	GLDP1	Glass dissolution model parameter	RIP	Waste package	normal	0 0	1 0					Frequency Comparison	Cumulative Comparison
507		GLDP1											
508													
509													
510													
511													
512													
513	GLDP2	Glass dissolution model parameter	RIP	Waste package	normal	0 0	1 0					Frequency Comparison	Cumulative Comparison
514		GLDP2											
515													
516													
517													
518													
519													
520													
521	GLDP3	Glass dissolution model parameter	RIP	Waste package	normal	0 0	1 0					Frequency Comparison	Cumulative Comparison
522		GLDP3											
523													
524													
525													
526													
527													
528													
529													

1	H		Q	P	D	R
	Score Plot	Root Criterion			Series Analysis (1)	Distribution of the logs of the sampled values
421	note: 10 of the 100 samples generated for the ISPA VA were 0.0. Frequency and cumulative comparisons are based on the 90 samples that were non zero	0.134	0.055			
422						
423						
424						
425						
426						
427						
428						
429						
430						
431						
432						
433						
434						
435						
436						
437						
438						
439						
440						
441						
442						
443						
444						
445						
446						
447						
448						
449						
450						
451						
452						
453						
454						
455						
456						
457						
458						
459						
460						
461						
462						
463						
464						
465						
466						
467						
468						
469						
470						
471						
472						
473						
474						
475						
476						
477						
478						
479						
480						
481						
482						
483						
484						
485						
486						
487						
488						
489						
490						
491						
492						
493						
494						
495						
496						
497						
498						
499						
500						
501						
502						
503						
504						
505						
506						
507						
508						
509						
510						
511						
512						
513						
514						
515						
516						
517						
518						
519						
520						
521						
522						
523						
524						
525						
526						
527						
528						
529						

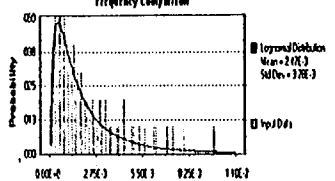
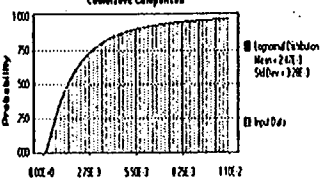
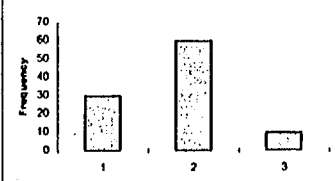

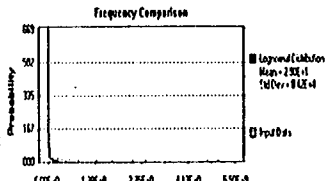
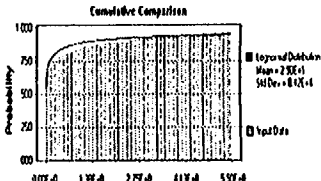
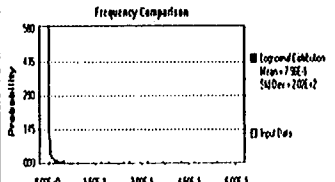
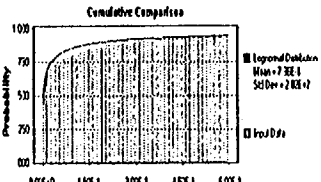
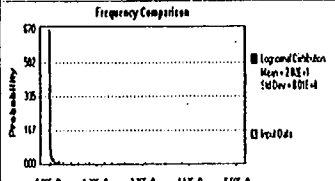
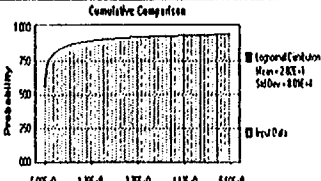
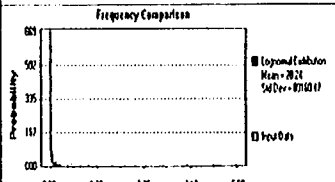
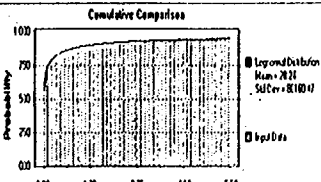


Parameter Name	Description	Code	Use in the Calculation and/or Process Model	Distribution Type	Mean	Std Dev	Minimum	Maximum	Correlated to Correlation Coefficient	SRVY	1.0
1	Sample data type (normal, skewed, lognormal, etc.)	A									
2	Class dissolution model parameter	B									
3	Waste package	C									
4	Use in the Calculation and/or Process Model	D									
5	Frequency Distribution of TSPA-VIA Output (1)	E									
6	Cumulative Distribution of TSPA-VIA Output	F									
7	Frequency Distribution of TSPA-VIA Output (2)	G									
8	Cumulative Distribution of TSPA-VIA Output	H									
9	Frequency Distribution of TSPA-VIA Output (3)	I									
10	Cumulative Distribution of TSPA-VIA Output	J									
11	Frequency Distribution of TSPA-VIA Output (4)	K									
12	Cumulative Distribution of TSPA-VIA Output	L									
13	Frequency Distribution of TSPA-VIA Output (5)	M									
14	Cumulative Distribution of TSPA-VIA Output	N									
15	Frequency Distribution of TSPA-VIA Output (6)	O									
16	Cumulative Distribution of TSPA-VIA Output	P									
17	Frequency Distribution of TSPA-VIA Output (7)	Q									
18	Cumulative Distribution of TSPA-VIA Output	R									
19	Frequency Distribution of TSPA-VIA Output (8)	S									
20	Cumulative Distribution of TSPA-VIA Output	T									
21	Frequency Distribution of TSPA-VIA Output (9)	U									
22	Cumulative Distribution of TSPA-VIA Output	V									
23	Frequency Distribution of TSPA-VIA Output (10)	W									
24	Cumulative Distribution of TSPA-VIA Output	X									
25	Frequency Distribution of TSPA-VIA Output (11)	Y									
26	Cumulative Distribution of TSPA-VIA Output	Z									
27	Frequency Distribution of TSPA-VIA Output (12)	AA									
28	Cumulative Distribution of TSPA-VIA Output	AB									
29	Frequency Distribution of TSPA-VIA Output (13)	AC									
30	Cumulative Distribution of TSPA-VIA Output	AD									
31	Frequency Distribution of TSPA-VIA Output (14)	AE									
32	Cumulative Distribution of TSPA-VIA Output	AF									
33	Frequency Distribution of TSPA-VIA Output (15)	AG									
34	Cumulative Distribution of TSPA-VIA Output	AH									
35	Frequency Distribution of TSPA-VIA Output (16)	AI									
36	Cumulative Distribution of TSPA-VIA Output	AJ									
37	Frequency Distribution of TSPA-VIA Output (17)	AK									
38	Cumulative Distribution of TSPA-VIA Output	AL									
39	Frequency Distribution of TSPA-VIA Output (18)	AM									
40	Cumulative Distribution of TSPA-VIA Output	AN									
41	Frequency Distribution of TSPA-VIA Output (19)	AO									
42	Cumulative Distribution of TSPA-VIA Output	AP									
43	Frequency Distribution of TSPA-VIA Output (20)	AQ									
44	Cumulative Distribution of TSPA-VIA Output	AR									
45	Frequency Distribution of TSPA-VIA Output (21)	AS									
46	Cumulative Distribution of TSPA-VIA Output	AT									
47	Frequency Distribution of TSPA-VIA Output (22)	AU									
48	Cumulative Distribution of TSPA-VIA Output	AV									
49	Frequency Distribution of TSPA-VIA Output (23)	AW									
50	Cumulative Distribution of TSPA-VIA Output	AX									
51	Frequency Distribution of TSPA-VIA Output (24)	AY									
52	Cumulative Distribution of TSPA-VIA Output	AZ									
53	Frequency Distribution of TSPA-VIA Output (25)	BA									
54	Cumulative Distribution of TSPA-VIA Output	BB									
55	Frequency Distribution of TSPA-VIA Output (26)	BC									
56	Cumulative Distribution of TSPA-VIA Output	BD									
57	Frequency Distribution of TSPA-VIA Output (27)	BE									
58	Cumulative Distribution of TSPA-VIA Output	BF									
59	Frequency Distribution of TSPA-VIA Output (28)	BG									
60	Cumulative Distribution of TSPA-VIA Output	BH									
61	Frequency Distribution of TSPA-VIA Output (29)	BI									
62	Cumulative Distribution of TSPA-VIA Output	BJ									
63	Frequency Distribution of TSPA-VIA Output (30)	BK									
64	Cumulative Distribution of TSPA-VIA Output	BL									
65	Frequency Distribution of TSPA-VIA Output (31)	BM									
66	Cumulative Distribution of TSPA-VIA Output	BN									
67	Frequency Distribution of TSPA-VIA Output (32)	BO									
68	Cumulative Distribution of TSPA-VIA Output	BP									
69	Frequency Distribution of TSPA-VIA Output (33)	BQ									
70	Cumulative Distribution of TSPA-VIA Output	BR									
71	Frequency Distribution of TSPA-VIA Output (34)	BS									
72	Cumulative Distribution of TSPA-VIA Output	BT									
73	Frequency Distribution of TSPA-VIA Output (35)	BU									
74	Cumulative Distribution of TSPA-VIA Output	BV									
75	Frequency Distribution of TSPA-VIA Output (36)	BW									
76	Cumulative Distribution of TSPA-VIA Output	BX									
77	Frequency Distribution of TSPA-VIA Output (37)	BY									
78	Cumulative Distribution of TSPA-VIA Output	BZ									
79	Frequency Distribution of TSPA-VIA Output (38)	CA									
80	Cumulative Distribution of TSPA-VIA Output	CB									
81	Frequency Distribution of TSPA-VIA Output (39)	CC									
82	Cumulative Distribution of TSPA-VIA Output	CD									
83	Frequency Distribution of TSPA-VIA Output (40)	CE									
84	Cumulative Distribution of TSPA-VIA Output	CF									
85	Frequency Distribution of TSPA-VIA Output (41)	CG									
86	Cumulative Distribution of TSPA-VIA Output	CH									
87	Frequency Distribution of TSPA-VIA Output (42)	CI									
88	Cumulative Distribution of TSPA-VIA Output	CJ									
89	Frequency Distribution of TSPA-VIA Output (43)	CK									
90	Cumulative Distribution of TSPA-VIA Output	CL									
91	Frequency Distribution of TSPA-VIA Output (44)	CM									
92	Cumulative Distribution of TSPA-VIA Output	CN									
93	Frequency Distribution of TSPA-VIA Output (45)	CO									
94	Cumulative Distribution of TSPA-VIA Output	CP									
95	Frequency Distribution of TSPA-VIA Output (46)	CQ									
96	Cumulative Distribution of TSPA-VIA Output	CR									
97	Frequency Distribution of TSPA-VIA Output (47)	CS									
98	Cumulative Distribution of TSPA-VIA Output	CT									
99	Frequency Distribution of TSPA-VIA Output (48)	CU									
100	Cumulative Distribution of TSPA-VIA Output	CV									
101	Frequency Distribution of TSPA-VIA Output (49)	CW									
102	Cumulative Distribution of TSPA-VIA Output	CX									
103	Frequency Distribution of TSPA-VIA Output (50)	CY									
104	Cumulative Distribution of TSPA-VIA Output	CZ									
105	Frequency Distribution of TSPA-VIA Output (51)	DA									
106	Cumulative Distribution of TSPA-VIA Output	DB									
107	Frequency Distribution of TSPA-VIA Output (52)	DC									
108	Cumulative Distribution of TSPA-VIA Output	DD									
109	Frequency Distribution of TSPA-VIA Output (53)	DE									
110	Cumulative Distribution of TSPA-VIA Output	DF									
111	Frequency Distribution of TSPA-VIA Output (54)	DG									
112	Cumulative Distribution of TSPA-VIA Output	DH									
113	Frequency Distribution of TSPA-VIA Output (55)	DI									
114	Cumulative Distribution of TSPA-VIA Output	DJ									
115	Frequency Distribution of TSPA-VIA Output (56)	DK									
116	Cumulative Distribution of TSPA-VIA Output	DL									
117	Frequency Distribution of TSPA-VIA Output (57)	DM									
118	Cumulative Distribution of TSPA-VIA Output	DN									
119	Frequency Distribution of TSPA-VIA Output (58)	DO									
120	Cumulative Distribution of TSPA-VIA Output	DP									
121	Frequency Distribution of TSPA-VIA Output (59)	DQ									
122	Cumulative Distribution of TSPA-VIA Output	DR									
123	Frequency Distribution of TSPA-VIA Output (60)	DS									
124	Cumulative Distribution of TSPA-VIA Output	DT									
125	Frequency Distribution of TSPA-VIA Output (61)	DU									
126	Cumulative Distribution of TSPA-VIA Output	DV									
127	Frequency Distribution of TSPA-VIA Output (62)	DW									
128	Cumulative Distribution of TSPA-VIA Output	DX									
129	Frequency Distribution of TSPA-VIA Output (63)	DY									
130	Cumulative Distribution of TSPA-VIA Output	DZ									
131	Frequency Distribution of TSPA-VIA Output (64)	EA									
132	Cumulative Distribution of TSPA-VIA Output	EB									
133	Frequency Distribution of TSPA-VIA Output (65)	EC									
134	Cumulative Distribution of TSPA-VIA Output	ED									
135	Frequency Distribution of TSPA-VIA Output (66)	EE									
136	Cumulative Distribution of TSPA-VIA Output	EF									
137	Frequency Distribution of TSPA-VIA Output (67)	EG									
138	Cumulative Distribution of TSPA-VIA Output	EH									
139	Frequency Distribution of TSPA-VIA Output (68)	EI									
140	Cumulative Distribution of TSPA-VIA Output	EJ									
141	Frequency Distribution of TSPA-VIA Output (69)	EK									
142	Cumulative Distribution of TSPA-VIA Output	EL									
143	Frequency Distribution of TSPA-VIA Output (70)	EM									
144	Cumulative Distribution of TSPA-VIA Output	EN									
145	Frequency Distribution of TSPA-VIA Output (71)	EO									
146	Cumulative Distribution of TSPA-VIA Output	EP									
147	Frequency Distribution of TSPA-VIA Output (72)	EQ									
148	Cumulative Distribution of TSPA-VIA Output	ER									
149	Frequency Distribution of TSPA-VIA Output (73)	ES									
150	Cumulative Distribution of TSPA-VIA Output	ET									
151	Frequency Distribution of TSPA-VIA Output (74)	EU									
152	Cumulative Distribution of TSPA-VIA Output	EV									
153	Frequency Distribution of TSPA-VIA Output (75)	EW									
154	Cumulative Distribution of TSPA-VIA Output	EX									
155	Frequency Distribution of TSPA-VIA Output (76)	EY									
156	Cumulative Distribution of TSPA-VIA Output	EZ									
157	Frequency Distribution of TSPA-VIA Output (77)	FA									
158	Cumulative Distribution of TSPA-VIA Output	FB									
159	Frequency Distribution of TSPA-VIA Output (78)	FC									
160	Cumulative Distribution of TSPA-VIA Output	FD									
161	Frequency Distribution of TSPA-VIA Output (79)	FE									
162	Cumulative Distribution of TSPA-VIA Output	FF									
163	Frequency Distribution of TSPA-VIA Output (80)	FG									
164	Cumulative Distribution of TSPA-VIA Output	FH									
165	Frequency Distribution of TSPA-VIA Output (81)	FI									
166	Cumulative Distribution of TSPA-VIA Output	FJ									
167	Frequency Distribution of TSPA-VIA Output (82)	FK									
168	Cumulative Distribution of TSPA-VIA Output	FL									
169	Frequency Distribution of TSPA-VIA Output (83)	FM									
170	Cumulative Distribution of TSPA-VIA Output	FN									
171	Frequency Distribution of TSPA-VIA Output (84)	FO									
172	Cumulative Distribution of TSPA-VIA Output	FP									
173	Frequency Distribution of TSPA-VIA Output (85)	FQ									
174	Cumulative Distribution of TSPA-VIA Output	FR									
175	Frequency Distribution of TSPA-VIA Output (86)	FS									
176	Cumulative Distribution of TSPA-VIA Output	FT									
177	Frequency Distribution of TSPA-VIA Output (87)	FU									
178	Cumulative Distribution of TSPA-VIA Output	FV									
179	Frequency Distribution of TSPA-VIA Output (88)	FW									
180	Cumulative Distribution of TSPA-VIA Output	FX									
181	Frequency Distribution of TSPA-V										

1	N	Scatter Plot	0	Rank Correlation	0.914	P	Linear Correlation	0.895	Q	Series Analysis (2)	R	Distribution of the logs of the sampled values
530												
531												
532												
533												
534												
535												
536												
537												
538												
539												
540												
541												
542												
543												
544												
545												
546												
547												
548												
549												
550												
551												
552												
553												
554												
555												
556												
557												
558												
559												
560												
561												
562												
563												
564												
565												
566												
567												
568												
569												
570												
571												
572												
573												
574												
575												
576												
577												

A		B	C	D	E	F	G	H	I	J	K	L	M
Parameter Name		Description	Code	Use in the Calculation and/or Process Model	Distribution Type	Mean	Std Dev	Minimum	Maximum	Correlated To	Correlation Coefficient	Frequency Distribution of TSPA-VA Output (1)	Cumulative Distribution of TSPA-VA Output
578	AEOL1	Sample 6.66E-02 (m) from 200 - 1,000 years	RIP	Geochemical environment	lognormal	2.6E-02	1.5E-02	0.0	1.0	SFDRY1	1.0	Frequency Comparison	Cumulative Comparison
579		ICOL1											
580													
581		5.6E-3 7.0E-3 5.0E-2 7.3E-2 6.5E-2											
582													
583													
584													
585													
586	ICOL2	Ionic strength (M) from 200 - 1,000 years	RIP	Geochemical environment	lognormal	1.6E-02	8.4E-03					Frequency Comparison	Cumulative Comparison
587		ICOL2											
588													
589		3.2E-3 1.8E-2 3.7E-2 4.7E-2 6.7E-2											
590													
591													
592													
593	ICOL3	Ionic strength (M) from 1,000 - 2,000 years	RIP	Geochemical environment	lognormal	1.9E-02	1.1E-02					Frequency Comparison	Cumulative Comparison
594		ICOL3											
595													
596		1.3E-3 2.3E-2 4.2E-2 6.3E-2 8.7E-2											
597													
598													
599													
600													
601	ICOL4	Ionic strength (M) from 2,000 - 4,000 years	RIP	Geochemical environment	lognormal	3.2E-03	1.7E-03					Frequency Comparison	Cumulative Comparison
602		ICOL4											
603													
604		5.3E-4 3.6E-3 6.6E-3 9.8E-3 1.7E-2											
605													
606													
607													
608													
609	ICOL5	Ionic strength (M) from 4,000 - 10,000 years	RIP	Geochemical environment	lognormal	4.7E-03	2.7E-03					Frequency Comparison	Cumulative Comparison
610		ICOL5											
611													
612		8.2E-4 5.6E-3 1.0E-2 1.5E-2 2.0E-2											
613													
614													
615													
616													
617	ICOL6	Ionic strength (M) from 10,000 - 100,000 years	RIP	Geochemical environment	lognormal	6.4E-03	3.4E-03					Frequency Comparison	Cumulative Comparison
618		ICOL6											
619													
620		1.2E-3 7.2E-3 1.2E-2 1.9E-2 2.5E-2											
621													
622													
623													
624													
625													

--	--	--	--	--	--	--	--	--	--	--	--	--	--	--	--	--	--	--	--	--	--	--	--	--	--	--	--	--	--	--	--	--	--	--	--	--	--	--	--	--	--	--	--	--	--	--	--	--	--	--	--	--	--	--	--	--	--	--	--	--	--	--	--	--	--	--	--	--	--	--	--	--	--	--	--	--	--	--	--	--	--	--	--	--	--	--	--	--	--	--	--	--	--	--	--	--	--	--	--	--	--	--	--	--	--	--	--	--	--	--	--	--	--	--	--	--	--	--	--	--	--	--	--	--	--	--	--	--	--	--	--	--	--	--	--	--	--	--	--	--	--	--	--	--	--	--	--	--	--	--	--	--	--	--	--	--	--	--	--	--	--	--	--	--	--	--	--	--	--	--	--	--	--	--	--	--	--	--	--	--	--	--	--	--	--	--	--	--	--	--	--	--	--	--	--	--	--	--	--	--	--	--	--	--	--	--	--	--	--	--	--	--	--	--	--	--	--	--	--	--	--	--	--	--	--	--	--	--	--	--	--	--	--	--	--	--	--	--	--	--	--	--	--	--	--	--	--	--	--	--	--	--	--	--	--	--	--	--	--	--	--	--	--	--	--	--	--	--	--	--	--	--	--	--	--	--	--	--	--	--	--	--	--	--	--	--	--	--	--	--	--	--	--	--	--	--	--	--	--	--	--	--	--	--	--	--	--	--	--	--	--	--	--	--	--	--	--	--	--	--	--	--	--	--	--	--	--	--	--	--	--	--	--	--	--	--	--	--	--	--	--	--	--	--	--	--	--	--	--	--	--	--	--	--	--	--	--	--	--	--	--	--	--	--	--	--	--	--	--	--	--	--	--	--	--	--	--	--	--	--	--	--	--	--	--	--	--	--	--	--	--	--	--	--	--	--	--	--	--	--	--	--	--	--	--	--	--	--	--	--	--	--	--	--	--	--	--	--	--	--	--	--	--	--	--	--	--	--	--	--	--	--	--	--	--	--	--	--	--	--	--	--	--	--	--	--	--	--	--	--	--	--	--	--	--	--	--	--	--	--	--	--	--	--	--	--	--	--	--	--	--	--	--	--	--	--	--	--	--	--	--	--	--	--	--	--	--	--	--	--	--	--	--	--	--	--	--	--	--	--	--	--	--	--	--	--	--	--	--	--	--	--	--	--	--	--	--	--	--	--	--	--	--	--	--	--	--	--	--	--	--	--	--	--	--	--	--	--	--	--	--	--	--	--	--	--	--	--	--	--	--	--	--	--	--	--	--	--	--	--	--	--	--	--	--	--	--	--	--	--	--	--	--	--	--	--	--	--	--	--	--	--	--	--	--	--	--	--	--	--	--	--	--	--	--	--	--	--	--	--	--	--	--	--	--	--	--	--	--	--	--	--	--	--	--	--	--	--	--	--	--	--	--	--	--	--	--	--	--	--	--	--	--	--	--	--	--	--	--	--	--	--	--	--	--	--	--	--	--	--	--	--	--	--	--	--	--	--	--	--	--	--	--	--	--	--	--	--	--	--	--	--	--	--	--	--	--	--	--	--	--	--	--	--	--	--	--	--	--	--	--	--	--	--	--	--	--	--	--	--	--	--	--	--	--	--	--	--	--	--	--	--	--	--	--	--	--	--	--	--	--	--	--	--	--	--	--	--	--	--	--	--	--	--	--	--	--	--	--	--	--	--	--	--	--	--	--	--	--	--	--	--	--	--	--	--	--	--	--	--	--	--	--	--	--	--	--	--	--	--	--	--	--	--	--	--	--	--	--	--	--	--	--	--	--	--	--	--	--	--	--	--	--	--	--	--	--	--	--	--	--	--	--	--	--	--	--	--	--	--	--	--	--	--	--	--	--	--	--	--	--	--	--	--	--	--	--	--	--	--	--	--	--	--	--	--	--	--	--	--	--	--	--	--	--	--	--	--	--	--	--	--	--	--	--	--	--	--	--	--	--	--	--	--	--	--	--	--	--	--	--	--	--	--	--	--	--	--	--	--	--	--	--	--	--	--	--	--	--	--	--	--	--	--	--	--	--	--	--	--	--	--	--	--	--	--	--	--	--	--	--	--	--	--	--	--	--	--	--	--	--	--	--	--	--	--	--	--	--	--	--	--	--	--	--	--	--	--	--	--	--	--	--	--	--	--	--	--	--	--	--	--	--	--	--	--	--	--	--	--	--	--	--	--	--	--	--	--	--	--	--	--	--	--	--	--	--	--	--	--	--	--	--	--	--	--	--	--	--	--	--	--	--	--	--	--	--	--	--	--	--	--	--	--	--	--	--	--	--	--	--	--	--	--	--	--	--	--	--	--	--	--	--	--	--	--	--	--	--	--	--	--	--	--	--	--	--	--	--	--	--	--	--	--	--	--	--	--	--	--	--	--	--	--	--	--	--	--	--	--	--	--	--	--	--	--	--	--	--	--	--	--	--	--	--	--	--	--	--	--	--	--	--	--	--	--	--	--	--	--	--	--	--	--	--	--	--	--	--	--	--	--	--	--	--	--	--	--	--	--	--	--	--	--	--	--	--	--	--	--	--	--	--	--	--	--	--	--	--	--	--	--	--	--	--	--	--	--	--	--	--	--	--	--	--	--	--	--	--	--	--	--	--	--	--	--	--	--	--	--	--	--	--	--	--	--	--	--	--	--	--	--	--	--	--	--	--	--	--	--	--	--	--	--	--	--	--	--	--	--	--	--	--	--	--	--	--	--	--	--	--	--	--	--	--	--	--	--	--	--	--	--	--	--	--	--	--	--	--	--	--	--	--	--	--	--	--	--	--	--	--	--	--	--	--	--	--	--	--	--	--	--	--	--	--	--	--	--	--	--	--	--	--	--	--	--	--	--	--	--	--	--	--	--	--	--	--	--	--	--	--	--	--	--	--	--	--	--	--	--	--	--	--	--	--	--	--	--	--	--	--	--	--	--	--	--	--	--	--	--	--	--	--	--	--	--	--	--	--	--	--	--	--	--	--	--	--	--	--	--	--	--	--	--	--	--	--	--	--	--	--	--	--	--	--	--	--	--	--	--	--	--	--	--	--	--	--	--	--	--	--	--	--	--	--	--	--	--	--	--	--	--	--	--

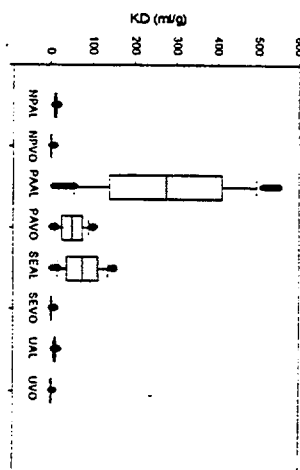
I	A	B	C	D	E	F	G	H	I	J	K	L		M
	Parameter Name	Description	Code	Use in the Calculation and/or Process Model	Distribution Type	Mean	Std Dev	Minimum	Maximum	Correlated To	Correlation Coefficient	Frequency Distribution of TSPA-VA Output (1)		Cumulative Distribution of TSPA-VA Output
626	ACOM1	Standard lognormal distribution	RIP	Geocell reinforcement	lognormal	2.5E+03	3.4E+03	0.0	1.0	SFDRV1	1.0			
627		100L7												
628														
629														
630														
631														
632														
633	INFMT1	Weights for UZ flow cases	RIP	Unsaturation zone flow	discrete									
634		INFMT1												
635														
636														
637														
638														
639														
640														
641	KCHLW	Kc for HLW colloids	RIP	Flow and transport	log uniform			1 E-05	10.0					
642		LOG KCHLW												
643														
644														
645														
646														
647														
648														
649	KCSF	Kc for SF colloids	RIP	Flow and transport	log uniform			1 E-05	10.0					
650		LOG KCSF												
651														
652														
653														
654														
655														
656														
657	KCPU	Kc, Pu, unsaturated zone	FEHM (UZ)	Unsaturation zone flow and transport	log uniform			1 E-05	10.0					
658		LOG KCPU												
659														
660														
661														
662														
663														
664														
665	KCPUSZ	Kc, Pu, saturated zone units	FEHM (SZ)	Saturated zone flow and transport	log uniform			1 E-05	10.0					
666		LOG KCPUSZ												
667														
668														
669														
670														
671														
672														
673														



	N Scatter Plot	O Rank Correlation	P Linear Correlation	Q Series Analysis (?)	R Distribution of the logs of the sampled values
626		0.934	0.695		
627					
628					
629					
630					
631					
632					
633					
634					
635					
636					
637					
638					
639					
640					
641					
642					<p>Frequency Comparison</p>
643					<p>Frequency Comparison</p>
644					
645					
646					
647					
648					
649					
650					
651					
652					
653					
654					
655					
656					
657					
658					<p>Frequency Comparison</p>
659					
660					
661					
662					
663					
664					
665					
666					
667					
668					
669					
670					
671					
672					
673					

A		B	C	D	E	F	G	H	I	J	K	L	M
Parameter Name		Description	Code	Use in the Calculation and/or Process Model	Distribution Type	Mean	Std Dev	Minimum	Maximum	Correlated To	Correlation Coefficient	Frequency Distribution of TSPA-VA Output (1)	Cumulative Distribution of TSPA-VA Output
674	K6NPAL	Sampled $K_d$ (mL/g) for neptunium, volcanic units	FEHM(SZ)	Saturated zone flow and transport	uniform	FMHL1	FSD11	0.0	15.0	SFDRV1	1.0	Frequency Comparison	Cumulative Comparison
675		K6NPAL											
676													
677													
678													
679													
680													
681	K6NPVO	$K_d$ (mL/g) for neptunium, volcanic units	FEHM(SZ)	Saturated zone flow and transport	beta	1.5	1.3	0.0	15.0			Frequency Comparison	Cumulative Comparison
682		K6NPVO											
683													
684													
685													
686													
687													
688													
689	K6PAAL	$K_d$ (mL/g) for Pa-231, alluvium	FEHM(SZ)	Saturated zone flow and transport	uniform			0.0	550.0			Frequency Comparison	Cumulative Comparison
690		K6PAAL											
691													
692													
693													
694													
695													
696													
697	K6PAVO	$K_d$ (mL/g) for Pa-231, volcanic units	FEHM(SZ)	Saturated zone flow and transport	uniform			0.0	100.0			Frequency Comparison	Cumulative Comparison
698		K6PAVO											
699													
700													
701													
702													
703													
704													
705	K6SEAL	$K_d$ (mL/g) for Se, alluvium	FEHM(SZ)	Saturated zone flow and transport	uniform			0.0	150.0			Frequency Comparison	Cumulative Comparison
706		K6SEAL											
707													
708													
709													
710													
711													
712													
713	K6SEVO	$K_d$ (mL/g) for Se, volcanic units	FEHM(SZ)	Saturated zone flow and transport	beta	2.0	1.7	0.0	15.0			Frequency Comparison	Cumulative Comparison
714		K6SEVO											
715													
716													
717													
718													
719													
720													
721													

I	H		O	P	Q	R
	Scatter Plot	Rank Correlation				
1		0.914	0.895			
674						
675						
676						
677						
678						
679						
680						
681						
682						
683						
684						
685						
686						
687						
688						
689						
690						
691						
692						
693						
694						
695						
696						
697						
698						
699						
700						
701						
702						
703						
704						
705						
706						
707						
708						
709						
710						
711						
712						
713						
714						
715						
716						
717						
718						
719						
720						
721						







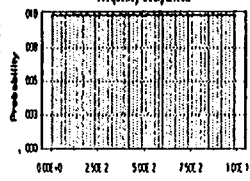
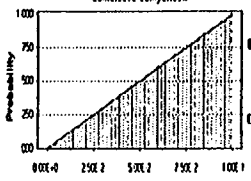
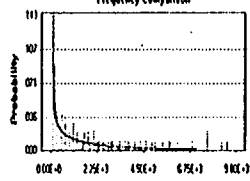
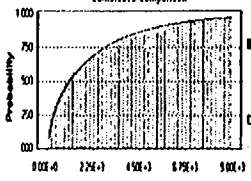
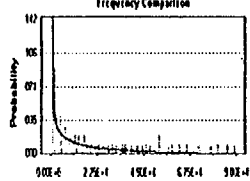
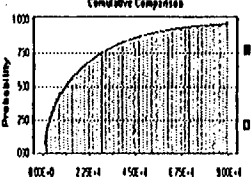
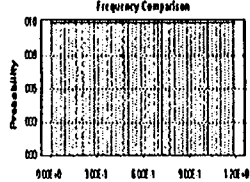
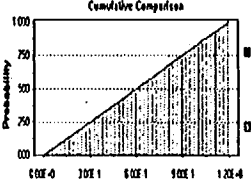
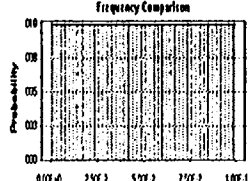
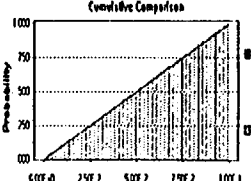
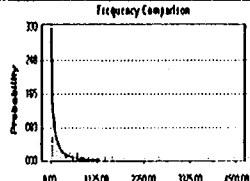
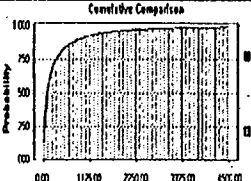
	A	B	C	D	E	F	G	H	I	J	K	L	M
	Parameter Name	Description	Code	Use in the Calculation and/or Process Model	Distribution Type	Mean	Std Dev	Minimum	Maximum	Correlated To	Correlation Coefficient	Frequency Distribution of TSPA-VA Output (1)	Cumulative Distribution of TSPA-VA Output
770	KOPAV	Sampled fraction of type A, deep, long term	FEHM (UZ)	Unsaturation flow and transport	Uniform	FMHL1	FSD1	0.0	100.0	SFDV1	1.0	Frequency Comparison	Cumulative Comparison
771		KOPAV											
772													
773													
774													
775													
776													
777	KOPAZ	Kd (ml/g), Pa, zeolitic	FEHM (UZ)	Unsaturation zone flow and transport	Uniform			0.0	100.0			Frequency Comparison	Cumulative Comparison
778		KOPAZ											
779													
780													
781													
782													
783													
784													
785	KOPUD	Kd (ml/g), Pu, devirified	FEHM (UZ)	Unsaturation zone flow and transport	Beta	100	25	20.0	200.0			Frequency Comparison	Cumulative Comparison
786		KOPUD											
787													
788													
789													
790													
791													
792													
793	KOPUV	Kd (ml/g), Pu, viric	FEHM (UZ)	Unsaturation zone flow and transport	Beta	100	25	50.0	200.0			Frequency Comparison	Cumulative Comparison
794		KOPUV											
795													
796													
797													
798													
799													
800													
801	KOPUZ	Kd (ml/g), Pu, zeolitic	FEHM (UZ)	Unsaturation zone flow and transport	Beta	100	25	30.0	200.0			Frequency Comparison	Cumulative Comparison
802		KOPUZ											
803													
804													
805													
806													
807													
808													
809	KOSED	Kd (ml/g), Se, devirified	FEHM (UZ)	Unsaturation zone flow and transport	Beta	3	3	0.0	30.0			Frequency Comparison	Cumulative Comparison
810		KOSED											
811													
812													
813													
814													
815													
816													
817													

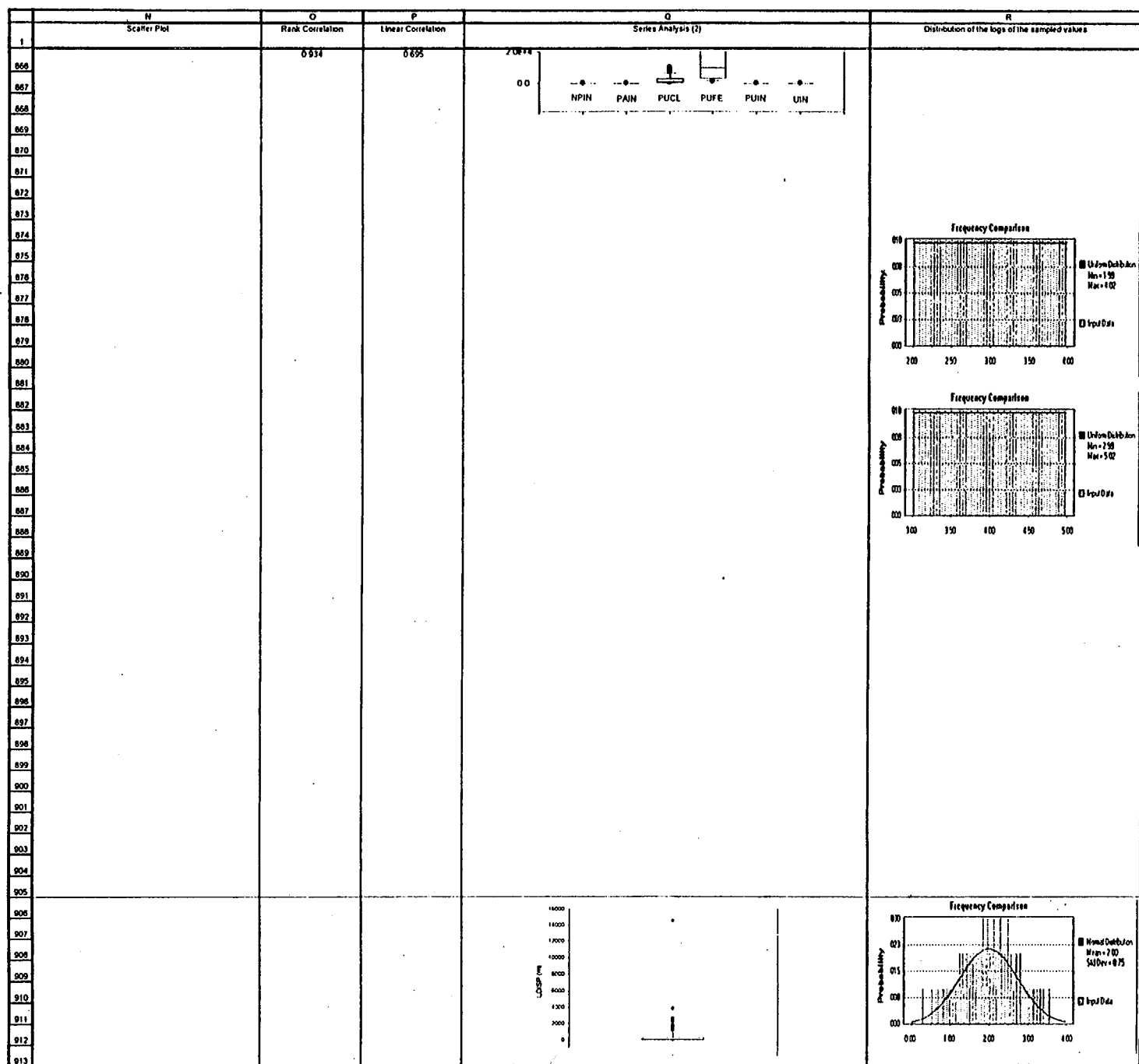
	N	O	P	Q	R
1	Scatter Plot	Rank Correlation	Linear Correlation	Series Analysis (2)	Distribution of the logs of the sampled values
770		0.934	0.695		
771					
772					
773					
774					
775					
776					
777					
778					
779					
780					
781					
782					
783					
784					
785					
786					
787					
788					
789					
790					
791					
792					
793					
794					
795					
796					
797					
798					
799					
800					
801					
802					
803					
804					
805					
806					
807					
808					
809					
810					
811					
812					
813					
814					
815					
816					
817					





	N	Stem Plot	Rank Correlation	P	Linear Correlation	Series Analysis (t)	R	Distribution of the logs of the sampled values
016			0.914		0.895			
017								
018								
019								
020								
021								
022								
023								
024								
025								
026								
027								
028								
029								
030								
031								
032								
033								
034								
035								
036								
037								
038								
039								
040								
041								
042								
043								
044								
045								
046								
047								
048								
049								
050								
051								
052								
053								
054								
055								
056								
057								
058								
059								
060								
061								
062								
063								
064								
065								

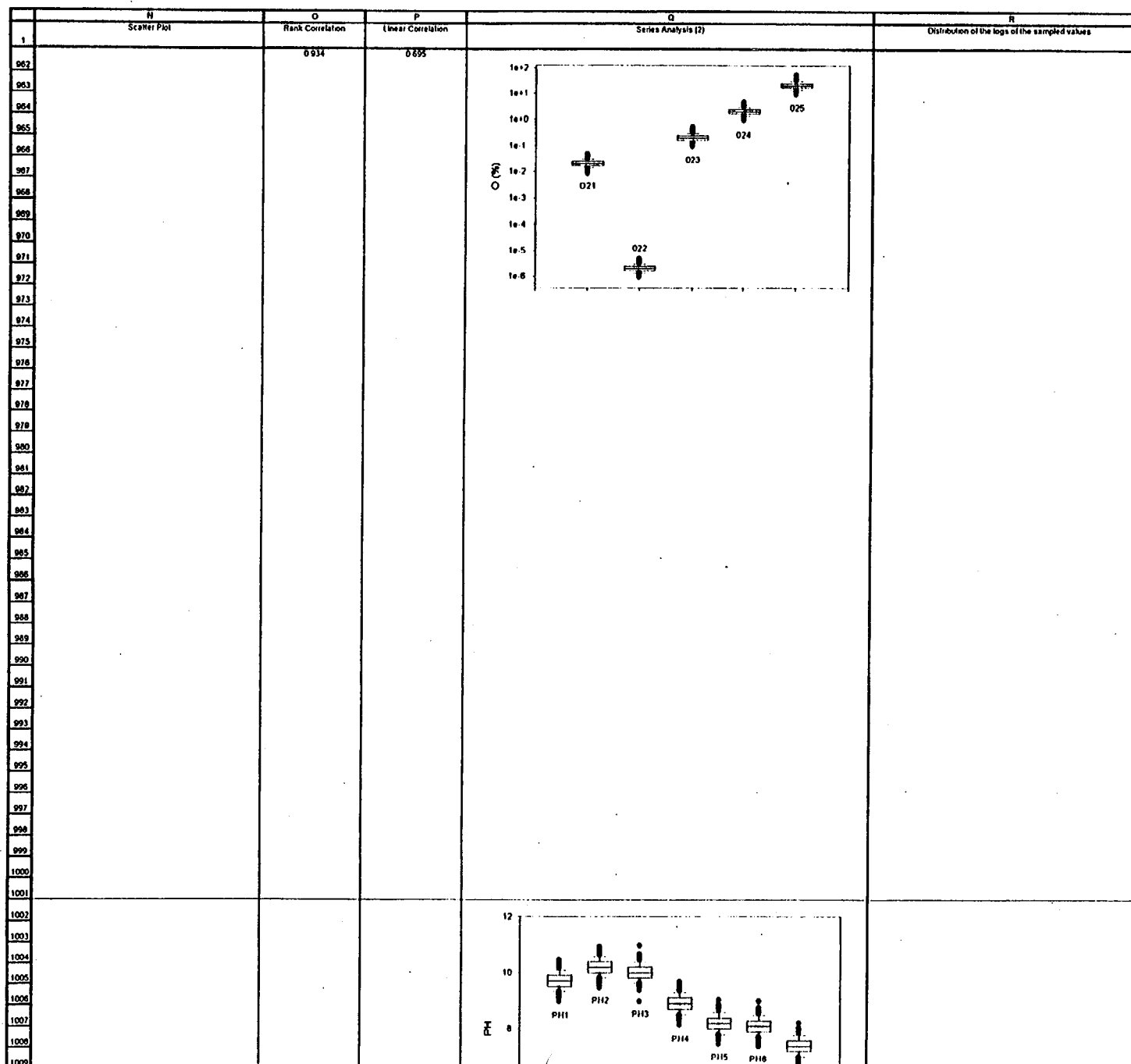
	A	B	C	D	E	F	G	H	I	J	K	L	M
	Parameter Name	Description	Code	Use in the Calculation and/or Process Model	Distribution Type	Mean	Std Dev	Minimum	Maximum	Correlated To	Correlation Coefficient	Frequency Distribution of TSPA-VA Output (1)	Cumulative Distribution of TSPA-VA Output
866	ADPMN	Sampled fraction of radionuclide in pore water, long term	RIP	Flow and transport in the engineered barrier system	uniform	FANL1	FSDL1	0.0	0.0	SFDY1	1.0		
867		KDPAN											
868													
869													
870													
871													
872													
873	KDPUCL	Kd (m3/kg) for Pu in clay colloids	RIP	Unsatulated zone flow and transport	log uniform			100.0	10000.0				
874		LOG KDPUCL											
875													
876													
877													
878													
879													
880													
881	KDPUFE	Kd (m3/kg) for Pu in Fe-oxide colloids	RIP	Unsatulated zone flow and transport	log uniform			1000.0	100000.0				
882		LOG KDPUFE											
883													
884													
885													
886													
887													
888													
889	KDPUH	Kd (m3/kg) in the invert for Pu	RIP	Flow and transport in the engineered barrier system	uniform			0.0	1.2				
890		KDPUH											
891													
892													
893													
894													
895													
896													
897	KDUIN	Kd (m3/kg) in the invert for U	RIP	Flow and transport in the engineered barrier system	uniform			0.0	0.1				
898		KDUIN											
899													
900													
901													
902													
903													
904													
905	LDISP	Longitudinal dispersivity (m), all units	FEHM (SZ)	Saturated zone flow and transport	lognormal	2 (logmean)	0.753 (logSD)						
906		LOG LDISP											
907													
908													
909													
910													
911													
912													
913													



A		B	C	D	E	F	G	H	I	J	K	L		M	
Parameter Name	Description	Code	Use in the Calculation and/or Process Model	Distribution Type	Mean	Std Dev	Minimum	Maximum	Correlated To	Correlation Coefficient	Frequency Distribution of TSPA-VA Output (1)	Cumulative Distribution of TSPA-VA Output			
ALPHA1	Saturated zone porosity - Albion (vol %)	FEHM	60/100/100/100	Uniform	FMHL1	FSD11	60000.0	100000.0	SFDY1	1.0	Frequency Comparison	Cumulative Comparison			
	LTA														
ITAL	Effective porosity - Albion	FEHM (SZ)	Saturated zone flow	truncated normal	0.25	0.075	0.0	1.0			Frequency Comparison	Cumulative Comparison			
	NNL														
HMVA	Effective porosity - Middle Volcanic Aquifer	FEHM (SZ)	Saturated zone flow	log triangular	2.00E-02		1.00E-05	0.23			Frequency Comparison	Cumulative Comparison			
	LOG HMVA														
HMVCU	Effective porosity - Middle Volcanic Confining Unit	FEHM (SZ)	Saturated zone flow	log triangular	2.00E-02		1.00E-05	0.3			Frequency Comparison	Cumulative Comparison			
	LOG HMVCU														
HPU	Effective porosity - Plutonium - Volcanic Units	FEHM (SZ)	Saturated zone flow	log uniform			1.0E-05	1.0E-03			Frequency Comparison	Cumulative Comparison			
	LOG HPU														
HUVA	Effective porosity - Upper Volcanic Aquifer	FEHM (SZ)	Saturated zone flow	log triangular	2.00E-02		1.00E-05	0.16			Frequency Comparison	Cumulative Comparison			
	NNVA														

1	Scatter Plot	Rank Correlation	0.934																																																																																																																																																																																																																																																																																																																																																																																																																																																																																																																																																																																																																																																																																																																																																																																																																																																																																																																																																																																																																																																																																																																																																																																																																																																																																																																																																																																																														
---	--------------	------------------	-------	--	--	--	--	--	--	--	--	--	--	--	--	--	--	--	--	--	--	--	--	--	--	--	--	--	--	--	--	--	--	--	--	--	--	--	--	--	--	--	--	--	--	--	--	--	--	--	--	--	--	--	--	--	--	--	--	--	--	--	--	--	--	--	--	--	--	--	--	--	--	--	--	--	--	--	--	--	--	--	--	--	--	--	--	--	--	--	--	--	--	--	--	--	--	--	--	--	--	--	--	--	--	--	--	--	--	--	--	--	--	--	--	--	--	--	--	--	--	--	--	--	--	--	--	--	--	--	--	--	--	--	--	--	--	--	--	--	--	--	--	--	--	--	--	--	--	--	--	--	--	--	--	--	--	--	--	--	--	--	--	--	--	--	--	--	--	--	--	--	--	--	--	--	--	--	--	--	--	--	--	--	--	--	--	--	--	--	--	--	--	--	--	--	--	--	--	--	--	--	--	--	--	--	--	--	--	--	--	--	--	--	--	--	--	--	--	--	--	--	--	--	--	--	--	--	--	--	--	--	--	--	--	--	--	--	--	--	--	--	--	--	--	--	--	--	--	--	--	--	--	--	--	--	--	--	--	--	--	--	--	--	--	--	--	--	--	--	--	--	--	--	--	--	--	--	--	--	--	--	--	--	--	--	--	--	--	--	--	--	--	--	--	--	--	--	--	--	--	--	--	--	--	--	--	--	--	--	--	--	--	--	--	--	--	--	--	--	--	--	--	--	--	--	--	--	--	--	--	--	--	--	--	--	--	--	--	--	--	--	--	--	--	--	--	--	--	--	--	--	--	--	--	--	--	--	--	--	--	--	--	--	--	--	--	--	--	--	--	--	--	--	--	--	--	--	--	--	--	--	--	--	--	--	--	--	--	--	--	--	--	--	--	--	--	--	--	--	--	--	--	--	--	--	--	--	--	--	--	--	--	--	--	--	--	--	--	--	--	--	--	--	--	--	--	--	--	--	--	--	--	--	--	--	--	--	--	--	--	--	--	--	--	--	--	--	--	--	--	--	--	--	--	--	--	--	--	--	--	--	--	--	--	--	--	--	--	--	--	--	--	--	--	--	--	--	--	--	--	--	--	--	--	--	--	--	--	--	--	--	--	--	--	--	--	--	--	--	--	--	--	--	--	--	--	--	--	--	--	--	--	--	--	--	--	--	--	--	--	--	--	--	--	--	--	--	--	--	--	--	--	--	--	--	--	--	--	--	--	--	--	--	--	--	--	--	--	--	--	--	--	--	--	--	--	--	--	--	--	--	--	--	--	--	--	--	--	--	--	--	--	--	--	--	--	--	--	--	--	--	--	--	--	--	--	--	--	--	--	--	--	--	--	--	--	--	--	--	--	--	--	--	--	--	--	--	--	--	--	--	--	--	--	--	--	--	--	--	--	--	--	--	--	--	--	--	--	--	--	--	--	--	--	--	--	--	--	--	--	--	--	--	--	--	--	--	--	--	--	--	--	--	--	--	--	--	--	--	--	--	--	--	--	--	--	--	--	--	--	--	--	--	--	--	--	--	--	--	--	--	--	--	--	--	--	--	--	--	--	--	--	--	--	--	--	--	--	--	--	--	--	--	--	--	--	--	--	--	--	--	--	--	--	--	--	--	--	--	--	--	--	--	--	--	--	--	--	--	--	--	--	--	--	--	--	--	--	--	--	--	--	--	--	--	--	--	--	--	--	--	--	--	--	--	--	--	--	--	--	--	--	--	--	--	--	--	--	--	--	--	--	--	--	--	--	--	--	--	--	--	--	--	--	--	--	--	--	--	--	--	--	--	--	--	--	--	--	--	--	--	--	--	--	--	--	--	--	--	--	--	--	--	--	--	--	--	--	--	--	--	--	--	--	--	--	--	--	--	--	--	--	--	--	--	--	--	--	--	--	--	--	--	--	--	--	--	--	--	--	--	--	--	--	--	--	--	--	--	--	--	--	--	--	--	--	--	--	--	--	--	--	--	--	--	--	--	--	--	--	--	--	--	--	--	--	--	--	--	--	--	--	--	--	--	--	--	--	--	--	--	--	--	--	--	--	--	--	--	--	--	--	--	--	--	--	--	--	--	--	--	--	--	--	--	--	--	--	--	--	--	--	--	--	--	--	--	--	--	--	--	--	--	--	--	--	--	--	--	--	--	--	--	--	--	--	--	--	--	--	--	--	--	--	--	--	--	--	--	--	--	--	--	--	--	--	--	--	--	--	--	--	--	--	--	--	--	--	--	--	--	--	--	--	--	--	--	--	--	--	--	--	--	--	--	--	--	--	--	--	--	--	--	--	--	--	--	--	--	--	--	--	--	--	--	--	--	--	--	--	--	--	--	--	--	--	--	--	--	--	--	--	--	--	--	--	--	--	--	--	--	--	--	--	--	--	--	--	--	--	--	--	--	--	--	--	--	--	--	--	--	--	--	--	--	--	--	--	--	--	--	--	--	--	--	--	--	--	--	--	--	--	--	--	--	--	--	--	--	--	--	--	--	--	--	--	--	--	--	--	--	--	--	--	--	--	--	--	--	--	--	--	--	--	--	--	--	--	--	--	--	--	--	--	--	--	--	--	--	--	--	--	--	--	--	--	--	--	--	--	--	--	--	--	--	--	--	--	--	--	--	--	--	--	--	--	--	--	--	--	--	--	--	--	--	--	--	--	--	--	--	--	--	--	--	--	--	--	--	--	--	--	--	--	--	--	--	--	--	--	--	--	--	--	--	--	--	--	--	--	--	--	--	--	--	--	--	--	--	--	--	--	--	--	--	--	--	--	--	--	--	--	--	--	--	--	--	--	--	--	--	--	--	--	--	--	--	--	--	--	--	--	--	--	--	--	--	--	--	--	--	--	--	--	--	--	--	--	--	--	--	--	--	--	--	--	--	--	--	--	--	--	--	--	--	--	--	--	--	--	--	--	--	--	--	--	--	--	--	--	--	--	--	--	--	--	--	--	--	--	--	--	--	--	--	--	--	--	--	--	--	--	--	--	--	--	--	--	--	--	--	--	--	--	--	--	--	--	--	--	--	--	--	--	--	--	--	--	--	--	--	--	--	--	--	--	--	--	--	--

	A	B	C	D	E	F	G	H	I	J	K	L	M
	Parameter Name	Description	Code	Use in the Calculation and/or Process Model	Distribution Type	Mean	Std Dev	Minimum	Maximum	Correlated To	Correlation Coefficient	Frequency Distribution of TSPA-VA Output (1)	Cumulative Distribution of TSPA-VA Output
962	A632A1	Scrapped plutonium pl waste from repository	RIP	Geochemical environment	lognormal	FMRL1	FSD11	0.0	1.0	SFDRY1	1.0	Frequency Comparison	Cumulative Comparison
963		O21											
964													
965													
966													
967													
968													
969													
970	O22	Oxygen partial pressure (%) from 200 - 1,000 years	RIP	Geochemical environment	lognormal							Frequency Comparison	Cumulative Comparison
971		O22											
972													
973													
974													
975													
976													
977													
978	O23	Oxygen partial pressure (%) from 1,000 - 2,000 years	RIP	Geochemical environment	lognormal							Frequency Comparison	Cumulative Comparison
979		O23											
980													
981													
982													
983													
984													
985													
986	O24	Oxygen partial pressure (%) from 2,000 - 4,000 years	RIP	Geochemical environment	lognormal							Frequency Comparison	Cumulative Comparison
987		O24											
988													
989													
990													
991													
992													
993													
994	O25	Oxygen partial pressure (%) from 4,000 - 1,000,000 years	RIP	Geochemical environment	lognormal							Frequency Comparison	Cumulative Comparison
995		O25											
996													
997													
998													
999													
1000													
1001													
1002	P11	pH of repository water from 0 - 200 years	RIP	Geochemical environment	normal	9.7	0.3					Frequency Comparison	Cumulative Comparison
1003		P11											
1004													
1005													
1006													
1007													
1008													
1009													

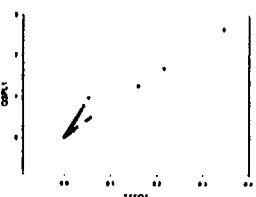
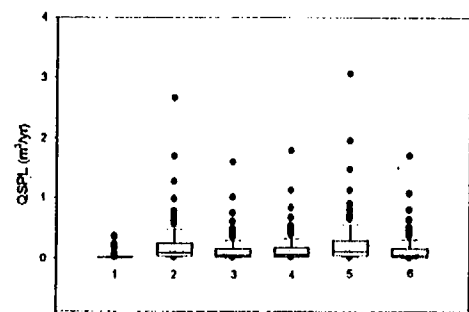
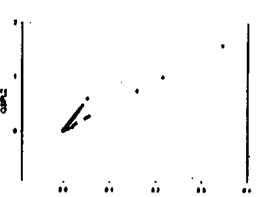
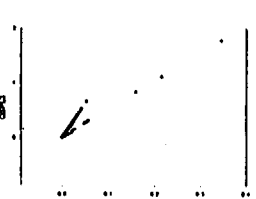
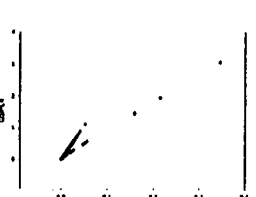
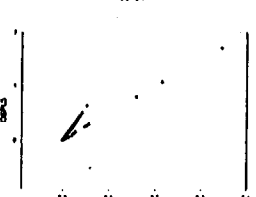
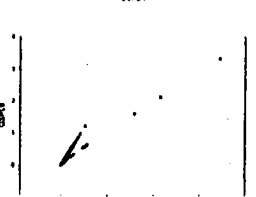
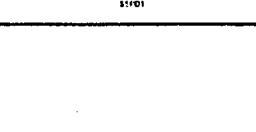






1	N	Rank Correlation	Linear Correlation	Series Analysis (2)	Distribution of the logs of the sampled values
1010	0	0.914	0.695	0	
1011					
1012					
1013					
1014					
1015					
1016					
1017					
1018					
1019					
1020					
1021					
1022					
1023					
1024					
1025					
1026					
1027					
1028					
1029					
1030					
1031					
1032					
1033					
1034					
1035					
1036					
1037					
1038					
1039					
1040					
1041					
1042					
1043					
1044					
1045					
1046					
1047					
1048					
1049					
1050					
1051					
1052					
1053					
1054					
1055					
1056					
1057					

A		B	C	D	E	F	G	H	I	J	K	L		M	
Parameter Name		Description	Code	Use in the Calculation and/or Process Model	Distribution Type	Mean	Std Dev	Minimum	Maximum	Correlated To	Coefficient	Frequency Distribution of TSPA via Output (1)		Cumulative Distribution of TSPA via Output	
1054	OSPL4	Sampled seepage flux (m3/yr), long term average climate, Region 4 30 simulations	RIP	Boundary condition	Beta	0.041	0.037	0.0	0.0415	OSPL4	1.0				
1055	OSPL2	Sampled seepage flux (m3/yr), long term average climate, Region 2 30 simulations	RIP	Boundary condition	Beta	0.041	0.037	0.0	0.0415	OSPL2	1.0				
1056	OSPL3	Sampled seepage flux (m3/yr), long term average climate, Region 3 30 simulations	RIP	Boundary condition	Beta	0.041	0.037	0.0	0.0415	OSPL3	1.0				
1057	OSPL4	Sampled seepage flux (m3/yr), long term average climate, Region 4 30 simulations	RIP	Boundary condition	Beta	0.041	0.037	0.0	0.0415	OSPL4	1.0				
1058	OSPL5	Sampled seepage flux (m3/yr), long term average climate, Region 5 30 simulations	RIP	Boundary condition	Beta	0.041	0.037	0.0	0.0415	OSPL5	1.0				
1059	OSPL6	Sampled seepage flux (m3/yr), long term average climate, Region 6 30 simulations	RIP	Boundary condition	Beta	0.041	0.037	0.0	0.0415	OSPL6	1.0				

	N Scatter Plot	O Rank Correlation	P Linear Correlation	Q Series Analysis (2)	R Distribution of the logs of the sampled values
1058		0.989	0.948		
1059					
1060					
1061					
1062					
1063		0.956	0.947		
1064					
1065					
1066					
1067					
1068		0.965	0.949		
1069					
1070					
1071					
1072					
1073		0.983	0.956		
1074					
1075					
1076					
1077					
1078		0.967	0.949		
1079					
1080					
1081					
1082					
1083		0.9985	0.957		
1084					
1085					
1086					
1087					
1088					
1089					
1090					
1091					
1092					
1093					
1094					
1095					
1096					
1097					
1098					
1099					
1100					
1101					
1102					
1103					
1104					
1105					
1106					
1107					

note: The parameters QSMXL, QSSDL, and QSUBL, 1 through 6, are defined as the mean, standard deviation and upper bound of QSP1, 1 through 6, respectively.

The specification of the input distribution as a function of three different sets of mean and standard deviation and the unequal sampling frequency generated ensemble statistics strongly skewed to the right

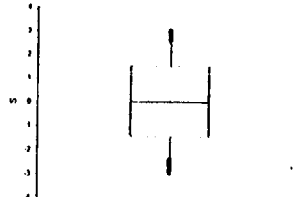
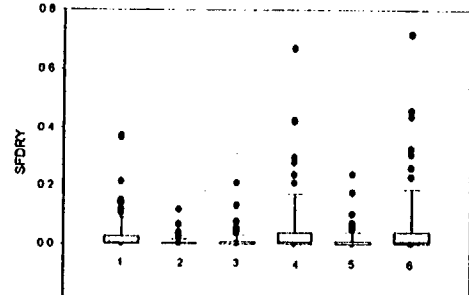
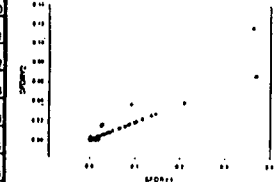
A		B	C	D	E	F	G	H	I	J	K	L	M
Parameter Name		Description	Code	Use in the Calculation and/or Process Model	Distribution Type	Mean	Std Dev	Minimum	Maximum	Correlated To	Correlation Coefficient	Frequency Distribution of ISPA-VA Output (1)	Cumulative Distribution of ISPA-VA Output
1105	45248	Sampled seepage flux (m3/yr), super physical climate, Region 1 30 simulations 60 simulations 10 simulations	RIP	Boundary condition	beta	0.143	0.137	0.0	0.50531	SSPD1	1.0		
1106	OSP52	Sampled seepage flux (m3/yr), super physical climate, Region 2 30 simulations 60 simulations 10 simulations	RIP	Boundary condition	beta	0.178	0.173	0.0	0.50532	SSPD1	1.0		
1107	OSP53	Sampled seepage flux (m3/yr), super physical climate, Region 3 30 simulations 60 simulations 10 simulations	RIP	Boundary condition	beta	0.133	0.13	0.0	0.50533	SSPD1	1.0		
1108	OSP54	Sampled seepage flux (m3/yr), super physical climate, Region 4 30 simulations 60 simulations 10 simulations	RIP	Boundary condition	beta	0.175	0.169	0.0	0.50534	SSPD1	1.0		
1109	OSP55	Sampled seepage flux (m3/yr), super physical climate, Region 5 30 simulations 60 simulations 10 simulations	RIP	Boundary condition	beta	0.105	0.101	0.0	0.50535	SSPD1	1.0		
1110	OSP56	Sampled seepage flux (m3/yr), super physical climate, Region 6 30 simulations 60 simulations 10 simulations	RIP	Boundary condition	beta	0.209	0.202	0.0	0.50536	SSPD1	1.0		

	N Scatter Plot	O Rank Correlation	P Linear Correlation	O Series Analysis (2)	R Distribution of the logs of the sampled values
1106		0.983	0.985		
1107					
1108					
1109					
1110					
1111					
1112		0.983	0.947		
1113					
1114					
1115					
1116					
1117					
1118		0.986	0.951		
1119					
1120					
1121					
1122					
1123					
1124		0.983	0.947		
1125					
1126					
1127					
1128					
1129					
1130		0.986	0.953		
1131					
1132					
1133					
1134					
1135					
1136		0.982	0.945		
1137					
1138					
1139					
1140					
1141					
1142					
1143					
1144					
1145					
1146					
1147					
1148					
1149					
1150					
1151					
1152					
1153					

note: The parameters OSMNS, QSSDS, and QSUBS, 1 through 6, are defined as the mean, standard deviation and upper bound of QSPS, 1 through 6, respectively.

The specification of the input distribution as a function of three different sets of mean and standard deviation and the unequal sampling frequency generated ensemble statistics strongly skewed to the right.

A		B	C	D	E	F	G	H	I	J	K	L	M
Parameter Name		Description	Code	Use in the Calculation and/or Process Model	Distribution Type	Mean	Std Dev	Minimum	Maximum	Correlated To	Correlation Coefficient	Frequency Distribution of TSPA-VA Output (1)	Cumulative Distribution of TSPA-VA Output
1154	ATUJA1	Sample fraction of packages with leaks, dry climate, Region 1	RIP	Waste package	Uniform	FMH1	FSD1	0.0	1.0	SFDRY1	1.0	Frequency Comparison	Cumulative Comparison
1155													
1156													
1157													
1158													
1159													
1160													
1161													
1162	SFDRY1	Sampled fraction of packages with leaks, dry climate, Region 1	RIP	Waste package	beta	FMH1	FSD1	0.0	1.0			Frequency Comparison	Cumulative Comparison
1163		30 simulations				3.50E-03	5.97E-03						
1164		60 simulations				4.60E-02	7.80E-02						
1165		10 simulations				2.21E-01	3.16E-01						
1166													
1167													
1168													
1169	SFDRY2	Sampled fraction of packages with leaks, dry climate, Region 2	RIP	Waste package	beta	FMH2	FSD2	0.0	1.0	SFDRY1	1.0	Frequency Comparison	Cumulative Comparison
1170		30 simulations				1.00E-07	1.00E-07						
1171		60 simulations				8.22E-03	1.40E-02						
1172		10 simulations				9.66E-02	1.64E-01						
1173													
1174													
1175													
1176													
1177	SFDRY3	Sampled fraction of packages with leaks, dry climate, Region 3	RIP	Waste package	beta	FMH3	FSD3	0.0	1.0	SFDRY1	1.0	Frequency Comparison	Cumulative Comparison
1178		30 simulations				1.00E-07	1.00E-07						
1179		60 simulations				1.63E-02	2.72E-02						
1180		10 simulations				1.69E-01	2.84E-01						
1181													
1182													
1183													
1184													
1185	SFDRY4	Sampled fraction of packages with leaks, dry climate, Region 4	RIP	Waste package	beta	FMH4	FSD4	0.0	1.0	SFDRY1	1.0	Frequency Comparison	Cumulative Comparison
1186		30 simulations				8.50E-03	1.11E-02						
1187		60 simulations				8.59E-02	1.46E-01						
1188		10 simulations				2.42E-01	3.20E-01						
1189													
1190													
1191													
1192													
1193	SFDRY5	Sampled fraction of packages with leaks, dry climate, Region 5	RIP	Waste package	beta	FMH5	FSD5	0.0	1.0	SFDRY1	1.0	Frequency Comparison	Cumulative Comparison
1194		30 simulations				1.00E-07	1.00E-07						
1195		60 simulations				2.17E-02	3.69E-02						
1196		10 simulations				1.79E-01	2.90E-01						
1197													
1198													
1199													
1200													
1201													

I	II	O	P	Q	R
	Scatter Plot	Rank Correlation	Linear Correlation	Series Analysis (2)	Distribution of the logs of the sampled values
1154		0.934	0.695		
1155					
1156					
1157					
1158					
1159					
1160					
1161					
1162					
1163					
1164				 <p>note: The parameters FMND and FSDD, 1 through 6, are defined as the mean and standard deviation of SFDRY, 1 through 6, respectively.</p> <p>The specification of the input distribution as a function of three different sets of mean and standard deviation and the unequal sampling frequency generated ensemble statistics strongly skewed to the right.</p>	
1165					
1166					
1167					
1168					
1169					
1170		0.917	0.949		
1171					
1172					
1173					
1174					
1175					
1176					
1177					
1178		0.908	0.972		
1179					
1180					
1181					
1182					
1183					
1184					
1185					
1186		0.997	0.981		
1187					
1188					
1189					
1190					
1191					
1192					
1193					
1194		0.896	0.907		
1195					
1196					
1197					
1198					
1199					
1200					
1201					

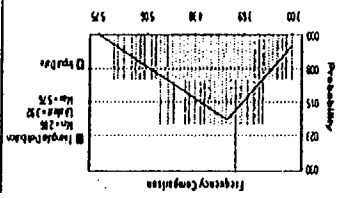
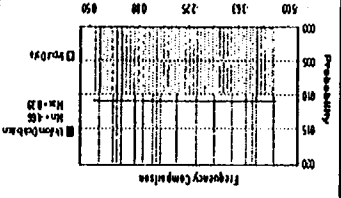
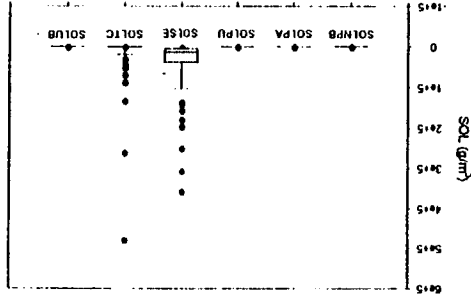


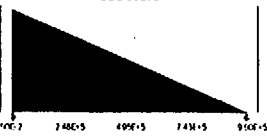




1	Scatter Plot		1202 1203 1204 1205 1206 1207 1208 1209
2	Rank Correlation	0.956	1210 1211 1212 1213 1214 1215 1216 1217 1218 1219 1220 1221
3	Linear Correlation	0.955	1222 1223 1224 1225 1226 1227 1228 1229 1230 1231 1232 1233 1234 1235 1236 1237 1238 1239 1240 1241 1242 1243 1244 1245 1246 1247 1248 1249
4	Series Analysis (2)		
5	Distribution of the logs of the sampled values		

	A	B	C	D	E	F	G	H	I	J	K	L	M
	Parameter Name	Description	Code	Use in the Calculation and/or Process Model	Distribution Type	Mean	Std Dev	Minimum	Maximum	Correlated To	Correlation Coefficient	Frequency Distribution of TSPA-VA Output (1)	Cumulative Distribution of TSPA-VA Output
1250	AS1761	Sample dissolution model parameter term	RIP	Waste package	normal	0.00	1.00	0.00	1.00	STORY1	1.00	Frequency Comparison	Cumulative Comparison
1251		SFM											
1252													
1253													
1254													
1255													
1256													
1257													
1258	SF117	Spent fuel dissolution model parameter	RIP	Waste Package	normal	0.00	1.00					Frequency Comparison	Cumulative Comparison
1259		SFM											
1260													
1261													
1262													
1263													
1264													
1265													
1266	SOLHP8	Solubility of H <sub>2</sub> PO <sub>4</sub> (g/m <sup>3</sup> )	RIP	Geochemical environment	log beta	0.4685	0.5622	-1.9208	1.3802			Frequency Comparison	Cumulative Comparison
1267		LOG SOLHP8											
1268													
1269													
1270													
1271													
1272													
1273													
1274	SOLPA	Solubility of Pa (g/m <sup>3</sup> )	RIP	Geochemical environment	log uniform			2.3E-05	2.3			Frequency Comparison	Cumulative Comparison
1275		LOG SOLPA											
1276													
1277													
1278													
1279													
1280													
1281													
1282	SOLPU	Solubility of U (g/m <sup>3</sup> )	RIP	Geochemical environment	uniform			2.4E-03	2.4E-01			Frequency Comparison	Cumulative Comparison
1283		SOLPU											
1284													
1285													
1286													
1287													
1288													
1289													
1290	SOLSE	Solubility of Se (g/m <sup>3</sup> )	RIP	Geochemical environment	log triangular	7.9E+03		7.9E+02	5.5E+05			Frequency Comparison	Cumulative Comparison
1291		LOG SOLSE											
1292													
1293													
1294													
1295													
1296													
1297													

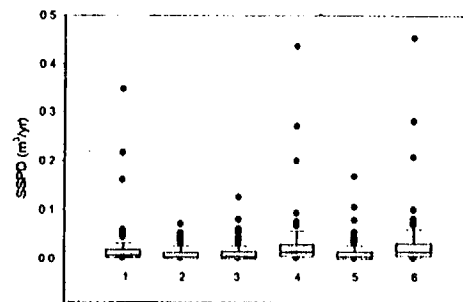
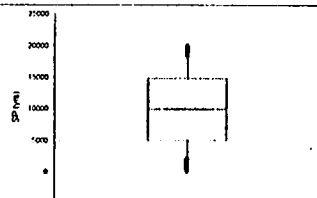
1	Scatter Plot	N				1290
	Rank Correlation	R	0.934			1291
	Linear Correlation	P	0.695			1292
	Series Analysis (2)	Q				1293
	Distribution of the tops of the sampled values	R				1294
						1295
						1296
						1297
						1298
						1299
						1300
						1301
						1302
						1303
						1304
						1305
						1306
						1307
						1308
						1309
						1310
						1311
						1312
						1313
						1314
						1315
						1316
						1317
						1318
						1319
						1320
						1321
						1322
						1323
						1324
						1325
						1326
						1327
						1328
						1329
						1330
						1331
						1332
						1333
						1334
						1335
						1336
						1337
						1338
						1339
						1340
						1341
						1342
						1343
						1344
						1345
						1346
						1347
						1348
						1349
						1350
						1351
						1352
						1353
						1354
						1355
						1356
						1357
						1358
						1359
						1360
						1361
						1362
						1363
						1364
						1365
						1366
						1367
						1368
						1369
						1370
						1371
						1372
						1373
						1374
						1375
						1376
						1377
						1378
						1379
						1380
						1381
						1382
						1383
						1384
						1385
						1386
						1387
						1388
						1389
						1390
						1391
						1392
						1393
						1394
						1395
						1396
						1397
						1398
						1399
						1400



A		B	C	D	E	F	G	H	I	J	K	L	M
Parameter Name		Description	Code	Use in the Calculation and/or Process Model	Distribution Type	Mean	Std Dev	Minimum	Maximum	Correlated To	Correlation Coefficient	Frequency Distribution of TSPA-VA Output (1)	Cumulative Distribution of TSPA-VA Output
1298	AKUT1	Sampled fracture permeability, long term	RIP	Geological environment	log triangular	7.0E-1	7.5E-1	3.5E-2	9.9E-1	SFDY1	1.0	Frequency Comparison	Cumulative Comparison
1299		LOG SOLTC											
1300													
1301													
1302													
1303													
1304													
1305	SOLUB	Solubility of U (g/m3)	RIP	Geochemical environment	beta	0.88	0.8976	2.6198	3.38			Frequency Comparison	Cumulative Comparison
1306													
1307													
1308													
1309													
1310													
1311													
1312													
1313	SP	Duration of super physical climate (years)	RIP	boundary condition	uniform			0.0	20000.0			Frequency Comparison	Cumulative Comparison
1314													
1315													
1316													
1317													
1318													
1319													
1320													
1321	SSPD1	Sampled seepage flux (m3/yr), dry climate, Region 1	RIP	boundary condition	beta	OSMND1	OSSD1	0.0	OSUB1			Frequency Comparison	Cumulative Comparison
1322		30 simulations				5.10E-03	4.60E-03		5.10E-02				
1323		60 simulations				1.24E-02	1.12E-02		1.24E-01				
1324		10 simulations				1.14E-01	1.09E-01		1.20E+00				
1325													
1326													
1327													
1328													
1329	SSPD2	Sampled seepage flux (m3/yr), dry climate, Region 2	RIP	boundary condition	beta	OSMND2	OSSD2	0.0	OSUB2	SSPD1	1.0	Frequency Comparison	Cumulative Comparison
1330		30 simulations				1.00E-07	1.00E-07		1.00E-06				
1331		60 simulations				1.20E-02	1.08E-02		1.20E-01				
1332		10 simulations				2.40E-02	2.17E-02		2.41E-01				
1333													
1334													
1335													
1336													
1337	SSPD3	Sampled seepage flux (m3/yr), dry climate, Region 3	RIP	boundary condition	beta	OSMND3	OSSD3	0.0	OSUB3	SSPD1	1.0	Frequency Comparison	Cumulative Comparison
1338		30 simulations				1.00E-07	1.00E-07		1.00E-06				
1339		60 simulations				1.23E-02	1.11E-02		1.23E-01				
1340		10 simulations				4.26E-02	3.88E-02		4.31E-01				
1341													
1342													
1343													
1344													
1345													

	N Scatter Plot	O Rank Correlation	P Linear Correlation	Q Series Analysis (2)	R Distribution of the logs of the sampled values
1298		0.934	0.695		<p>Frequency Comparison</p> <p>Cumulative Comparison</p>
1299					
1300					
1301					
1302					
1303					
1304					
1305					
1306					
1307					
1308					
1309					
1310					
1311					
1312					
1313					
1314					
1315					
1316					
1317					
1318					
1319					
1320					
1321					
1322					
1323					
1324					
1325					
1326					
1327					
1328					
1329					
1330		0.834	0.748		
1331					
1332					
1333					
1334					
1335					
1336					
1337					
1338		0.857	0.915		
1339					
1340					
1341					
1342					
1343					
1344					
1345					

note: Crystal Ball does not show beta distributions with negative values. To fit the beta distribution illustrated in the next column, 100 was added to each of the sample values. The p-value for the Chi-Square test was 0.998.

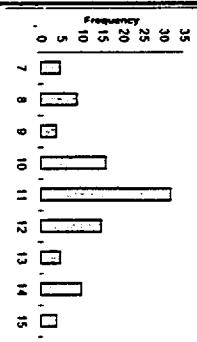
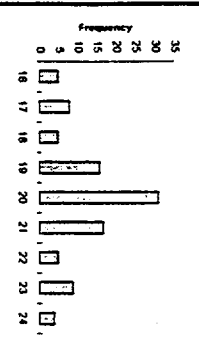
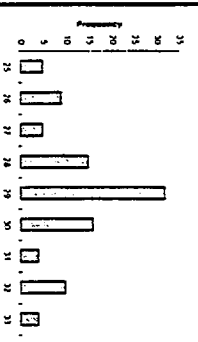
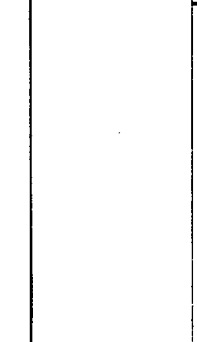






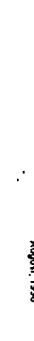






note: The parameters QSMND, QSSDD, and QSUBD, 1 through 6, are defined as the mean, standard deviation and upper bound of SSPO, 1 through 6, respectively.

The specification of the input distribution as a function of three different sets of mean and standard deviation and the unequal sampling frequency generated ensemble statistics strongly skewed to the right.

i	Parameter Name	Description	C	O	E	F	G	H	I	J	K	Cumulative Distribution of TSPA.VA Output	
												Frequency Distribution of TSPA.VA Output (1)	M
1346	ASD01	Sampled seepage flux (m/yr), dry climate, Region 5 30 simulations 60 simulations 10 simulations	RIP	uniform package	beta	OSM004 9.47E-02 2.18E-01 1.51E-00	OSD04 0.0	0.0	OSUB01 9.47E-02 2.18E-01 1.51E-00	SSPD1	1.0	Frequency Cumulative Lognormal Distribution Min=13E-2 Max=15E-1 D=10000	Cumulative Cumulative Lognormal Distribution Min=13E-2 Max=15E-1 D=10000
1347													
1348													
1349													
1350													
1351													
1352													
1353	SSPD5	Sampled seepage flux (m/yr), dry climate, Region 5 30 simulations 60 simulations 10 simulations	RIP	boundary condition	beta	OSM005 1.0E-07 1.23E-02 5.60E-02	OSD05 0.0	0.0	OSUB05 1.0E-06 1.23E-01 5.75E-01	SSPD1	1.0	Frequency Cumulative Lognormal Distribution Min=10E-5 Max=15E-1 D=10000	Cumulative Cumulative Lognormal Distribution Min=10E-5 Max=15E-1 D=10000
1354													
1355													
1356													
1357													
1358													
1359													
1360													
1361													
1362	SSPD6	Sampled seepage flux (m/yr), dry climate, Region 6 30 simulations 60 simulations 10 simulations	RIP	boundary condition	beta	OSM006 1.0E-02 2.33E-02 1.4E-01	OSD06 0.0	0.0	OSUB06 1.0E-01 2.33E-01 1.57E-00	SSPD1	1.0	Frequency Cumulative Lognormal Distribution Min=13E-2 Max=15E-1 D=10000	Cumulative Cumulative Lognormal Distribution Min=13E-2 Max=15E-1 D=10000
1363													
1364													
1365													
1366													
1367													
1368													
1369	UPATCH	Uniform random number for seepage through patches	RIP	Waste package	uniform			1.0	10.0			Frequency Cumulative Uniform Distribution Min=0.0 Max=10.0 D=10000	Cumulative Cumulative Uniform Distribution Min=0.0 Max=10.0 D=10000
1370													
1371													
1372													
1373													
1374													
1375													
1376													
1377	UPIT	Uniform random number for seepage through pits	RIP	Waste package	uniform			0.0	2.0			Frequency Cumulative Uniform Distribution Min=0.0 Max=2.0 D=10000	Cumulative Cumulative Uniform Distribution Min=0.0 Max=2.0 D=10000
1378													
1379													
1380													
1381													
1382													
1383													
1384													
1385	UPRAID	Uniform random number for selecting UZ transport parameters	RIP	Unshielded zone transport parameters	uniform			1.0	101.0			Frequency Cumulative Uniform Distribution Min=1.0 Max=101.0 D=10000	Cumulative Cumulative Uniform Distribution Min=1.0 Max=101.0 D=10000
1386													
1387													
1388													
1389													
1390													
1391													
1392													
1393													

I	H	O	P	D	R
	Scatter Plot	Rank Correlation	Linear Correlation	Series Analysis (2)	Distribution of the logs of the sampled values
1346		0.997	0.996		
1347					
1348					
1349					
1350					
1351					
1352					
1353		0.864	0.961		
1354					
1355					
1356					
1357					
1358					
1359					
1360					
1361		0.997	0.994		
1362					
1363					
1364					
1365					
1366					
1367					
1368					
1369					
1370					
1371					
1372					
1373					
1374					
1375					
1376					
1377					
1378					
1379					
1380					
1381					
1382					
1383					
1384					
1385					
1386					
1387					
1388					
1389					
1390					
1391					
1392					
1393					

A	B	C	D	E	F	G	H	I	J	K	L	M
Parameter Name	Description	Code	Use in the Calculation and/or Process Model	Outlook Type	Mean FAMCT	Std Dev FSOCT	Maximum 0.0	Maximum 1.0	Counted FSOCT	Counted Coefficient	Frequency Distribution of ISPA-VIA Output (1)	Cumulative Distribution of ISPA-VIA Output
1394	WAPR101	WAPR101	White package	discrete								
1395	WAPR102	WAPR102	White package	discrete								
1396	WAPR103	WAPR103	White package	discrete								
1397	WAPR104	WAPR104	White package	discrete								
1398	WAPR105	WAPR105	White package	discrete								
1399	WAPR106	WAPR106	White package	discrete								
1400	WAPR107	WAPR107	White package	discrete								
1401	WAPR108	WAPR108	White package	discrete								
1402	WAPR109	WAPR109	White package	discrete								
1403	WAPR110	WAPR110	White package	discrete								
1404	WAPR111	WAPR111	White package	discrete								
1405	WAPR112	WAPR112	White package	discrete								
1406	WAPR113	WAPR113	White package	discrete								
1407	WAPR114	WAPR114	White package	discrete								
1408	WAPR115	WAPR115	White package	discrete								
1409	WAPR116	WAPR116	White package	discrete								
1410	WAPR117	WAPR117	White package	discrete								
1411	WAPR118	WAPR118	White package	discrete								
1412	WAPR119	WAPR119	White package	discrete								
1413	WAPR120	WAPR120	White package	discrete								
1414	WAPR121	WAPR121	White package	discrete								
1415	WAPR122	WAPR122	White package	discrete								
1416	WAPR123	WAPR123	White package	discrete								
1417	WAPR124	WAPR124	White package	discrete								
1418	WAPR125	WAPR125	White package	discrete								
1419	WAPR126	WAPR126	White package	discrete								
1420	WAPR127	WAPR127	White package	discrete								
1421	WAPR128	WAPR128	White package	discrete								
1422	WAPR129	WAPR129	White package	discrete								
1423	WAPR130	WAPR130	White package	discrete								

(1) Each of the figures in this column displays the frequency distribution of the random variable as sampled in the ISPA-VIA and a "best fit" continuous distribution represented by the solid green curve. The "best fit" distribution is determined by a series of mathematical tests performed to find the best fit between a standard probability distribution and the distribution of a set of data. The adjacent column is titled by the same information plotted as a cumulative distribution of the sampled data. The continuous distributions were fit to the sample data using Crystal Ball Version 4.0.

(2) Since data is displayed as a bar plot, the boundary of the bar closest to zero indicates the 25th percentile, the bar within the bar marks the median, and the boundary of the bar furthest from zero indicates the 75th percentile. Whiskers above and below the box indicate the 50th and 10th percentiles. Outlying data values are plotted above and below the whiskers. The box plots were generated using SigmaStat, Version 2.0 and edited using SigmaPlot 4.0 for Windows.



																																																																																																																																																																																																																																																																																																																																																																																																																																																																																																																																																																																																																																																																																																																																																																																																																																																																																																																																																																																																																																																																																																																																																																																																																																																																																																																																																																																																																					</
--	--	--	--	--	--	--	--	--	--	--	--	--	--	--	--	--	--	--	--	--	--	--	--	--	--	--	--	--	--	--	--	--	--	--	--	--	--	--	--	--	--	--	--	--	--	--	--	--	--	--	--	--	--	--	--	--	--	--	--	--	--	--	--	--	--	--	--	--	--	--	--	--	--	--	--	--	--	--	--	--	--	--	--	--	--	--	--	--	--	--	--	--	--	--	--	--	--	--	--	--	--	--	--	--	--	--	--	--	--	--	--	--	--	--	--	--	--	--	--	--	--	--	--	--	--	--	--	--	--	--	--	--	--	--	--	--	--	--	--	--	--	--	--	--	--	--	--	--	--	--	--	--	--	--	--	--	--	--	--	--	--	--	--	--	--	--	--	--	--	--	--	--	--	--	--	--	--	--	--	--	--	--	--	--	--	--	--	--	--	--	--	--	--	--	--	--	--	--	--	--	--	--	--	--	--	--	--	--	--	--	--	--	--	--	--	--	--	--	--	--	--	--	--	--	--	--	--	--	--	--	--	--	--	--	--	--	--	--	--	--	--	--	--	--	--	--	--	--	--	--	--	--	--	--	--	--	--	--	--	--	--	--	--	--	--	--	--	--	--	--	--	--	--	--	--	--	--	--	--	--	--	--	--	--	--	--	--	--	--	--	--	--	--	--	--	--	--	--	--	--	--	--	--	--	--	--	--	--	--	--	--	--	--	--	--	--	--	--	--	--	--	--	--	--	--	--	--	--	--	--	--	--	--	--	--	--	--	--	--	--	--	--	--	--	--	--	--	--	--	--	--	--	--	--	--	--	--	--	--	--	--	--	--	--	--	--	--	--	--	--	--	--	--	--	--	--	--	--	--	--	--	--	--	--	--	--	--	--	--	--	--	--	--	--	--	--	--	--	--	--	--	--	--	--	--	--	--	--	--	--	--	--	--	--	--	--	--	--	--	--	--	--	--	--	--	--	--	--	--	--	--	--	--	--	--	--	--	--	--	--	--	--	--	--	--	--	--	--	--	--	--	--	--	--	--	--	--	--	--	--	--	--	--	--	--	--	--	--	--	--	--	--	--	--	--	--	--	--	--	--	--	--	--	--	--	--	--	--	--	--	--	--	--	--	--	--	--	--	--	--	--	--	--	--	--	--	--	--	--	--	--	--	--	--	--	--	--	--	--	--	--	--	--	--	--	--	--	--	--	--	--	--	--	--	--	--	--	--	--	--	--	--	--	--	--	--	--	--	--	--	--	--	--	--	--	--	--	--	--	--	--	--	--	--	--	--	--	--	--	--	--	--	--	--	--	--	--	--	--	--	--	--	--	--	--	--	--	--	--	--	--	--	--	--	--	--	--	--	--	--	--	--	--	--	--	--	--	--	--	--	--	--	--	--	--	--	--	--	--	--	--	--	--	--	--	--	--	--	--	--	--	--	--	--	--	--	--	--	--	--	--	--	--	--	--	--	--	--	--	--	--	--	--	--	--	--	--	--	--	--	--	--	--	--	--	--	--	--	--	--	--	--	--	--	--	--	--	--	--	--	--	--	--	--	--	--	--	--	--	--	--	--	--	--	--	--	--	--	--	--	--	--	--	--	--	--	--	--	--	--	--	--	--	--	--	--	--	--	--	--	--	--	--	--	--	--	--	--	--	--	--	--	--	--	--	--	--	--	--	--	--	--	--	--	--	--	--	--	--	--	--	--	--	--	--	--	--	--	--	--	--	--	--	--	--	--	--	--	--	--	--	--	--	--	--	--	--	--	--	--	--	--	--	--	--	--	--	--	--	--	--	--	--	--	--	--	--	--	--	--	--	--	--	--	--	--	--	--	--	--	--	--	--	--	--	--	--	--	--	--	--	--	--	--	--	--	--	--	--	--	--	--	--	--	--	--	--	--	--	--	--	--	--	--	--	--	--	--	--	--	--	--	--	--	--	--	--	--	--	--	--	--	--	--	--	--	--	--	--	--	--	--	--	--	--	--	--	--	--	--	--	--	--	--	--	--	--	--	--	--	--	--	--	--	--	--	--	--	--	--	--	--	--	--	--	--	--	--	--	--	--	--	--	--	--	--	--	--	--	--	--	--	--	--	--	--	--	--	--	--	--	--	--	--	--	--	--	--	--	--	--	--	--	--	--	--	--	--	--	--	--	--	--	--	--	--	--	--	--	--	--	--	--	--	--	--	--	--	--	--	--	--	--	--	--	--	--	--	--	--	--	--	--	--	--	--	--	--	--	--	--	--	--	--	--	--	--	--	--	--	--	--	--	--	--	--	--	--	--	--	--	--	--	--	--	--	--	--	--	--	--	--	--	--	--	--	--	--	--	--	--	--	--	--	--	--	--	--	--	--	--	--	--	--	--	--	--	--	--	--	--	--	--	--	--	--	--	--	--	--	--	--	--	--	--	--	--	--	--	--	--	--	--	--	--	--	--	--	--	--	--	--	--	--	--	--	--	--	--	--	--	--	--	--	--	--	--	--	--	--	--	--	--	--	--	--	--	--	--	--	--	--	--	--	--	--	--	--	--	--	--	--	--	--	--	--	--	--	--	--	--	--	--	--	--	--	--	--	--	--	--	--	--	--	--	--	--	--	--	--	--	--	--	--	--	--	--	--	--	--	--	--	--	--	--	--	--	--	--	--	--	--	--	--	--	--	--	--	--	--	--	--	--	--	--	--	--	--	--	--	--	--	--	--	--	--	--	--	--	--	--	--	--	--	--	--	--	--	--	--	--	--	--	--	--	--	--	--	--	--	--	--	--	--	--	--	--	--	--	--	--	--	--	--	--	--	--	--	--	--	--	--	--	--	--	--	--	--	--	--	--	--	--	--	--	--	--	--	--	--	--	--	--	--	--	--	--	--	--	--	--	--	--	--	--	--	--	--	--	--	--	--	--	--	--	--	--	--	--	--	--	--	--	--	--	--	--	--	--	--	--	--	--	--	--	--	--	--	--	--	--	--	--	--	--	--	--	--	--	--	--	--	--	--	--	--	--	--	--	--	--	--	--	--	--	--	--	--	--	--	--	--	--	--	--	--	--	--	--	--	--	--	--	--	--	--	--	--	--	--	--	--	--	--	----

## **Chapter 11**

### **Figures**

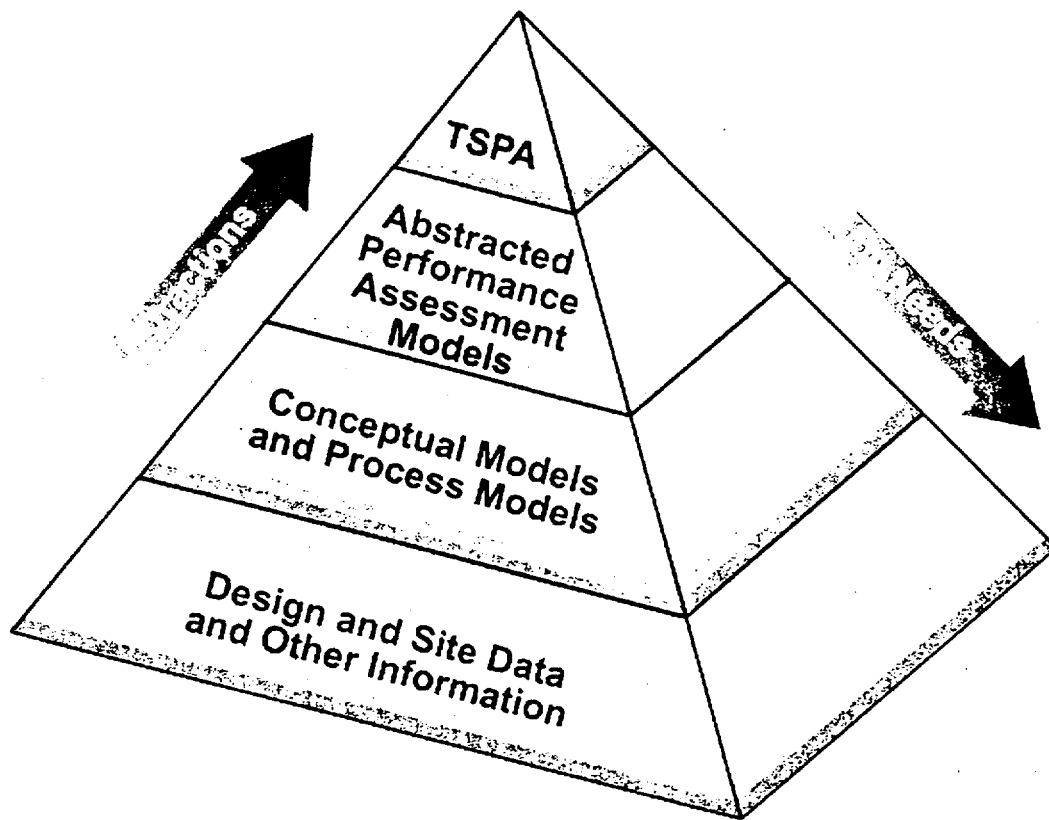


Figure 11-1. Performance assessment information flow pyramid.

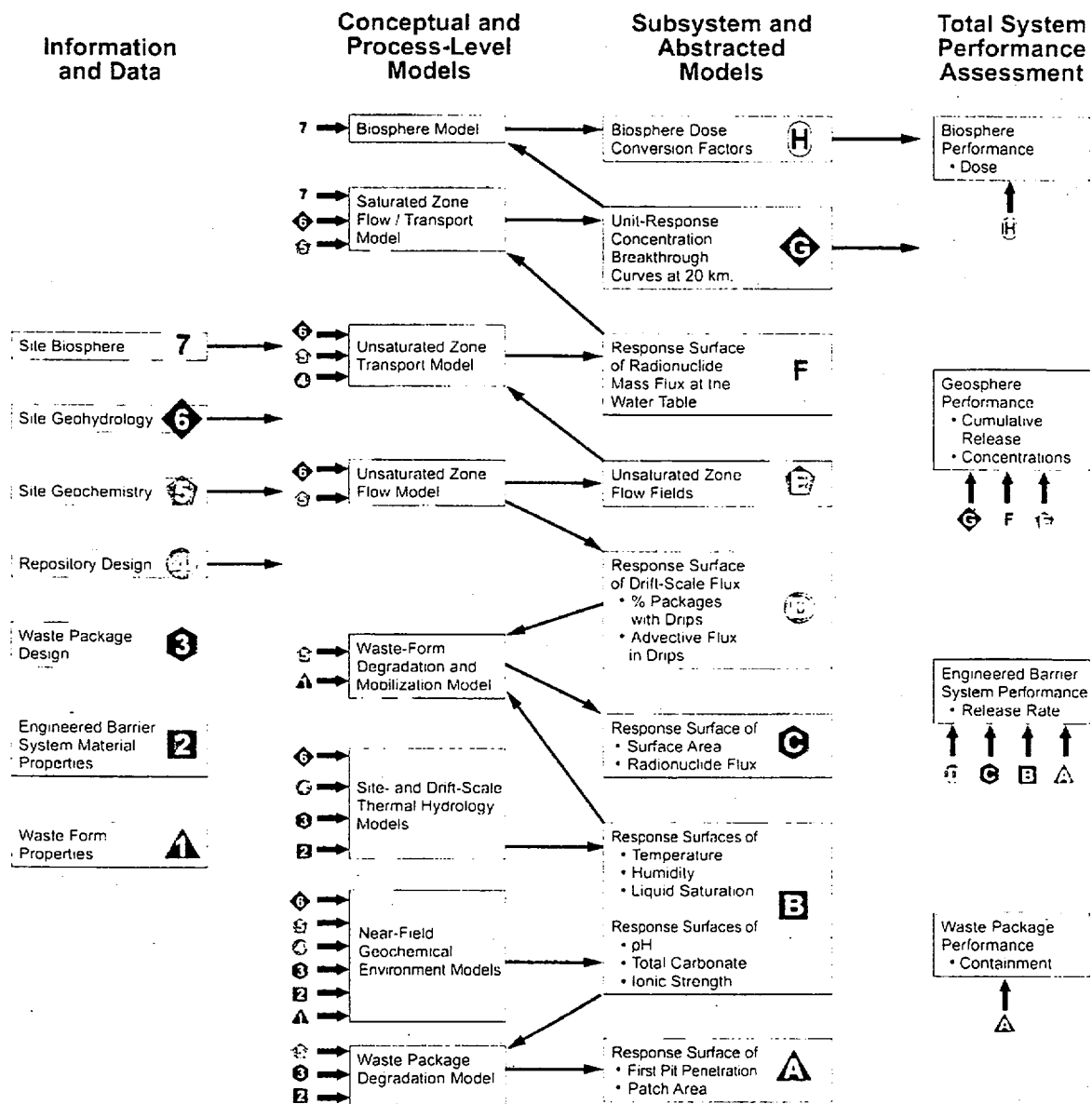
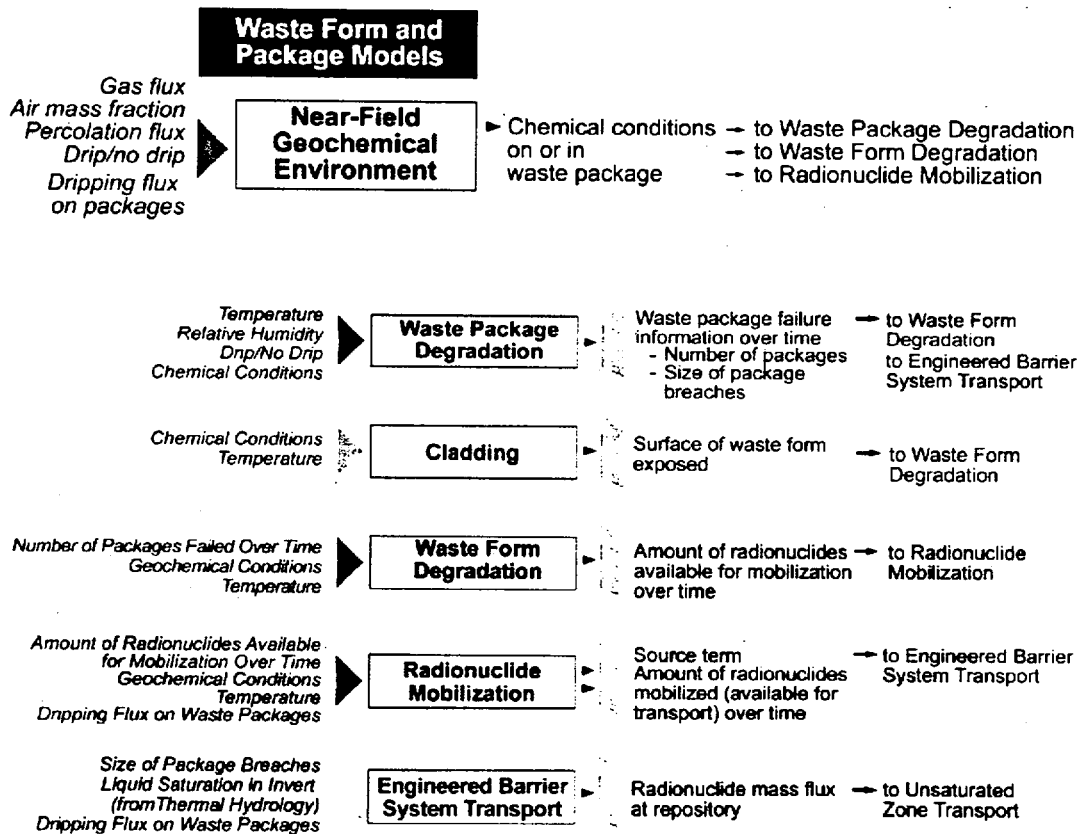
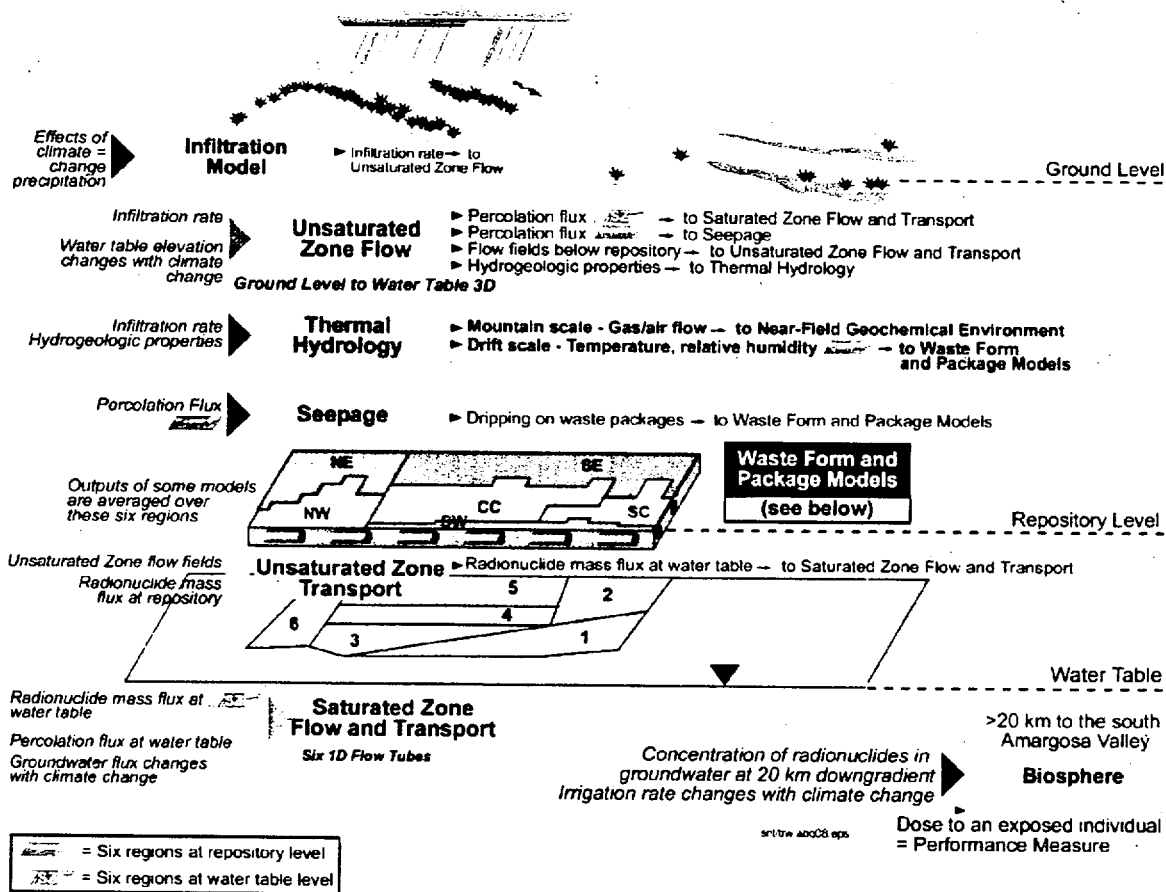


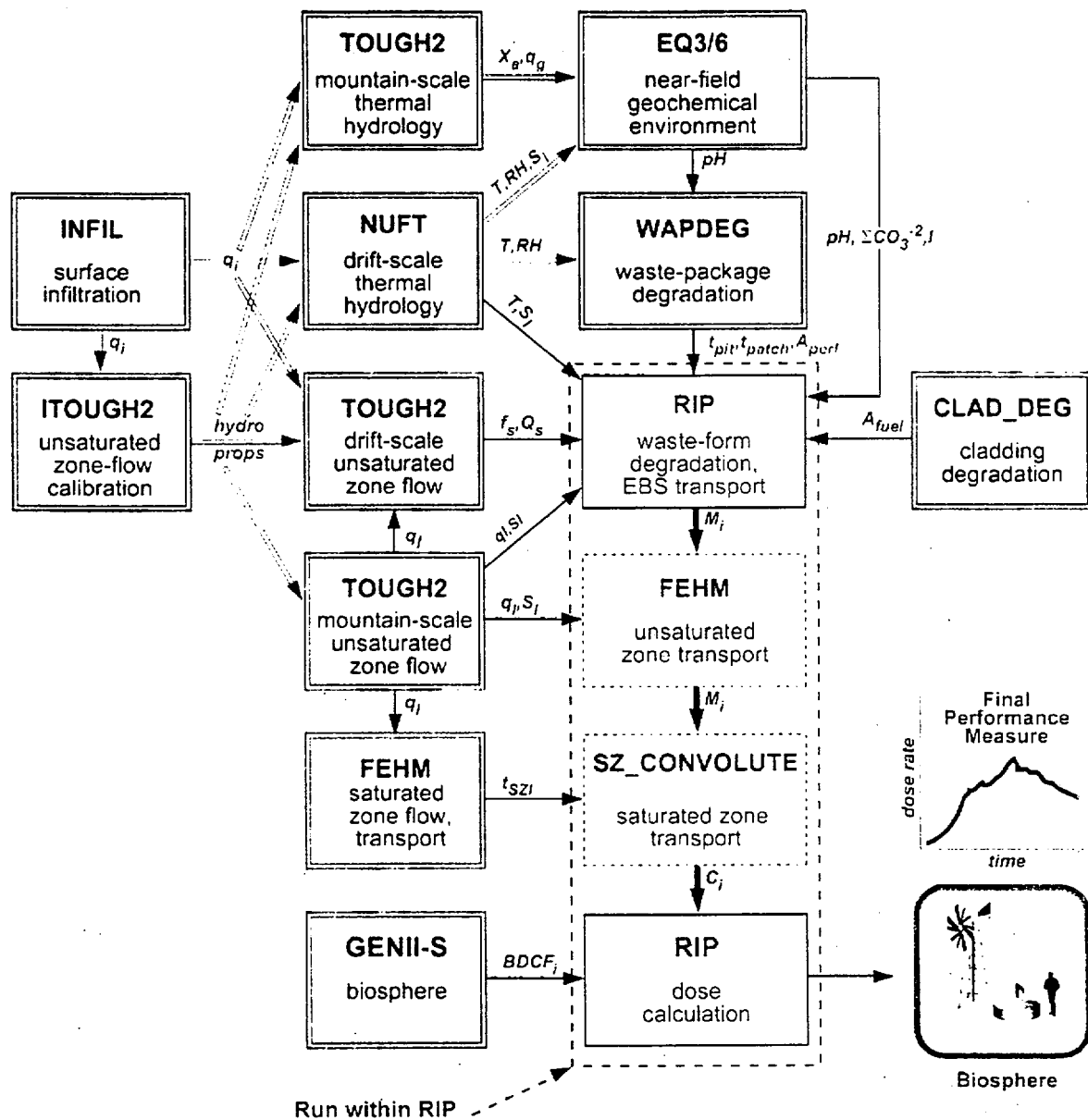
Figure 11-2. Simplified representation of information flow in TSPA-VA between data, process models, and abstracted models.



snltw abq22 eds

= six regions at repository level

Figure 11-3. Detailed representation of information flow in TSPA-VA.



#### OUTPUT Parameters

$T$	Temperature	$Q_s$	Seep flow rate
$RH$	Relative humidity	$pH$	pH
$S_i$	Liquid saturation	$\Sigma CO_3^{2-}$	Carbonate concentration
$X_a$	Air mass fraction	$I$	Ionic strength
$q_g$	Gas flux	$t_{pit}$	Initial-pit-penetration time
$q_l$	Liquid flux	$t_{patch}$	Initial-patch-penetration time
$q_i$	Infiltration flux	$A_{perf}$	Perforated container area
$M_i$	Radionuclide mass flux	$A_{fuel}$	Exposed fuel area
$C_i$	Radionuclide concentration	$t_{SZi}$	Saturated zone transport time
$f_s$	Fraction of WPs with seeps	$BDCF_i$	Biosphere dose conversion factor
		<b>EBS</b>	Engineered Barrier System

#### Legend

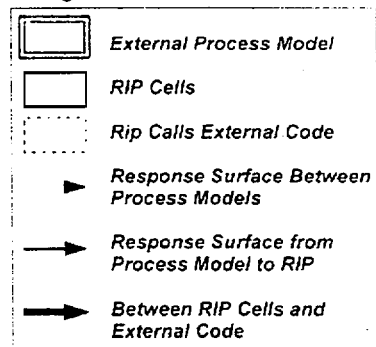


Figure 11-4. TSPA-VA code configuration: Information flow among component computer codes.

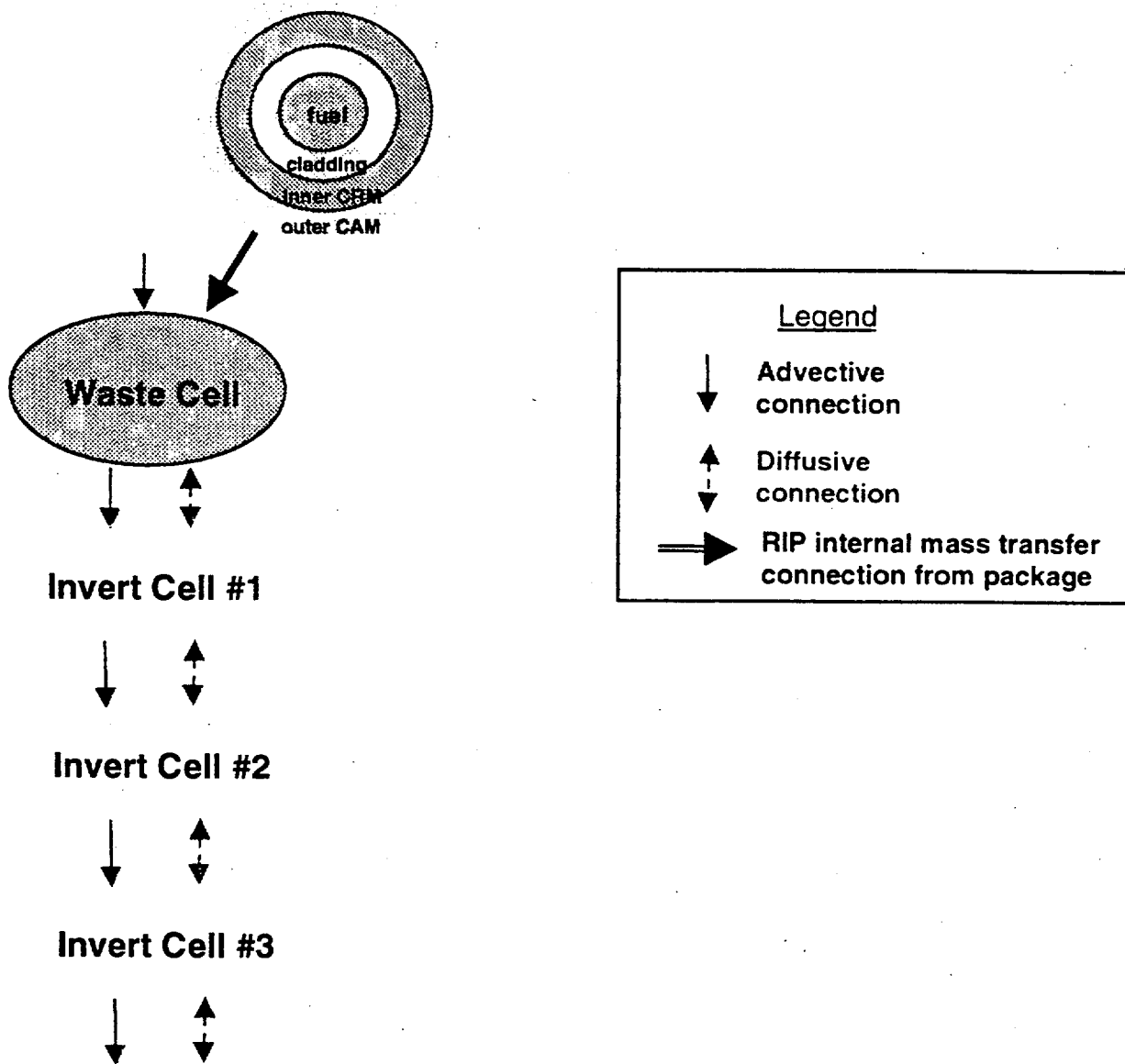


Figure 11-5. Configuration of cells in the RIP program for EBS transport in the TSPA-VA base case. CAM means corrosion allowance material and is the outer waste-package layer made of carbon steel. CRM means corrosion resistant material and is the inner waste-package layer made of Alloy 22.

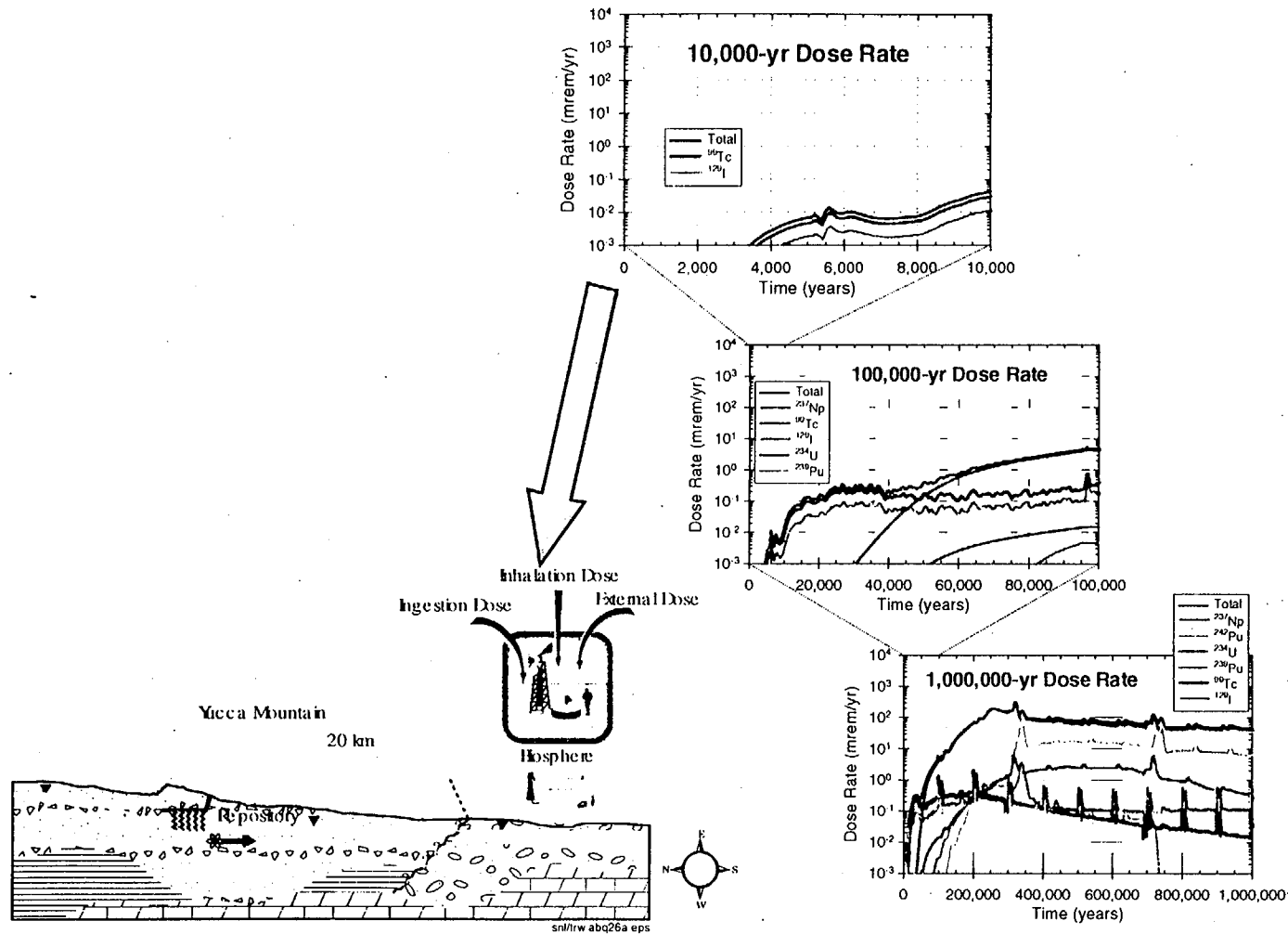


Figure 11-6. Dose rate to an "average" individual withdrawing water from a well penetrating the maximum plume concentration in the SZ, 20 km downgradient from the repository. This figure shows the most important radionuclides in different time periods: Tc-99 and I-129 within the first 10,000 years; Tc-99 and Np-237 within the first 100,000 years; and Np-237 and Pu-242 within the first 1,000,000 years.



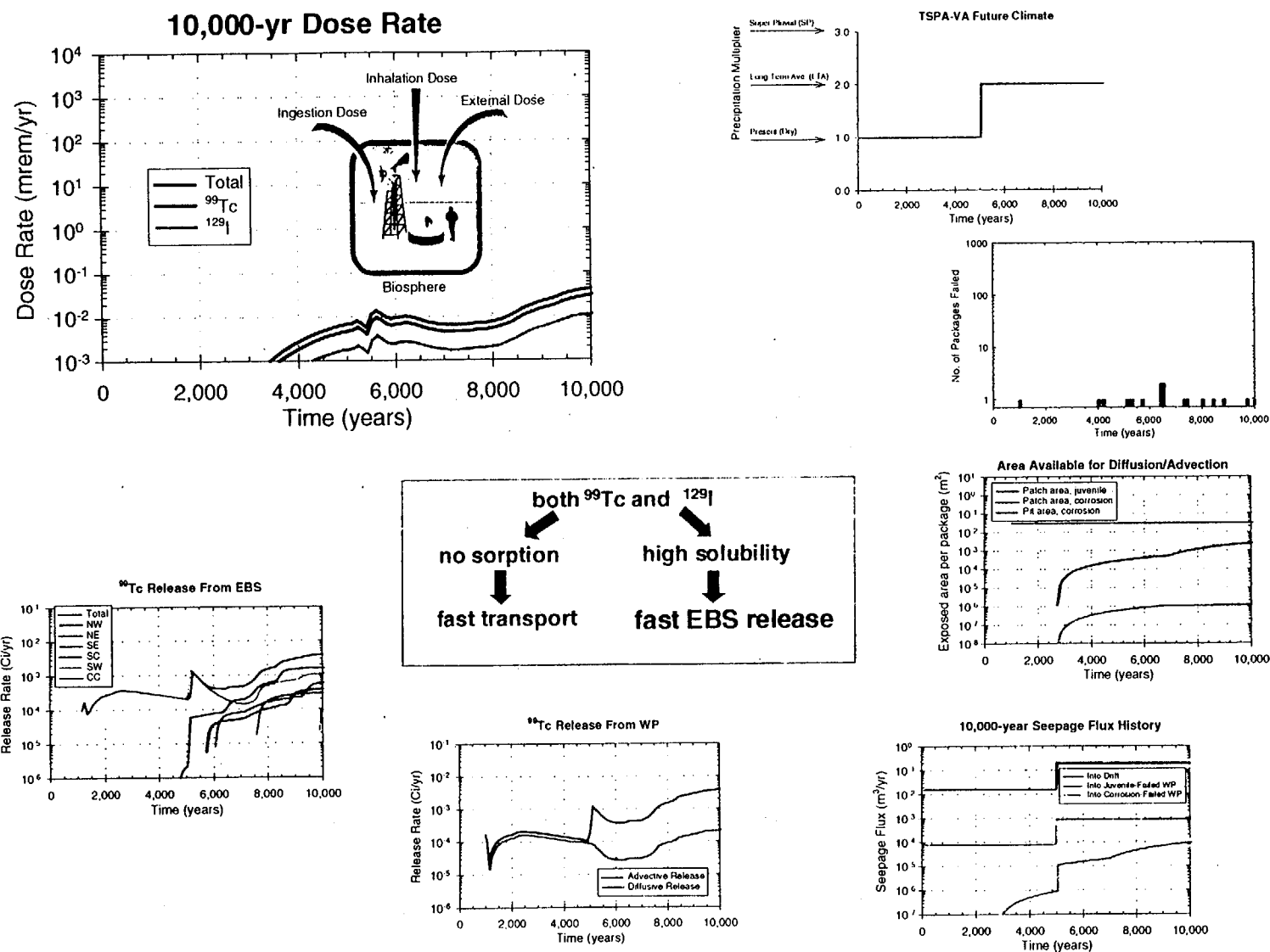


Figure 11-7. Effects of climate change, seepage flux, and waste-package degradation on EBS releases and dose rates in the first 10,000 years after waste emplacement.

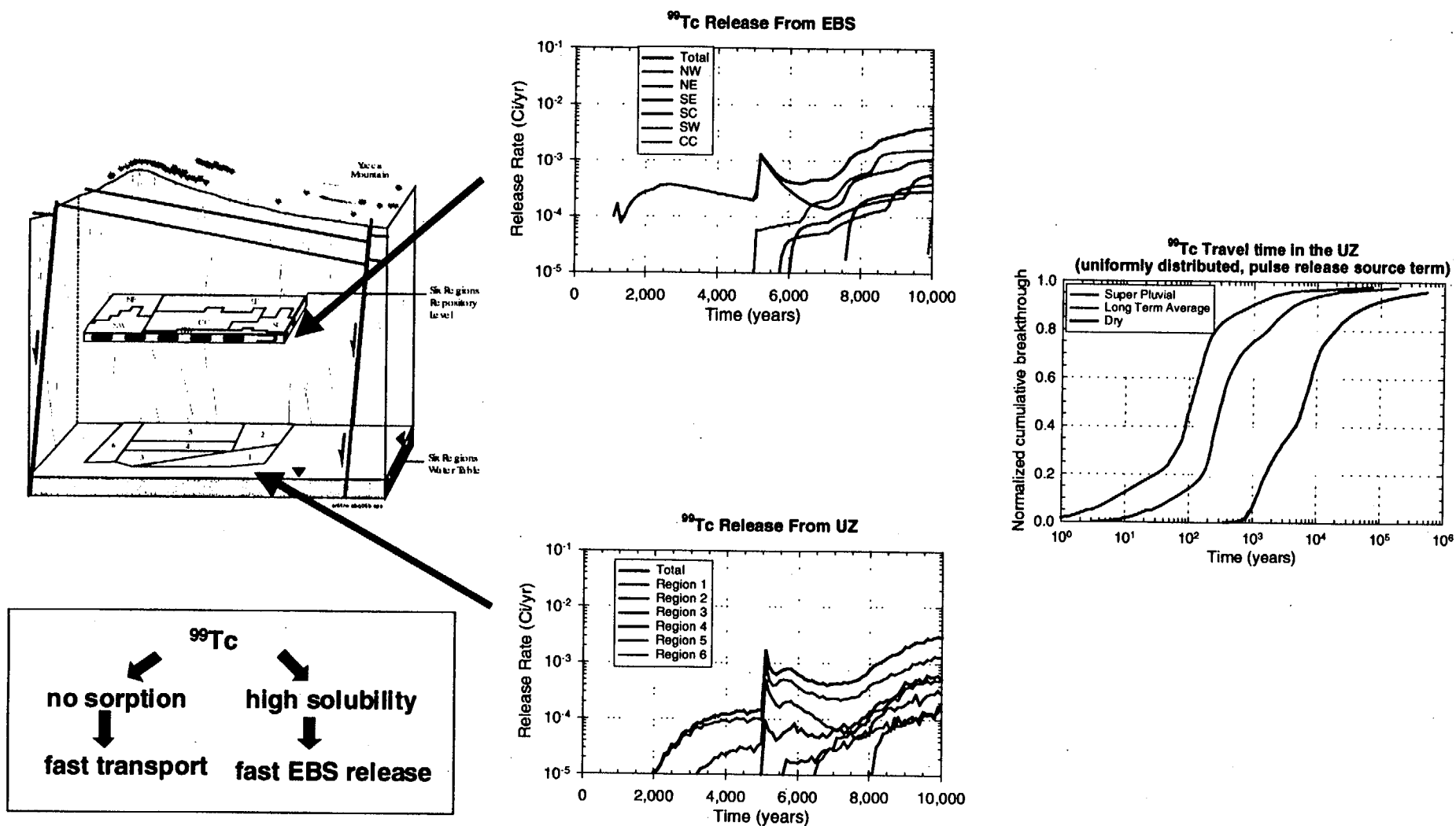


Figure 11.8. Performance of the UZ with respect to Tc-99 during the first 10,000 years after waste emplacement. Shown is the effect of different climate states, the EBS released from various repository regions, and the UZ releases to the various water table regions.

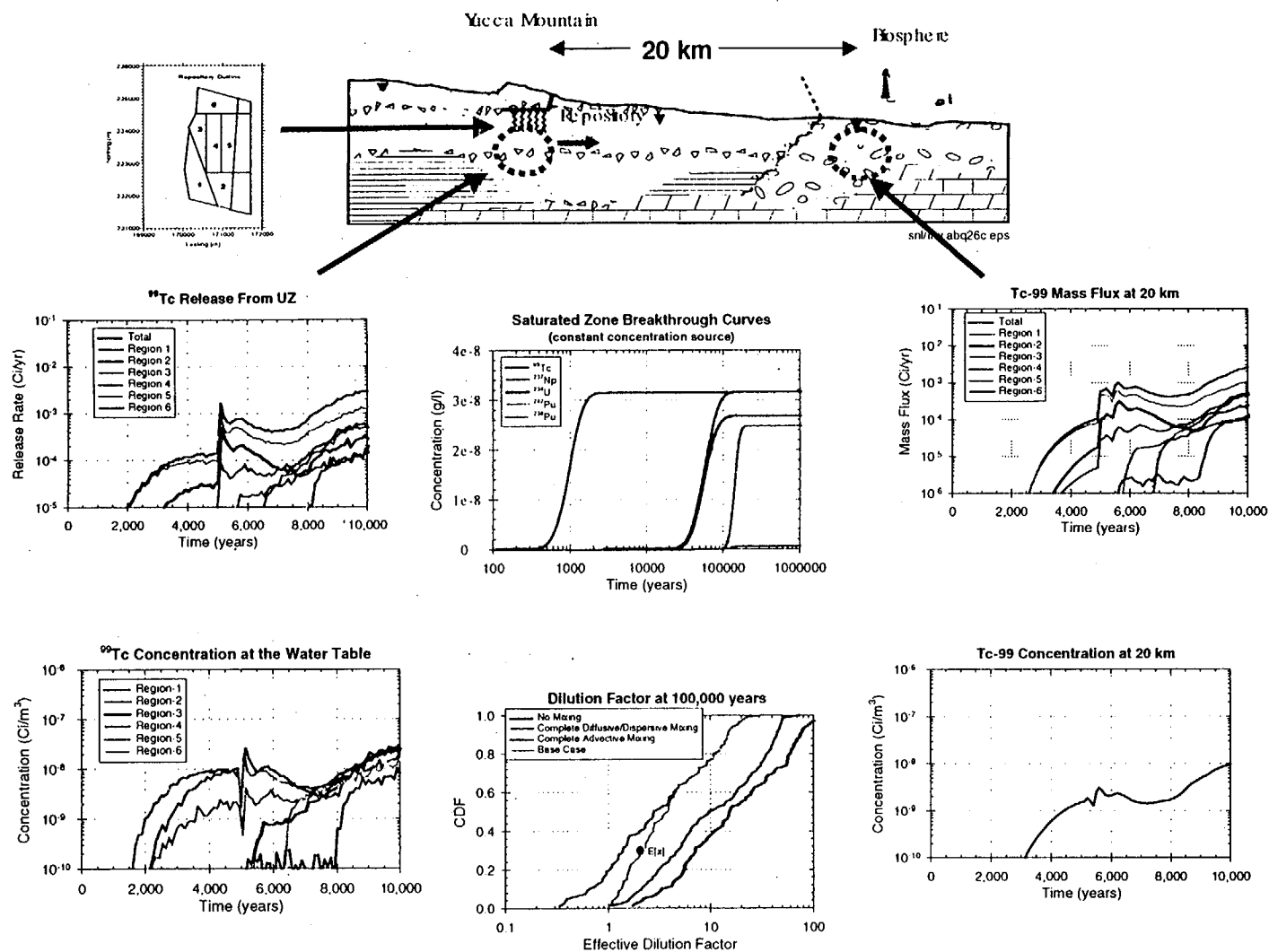


Figure 11-9. Performance of the SZ with respect to Tc-99 during the first 10,000 years after waste emplacement. Shown are concentration and releases in six stream tubes (each associated with one of six regions at the water-table level) and the impact of dilution in the SZ. Shown in the upper left corner are the six water-table regions.

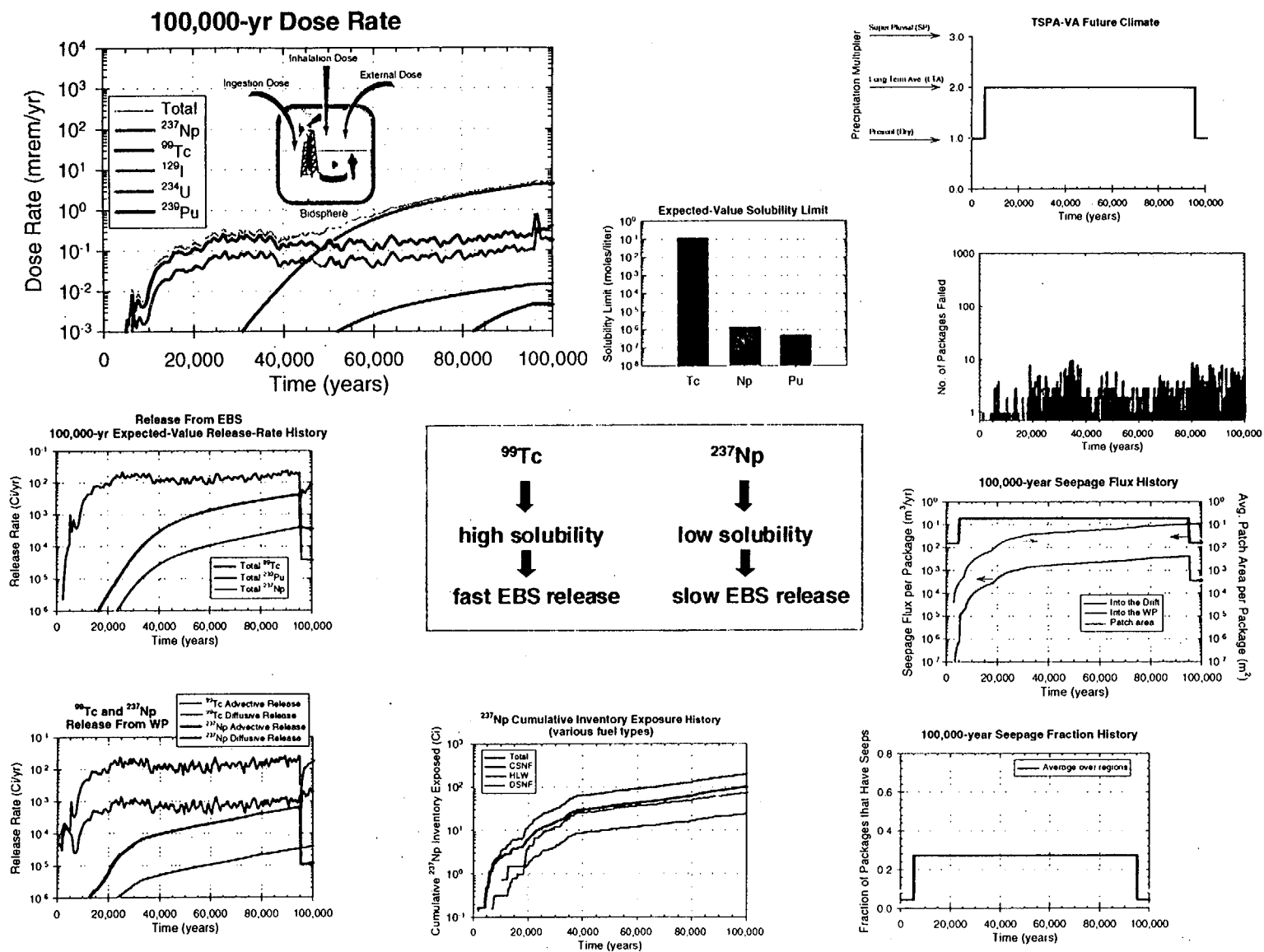


Figure 11-10. Effects of climate change, seepage flux, and waste-package degradation on EBS releases and dose rates in the first 100,000 years after waste emplacement.

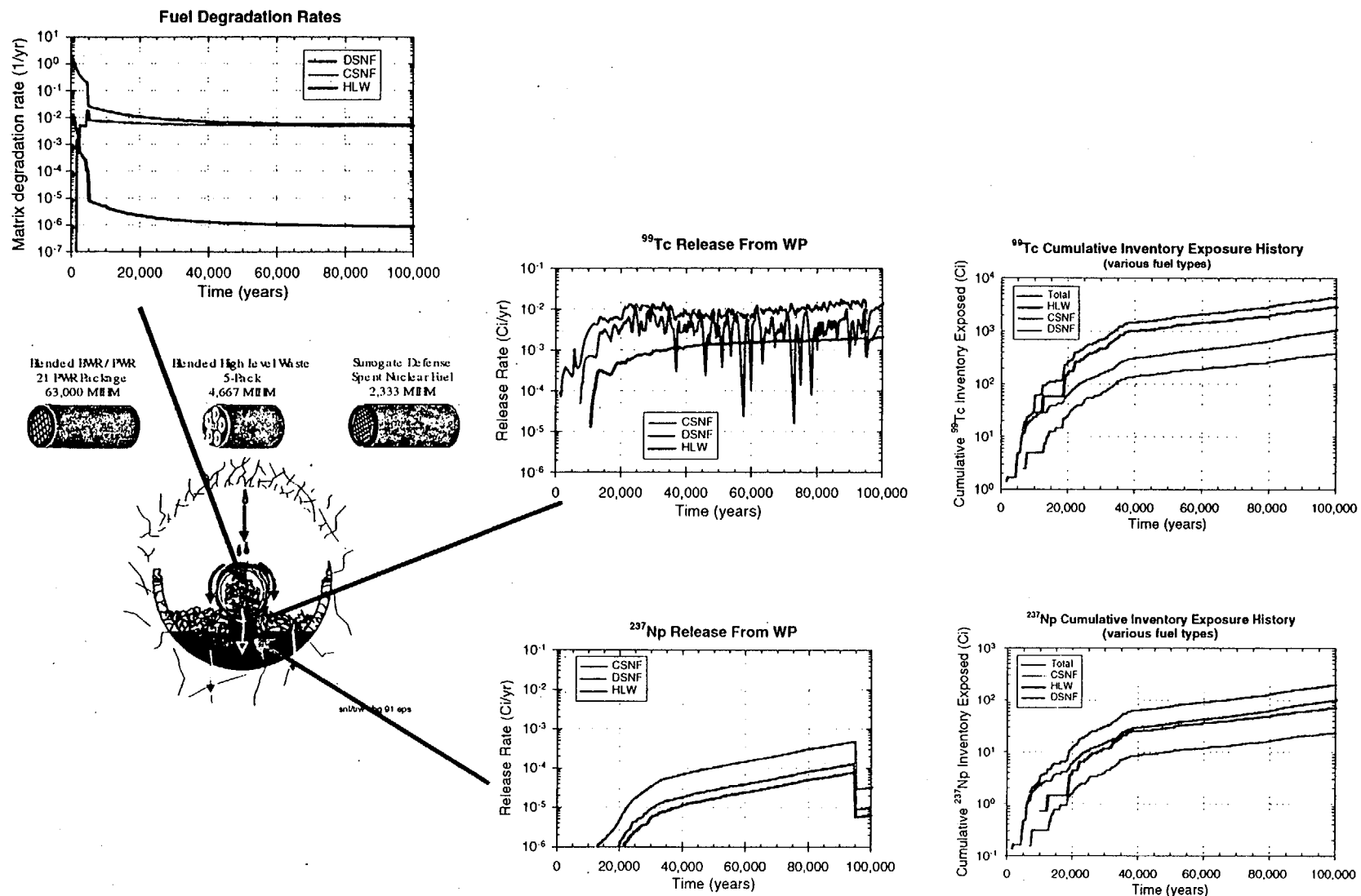


Figure 11-11. Effects of matrix degradation rate and inventory exposure rate on the releases of the three different fuel types: CSNF, DSNF, and HLW. WP means waste package.

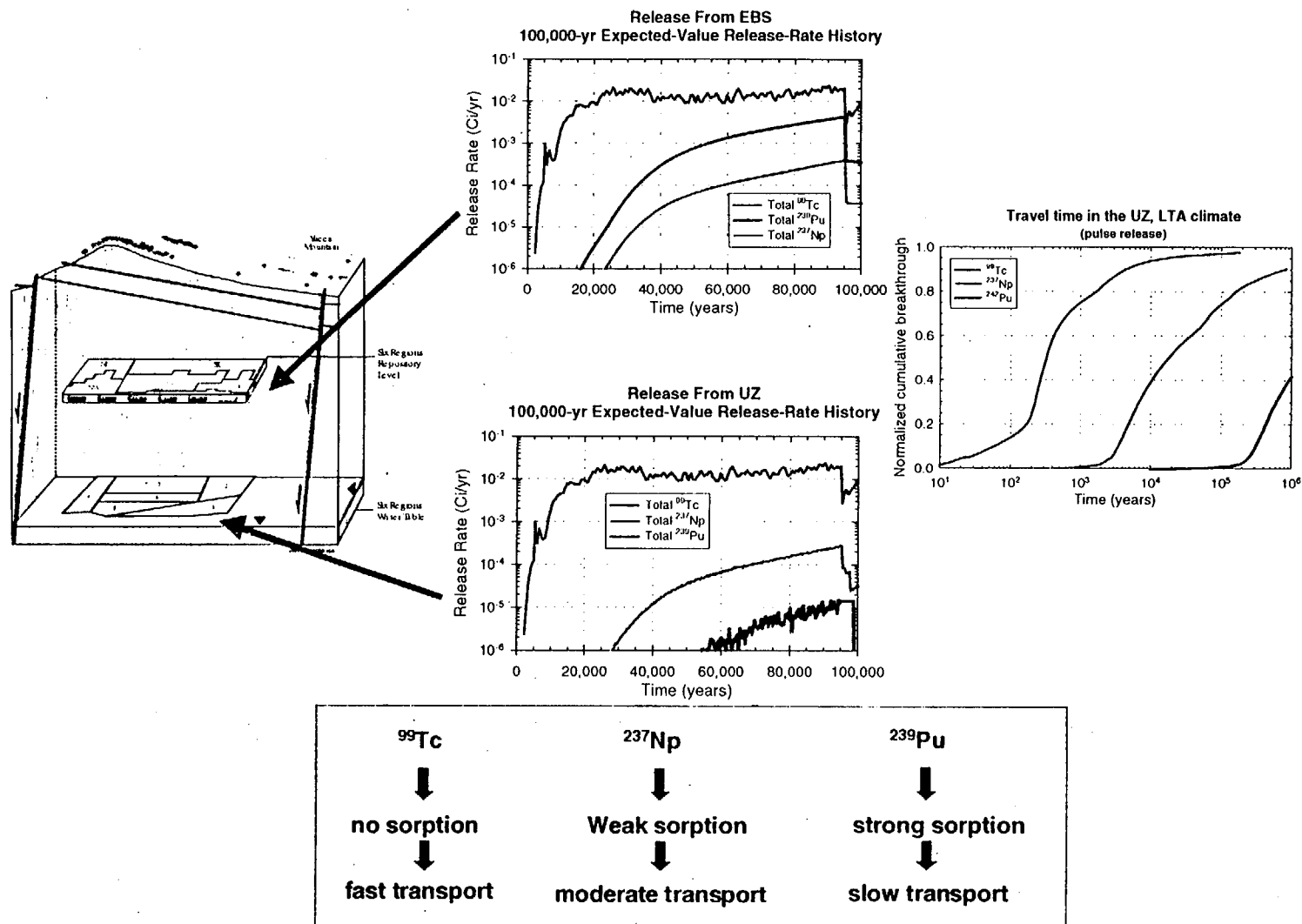


Figure 11-12. Performance of the UZ during the first 100,000 years after waste emplacement with respect to Tc-99, Np-237, and Pu-239. Shown is the importance of sorption in the UZ. EBS means engineered barrier system. LTA means long term average. Pu-242 breakthrough curve is approximate only, see discussion in Section 11.4.1.3.

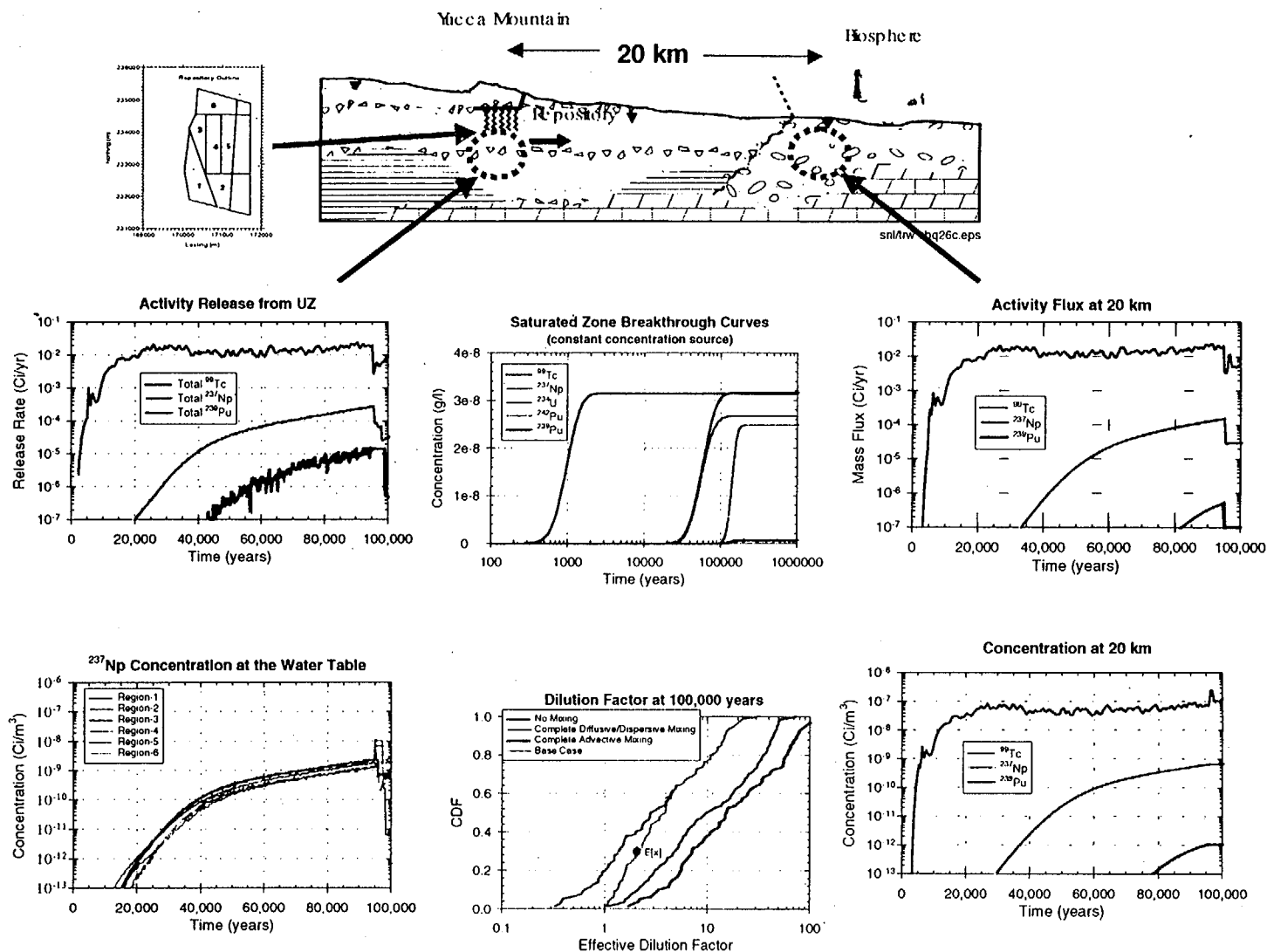


Figure 11-13. Performance of the SZ during the first 100,000 years after waste emplacement with respect to Tc-99, Np-237, and Pu-239. Shown is the importance of sorption and dilution in the SZ. UZ means unsaturated zone. CDF means cumulative distribution function.

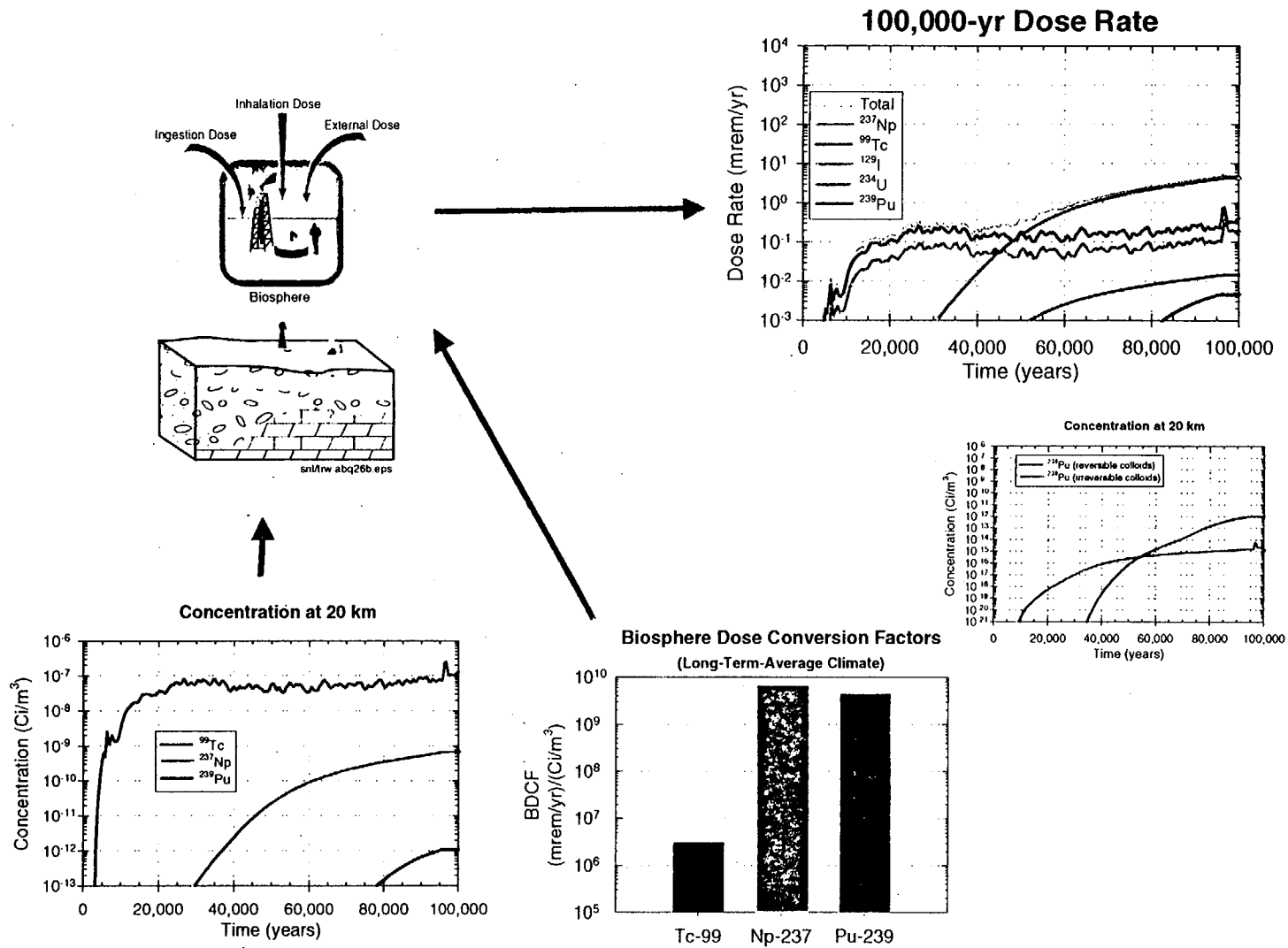


Figure 11-14. Importance of biosphere dose conversion factors (BDCF) in the first 100,000 years after waste emplacement. Also shown is the impact of colloidal transport of irreversibly sorbed Pu-239.



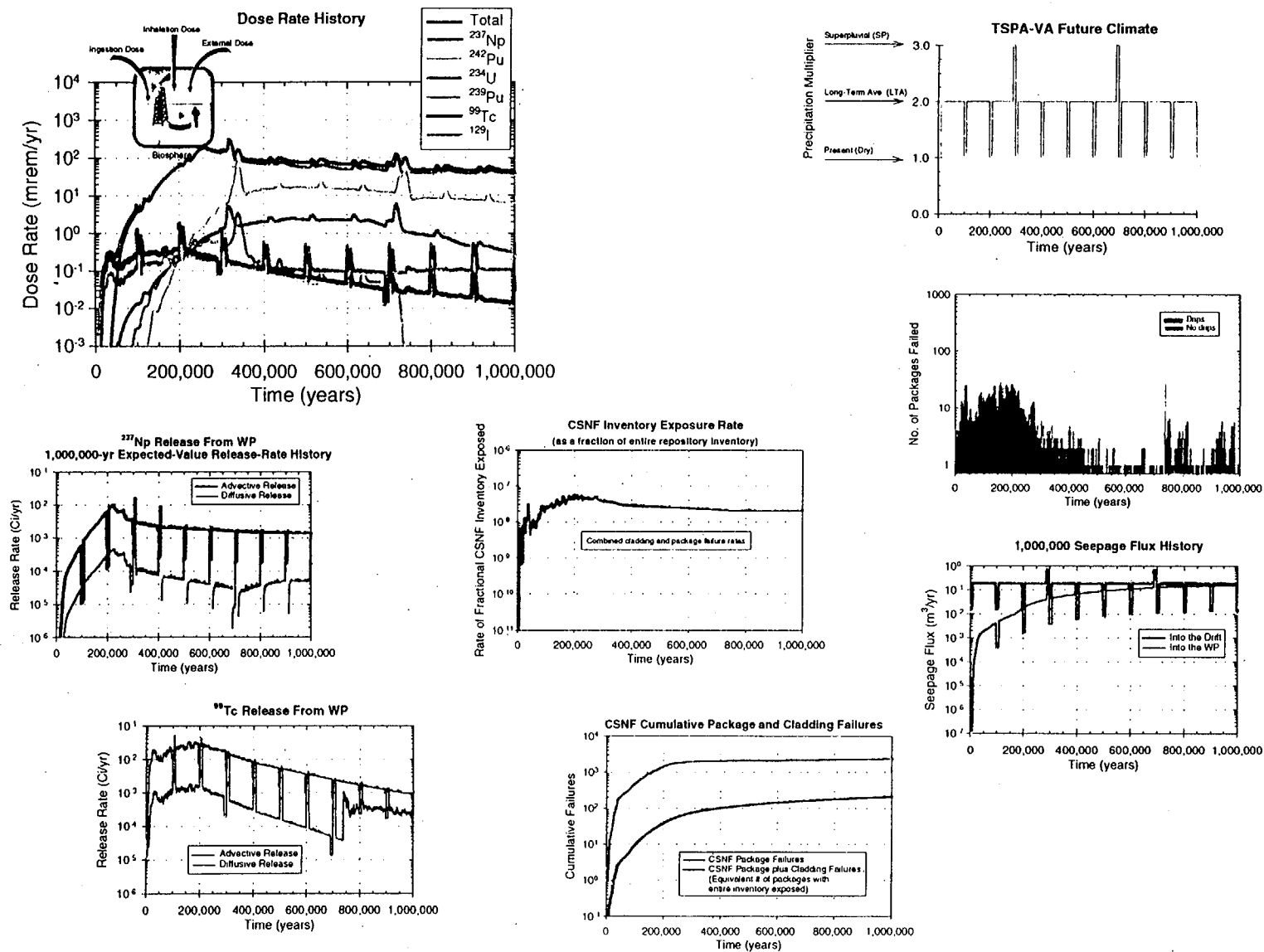


Figure 11-15. Effects of climate change, seepage flux, waste-package degradation, and cladding degradation on waste-package (WP) releases and dose rates in the first 1,000,000 years after waste emplacement. CSNF means commercial spent nuclear fuel.

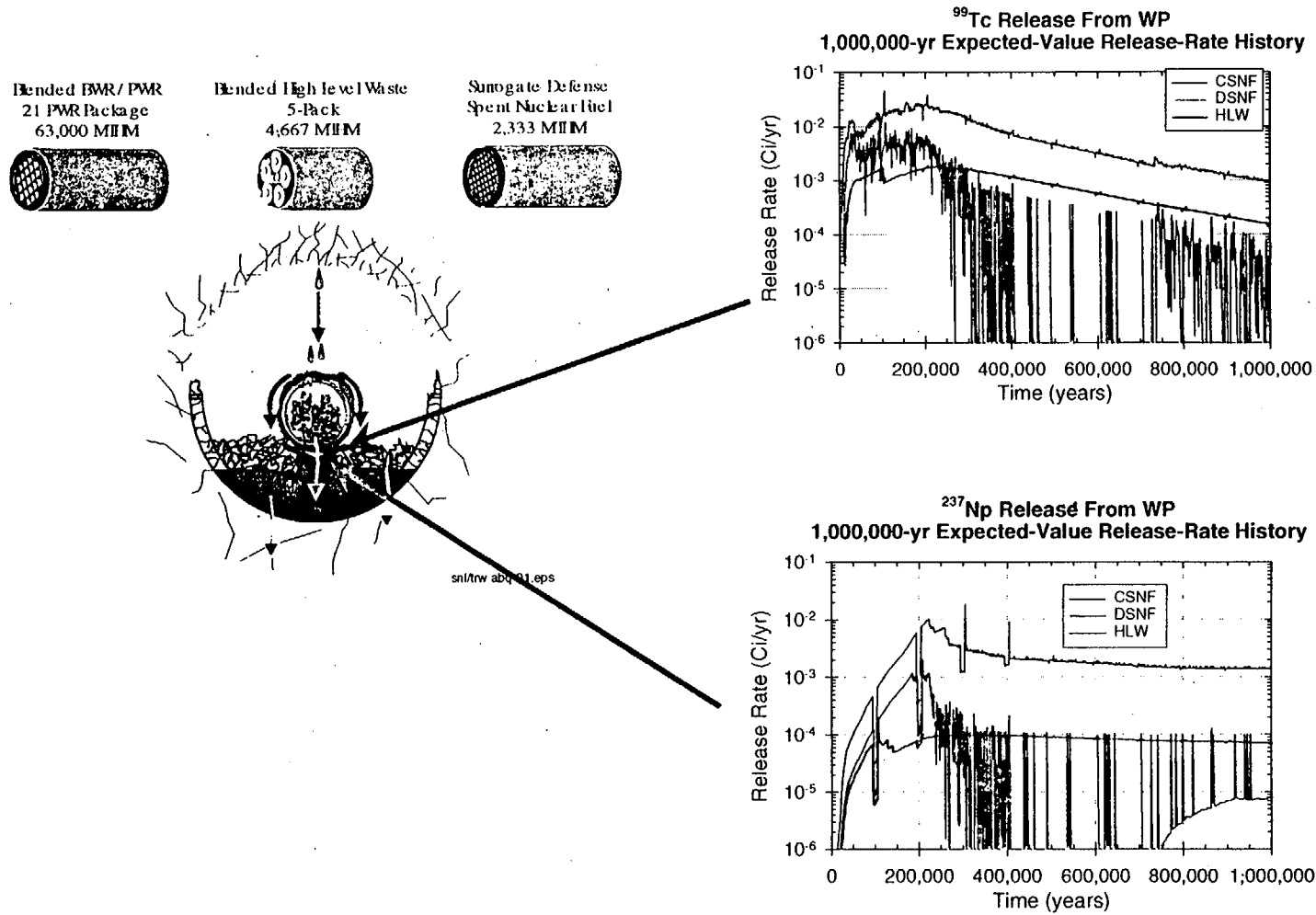


Figure 11-16. Waste-package (WP) releases during 1,000,000 years after waste emplacement for the three inventory types: CSNF, DSNF, and HLW.

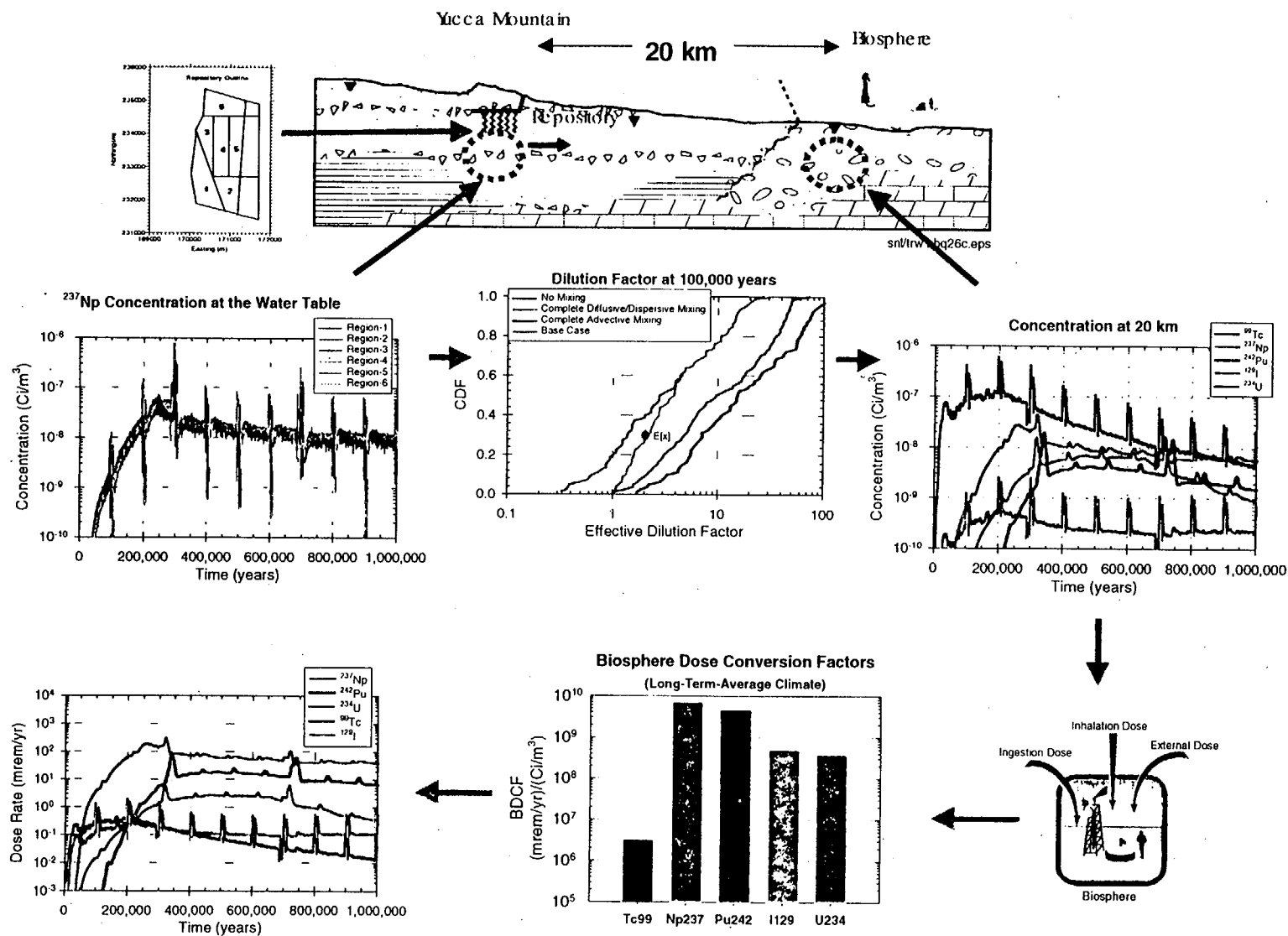


Figure 11-17. Effects of SZ dilution and BDCF on 1,000,000-year dose rates. The inset at upper left shows the six water table regions.

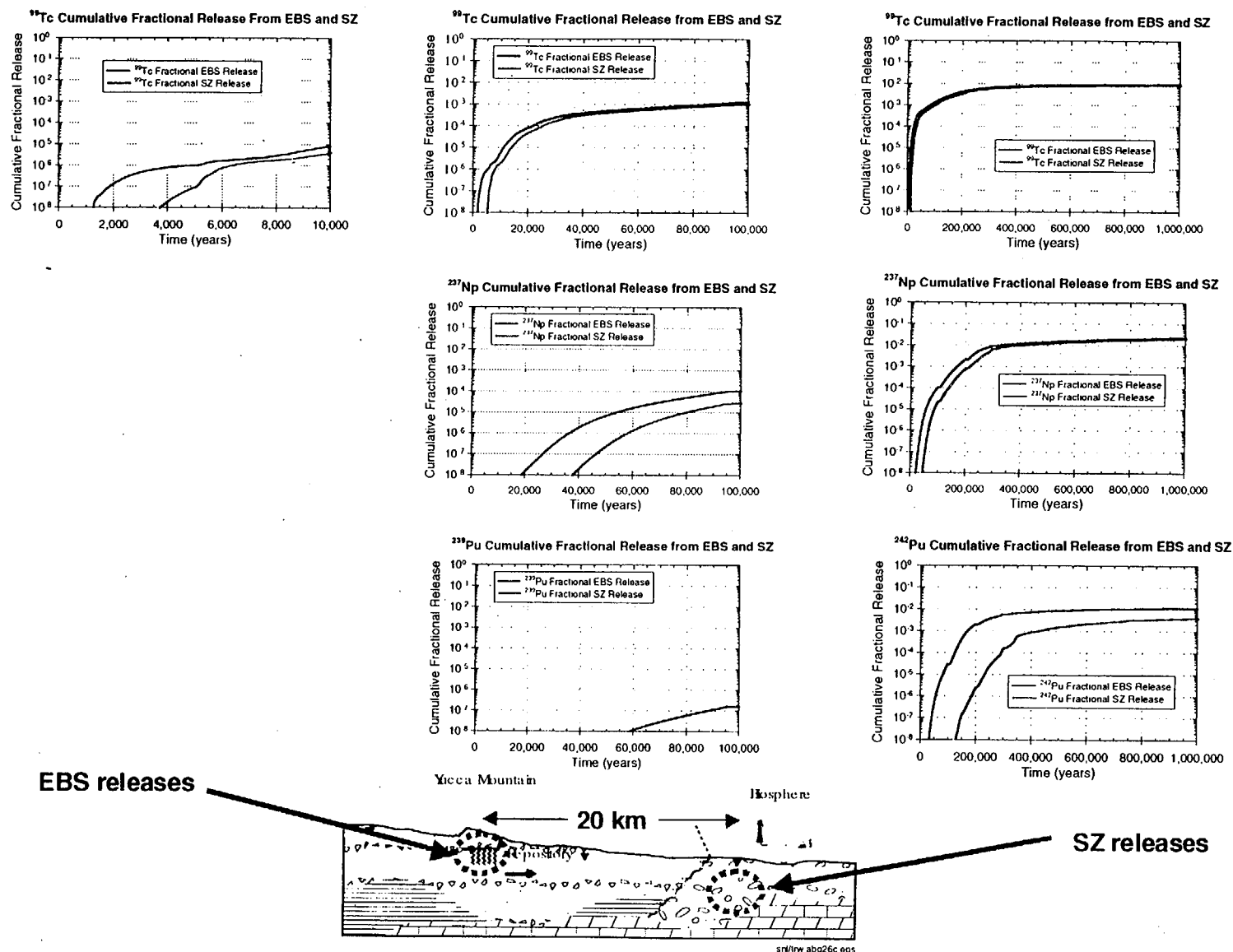


Figure 11-18. Cumulative fractional inventory releases of Tc-99, Np-237, Pu-239, and Pu-242 from the EBS and the 20-km SZ boundary, normalized to the initial inventory. Shown are the effects of sorption and decay of radionuclides.

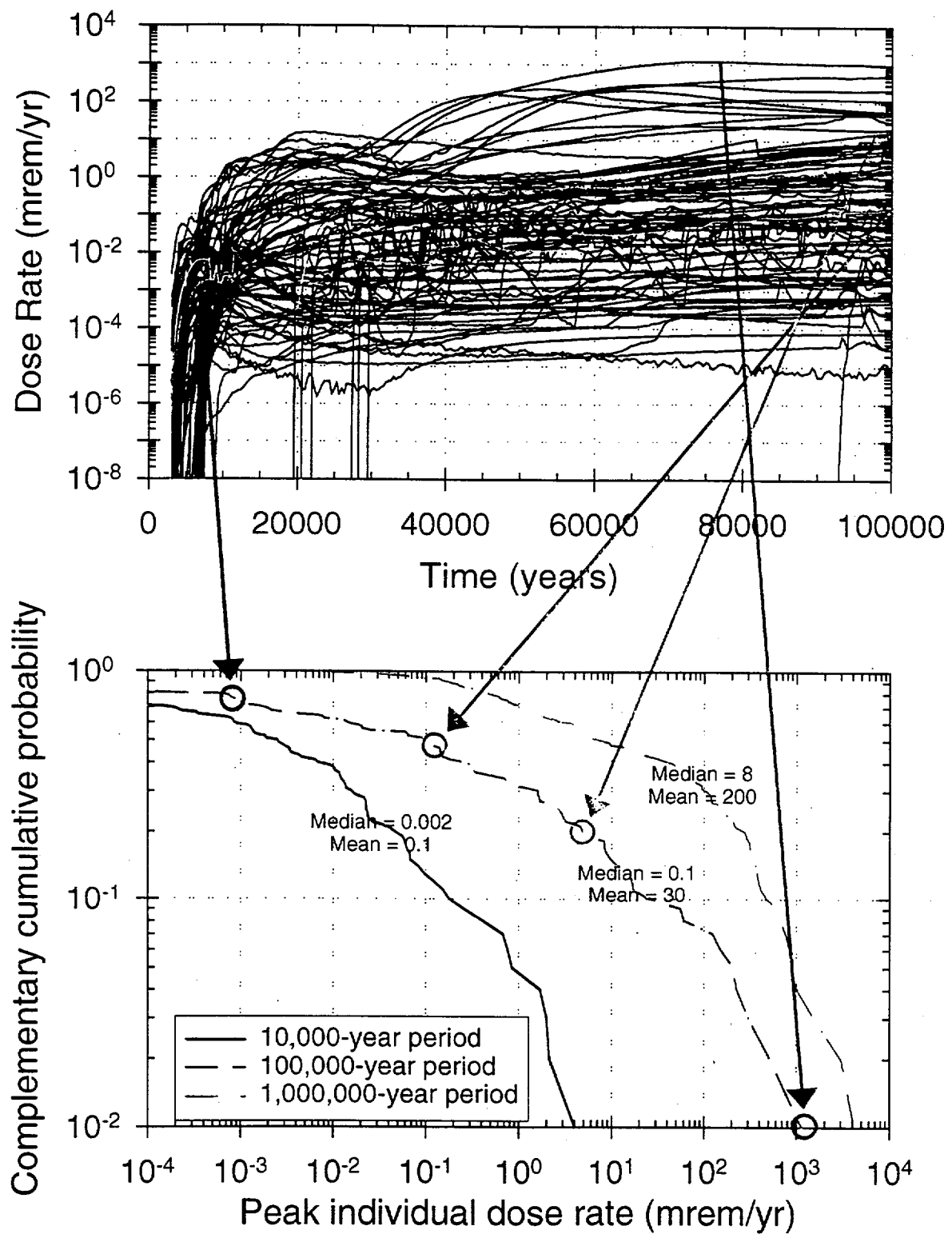
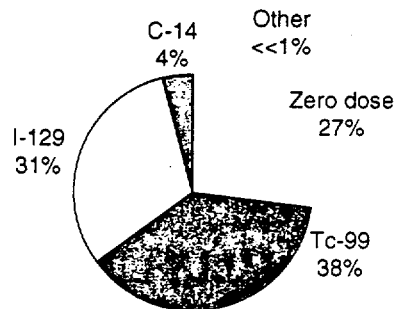
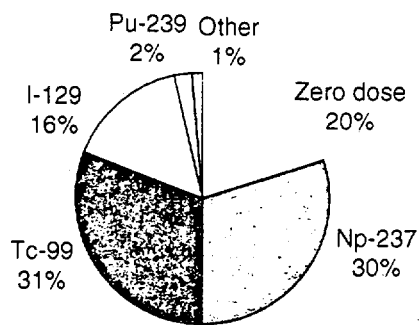


Figure 11-19. The base-case distribution of peak-dose rates for three time periods (bottom) and their relation to dose-rate time histories (top). Twenty dose-rate histories do not appear on the top plot because they have no computed dose for the first 100,000 years.

### 10,000-Year Period



### 100,000-Year Period



### 1,000,000-Year Period

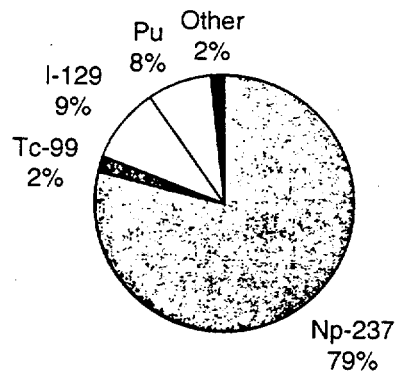


Figure 11-20. Average contribution to peak-dose rate of different radionuclides for three time periods. Note that for the earlier two time periods, many realizations have no computed dose.

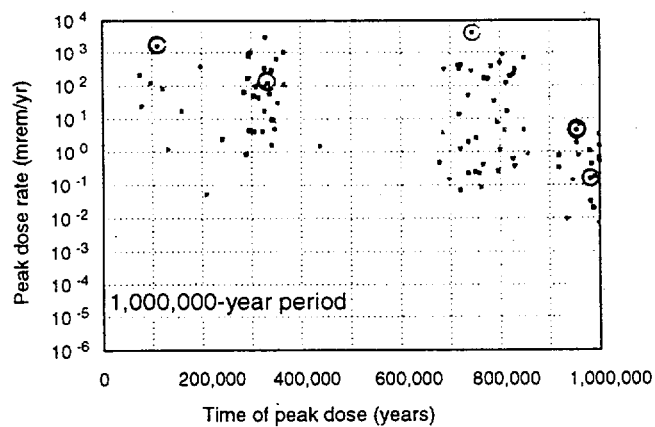
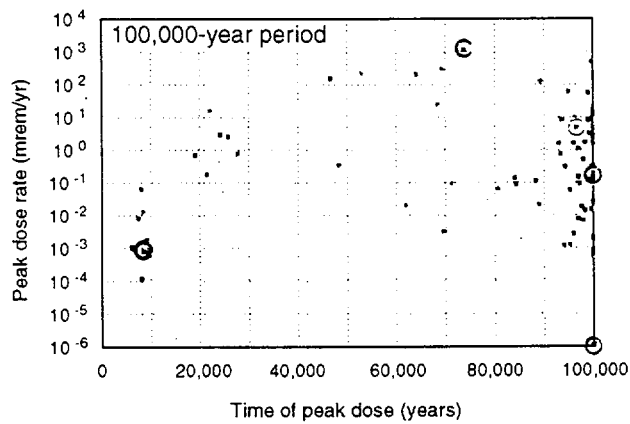
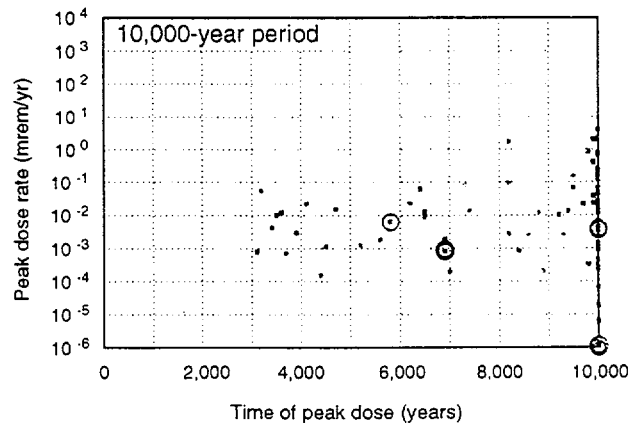


Figure 11-21. Peak-dose-rate vs. time of peak-dose rate for three time periods. Pink dots at the bottom indicate realizations with zero dose (which are off the scale of the log plot). The colored circles refer to the selected realizations highlighted in Figure 11-19, plus one that is not in Figure 11-19 because of having no computed dose for the first 100,000 years.

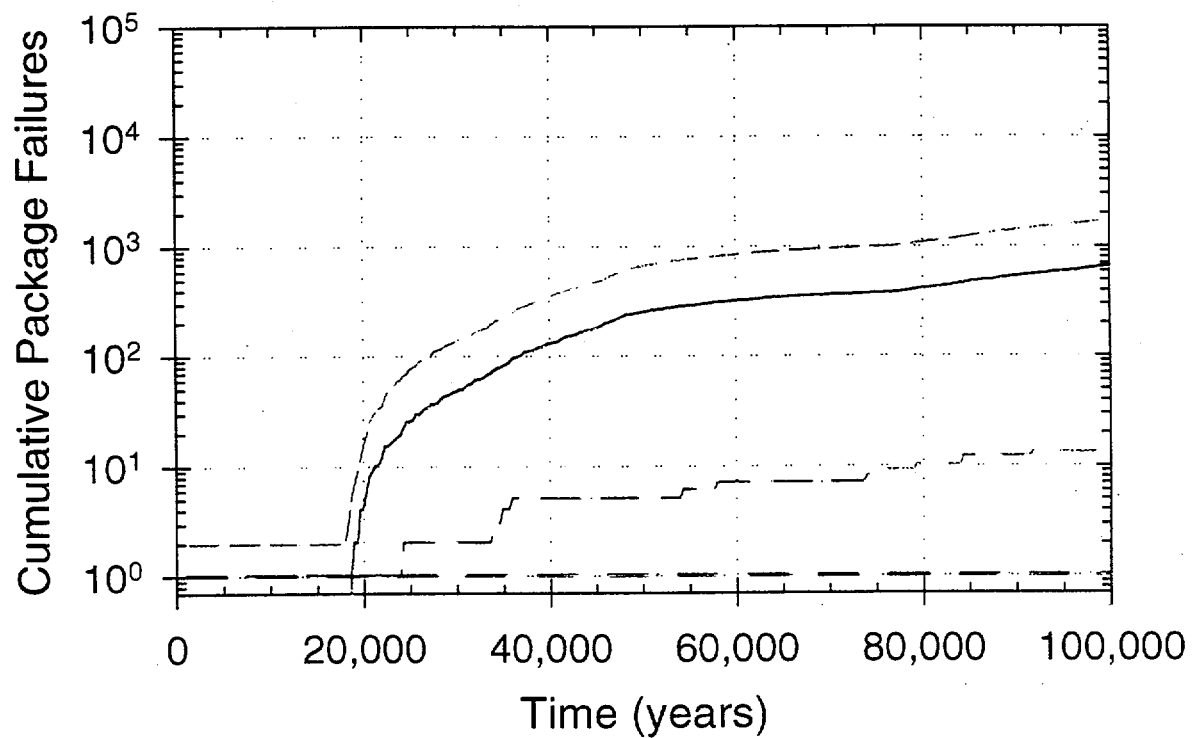


Figure 11-22. Number of failed waste packages over time for the selected realizations for 100,000 years. There is no curve for one realization because it has no waste-package failures in the first 100,000 years. The realizations were chosen to have a spread of peak-dose rates and peak-dose times and, therefore, a variety of different behaviors.



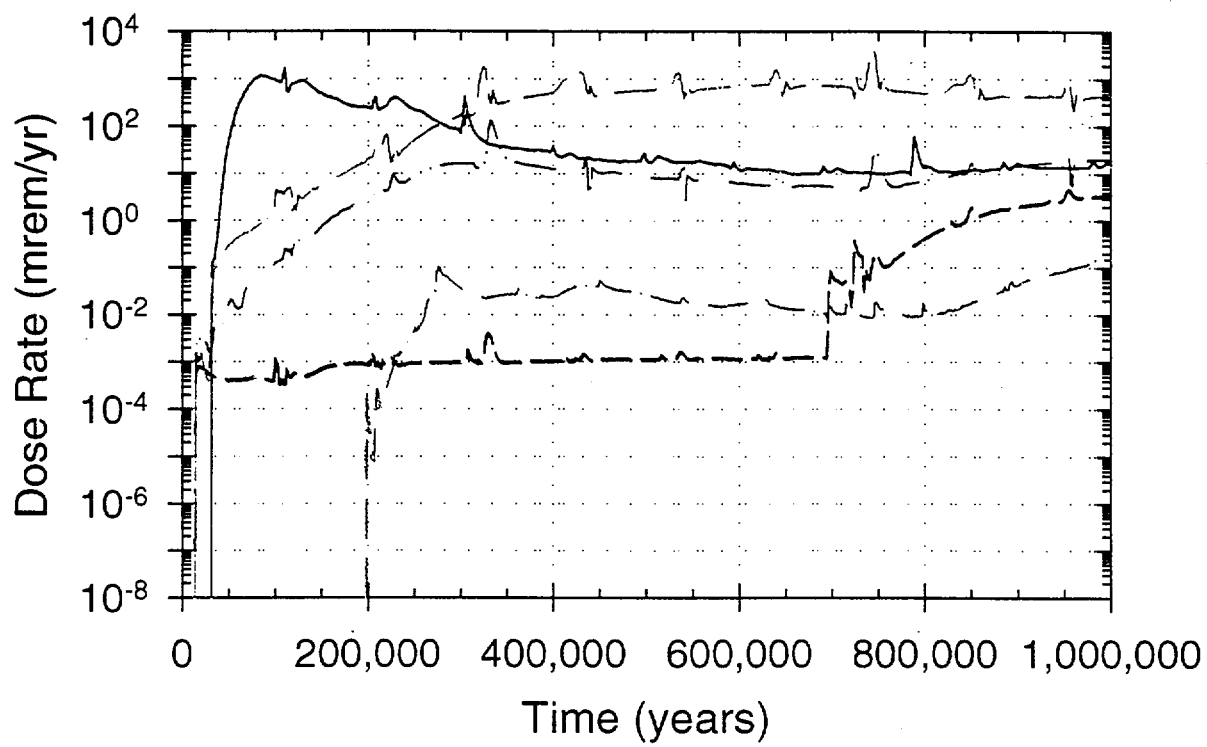


Figure 11-23. Dose-rate time histories for 1,000,000 years for the five selected realizations. Regularly spaced spikes in the curves are caused by the climate changes that occur roughly every 100,000 years.

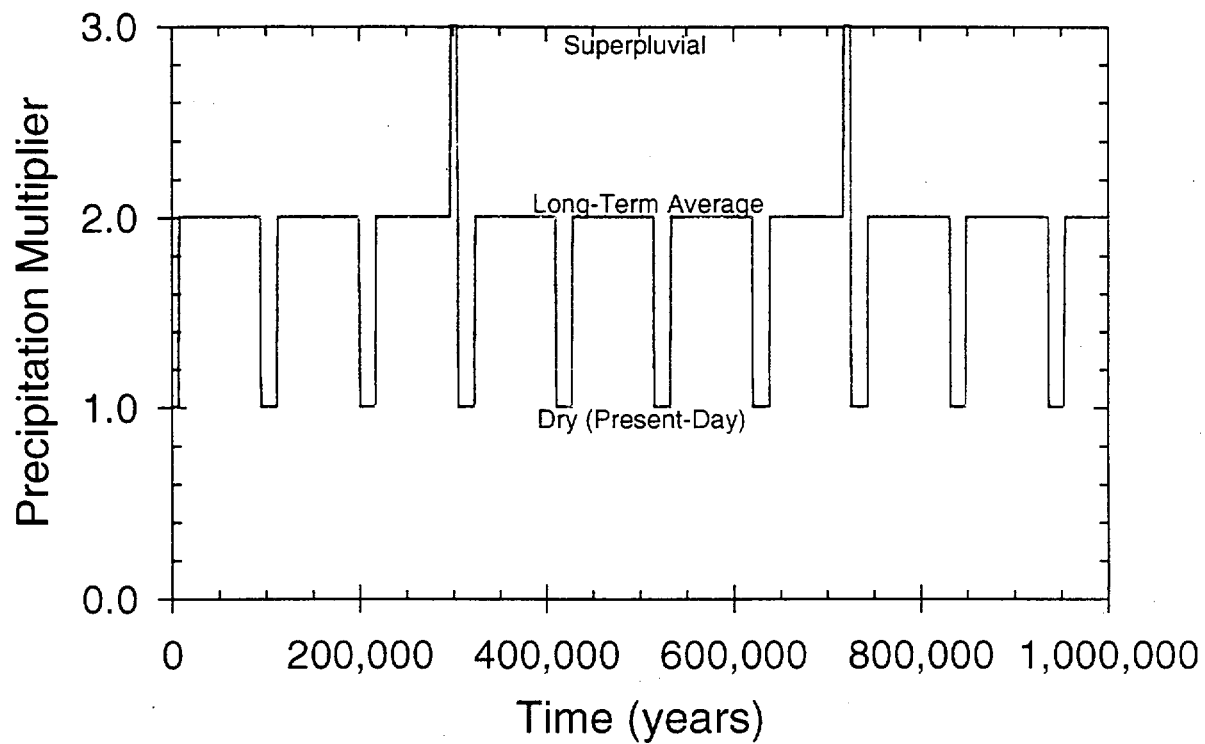


Figure 11-24. Climate history for one realization. The others look similar. Most of the peak-dose rates occur at one of the two superpluvial climates.

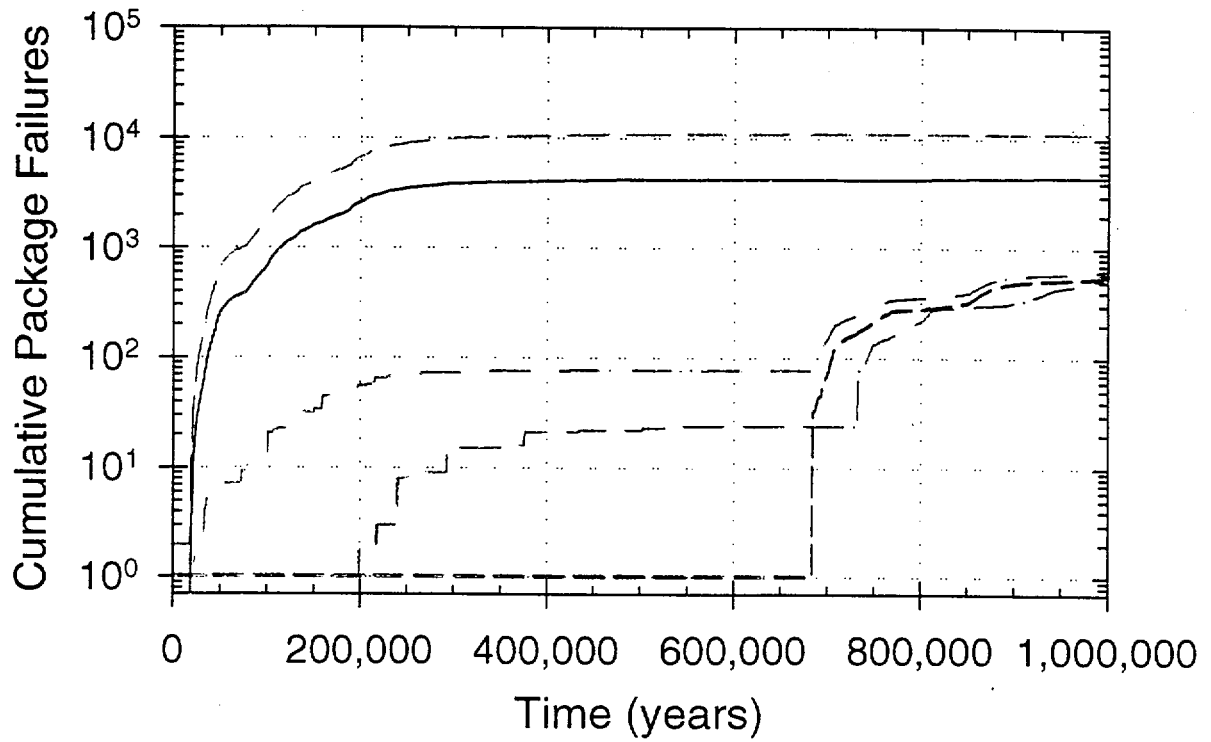


Figure 11-25. Number of failed waste packages over time for the selected realizations for 1,000,000 years. The waste-package failures starting at about 700,000 years are waste packages with no seeps dripping on them.

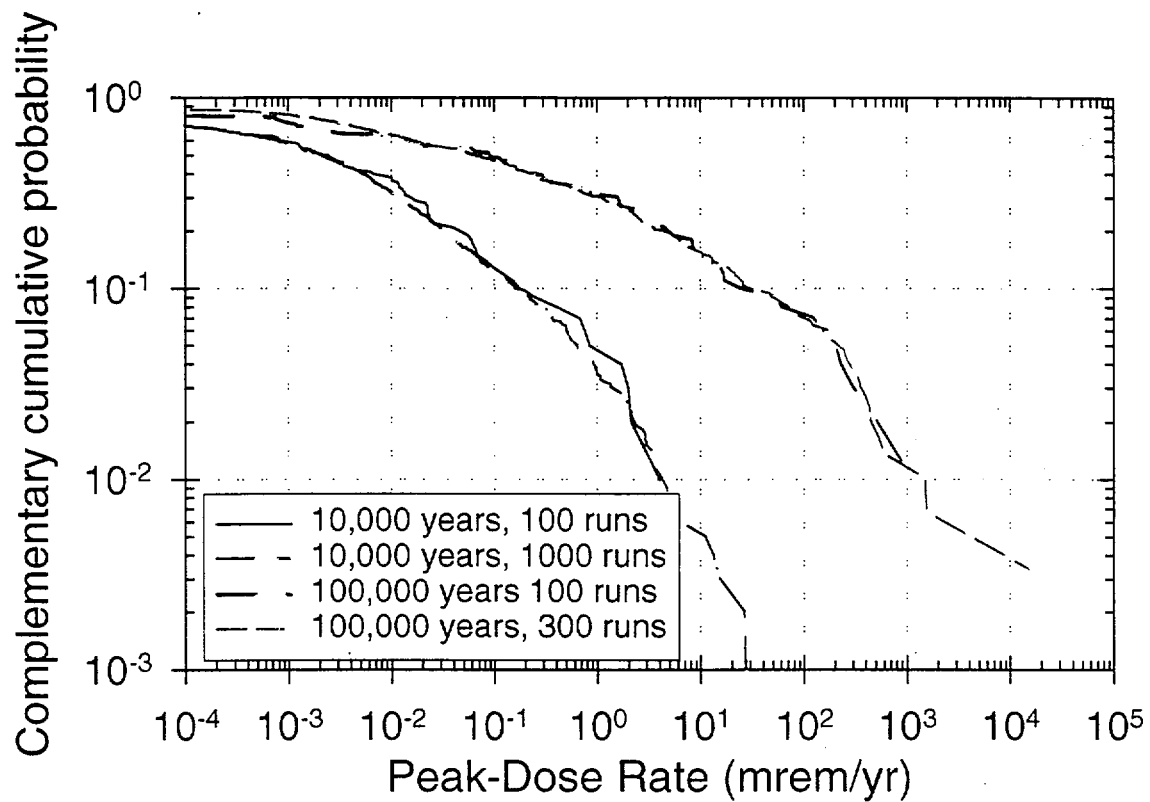


Figure 11-26. Comparison of peak-dose-rate distributions determined from simulations with different numbers of realizations (runs). The distributions are found to be quite similar, indicating reasonable stability with respect to number of realizations.

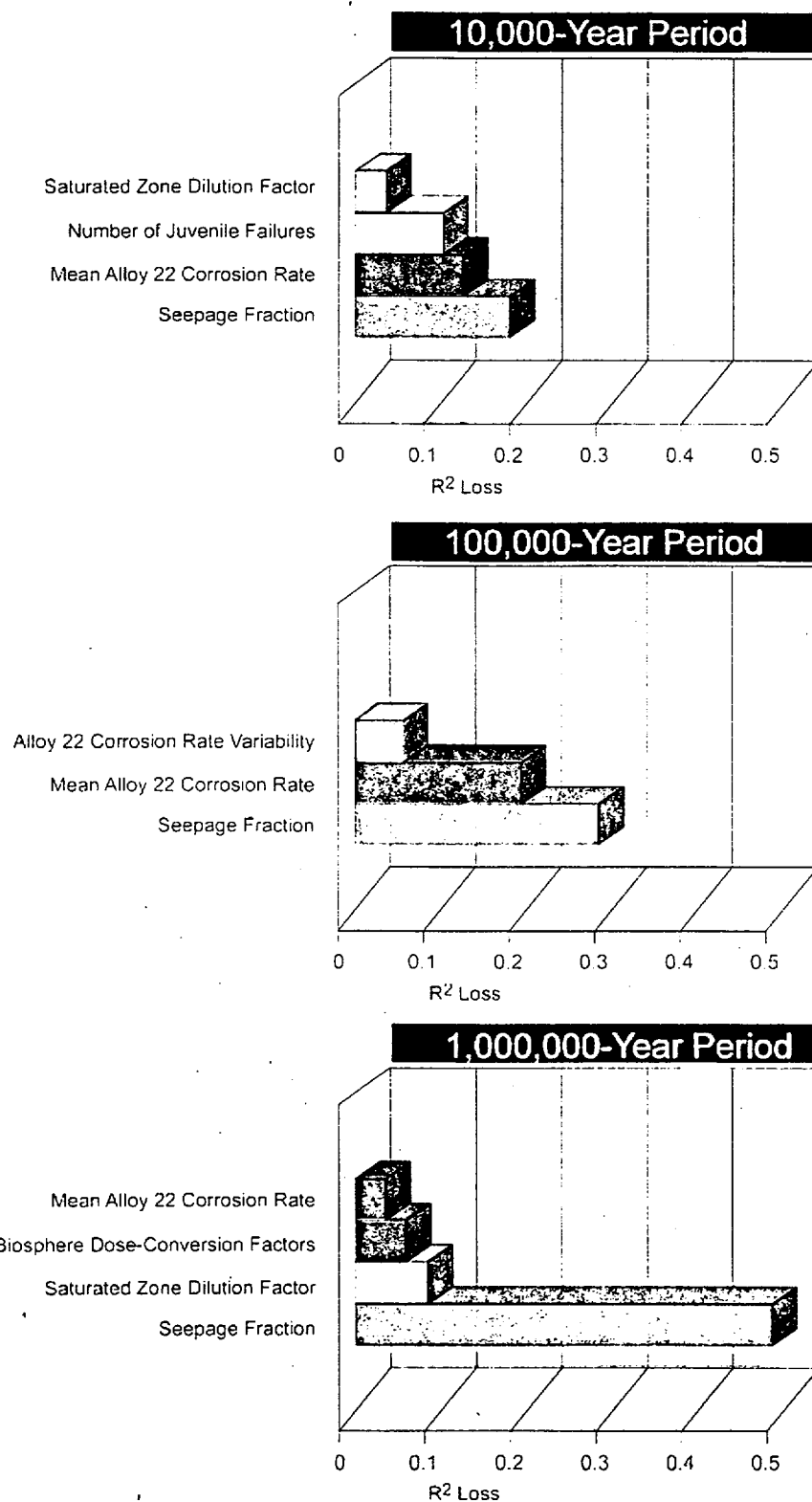


Figure 11-27. Most important parameters from stepwise regression analysis for three time periods. These charts show the relative importance of various parameters to the calculated uncertainty in dose rate for the three time periods. Importance of an individual parameter is shown by  $R^2$ -loss, the reduction in goodness of the regression fit when the parameter is left out of the calculation, as described in the text.

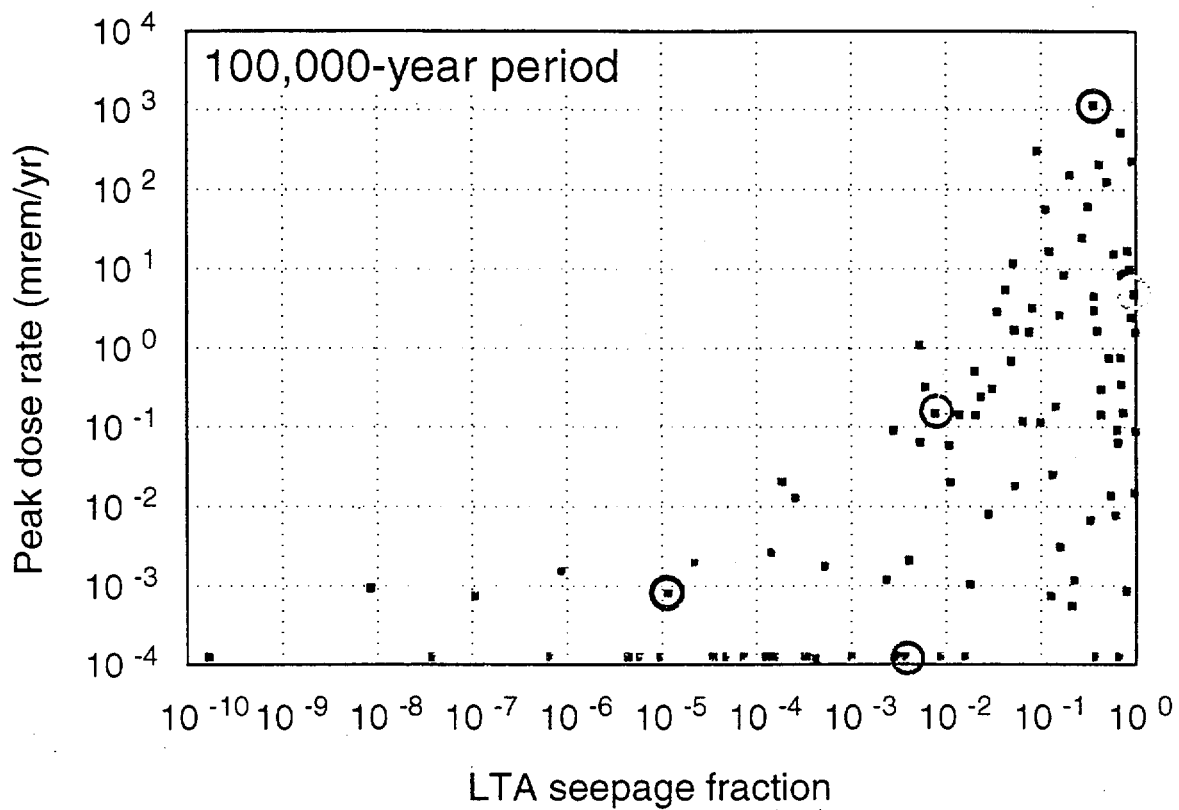


Figure 11-28. Scatter plot of seepage fraction (fraction of waste packages contacted by seeps) for the long-term-average climate against peak dose rate for a 100,000-year period. Pink dots at the bottom indicate realizations with zero dose (which are off the scale of the log plot). The colored circles refer to the selected realizations highlighted in Figure 11-19.

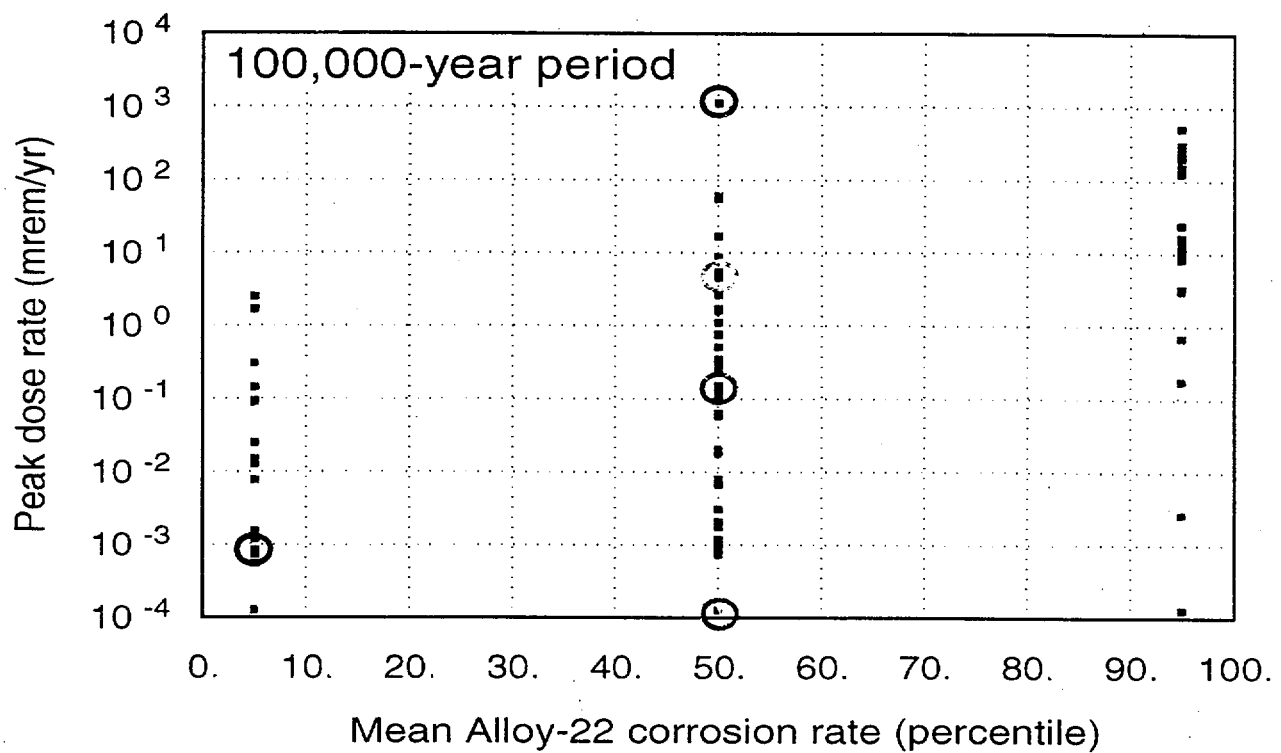


Figure 11-29. Scatter plot of mean Alloy 22 corrosion rate (in terms of percentile from the uncertainty distribution) against peak-dose rate for a 100,000-year period. Pink dots at the bottom indicate realizations with zero dose (which are off the scale of the log plot). The colored circles refer to the selected realizations highlighted in Figure 11-19.

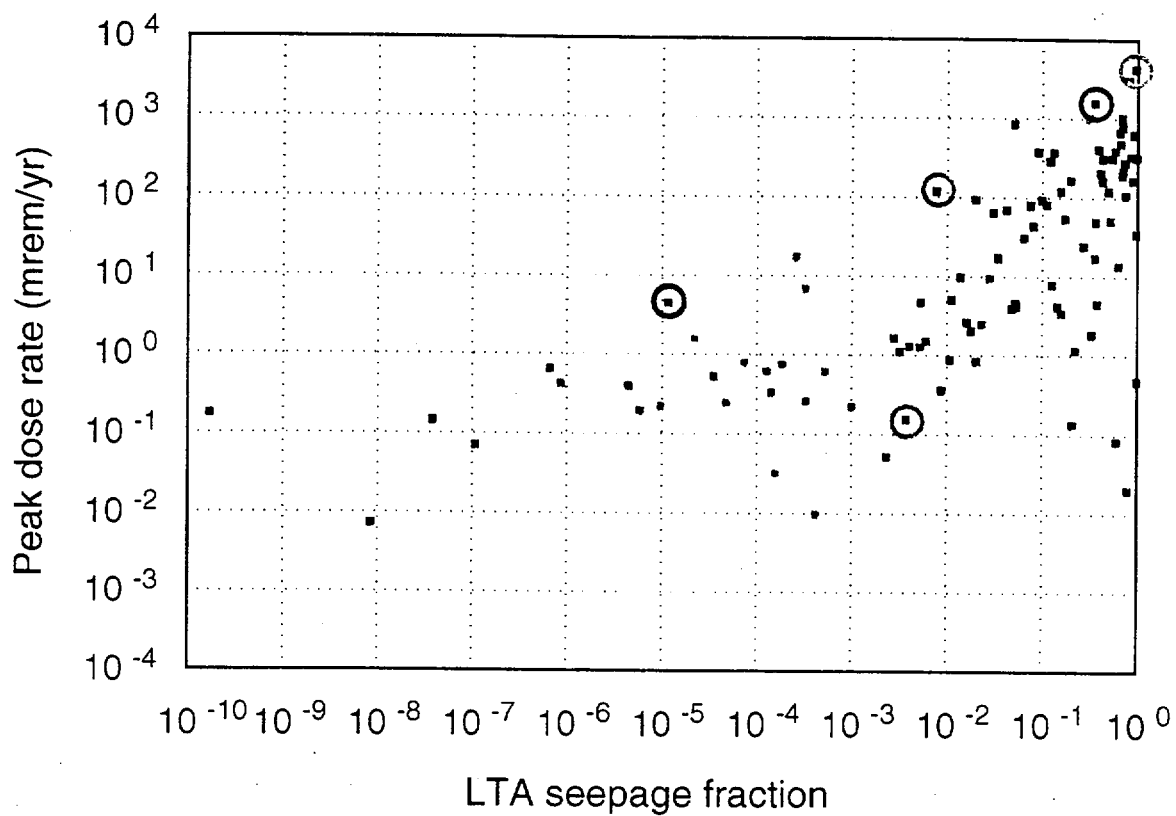


Figure 11-30. Scatter plot of seepage fraction (fraction of waste packages contacted by seeps) for the long-term-average climate against peak-dose rate for a 1,000,000-year period. The colored circles refer to the selected realizations shown in Figure 11-23.



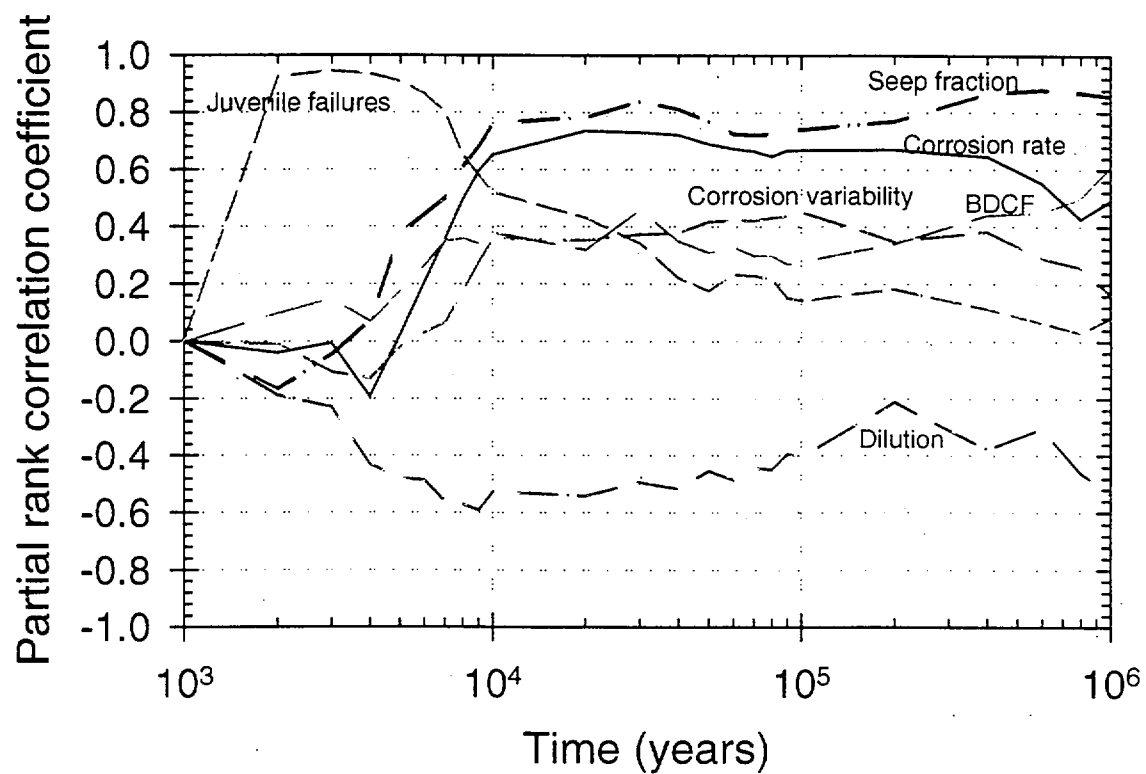


Figure 11-31. Partial rank correlation coefficients as a function of time for six uncertain parameters that are most important to uncertainty in dose rate. This figure illustrates another way to show the change of importance of parameters through time from that shown in Figure 11-27.

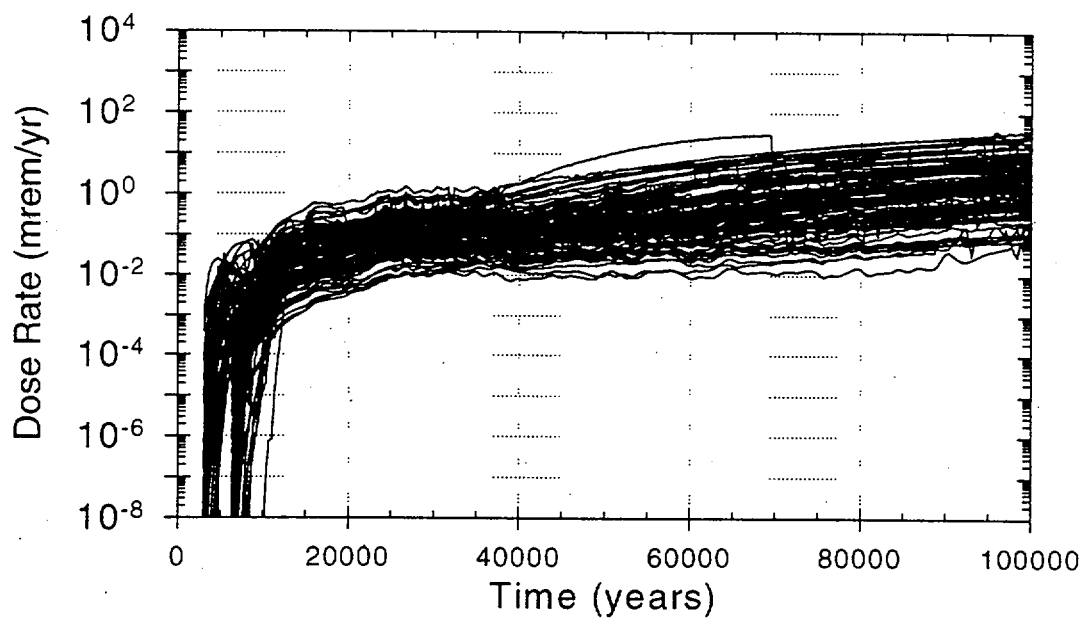
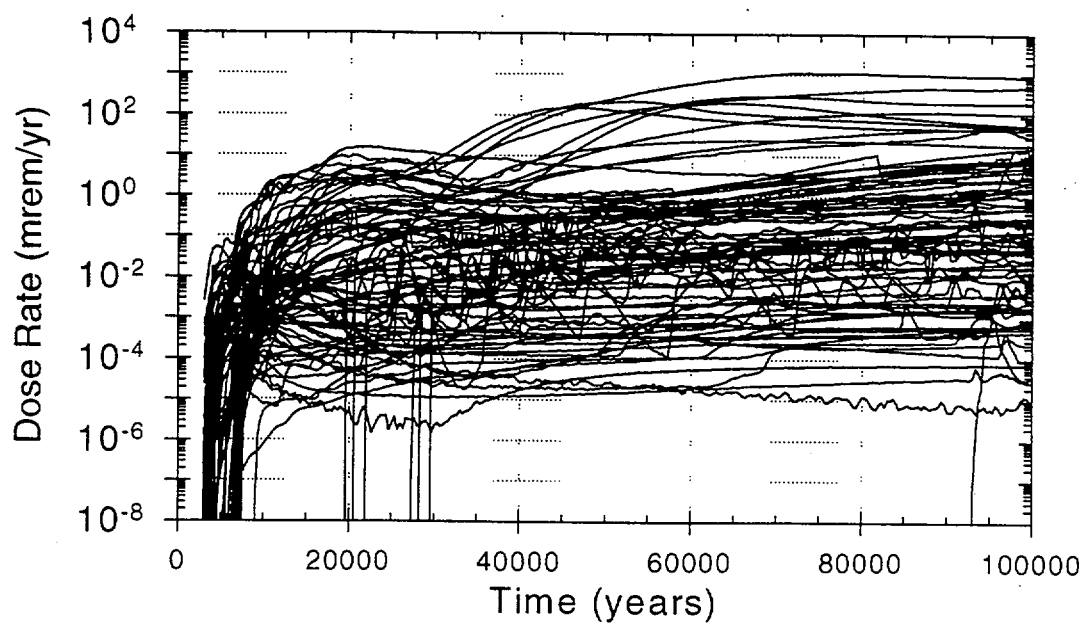


Figure 11-32. Dose-rate time histories for 100,000 years for the base case (top) and the modified-parameter case (bottom).

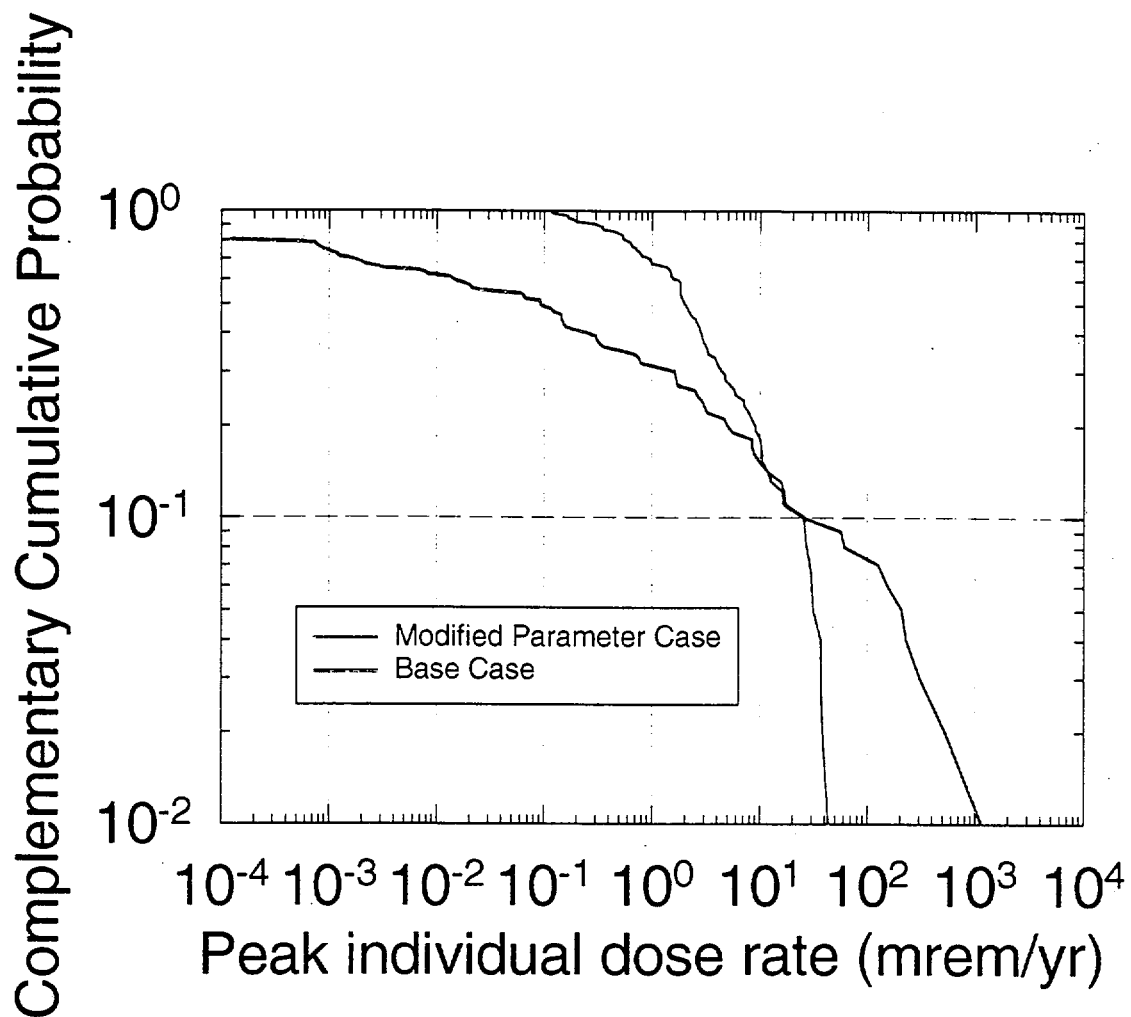


Figure 11-33. Base case and modified-parameter case distributions of peak-dose rates for the 100,000-year time period.

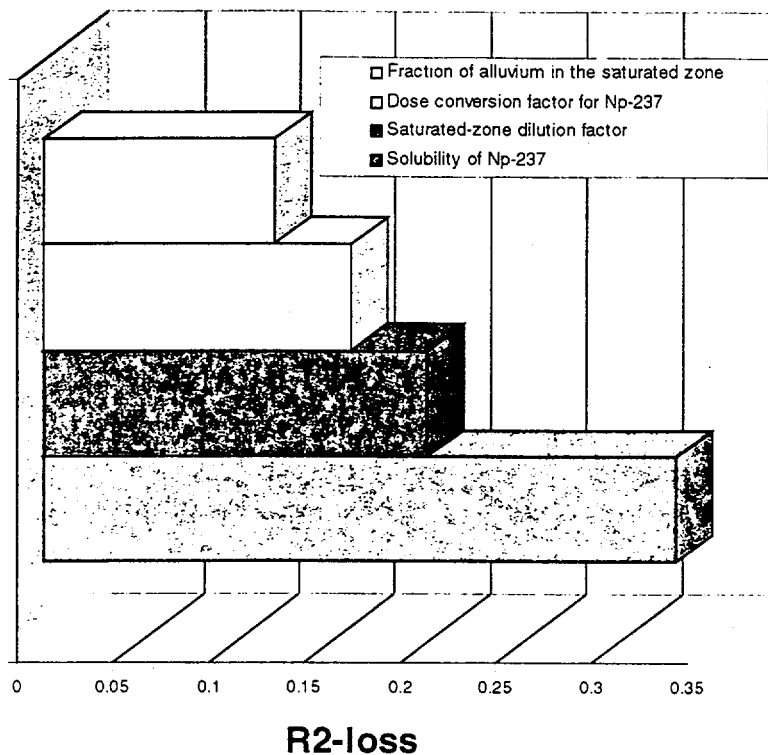


Figure 11-34. Most important parameters from stepwise regression analysis for the modified-parameter case. This chart shows the relative importance of various parameters to the calculated uncertainty in dose rate. Importance of an individual parameter is shown by  $R^2$ -loss, the reduction in goodness of the regression fit when the parameter is left out of the calculation.

## **Chapter 11**

### **Tables**

Table 11-1. Summary of input and output files, plot file names (SigmaPlot), and data tracking numbers (DTNs) associated with the TSPA-VA figures in Sections 4.2 and 5 of DOE (1998).

Figure Number	Plot File Name	Plot Description	Input Files	Output Files	Data Tracking Number
11-6 4.2-1	tspava001	Base case 10,000-year expected-value dose-rate plot	Case0ee4* UZ Files** SZ Files***	Case0ee4.btr	MO9807MWDRIP00.000
11-6 4.2-1	tspava002	Base Case 100,000-year expected-value dose-rate plot	Case0ee5* UZ Files** SZ Files***	Case0ee5.btr	MO9807MWDRIP00.000
11-6 4.2-1	tspava003	Base Case 1,000,000-year expected-value dose-rate plot	Case0ee6* UZ Files** SZ Files***	Case0ee6.btr	MO9807MWDRIP00.000
11-7 4.2-2	tspava001	Base case 10,000-year expected-value dose-rate plot	Case0ee4* UZ Files** SZ Files***	Case0ee4.btr	MO9807MWDRIP00.000
11-7 4.2-2	tspava004	Base Case 10,000-year expected-value Tc-99 EBS release from the different regions	Case0ee4* UZ Files** SZ Files***	Case0ee4.btr	MO9807MWDRIP00.000
11-7 4.2-2	tspava005	Base Case 10,000-year expected-value advective and diffusive release of Tc-99 from the waste package	Case0ee4* UZ Files** SZ Files***	Case0ee4.btr	MO9807MWDRIP00.000
11-7 4.2-2	tspava100	10,000-year plot of number of packages failed	"packages1e4.xls" Case0ee4* UZ Files** SZ Files***	Case0ee4.btr	MO9807MWDRIP00.000
11-8 4.2-3	tspava004	Base Case 10,000-year expected-value Tc-99 EBS release from the different regions	Case0ee4* UZ Files** SZ Files***	Case0ee4.btr	MO9807MWDRIP00.000
11-8 4.2-3	tspava006	Base Case 10,000-year expected-value Tc-99 UZ release from the different regions	Case0ee4* UZ Files** SZ Files***	Case0ee4.btr	MO9807MWDRIP00.000
11-8 4.2-3	tspava101	Tc-99 travel time through the UZ for various climates	****(see footnote)	****	MO9807MWDIFEIM.000

11-9 4.2-4	tspava006	Base Case 10,000-year expected-value Tc-99 UZ release from the different regions	Case0ee4* UZ Files** SZ Files***	Case0ee4.btr	MO9807MWDRIP00.000
11-9 4.2-4	tspava007	Base Case 10,000-year expected-value Tc-99 concentration at the water table	Case0ee4* UZ Files** SZ Files*** Uzflux.xls	Case0ee4.btr	MO9807MWDRIP00.000
11-9 4.2-4	tspava008	Cumulative distribution function of the effective dilution factors	Cas130m5* UZ Files** SZ Files**	Cas130m5.btr	MO9807MWDRIP00.000
11-9 4.2-4	tspava009	Base Case 10,000-year Tc-99 concentration at 20 km from the repository boundary	Case0ee4* UZ Files** SZ Files***	Case0ee4.btr	MO9807MWDRIP00.000
11-9 4.2-4	tspava010	Base Case 10,000-year Tc-99 mass flux at 20 km from the six different streamtubes	Case0ee4* UZ Files** SZ Files***	Case0ee4.btr	MO9807MWDRIP00.000
11-9 4.2-4	tspava102	Saturated zone breakthrough curves for various radionuclides	trans.dat trac[1-11].0000 zone1.0000	sz[01-11]_01.0000	SNT05082597001.P05
11-10 4.2-5	tspava002	Base Case 100,000-year expected-value dose-rate plot	Case0ee5* UZ Files** SZ Files***	Case0ee5.btr	MO9807MWDRIP00.000
11-10 4.2-5	tspava011	100,000-year Tc-99, Pu-239 and Np-237 release from the EBS	Case0ee5* UZ Files** SZ Files***	Case0ee5.btr	MO9807MWDRIP00.000
11-10 4.2-5	tspava012	100,000-year advective and diffusive release of Tc-99 and Np-237 from the waste package	Case0ee5* UZ Files** SZ Files***	Case0ee5.btr	MO9807MWDRIP00.000
11-10 4.2-5	tspava103	100,000-year plot of number of packages failed	"packages1e5.xls" Case0ee5* UZ Files** SZ Files***	Case0ee5.btr	MO9807MWDRIP00.000

11-10 4.2-5	tspava104	Np-237 cumulative inventory exposure history	Convolute.f Convolute.exe Case0ee5* UZ Files** SZ Files***	Case0ee5.btr	MO9807MWDRIP00.000
11-11 4.2-6	tspava013	100,000-year Tc-99 release rate from waste package for different fuel types	Case0ee5* UZ Files** SZ Files***	Case0ee5.btr	MO9807MWDRIP00.000
11-11 4.2-6	tspava014	100,000-year Np-237 release rate from waste package for different fuel types	Case0ee5* UZ Files** SZ Files***	Case0ee5.btr	MO9807MWDRIP00.000
11-11 4.2-6	tspava105	Tc-99 cumulative inventory exposure history	Convolute.f Convolute.exe Case0ee5* UZ Files** SZ Files***	Case0ee5.btr	MO9807MWDRIP00.000
11-11 4.2-6	tspava104	Np-237 cumulative inventory exposure history	Convolute.f Convolute.exe Case0ee5* UZ Files** SZ Files***	Case0ee5.btr	MO9807MWDRIP00.000
11-12 4.2-7	tspava011	100,000-year Tc-99, Pu-239 and Np-237 release from the EBS	Case0ee5* UZ Files** SZ Files***	Case0ee5.btr	MO9807MWDRIP00.000
11-12 4.2-7	tspava015	100,000-year Tc-99, Pu-239 and Np-237 release from the UZ	Case0ee5* UZ Files** SZ Files***	Case0ee5.btr	MO9807MWDRIP00.000
11-12 4.2-7	tspava106	Tc-99, Np-237 and Pu-242 travel time in the UZ for LTA climate	***** (see footnote)	*****	MO9807MWD1FEIM.000
11-13 4.2-8	tspava015	100,000-year Tc-99, Pu-239 and Np-237 release from the UZ	Case0ee5* UZ Files** SZ Files*** UZFlux.xls	Case0ee5.btr	MO9807MWDRIP00.000



11-13 4.2-8	tspava016	100,000-year Np-237 concentration at the water table	Case0ee5* UZ Files** SZ Files***	Case0ee5.btr	MO9807MWDRIP00.000
11-13 4.2-8	tspava008	Cumulative distribution function of the effective dilution factors	Cas130m5* UZ Files** SZ Files***	Cas130m5.btr	MO9807MWDRIP00.000
11-13 4.2-8	tspava017	100,000-year Tc-99, Pu-239 and Np-237 concentration at 20 km from the repository boundary	Case0ee5* UZ Files** SZ Files***	Case0ee5.btr	MO9807MWDRIP00.000
11-13 4.2-8	tspava018	100,000-year Tc-99, Pu-239 and Np-237 mass flux (Ci/yr) at 20 km from the repository boundary	Case0ee5* UZ Files** SZ Files***	Case0ee5.btr	MO9807MWDRIP00.000
11-13 4.2-8	tspava102	Saturated zone breakthrough curves for various radionuclides	trans.dat trac[1-11].0000 zone1.0000	sz[01-11]_01.0000	SNT05082597001.P05
11-14 4.2-9	tspava017	100,000-year Tc-99, Pu-239 and Np-237 concentration at 20 km from the repository boundary	Case0ee5* UZ Files** SZ Files***	Case0ee5.btr	MO9807MWDRIP00.000
11-14 4.2-9	tspava019	100,000-year Pu-239 concentration from irreversible and reversible colloids at 20 km	Case0ee5* UZ Files** SZ Files***	Case0ee5.btr	MO9807MWDRIP00.000
11-14 4.2-9	tspava002	Base Case 100,000-year expected-value dose-rate plot	Case0ee5* UZ Files** SZ Files***	Case0ee5.btr	MO9807MWDRIP00.000
11-15 4.2-10	tspava003	Base Case 1,000,000-year expected-value dose-rate plot	Case0ee6* UZ Files** SZ Files***	Case0ee6.btr	MO9807MWDRIP00.000
11-15 4.2-10	tspava020	1,000,000-year Np-237 advective and diffusive release from waste package	Case0ee6* UZ Files** SZ Files***	Case0ee6.btr	MO9807MWDRIP00.000
11-15 4.2-10	tspava021	1,000,000-year Tc-99 advective and diffusive release from waste package	Case0ee6* UZ Files** SZ Files***	Case0ee6.btr	MO9807MWDRIP00.000

11-15 4.2-10	tspava107	Inventory exposure rate history for 1,000,000 years	Convolute.f Convolute.exe Case0ee6* UZ Files** SZ Files***	Case0ee6.btr	MO9807MWDRIP00.000
11-15 4.2-10	tspava108	Np-237 cumulative inventory exposure history	Convolute.f Convolute.exe Case0ee6* UZ Files** SZ Files***	Case0ee6.btr	MO9807MWDRIP00.000
11-15 4.2-10	tspava109	1,000,000-year plot of number of packages failed	"packages.xls" Case0ee6* UZ Files** SZ Files***	Case0ee6.btr	MO9807MWDRIP00.000
11-16 4.2-11	tspava22	1,000,000-year Tc-99 release rate from waste package for different fuel types	Case0ee6* UZ Files** SZ Files***	Case0ee6.btr	MO9807MWDRIP00.000
11-16 4.2-11	tspava023	1,000,000-year Np-237 release rate from waste package for different fuel types	Case0ee6* UZ Files** SZ Files***	Case0ee6.btr	MO9807MWDRIP00.000
11-17 4.2-12	tspava024	1,000,000-year Np-237 Concentration at the water table	Case0ee6* UZ Files** SZ Files***	Case0ee6.btr	MO9807MWDRIP00.000
11-17 4.2-12	tspava025	Base Case 1,000,000-year dose-rate plot (no total dose-rate on plot)	Case0ee6* UZ Files** SZ Files***	Case0ee6.btr	MO9807MWDRIP00.000
11-17 4.2-12	tspava026	1,000,000-year concentration at 20 km from the six streamtubes for the top 5 radionuclides	Case0ee6* UZ Files** SZ Files***	Case0ee6.btr	MO9807MWDRIP00.000
11-18 4.2-13	tspava027	10,000-year Tc-99 cumulative fractional release from EBS and SZ	Case0ee4* UZ Files** SZ Files***	Case0ee4.btr	MO9807MWDRIP00.000
11-18 4.2-13	tspava028	100,000-year Tc-99 cumulative fractional release from EBS and SZ	Case0ee5* UZ Files** SZ Files***	Case0ee5.btr	MO9807MWDRIP00.000

11-18 4.2-13	tspava029	1,000,000-year Tc-99 cumulative fractional release from EBS and SZ	Case0ee6* UZ Files** SZ Files***	Case0ee6.btr	MO9807MWDRIP00.000
11-18 4.2-13	tspava030	100,000-year Np-237 cumulative fractional release from EBS and SZ	Case0ee5* UZ Files** SZ Files***	Case0ee5.btr	MO9807MWDRIP00.000
11-18 4.2-13	tspava031	1,000,000-year Np-237 cumulative fractional release from EBS and SZ	Case0ee6* UZ Files** SZ Files***	Case0ee6.btr	MO9807MWDRIP00.000
11-18 4.2-13	tspava032	100,000-year Pu-239 cumulative fractional release from EBS and SZ	Case0ee5* UZ Files** SZ Files***	Case0ee5.btr	MO9807MWDRIP00.000
11-18 4.2-13	tspava033	1,000,000-year Pu-242 cumulative fractional release from EBS and SZ	Case0ee6* UZ Files** SZ Files***	Case0ee6.btr	MO9807MWDRIP00.000
4.5-4	tspava034	1,000,000-year dose rate history for base case vs. drip shield case	Case86e6* Case0ee6* UZ Files** SZ Files***	Case86e6.btr Case0ee6.btr	MO9807MWDRIP00.000
4.5-5	tspava035	1,000,000-year dose rate history for base case vs. ceramic coating case	Case28e6* Case0ee6* UZ Files** SZ Files***	Case28e6.btr Case0ee6.btr	MO9807MWDRIP00.000
5.1-1	tspava036	1,000,000-year dose rate history for base case vs. 50,000-year climate duration case	Case1ee6* Case0ee6* UZ Files** SZ Files***	Case1ee6.btr Case0ee6.btr	MO9807MWDRIP00.000
5.1-2	tspava037	1,000,000-year-dose rate history for base case vs. case with LTA climate only, SP climate only, and DRY climate only.	Case0ee6* Case2ee6* Case3ee6* Case4ee6* UZ Files** SZ Files***	Case0ee6.btr Case2ee6.btr Case3ee6.btr Case4ee6.btr	MO9807MWDRIP00.000

5.1-3	tspava038	Comparison of 100,000-year peak dose rate CCDF of the base case with the uncorrelated climate amplitudes case	Case5me6* Case0me6* UZ Files** SZ Files***	Case5me6.btr Case0me6.btr	MO9807MWDRIP00.000
5.1-4	tspava039	Comparison of 100,000-year peak dose rate CCDF of the base case with the modified infiltration weights case	Case23m5* Case0me5* UZ Files** SZ Files***	Case23m5.btr Case0me5.btr	MO9807MWDRIP00.000
5.1-5	tspava040	100,000-year expected value dose rate history for base case and cases with various infiltration and fracture alpha values.	Case0ee5* Case6ee5* Case7ee5* Case8ee5* Case9ee5* UZ Files** SZ Files***	Case0ee5.btr Case6ee5.btr Case7ee5.btr Case8ee5.btr Case9ee5.btr	MO9807MWDRIP00.000
5.1-6	tspava041	100,000-year expected value dose rate history for base case vs. dual permeability/veeps model	Case0ee5* Case11e5* UZ Files** SZ Files***	Case0ee5.btr Case11e5.btr	MO9807MWDRIP00.000
5.1-7	tspava042	Comparison of 100,000 year peak dose rate CCDF of the base case with DKM/Weeps UZ Flow model case	Case19m5* Case0me5* UZ Files** SZ Files***	Case19m5.btr Case0me5.btr	MO9807MWDRIP00.000
5.1-8	tspava043	Comparison of 100,000 year peak-dose-rate CCDF of the base case with increased fracture aperture case, decreased fracture aperture case and narrow variance of fractures case	Case0m5* Case21me5* Case22me5* Case24me5* UZ Files** SZ Files***	Case0m5.btr Case21me5.btr Case22me5.btr Case24me5.btr	MO9807MWDRIP00.000
5.3-1	tspava044	10,000-year EBS release-rate history for base case and concrete modified water case	Case0ee4* Case57e4* UZ Files** SZ Files***	Case0ee4.btr Case57e4.btr	MO9807MWDRIP00.000

5.3-2	tspava045	100,000-year EBS release-rate history for base case and concrete modified water case	Case0ee5* Case30e5* UZ Files** SZ Files***	Case0ee5.btr Case30e5.btr	MO9807MWDRIP00.000
5.3-3	tspava046	100,000-year release-rate history for concrete modified water case with several radionuclides	Case30e5* UZ Files** SZ Files***	Case30e5.btr	MO9807MWDRIP00.000
5.3-4	tspava047	10,000-year dose-rate history for base case and concrete modified water case	Case0ee4* Case57e4* UZ Files** SZ Files***	Case0ee4.btr Case57e4.btr	MO9807MWDRIP00.000
5.3-5	tspava048	100,000-year dose-rate history for base case and concrete modified water case	Case0ee5* Case30e5* UZ Files** SZ Files***	Case0ee5.btr Case30e5.btr	MO9807MWDRIP00.000
5.4-1	tspava049	100,000-year dose-rate history for base case vs. CRM 5 <sup>th</sup> and 95 <sup>th</sup> percentile corrosion rate cases	Case0ee5* Case65e5* Case66e5* UZ Files** SZ Files***	Case0ee5.btr Case65e5.btr Case66e5.btr	MO9807MWDRIP00.000
5.4-4	tspava045	100,000-year EBS release-rate history for base case and concrete modified water case	Case0ee5* Case30e5* UZ Files** SZ Files***	Case0ee5.btr Case30e5.btr	MO9807MWDRIP00.000
5.4-5	tspava050	100,000-year dose-rate history for base case and 95 <sup>th</sup> percentile juvenile failures case	Case0ee5* Case58e5* UZ Files** SZ Files***	Case0ee5.btr Case58e5.btr	MO9807MWDRIP00.000
5.4-6	tspava051	1,000,000-year dose rate history showing sensitivity to corrosion patch size	Case87e6* Case88e6* case0ee6* UZ Files** SZ Files***	Case87e6.btr Case88e6.btr case0ee6.btr	MO9807MWDRIP00.000

5.5-1	tspava052	1,000,000-year dose-rate history for base case, 5 <sup>th</sup> and 95 <sup>th</sup> percentile value of Np-237 solubility	Case0ee6* Case67e6* Case68e6* UZ Files** SZ Files***	Case0ee6.btr Case67e6.btr Case68e6.btr	MO9807MWDRIP00.000
5.5-2	tspava053	1,000,000-year dose-rate history for base case and secondary phase concentration case	Case0ee6* Case32e6* UZ Files** SZ Files***	Case0ee6.btr Case32e6.btr	MO9807MWDRIP00.000
5.5-3	tspava054	1,000,000-year dose rate history for base case, 5 <sup>th</sup> and 95 <sup>th</sup> percentile value of cladding failure fraction	Case0ee6* Case79e6* Case80e6* UZ Files** SZ Files***	Case0ee6.btr Case79e6.btr Case80e6.btr	MO9807MWDRIP00.000
5.5-4	tspava055	1,000,000-year dose rate history for base case, no cladding case and cases for cladding degraded at 10,000, 100,000 and 200,000 years	Case0ee6* Case31e6* Case81e6* Case82e6* Case83e6* UZ Files** SZ Files***	Case0ee6.btr Case81e6.btr Case82e6.btr Case83e6.btr Case31e6.btr	MO9807MWDRIP00.000
5.5-4	tspava056	1,000,000-year dose rate for base case, no cladding case and cases for cladding failure at 100,000 and 1,000,000 years	Case0ee6* Case31e6 Case82e6* Case84e6* UZ Files** SZ Files***	Case0ee6.btr Case82e6.btr Case84e6.btr Case31e6.btr	MO9807MWDRIP00.000
5.5-5	tspava057	100,000-year CCDF of peak dose rate values for base case and no cladding case	Case0me5* Case31m5* UZ Files** SZ Files***	Case0me5.btr Case31m5.btr	MO9807MWDRIP00.000
5.5-6	tspava058	1,000,000-year dose rate for base case, 5 <sup>th</sup> and 95 <sup>th</sup> percentile seepage flux values	Case0ee6* Case71e6* Case72e6* UZ Files** SZ Files***	Case0ee6.btr Case71e6.btr Case72e6.btr	MO9807MWDRIP00.000

5.5-9	tspava059	100,000-year dose rate history for base case and case with $K_d=0$ in the invert for Np-237, Pu-239 and U-234	Case0ee5* Case89e5* UZ Files** SZ Files***	Case0ee5.btr Case89e5.btr	MO9807MWDRIP00.000
5.5-9	tspava060	100,000-year dose rate for base case and case with $K_d=0$ in the invert	Case0ee5* Case89e5* UZ Files** SZ Files***	Case0ee5.btr Case89e5.btr	MO9807MWDRIP00.000
5.6-1	tspava002	Base Case 100,000-year expected-value dose-rate plot	Case0ee5* UZ Files** SZ Files***	Case0ee5.btr	MO9807MWDRIP00.000
5.6-2	tspava061	100,000-year dose rate for base case and no matrix diffusion in UZ case	Case0ee5* Case33e5* UZ Files** SZ Files***	Case0ee5.btr Case33e5.btr	MO9807MWDRIP00.000
5.6-3	tspava062	100,000-year dose rate for dual permeability/weepers case with and without matrix diffusion in UZ	Case11e5* Case39e5* UZ Files** SZ Files***	Case11e5.btr Case39e5.btr	MO9807MWDRIP00.000
5.6-4	tspava063	100,000-year dose rate for 1/3 and max alpha case with and without matrix diffusion	Case8ee5* Case36e5* UZ Files** SZ Files***	Case8ee5.btr Case36e5.btr	MO9807MWDRIP00.000
5.6-5	tspava064	100,000-year dose rate for 1/3 and min alpha case with and without matrix diffusion	Case9ee5* Case37e5* UZ Files** SZ Files***	Case9ee5.btr Case37e5.btr	MO9807MWDRIP00.000
5.6-6	tspava065	100,000-year Np-237 dose rate for base case and the case with $K_d=0$ for actinides in UZ	Case0ee5* Case46e5* UZ Files** SZ Files***	Case0ee5.btr Case46e5.btr	MO9807MWDRIP00.000
5.6-7	tspava066	100,000-year Pu-239 dose rate for base case and the case with $K_d=0$ for actinides in UZ	Case0ee5* Case46e5* UZ Files** SZ Files***	Case0ee5.btr Case46e5.btr	MO9807MWDRIP00.000

5.6-8	tspava067	100,000-year Pu-242 dose rate for base case and the case with Kd=0 for actinides in UZ	Case0ee5* Case46e5* UZ Files** SZ Files***	Case0ee5.btr Case46e5.btr	MO9807MWDRIP00.000
5.6-9	tspava068	100,000-year dose rate for base case and the case with Kd=0 for actinides in the UZ for the important radionuclides	Case0ee5* Case46e5* UZ Files** SZ Files***	Case0ee5.btr Case46e5.btr	MO9807MWDRIP00.000
5.6-10	tspava069	100,000 year total dose-rate for base case and the case with concrete modified water and Kd=0 for actinides in UZ	Case0ee5* Case57e5* UZ Files** SZ Files***	Case0ee5.btr Case57e5.btr	MO9807MWDRIP00.000
5.6-11	tspava070	100,000-year dose rate history for the case with concrete modified water and Kd=0 for actinides in UZ	Case57e5* UZ Files** SZ Files***	Case57e5.btr	MO9807MWDRIP00.000
5.7-1	tspava071	1,000,000-year dose rate for base case, 5 <sup>th</sup> and 95 <sup>th</sup> percentile of SZ dilution factor	Case0ee6* UZ Files** SZ Files***	Case0ee6.btr	MO9807MWDRIP00.000
5.7-2	tspava072	100,000-year dose rate comparison for base case, using maximum concentration and weighted average concentration from the six streamtubes in the SZ	Case0ee5* UZ Files** SZ Files***	Case0ee5.btr	MO9807MWDRIP00.000
5.8-1	tspava099	100,000-year dose rate for base case, 5 <sup>th</sup> and 95 <sup>th</sup> percentile Biosphere Dose Conversion Factors (BDCF)	Case0ee5* Case63e5* Case64e5* UZ Files** SZ Files***	Case0ee5.btr Case63e5.btr Case64e5.btr	MO9807MWDRIP00.000

\*RIP input files. Name listed is the file name ("filename") representing the files with the following extensions:

filename.bak	filename.bpf	filename.bsr	filename.btf
filename.rp	filename.t01	filename.t02	filename.t03
filename.t04	filename.t05	filename.t06	filename.t07
filename.t08	filename.t09	filename.t10	filename.t11
filename.t12	filename.t13	filename.t14	filename.t15
filename.t16	filename.t17	filename.t18	filename.t19
filename.t20	filename.t21	filename.t22	filename.t23
filename.t24	filename.t25	filename.t26	filename.t27



filename.t28  
filename.t32  
filename.t36

filename.t29  
filename.t33  
filename.t37

filename.t30  
filename.t34

filename.t31  
filename.t35

**\*\* FEHM particle tracker input files for Unsaturated-zone transport:**

baserun1.chk  
baserun1.dat  
fmQb.rock  
ff0100.ini  
ff1300.ini  
ff2500.ini

baserun1.his  
fehmn.files  
fmQb.stor  
ff0300.ini  
ff1500.ini

baserun1.trc  
fmQb.dpdp  
fmQb.zone  
ff0500.ini  
ff2100.ini

fmQb.grid  
fmQb.zone6  
ff1100.ini  
ff2300.ini

ptrk.expval (used for expected-value runs)

ptrk.multrlz (used for multiple realization runs)

**\*\*\* SZ breakthrough curve files used as input to SZ\_Convolute for saturated-zone transport:**

SZ0A\_0B.0XXX

A= 1 through 11, represent the 9 radionuclides and the 2 irreversible Pu-239 and Pu-242 radionuclides tracked in the TSPA-VA model.

Radionuclide	Number (A)
C-14	1
I-129	2
Np-237	3
Pa-231	4
Pu-239	5
Pu-239 irreversible	6
Pu-242	7
Pu-242 irreversible	8
Se-79	9
Tc-99	10
U-234	11

B= 1 through 6 represent the six streamtubes used in the SZ transport

XXX= Used to represent the realization number

= 1 for expected-value runs

= 1 through 100 for multiple realization runs

\*\*\*\* tspava101 files:

Input Files	Output files
/present/mdi11.E-11/ zkd0vkd0dkd0.trn pirk fehmn.files	/present/mdi11.E-11/ zkd0vkd0dkd0_tc99.fin..output
/lta/mdi11.E-11/ zkd0vkd0dkd0.trn pirk fehmn.files	/lta/mdi11.E-11/ zkd0vkd0dkd0_tc99.fin..output
/sp/mdi11.E-11/ zkd0vkd0dkd0.trn pirk fehmn.files	/sp/mdi11.E-11/ zkd0vkd0dkd0_tc99.fin..output

\*\*\*\*\* tspava106 files:

Input Files	Output files
/lta/mdi11.E-11/ zkd0vkd0dkd0.trn pirk fehmn.files	/lta/mdi11.E-11/ zkd0vkd0dkd0_tc99.fin.output
/lta/mdi11.E-10/ zkd100vkd100dkd100/ zkd100vkd100dkd100.trn pirk fehmn.files	/lta/mdi11.E-10/ zkd100vkd100dkd100/ zkd100vkd100dkd100.output
/lta/mdi11.E-10/ zkd4vkd1dkd1/ zkd4vkd1dkd1.trn pirk fehmn.files	/lta/mdi11.E-10/ zkd4vkd1dkd1/ zkd4vkd1dkd1.output

Table 11- 2. Summary of Computer Codes\* that Comprise the Total System Model.\*

Computer Code	Version	Code Usage	QA Status
RIP	5.19.01	Total system integrator	NQ
SFDiss	1.0	Software routine coupled to RIP code to calculate CSNF rate	NQ
GLDiss	1.0	Software routine coupled to RIP code to calculate glass dissolution rate	NQ
EDC	1.0	Software routine coupled to RIP code to calculate effective diffusion coefficient in partially saturated medium	NQ
FEHMN	1.2	Particle tracker coupled to RIP for UZ transport	NQ
SZ_CONVOLUTE	1.0	Software routine coupled to RIP code to calculate SZ concentrations using SZ unit breakthrough curves	NQ

\*Software routine reports are currently being developed for SFDiss, GLDiss, and EDC. Codes are executed on 266/300Mz Pentium II dual processor personal computers.

Table 11- 3. Summary of Input and Output Files and Data Tracking Numbers Associated with the TSPA-VA  
(Figures 11-19 through 11-34 in Section 11.4 of this Chapter).\*

Figure Number	Input Filename	Data Tracking Number	Q Status	Output Filename	Data Tracking Number	Q Status
11-19 4.3-1	case0me4.zip base1e5.zip case0me6.zip	M09807MWDRIP00.000	NQ	Details.dat(1E4) Details.dat(1E5) Details.dat(1E6) hairplot_100k.jnb baseccdfs.jnb	SNT05070798001.001	NQ
11-20 4.3-2	case0me4.zip base1e5.zip case0me6.zip	M09807MWDRIP00.000	NQ	Details.dat(1E4) Details.dat(1E5) Details.dat(1E6) 10kcontr.xls 100kcontr.xls 1000kcontr.xls	SNT05070798001.001	NQ
11-21 4.3-3	case0me4.zip base1e5.zip case0me6.zip	M09807MWDRIP00.000	NQ	Details.dat(1E4) Details.dat(1E5) Details.dat(1E6) peaktime_10k.xls peaktime_100k.xls peaktime_1000k.xls	SNT05070798001.001	NQ
11-22 4.3-4	base1e5.zip	M09807MWDRIP00.000	NQ	Details.dat(1E4) Cumfail100k.jnb	SNT05070798001.001	NQ
11-23 4.3-5	case0me6.zip	M09807MWDRIP00.000	NQ	Details.dat(1E6) 1000kcurves.jnb	SNT05070798001.001	NQ
11-24 4.3-6	case0me6.zip	M09807MWDRIP00.000	NQ	Details.dat(1E6) Fracall.JNB (Climate Model, Real 87)	SNT05070798001.001	NQ
11-25 4.3-7	case0me6.zip	M09807MWDRIP00.000	NQ	Details.dat(1E6) Cumfail1000k.jnb	SNT05070798001.001	NQ

Table 11-3. (continued).

Figure Number	Input Filename	Data Tracking Number	Q Status	Output Filename	Data Tracking Number	Q Status
11-26 4.3-8	case0me4.zip base0me5.zip baseme4n.zip baseme5n.zip	M09807MWDRIP00.000	NQ	Details.dat(1E4) Details.dat(1E5) ccdf100k_100r.dat ccdf10k_1000r.dat bigccdf.jnb	SNT05070798001.001	NQ
11-27 4.3-9	case0me4.zip base1e5.zip case0me6.zip	M09807MWDRIP00.000	NQ	Details.dat(1E4) Details.dat(1E5) Details.dat(1E6) rankdos10k.xls rankdos100k.xls rankdos1000k.xls	SNT05070798001.001	NQ
11-28 4.3-10	base1e5.zip	M09807MWDRIP00.000	NQ	Details.dat(1E5) FI_C22_DOSE100k.xls	SNT05070798001.001	NQ
11-29 4.3-11	base1e5.zip	M09807MWDRIP00.000	NQ	Details.dat(1E5) FI_C22_DOSE100k.xls	SNT05070798001.001	NQ
11-30 4.3-12	case0me6.zip	M09807MWDRIP00.000	NQ	Details.dat(1E6) dos_fl_1000k.xls	SNT05070798001.001	NQ
11-31 4.3-13	case0me4.zip base1e5.zip case0me6.zip	M09807MWDRIP00.000	NQ	Details.dat(1E4) Details.dat(1E5) Details.dat(1E6) pcc.jnb	SNT05070798001.001	NQ
11-32	base1e5.zip case55m5.zip	M09807MWDRIP00.000	NQ	Details.dat(1E5) Details.dat(1E5,Case55) basevscase55.jnb	SNT05070798001.001	NQ
11-33	base1e5.zip case55m5.zip	M09807MWDRIP00.000	NQ	Details.dat(1E5) Details.dat(1E5,Case55) Case55vsbase_ccdf.jnb	SNT05070798001.001	NQ
11-34	case55m5.zip	M09807MWDRIP00.000	NQ	Details.dat(1E5,Case55) rank_dos100kcase55.xls	SNT05070798001.001	NQ

- \*.zip files are compressed RIP output files. Details.dat files are extracted from the \*.zip files after they are decompressed; these files contain the independent and dependent variables analyzed in the regression analysis. \*.jnb files are SigmaPlot files. \*.xls files are EXCEL files

Table 11-4. Summary of Computer Codes Used for the Uncertainty and Sensitivity Analysis (Codes were Executed on a Sun Ultra Sparc (UNIX Operating System).\*

Computer Code	Version	Code Usage	QA Status
PRESATOOL	1.5	Preprocessor for SATOOL	NQ
SATOOL	1.2	Perform regression analysis	NQ
PEAKCONTR	1.0	Calculate individual radionuclide contribution to peak dose rate	NQ
PEAKTIME	1.0	Extract time of peak-dose rate of RIP output	NQ
READPCC	1.1	Extract partial correlation coefficients from SATOOL output	NQ
STUFFIT	1.0	Insert zero peak-dose rates into RIP output	NQ

\* These computer codes are stored in Sandia National Laboratories' code configuration management system.

Table 11-5. Importance Ranking of Inputs for Engineered-Barrier-System Releases at 1,000,000 Years.

Rank	Variable	$R^2$ -loss	Partial Rank Correlation Coefficient
1	Fraction of waste packages contacted by seepage water	0.45	0.84
2	Number of cladding failures because of corrosion	0.07	0.52
3	Alloy 22 mean corrosion rate	0.06	0.51
4	Fraction of plutonium colloids transported with irreversible sorption	0.04	0.43

Regression Model: Input variables = 11,  $R^2$  = 0.82

Table 11-6. Summary of Calculated, Peak-Dose Rates at 20 km (12.4 Miles).

Simulation Period (years)	5 <sup>th</sup> Percentile (mrem/year)	Mean (mrem/year)	50 <sup>th</sup> Percentile (mrem/year)	95 <sup>th</sup> Percentile (mrem/year)	Coefficient of Variation
10,000	0	0.1	0.002	0.8	3.8
100,000	0	30	0.09	200	4.4
1 million	0.07	200	8	1,000	2.8